Functionalised Polymers by Surface Modification Using Diaryl Carbenes

Apichat Aphaiwong

St. John's College
University of Oxford

A thesis submitted for the degree of
Doctor of Philosophy
Trinity 2013

Abstract

Functionalised Polymers by Surface Modification Using Diaryl Carbenes

Apichat Aphaiwong, St. John's College, University of Oxford

A thesis submitted for the degree of D.Phil, Trinity Term 2013

This thesis is concerned with the synthesis of diazo compounds for the introduction of various functional groups on the surface of polymers by means of carbene insertion and diazonium coupling. Characterisation and investigation of their properties were conducted.

A library of functionalised polystyrene beads containing pyridine rings has been established for the coordination of metal ions and metal complexes. The pyridyl system on the surface has demonstrated its capability to bind with zinc complexes of bis(thiosemicarbazones) and release the corresponding copper complexes upon transmetallation.

A spiropyran derivative has been introduced onto the surface of polystyrene and polyethylene terephthalate. The chromophore on both polymers exhibited photoswitchability as determined from colour change and wettability.

Polystyrenes with either pyridine or spiropyran units have been investigated for reversible immobilisation of bioactive species. Materials coated with penicillin V gave significant inhibition zones in antibacterial assays, showing efficacy in drug delivery.

Finally, a range of diazo compounds with different substituents has been synthesised and their thermal stabilities have been assessed by differential scanning calorimetry technique.

Acknowledgements

Firstly, I would like to thank Prof Mark Moloney for his kind support and excellent supervision throughout my partII and DPhil. It is my pleasure to be one of your students. I would also like to thank the CRL staff, Dr Robert Jacobs for the ATR-IR and contact angle measurements, Wendy Sobey for the bioassay experiments, Dr Jeffrey Harmer for the EPR results, Dr Karl Harrison for professional photography, Benjamin Tan and Yongchul Jeong for bioactive compounds, Dr Martin Christlieb from the Gray Institute for Radiation Oncology & Biology Laboratory for the HPLC assay, Dr Jon-Paul Griffiths from the Oxford Advanced Surfaces group for the DSC analysis, Dr David J Morgan from the Cardiff Catalysis Institute for the XPS data, and Shuyun for massive help with my corrections.

I would like to thank the Royal Thai Government for financial support.

To past and present members of the Moloney group, especially Jeong, Anwar, Lawrence, Claire, Chandan, Emily, Beth, and Ben for lovely lab edutainment.

To all friends for awesome memories and experiences.

Finally, to papa, mama, p'Yui, p'Nui, and Mai. You make me feel so loved.

Table of Contents

Abbreviations

A^o	limiting area
Ar	aryl
ATR	attenuated total reflectance
B^o	magnetic field strength
Boc	*t*-butoxycarbonyl
Bu	butyl
Ceph C	Cephalosporin C
conc	concentrated
COSY	2D 1H correlation spectroscopy
δ	chemical shift
DBU	1,8-diazabicyclo[5.4.0]undec-7-ene
DCC	dicyclohexylcarbodiimide
DCM	dichloromethane
DEPT	distortionless enhancement by polarisation transfer
DMAP	4-dimethylaminopyridine
DMSO	dimethylsulphoxide
DNA	deoxyribonucleic acid
DSC	differential scanning calorimetry
E. coli	*Escherichia coli*
Et	ethyl
EPR	electron paramagnetic resonance
ESI	electrospray ionisation
FT	Fourier transform

h	hours
hv	irradiation
HMQC	heteronuclear multiple quantum correlation
HPLC	high-performance liquid chromatography
HRMS	high resolution mass spectrometry
HSQC	heteronuclear single quantum correlation
Hz	Hertz
ICP	inductively coupled plasma
IR	infra-red
J	coupling constant
λ	wavelength
λ_{max}	wavelength maxima
Me	methyl
MIC	minimum inhibitory concentration
min	minutes
mp	melting point
MS	mass spectrometry
m/z	mass/charge ratio
NBS	N-bromosuccinimide
NMR	nuclear magnetic resonance
PBS	phosphate buffered saline
PET	positron emission tomography
PET	polyethylene terephthalate
Ph	phenyl
ppm	part per million
PPTS	pyridinium *p*-toluenesulfonate

PS	polystyrene
PS XAD	polystyrene Amberlite® XAD4
R	alkyl
S. aureus	*Staphylococcus aureus*
t	*tert*
THF	tetrahydrofuran
TLC	thin layer chromatography
Ts	tosyl
UV	ultra-violet
ν_{max}	absorption maxima
v/v	volume/volume
VIS	visible
w/v	weight/volume
XPS	X-ray photoelectron spectroscopy

Chapter 1 Diazo Modification

1.1 Introduction

1.1.1 Surface Modification

Surface modification can be achieved with various techniques to introduce active functional groups onto materials. Common methods can be divided into mechanical treatments, chemical treatments, flame treatments, ionised gas treatments, radiation treatments, and atom bombardment.[1-4] These techniques, however, often require significant infrastructure and high operating cost. Nonetheless, chemical approaches do not always require specialised equipment and therefore can be performed in most laboratories although many processes utilise harsh reaction conditions and are limited to a specific range of material substrates which must posses appropriate functionality capable of direct modification.

Of interest in the context of this work was the use of carbene insertions to introduce and systematically control diverse chemical functionality on the surface of commonly-used polymers without alteration of bulk (for instance, flexibility or mechanical strength) properties of the materials. A class of organic compounds which is well-known as carbene precursors is diazirines, but these were thought not to be suitable as a result of their lengthy chemical synthesis.[5-7] Diazo compounds, or 1,1-diaryldiazo compounds in particular, are excellent alternatives to diazirines.

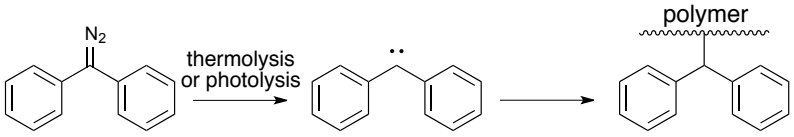

Figure 1 Surface modification by diaryldiazo compounds

Previous work in the group has proved success in surface modification with diaryldiazo compounds. This method was originally developed for colouration of a wide range of substrates, namely polystyrene, polythene, nylon, silica, glass, and polytetrafluoroethylene, by applying diaryldiazo compounds to the surface for carbene insertion followed by coupling with diazonium salts to give extended structures (**Figure 2**).[8] The modified silica, for example, displayed distinct colours as compared to the unmodified sample, demonstrated in **Figure 3**.

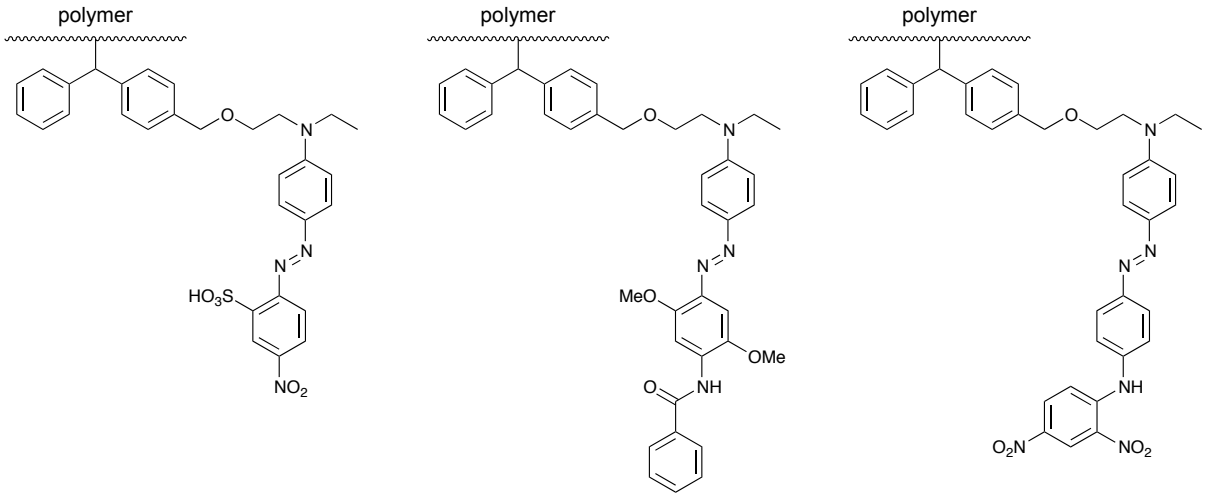

Figure 2 Structures of dyed polymers[8]

Figure 3 Comparison of white silica and dyed samples[8]

By using similar methods, polystyrenes were also introduced with various functional groups to vary protein binding, depending on the modified structure (**Figure 4**).[9] Surface characterisation using XPS was used to demonstrate the introduction of *tert*-butyl, hexyl, dimethylamino, and carboxylic acid groups onto otherwise unfunctionalised polystyrene. The significantly enhanced adhesion of the test protein bovine serum albumin (BSA) was observed for materials with these groups, in keeping with the known selectivity of BSA for these chemical functions. In addition, polymers with polar groups (NH_2, OH, and CH_2COOH) generally increased surface wettability and the more hydrophilicity attributed to a change in surface hydration.

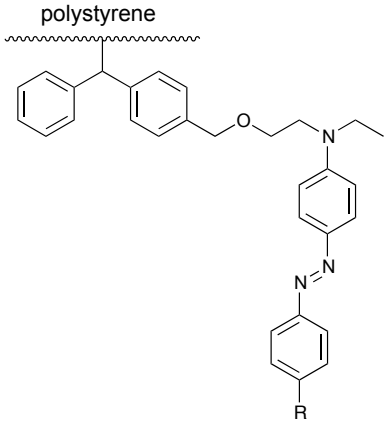

R = H, *t*-Bu, C_6H_{13}, I, NH_2, NMe_2, OH, $O(CH_2CH_2O)_3CH_3$, $CH_2P(O)(OEt)_2$, CH_2COOH

Figure 4 Structures of modified polystyrenes[9]

In addition, the use of diaryldiazo compounds for surface functionalisation was also demonstrated with hydrogen-terminated diamond samples, producing diamond surface with structures shown in **Figure 5**.[10] The incorporation of iodide onto the surface allowed detailed characterisation by XPS and the loading density was shown to be around 3 x 10^{14} molecules/cm^2.

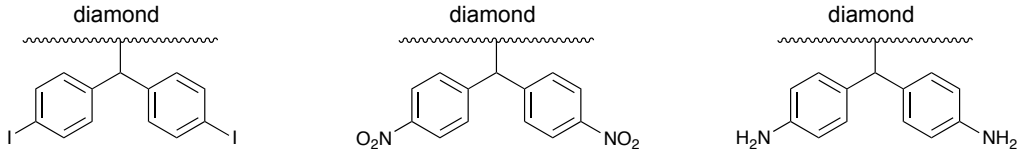

Figure 5 Structures of modified diamonds[10]

The sample with amino groups was then further modified by coupling with fluorescein isocyanate to generate fluorescent material.[11] Its structure and fluorescence microscopic examination is shown in **Figure 6**.

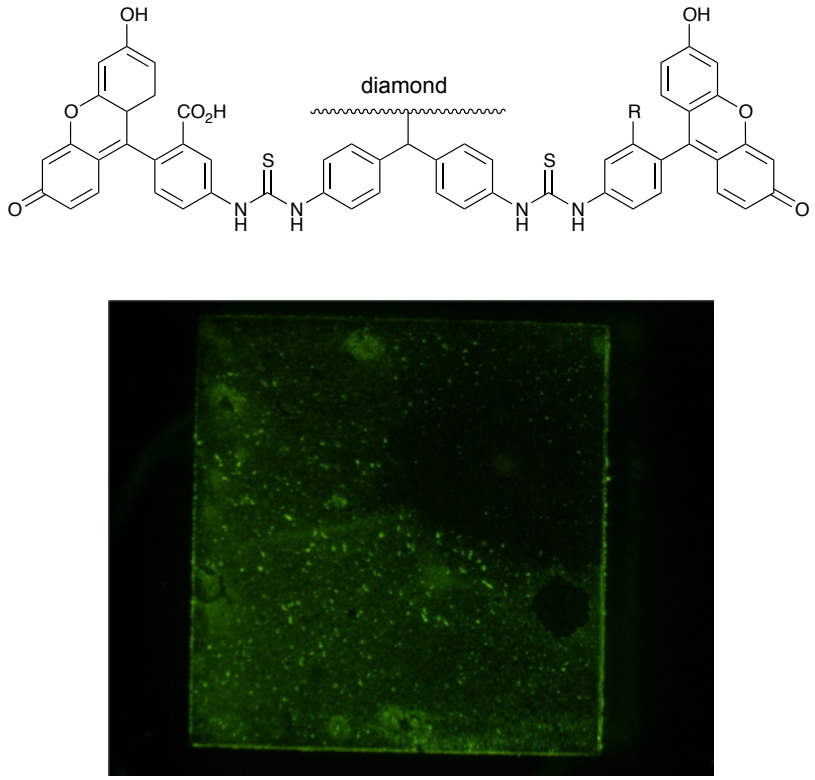

Figure 6 Structure and fluorescence microscopic examination of diamond sample[11]

The use of diarylcarbenes was also extended for incorporation of urea and thiourea groups to catch and release hydrogen peroxide as an antibacterial molecule.[11,12] Characterisation of the polymer indicated that incorporation of around 5.6 x 10^{12} urea molecules/cm^2 was achieved, and this could be used to bind H_2O_2 at a level of about 1.0 mmol/g. The fact that urea can effectively bind H_2O_2 is shown by the

existence of X-ray characterisation of $NH_2CONH_2.5H_2O_2$, and a similar binding of the modified polymer is assumed. Polymers with structures shown in **Figure 7** were therefore found to be effective in loading of hydrogen peroxide, and showed high activity against Gram-positive and Gram-negative bacteria.

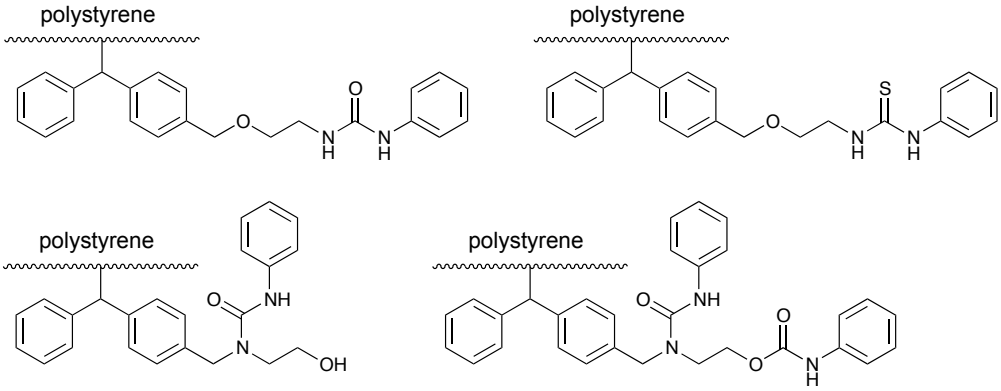

Figure 7 Structures of modified polystyrenes prior to loading of H_2O_2[11,12]

When phosphonate functional groups were introduced to the surface of Nylon and polystyrene followed by treatment with aqueous calcium hydroxide, the materials showed enhancement of biocompatibility (**Figure 8**).[13] This was demonstrated by the improved growth of human osteosarcoma cell line on the surface. The modified nylon and polystyrene materials exhibit improved cell proliferation after 13 days when compared to an unmodified samples.

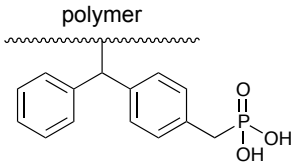

Figure 8 Structures of modified polystyrenes prior to treatment with $Ca(OH)_2$[13]

1.1.2 Diaryldiazo Compounds

The standard method for the preparation of diaryldiazo compounds involves either the formation of hydrazone from a carbonyl compound followed by oxidation or

base-mediated Bamford-Stevens-type elimination of a tosyl hydrazone. With the generation of a diaryldiazo molecule, solution coating and evaporation of the solvent is then carried out to deposit the pre-intermediate diazo substance on the surface as a thin film. Under mild conditions, either by thermolysis or photolysis, the diazo compound decomposes to produce a reactive intermediate carbene.[8-11,13-16] The carbene can then attach to available chemical groups of the polymer surface, in which the mechanism of the process is bond-insertion to X-H single bond (X=C, O, N, S) or addition reaction at C=C double bond in a chemically irreversible process.[8,11,16]

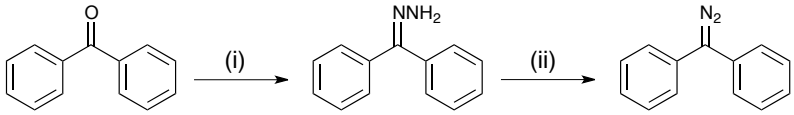

Figure 9 Synthesis of diaryldiazo compounds
H_2NNH_2 then oxidation or H_2NNHTs then base.

After the functionalisation process, the modified polymers will then be characterised by a combination of combustion analysis, Attenuated Total Reflectance (ATR) IR, X-ray photoelectron spectroscopy (XPS), and other relevant techniques based on the properties of the additional functional groups to obtain some direct information regarding changes in chemical and physical nature of the materials.

With this simple yet efficient, rapid, and versatile post-polymerisation protocol using inexpensive reagents, a wide range of materials, which might be chemically inert or have low surface energy, can be potentially derivatised with substituted diaryldiazomethanes, by the formation of carbenes with different functional groups to obtain modified polymers with a variety of desired surface chemical characteristics at controlled loading levels without compromise of bulk properties of substrates.

1.1.3 General Strategies

1.1.3.1 Indirect Modification

The general strategy for surface modification of polymers by carbene insertions involve a two-step process (**Figure 10**). Firstly, a polymer is pre-activated with an electron-rich diaryldiazo compound which is a carbene precursor substituted with strong or moderate electron donating groups, for example, alkoxy or N-alkyl amino groups. The presence of these electron-rich aromatic rings is essential for the last activation stage. Upon pre-activation, a change in colour of the material indicates successful irreversible covalent bond formation which cannot be detached by an extensive washing procedure involving sequential washes with water, acetone, methanol, alkali or acidic solution.

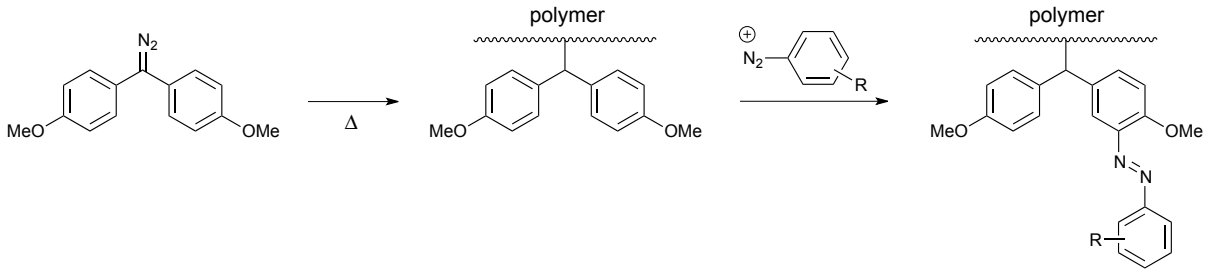

Figure 10 Indirect modification

Subsequently, the pre-modified substrate, which is activated to further electrophilic aromatic substitution for the desired surface functionality, can be treated with various diazonium salts in aqueous solution to allow azo coupling and produce highly intense colouration. The diazonium salts can be made from commercially available amines or independently synthesised amines with preferred functional groups, and the formation of diazonium groups is confirmed by H-acid test which gives an intense purple colour as a result of extended conjugation system (**Figure 11**).[9] It is worth noting that the production of diazonium salts is limited by both the

choice of substituents that must survive the diazonium formation condition, and the stability of desired aliphatic or aromatic diazonium compounds.[11,14,16]

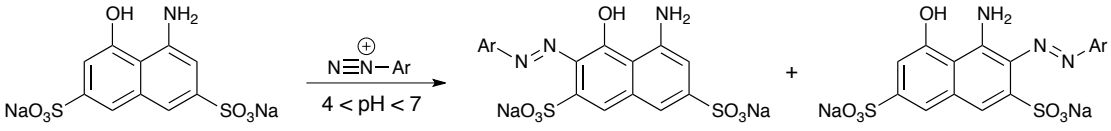

Figure 11 H-acid test

The advantage of this approach is that several detection and analysis techniques can be use to identify functional groups existing on the azo linkage, and vigorous dyeing of the polymer from both pre-activation and azo coupling stages can be a diagnostic step as it provides a UV/visible chromophore to immediately indicate a change in structure of polymer surfaces. The colours or absorption characteristics of modified materials are contributed by the structure of diazo compounds and diazonium salts corresponding to the structure of activated polymers, and the intensity of colouration implies degrees of loading of these reagents on the surface of materials.

An alternative structure of required diaryldiazo compounds is a benzophenone diazo molecule tethered with an electron-rich aromatic residue or arylamino side chain (**Figure 12**). The corresponding carbonyl compound is accessible by the reaction between 4-bromomethylbenzophenone and 2-(N-ethylanilino)ethanol, both are commercially available.[9,11,14,15]

This diaryldiazo molecule has one advantage over the other in that when 4,4'-(diazomethylene)bis(methoxybenzene) is used as a carbene precursor in **Figure 10**, although it is highly reactive due to conjugation from the strong electron donating groups and this is a crucial requirement for the next diazo coupling process as the methoxy-activated phenyl rings are important to ensure rapid coupling with the

relatively unstable diazonium salt, but the two methoxy groups also destabilise the diazo compound, aiding the decomposition by loss of nitrogen.[17,18] It was illustrated in **Figure 12** that the need for an electron-rich aromatic ring for diazo coupling is fulfilled by the presence of arylamine unit, as a result, electron donating groups are not necessary on the diaryldiazo part. However, any functional group on the arylamine unit must be resistant to reaction conditions used for diazo formation i.e. nucleophilic attack by the alpha-nucleophile H_2NNH_2 followed by oxidation, or reaction with another strong nucleophile, H_2NNHTs followed by elimination.

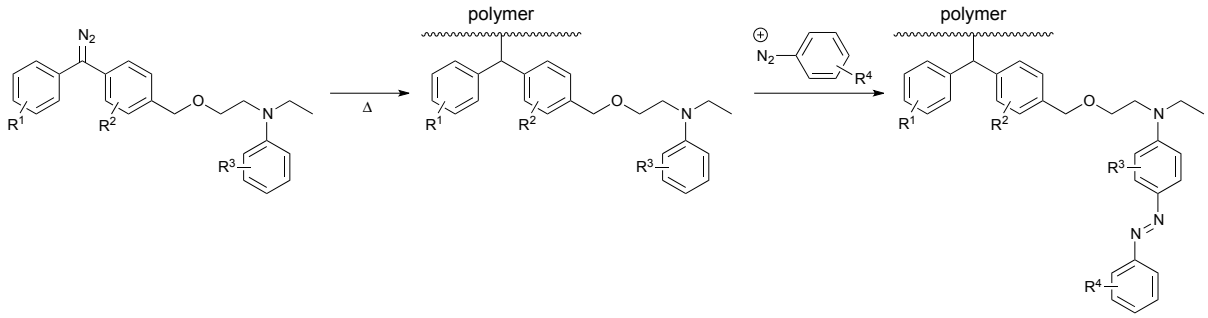

Figure 12 Indirect modification

1.1.3.2 Direct Modification

Another general strategy for the functionalisation of polymer surfaces via carbene insertions is to incorporate desired functional groups into the structure of diaryldiazo compounds prior to surface modification of polymers (**Figure 13**). This method requires the synthesis of diaryldiazo compounds with improved stability since they are used as a central core for coupling with other fragments and must be resistant to certain reaction conditions.[8,19]

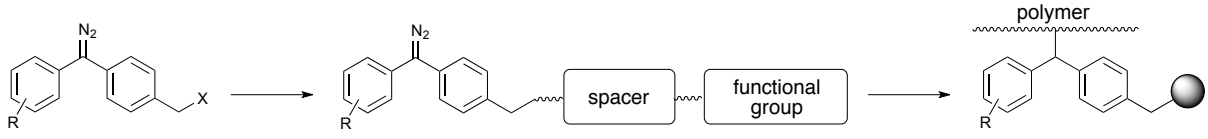

Figure 13 Direct modification

The choice of substituents on the aromatic rings depends on the balance between reactivity and stability of the diazo compound: the greater the electron density of the diazo unit, the more reactive towards surface modification of polymers, and the less stable the diazo group, and vice versa.[14,17,18,20] The terminal X group of diazo compounds can be either a leaving group or a nucleophile for conjugation with other molecules. The advantage of this method is that the desired functional groups do not need to be insensitive towards reaction conditions for the conversion of a carbonyl compound to the corresponding diazo compound as the diazo functional group is formed prior to the coupling step.

1.1.3.3 Choice of Polymers

Amberlite XAD4 polystyrene beads, purchased from Sigma-Aldrich Chemicals Ltd, are white translucent non-polar resins. They are generally used for adsorption of hydrophobic organic compounds with molecular weight up to 20000, and have large surface areas (725 m^2/g) as compared to other available polyaromatic resins, namely XAD-2, XAD-7, XAD-200, XAD-1180, and XAD-2010.[21]

This type of polymers was chosen as an example of non-polar hydrocarbon polymers in order to demonstrate the ability of diaryldiazo compounds to functionalise polymers with relatively inert surfaces (i.e. containing only phenyl groups and saturated hydrocarbon side chains) as compared to other polar materials. The large surface areas would be expected to facilitate the diazo modification process by increasing the degrees of adsorption prior to generation of carbenes. In addition, it is easy to handle these beads and they are stable for years at room temperature and their cross-linked structure (**Figure 14**) is resistant to acids, bases, and does not dissolve in organic solvents. It was decided that Amberlite XAD4 polystyrene beads would be used for work regarding surface modification described in this thesis.

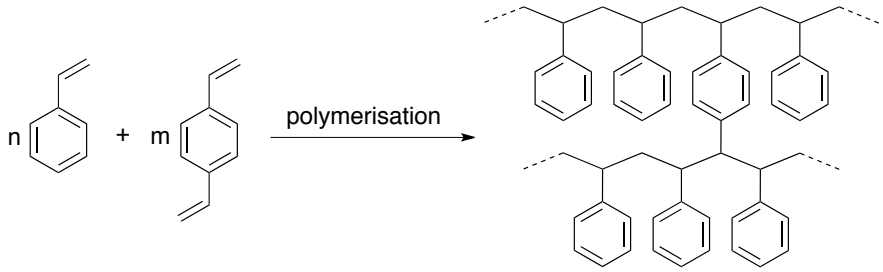

Figure 14 Cross-linked polystyrenes from styrene and divinylbenzene monomers

1.1.4 Structure and Reactivity of Carbenes

Carbenes, generally written as :CR_2, are neutral highly reactive intermediates containing a carbon atom with six valence electrons, usually in sp^2 hybridisation. Four electrons are located in two bonded sp^2 orbitals, while the other two electrons are non-bonding. Carbenes can be divided into two types depending on its electronic structure or the spin states of the two non-bonding electrons. When all of the electrons occupy the sp^2 orbitals and leave the p orbital empty, these electrons are paired and the electron arrangement is termed singlet (spin multiplicity = 1). However, the triplet state (spin multiplicity = 3) refers to the electronic distribution when there are two unpaired electrons with parallel spins, one electron in each of two molecular orbitals. These two spin states are frequently found to exist in equilibrium with each other by intersystem crossing.

singlet carbene triplet carbene

Figure 15 Structures of carbenes

Frequently, the triplet carbene is the ground state and it requires about 40 kJ/ mol to pair up the two electrons to convert to the singlet carbene. However, when

electron-rich substituents are present such as dichlorocarbene :CCl_2, overlap of lone-pair electrons from the substituents and the p orbital of carbenes produces a low-energy orbital which the two non-bonding electrons occupy, resulting in the singlet carbene ground state.[22] Nonetheless, carbenes can be formed in either ground or excited state depending on reaction conditions.

As carbenes have a carbon atom with only six electrons in its outer shell, both singlet and triplet carbenes are electron deficient and generally highly electrophilic. Carbenes that have electron-donating groups are therefore less electrophilic, and in some cases, can be nucleophilic such as diamino carbenes :$C(NR_2)_2$.[23] In addition, triplet carbenes, which have two unpaired electrons, exhibit the properties of diradicals and can be detected by EPR spectroscopy. Work described in this thesis is related to reactions of diarylcarbenes, generated from either thermolysis or photolysis of diaryldiazo compounds as previously mentioned, with polystyrenes and polyethylene terephthalates.

The mechanism of carbene reactions, as predicted by the Skell-Woodworth rules,[24] depends on the relative rates of cyclopropanation or other reactions and intersystem crossing, in other words, whether the reacting carbene is a singlet or a triplet. Singlet carbenes react in a concerted pathway, and hence, reactions are stereospecific as the geometry of substrates are preserved in products. When a singlet carbene reacts with an alkene, the cyclopropane adduct is formed via *syn* addition. Similarly, C-H insertion reactions by singlet carbenes occur in a concerted manner with retention of stereochemistry at a stereogenic centre.

In contrast, the structure of triplet carbenes is a diradical with unpaired spins. When a triplet carbene forms a C-C bond with an alkene in a radical reaction, the diradical intermediate has to flip one of the spins by intersystem crossing in order to form the other C-C bond. The rate of this spin-inversion process is comparable to

that of molecular rotations, thus, free rotations about single bonds result in loss of stereochemistry of the starting material and a mixture of diastereoisomers is produced. The need for spin inversion also applies when a triplet carbene inserts to a C-H bond via a stepwise hydrogen abstraction followed by recombination mechanism, leading to non-stereospecific insertion.

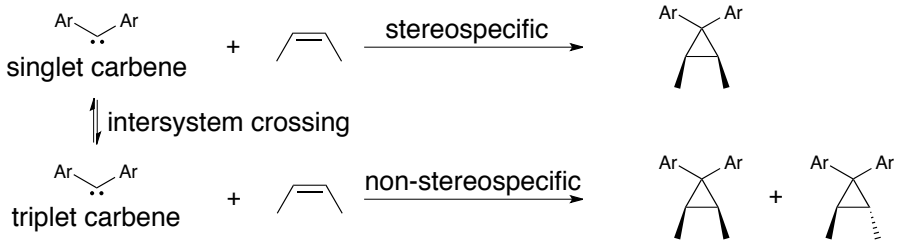

Figure 16 Cycloaddition of carbenes to alkenes

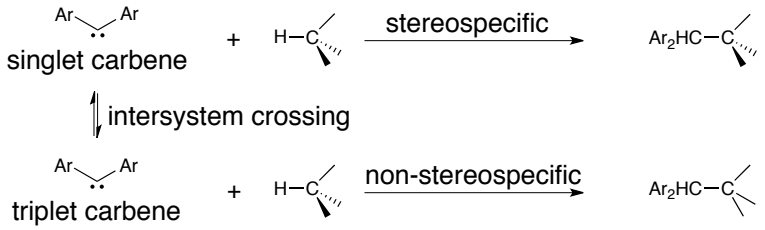

Figure 17 Insertion of carbenes into C-H bonds

Nonetheless, at room temperature most carbenes react via the singlet state even though the ground state is the triplet state. This is because reactions of singlet carbenes are usually much faster than those of triplet carbenes.[25,26]

1.1.5 Carbenes in Solidified Matrix

As previously described, the general method for surface modification is to apply a solution of diaryldiazo compounds to polymers and evaporate the solvents in order to deposit the substances as a thin film, and subsequently the corresponding carbenes generated from either thermolysis or photolysis will react with the polymers

in solid-state (i.e. in the absence of solvent) conditions. Studies have shown that the reactivity of carbenes in a solidified matrix at low temperature is different from that in solution phase at ambient temperature[27] and crucially at 77 K there is a change in reaction mechanism. Reactions of both singlet and triplet carbenes via classical mechanisms are exceedingly slow in solidified organic molecules where the motion of carbene intermediates are partially inhibited. As the classical reaction rates substantially decrease and become slower than the quantum mechanical rate as a result of rigid matrix environment, hydrogen atom tunnelling from the matrix to carbenes dominates the carbene decay, corresponding to hydrogen abstraction of triplet carbenes. The radical intermediates which are generated in close proximity then recombine to form the C-H insertion product without racemisation due to restricted motion and rotation of the radicals in the solid matrix. Thus, under these conditions, reaction via the triplet intermediate dominates, in contrast to the situation in solution described above.

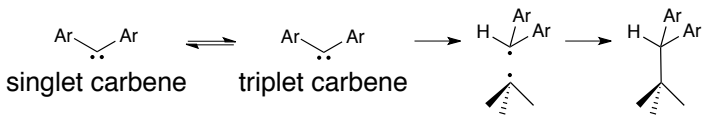

Figure 18 Reaction of carbenes in solid matrix

This solid state reactivity applies for a variety of substrates such as alkenes, alcohols, amines, alkyl halides, ethers, and ketones so that the ratio of C-H insertion products via hydrogen atom tunnelling increases, and interactions between singlet carbenes and double bonds or heteroatoms becomes more limited. For example, photolysis of phenyldiazomethane in *cis*-but-2-ene at 0°C produced cyclopropane **I1** via addition of a singlet carbene to the alkene with excellent yield, along with minor adduct **I2** from cycloaddition, and alkenes **I3**, **I4**, and **I5** via hydrogen abstraction-

recombination of a triplet carbene (**Figure 19**).[27] This product ratio, however, changed considerably in solidified *cis*-but-2-ene where the percentage of **I1** decreased from 93% to 44% while those of **I3** and **I5** increased by over 40% in total.

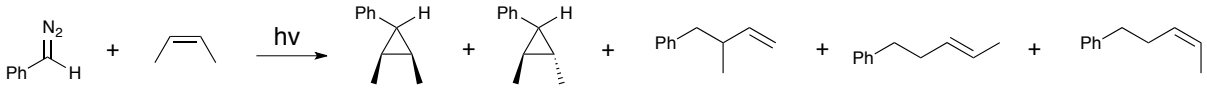

	I1	I2	I3	I4	I5
0 °C	92.7 %	2.1 %	1.4 %	0.4 %	3.5 %
-196 °C	43.9 %	3.2 %	18.5 %	4.9 %	29.0 %

Figure 19 Photolysis of phenyldiazomethane in *cis*-but-2-ene at 0°C and -196°C

With substrates containing heteroatoms such as alcohols, amines, and alkyl halides, there is also a dramatic change in product distributions when experiments were conducted in solidified organic molecules. In solution phase, ethanol, diethylamine, and isopropyl chloride reacted with phenyldiazomethane to predominantly give X-H insertion products (X=O, N, Cl), whereas in solid matrices, the major adducts were obtained from insertion into C-H bonds (**Figure 20**).[27]

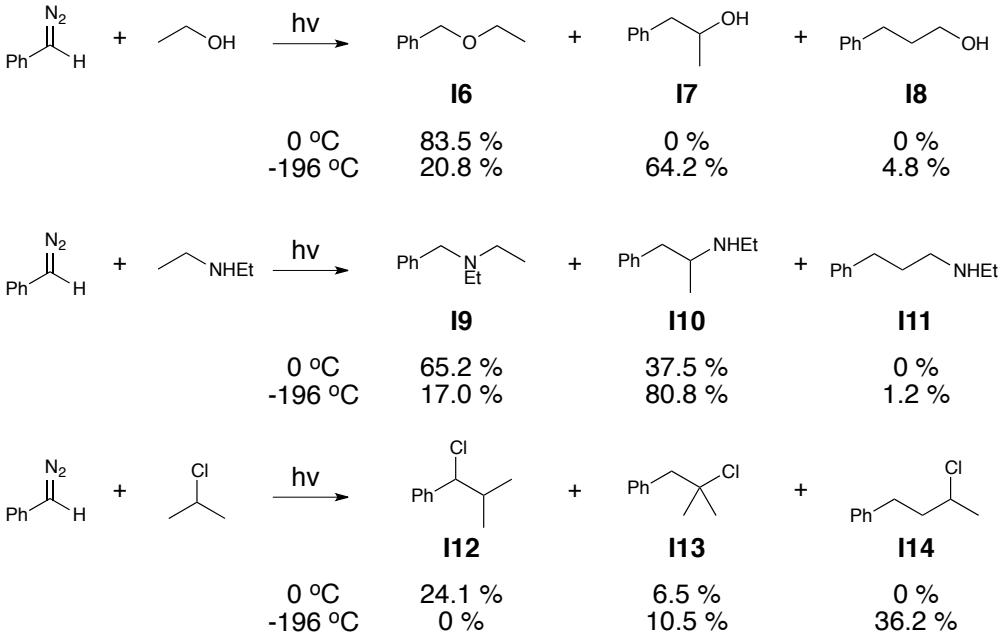

	I6	I7	I8
0 °C	83.5 %	0 %	0 %
-196 °C	20.8 %	64.2 %	4.8 %

	I9	I10	I11
0 °C	65.2 %	37.5 %	0 %
-196 °C	17.0 %	80.8 %	1.2 %

	I12	I13	I14
0 °C	24.1 %	6.5 %	0 %
-196 °C	0 %	10.5 %	36.2 %

Figure 20 Photolysis of phenyldiazomethane in various conditions

Photodecomposition of a solution of phenyldiazomethane in acetone at 0°C generated oxirane **I15**, vinyl ether **I16**, and dioxolane **I17** via a carbonyl ylide intermediate. In contrast, at -196°C, benzylacetone, which was not observed in the solution condition, was the main product through C-H bond insertion (**Figure 21**).[27]

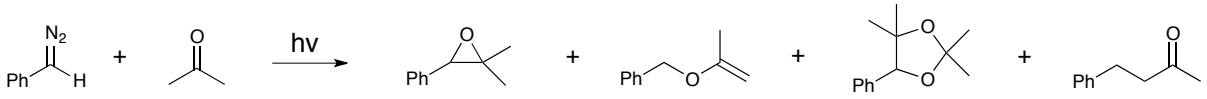

	I15	**I16**	**I17**	**I18**
0 °C	4.6 %	10.8 %	20.9 %	0 %
-196 °C	1.9 %	1.8 %	1.3 %	21.1 %

Figure 21 Photolysis of phenyldiazomethane in acetone at 0°C and -196°C

Phenyldiazomethane photodissociated in liquid diethyl ether to produce ethers **I19**, **I20**, and **I21** via an oxonium ylide intermediate. However, in the solid state, both of the products **I19** and **I20**, which were derived from the singlet carbene intermediate, were not present and only the C-H insertion products **I21** and **I22** were observed (**Figure 22**).[27]

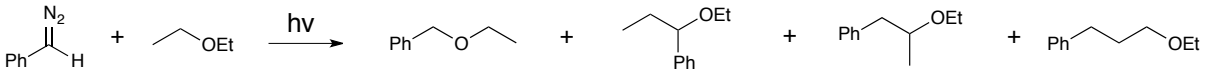

	I19	**I20**	**I21**	**I22**
0 °C	13.7 %	18.1 %	68.2 %	0 %
-196 °C	< 1 %	0 %	88.3 %	10.4 %

Figure 22 Photolysis of phenyldiazomethane in diethyl ether at 0°C and -196°C

Thus, the solution and solid state behaviour is very different, and crucially the less selective behaviour observed in the solid state is just what is required for a general methodology which would be applicable to a wide variety of polymer types.

For the surface modification of polymers using carbenes generated from diaryldiazo compounds, it can be expected that polymeric chains will produce a mixture of C-H insertion products through the quantum mechanical mechanism,

along with other adducts via classical mechanistic pathways, but the overall outcome, that of irreversible covalent bond formation leading to the introduction of new surface functionality, is what is of utmost importance.

1.2 Thesis Outline

The work described in this thesis relates to the synthesis of diazo compounds, their behaviour and the properties of polymers modified by them. Their application for the coordination of metal ions and metal complexes is discussed in **Chapter 2**, where the synthesis of a library of modified polystyrenes is demonstrated together with its capability in catch and release of metal-containing species.

Chapter 3 discusses photochromophores and particularly spiropyran-derived systems. This class of organic compound was introduced onto the surface of polymers which were then characterised using contact angle and colour change, and then investigated for photochromic properties.

With materials from both projects in hand, expansion of the polymer modification concept is outlined in **Chapter 4**. Polymers with different characteristics were combined with bioactive ions/molecules and used for bioassay experiments to prove the efficacy in drug delivery.

Lastly, **Chapter 5** discusses the synthesis of diazo compounds with a range of stabilising functional groups and determination of the stability of successfully made diazo compounds was conducted via differential scanning calorimetry.

Chapter 2 Metal Coordination

2.1 Introduction

2.1.1 Hypoxia Detection

Hypoxia is a pathological condition that occurs when deficiency of oxygen supply reaches a region of the body, known as tissue hypoxia, or the whole body, causing a disruption of cellular metabolism. It can occur when the vasculature cannot supply oxygen, associated with stroke, or when a tumour outgrows its oxygen demand.[28] When well-oxygenated cells are treated with irradiative therapy, the oxygen increases the lifetime of free radicals that are generated upon radiation. These reactive radicals kill influenced cells by breaking DNA double strands.[29] However, the presence of hypoxia can decrease the sensitivity of tumour cells towards ionising radiation, and also limit the effectiveness of chemotherapy, due to the lack of oxygen.[30] Several techniques have been developed for hypoxia measurements including the use of oxygen micro-electrodes and the comet fine-needle assay. However, these methods are invasive and require many observations for reliability of the results.[31] An alternative approach for detecting the presence and degree of hypoxia involves the use of nitroimidazoles - molecules that mimic the effect of oxygen. Nitroimidazole *in vivo* is reduced by nitroreductase enzymes to generate a radical anion which is oxidised to its original state by molecular oxygen in normal oxygenated cells, while in hypoxic tissues the radical anion is further reduced and irreversibly binds its fragments within the cell.[32]

The most commonly used derivative of nitroimidazole for imaging hypoxia in clinics is radioactive ^{18}F-fluoromisonidazole (**Figure 2**). This compound allows non-invasive identification of regions where oxygen supply is inadequate via the decay of

the fluorine-18 isotope which can be detected and quantified by positron emission tomography (PET).[28,29,33,34] However, the image contrast between normal and hypoxic cells is usually low due to slow blood clearance from non-target tissue.[28,30] In addition, with short half-life of 109.8 minutes, the radioactive molecule cannot be generated from a laboratory remote from the site-of-use as the quality will diminish by transportation, and the compound needs to be produced using complex synthesis facilities and handled by skilled specialists.

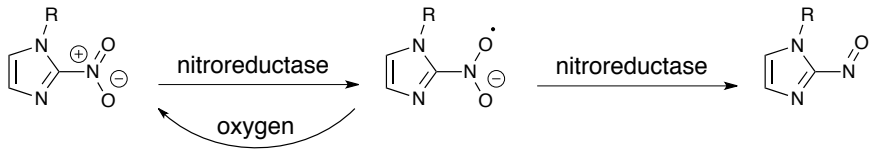

Figure 1 Reactions of nitroimidazoles

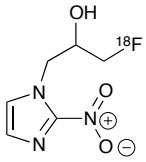

Figure 2 Structure of ^{18}F-fluoromisonidazole

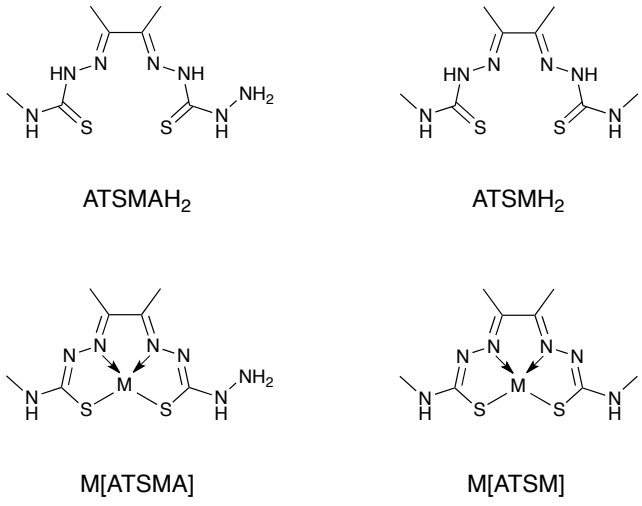

Figure 3 Examples of bis(thiosemicarbazones) and metal complexes

Copper-64, in contrast, with a much longer half-life of 12.7 hours, low positron emission energies, and therapeutic potential, is an alternative PET hypoxia marker in some tumour types.[35] The copper complex of bis(thiosemicarbazones) has been widely used in diagnostic and therapeutic radiopharmaceuticals as a highly effective imaging agent to locate hypoxic tissues.[28,36] It is a stable mononuclear square-planar complex which is permeable to membranes. Furthermore, it has good tumour uptakes and permits rapid radiolabeling at room temperature. Thiosemicarbazone ligands can form a chelate with transition metal ions through its sulphur atoms and deprotonated azomethinic nitrogen atoms. The neutral form of copper complexes can be easily transported into cells and reduced to an unstable Cu(I) form. In oxic cells, the Cu(I) complex can be re-oxidised to the Cu(II) species and diffuses out of cells. In tissues with low concentration of oxygen, the Cu(I) complex decomposes and reversibly binds within hypoxic cells.[37] The reduction potential and therefore selectivity for hypoxia of copper complexes also depend on substituents on the diketone backbone and the terminal nitrogen atoms of the ligand.[30]

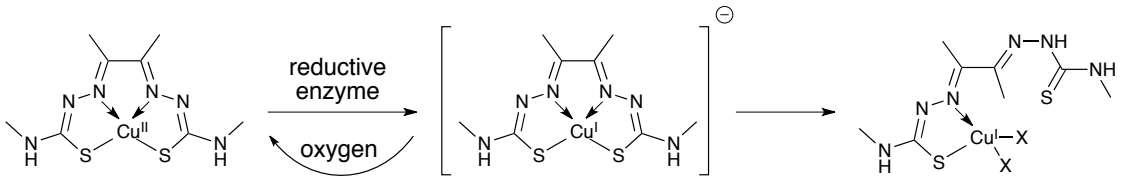

Figure 4 Reactions of Cu[ATSM] complexes

2.1.2 Transmetallation

One way to generate a Cu(II) complex is by transmetallation of the corresponding Zn(II) complex with a solution of Cu(II) ion. However, for clinical use the existence of unreacted Zn(II) complex can be regarded as a contaminant in the radiolabelled solution of Cu(II) complex. Nonetheless, studies on solid-phase preparation and purification of metallo-radiopharmaceuticals have been reported,

based on selective axial coordination of Zn(II) complexes to pyridine/DMAP-modified polystyrene resins.[38] The nitrogen atom of a pyridine moiety, having a lone pair electrons, can potentially bind with a pseudo-square-planar Zn[ATSM] complex as a fifth donor atom in an axial coordination site. Upon metal exchange with a Cu^{2+} ion, the interaction between the donor nitrogen atom from the heteroaromatic ring and the acceptor copper atom of the formed complex is weakened as a result of Jahn-Teller distortion that elongates the axial coordination bond. Therefore, the Cu[ATSM] complex is released from the solid phase substrate while the Zn^{2+} ion is still bound with the polymer by similar donor-acceptor interaction (**Figure 5**).

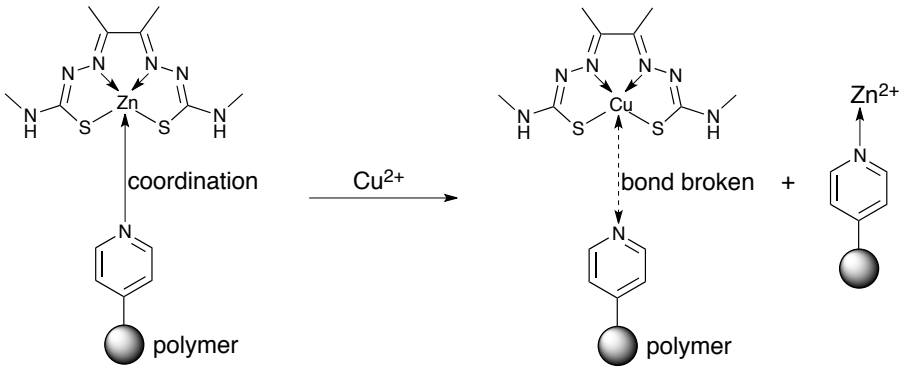

Figure 5 Solid-phase generation of Cu[ATSM]

For clinical application, it could be envisaged that a column could be preloaded with sterile resins bearing immobilised donor pyridyl groups that are tethered with Zn[ATSM] complexes by coordination bonds. Injection of a solution of 'hot' copper and gravity elution would enable transmetallation, and hence, generation of radioactive Cu[ATSM] complexes which would be collected from the bottom of the column ready for use. It might be expected that binding of the Zn^{2+} to the polymer would minimise the concentration of Zn^{2+} in solution as described above, leading to an enriched solution containing Cu^{2+}.

2.1.3 Aims of the project

Of interest to us was to establish a general method to incorporate pyridine/ DMAP systems onto the surface of polymers via direct and indirect modification. A library of modified materials capable of binding with metal complexes, performing transmetallation, and releasing desired species for diagnostic and therapeutic purposes would be constructed and characterised by elemental analysis, ATR-IR, and XPS. The efficiency of these processes would be investigated and assessed by inductively coupled plasma optical emission (ICP-OES), UV/visible spectrophotometry, EPR spectroscopy, and HPLC/MS analysis.

2.2 Results and Discussion

2.2.1 Indirect Modification

The required pre-activated polymer **PSM4** was prepared by using the published strategy (**Scheme 1**).[15] Starting from commercially available 4-methylbenzophenone, the ketone was brominated by NBS in the presence of light to give bromide **M1** with moderate yield, confirmed by ^{1}H NMR spectroscopic data. Conversion to ether **M2** was carried out by the reaction with 2-(N-ethylanilino)ethanol and NaH. The ^{1}H NMR spectrum showed additional aromatic peaks corresponding to the aniline group, and the MS spectra displayed peaks at 382($[M+Na]^+$) and 360 ($[M+H]^+$).

Addition of hydrazine monohydrate to the carbonyl **M2** gave the hydrazone intermediate **M3** with excellent yield. The observed MS spectra exhibited the base peak at 374($[M+H]^+$) and a peak at 396($[M+Na]^+$), and the aromatic region of the ^{1}H NMR spectrum became even more complicated upon formation of C=N bonds as a result of the existence of both *syn*- and *anti*- isomers. Oxidation of the condensed

product **M3** was done by MnO_2 in anhydrous basic solution of MeOH in the dark, producing benzophenone diazo compound **M4**. The presence of the diazo group was confirmed by IR spectroscopy, showing an absorption peak at 2038 cm^{-1} corresponding to N≡N stretching mode.

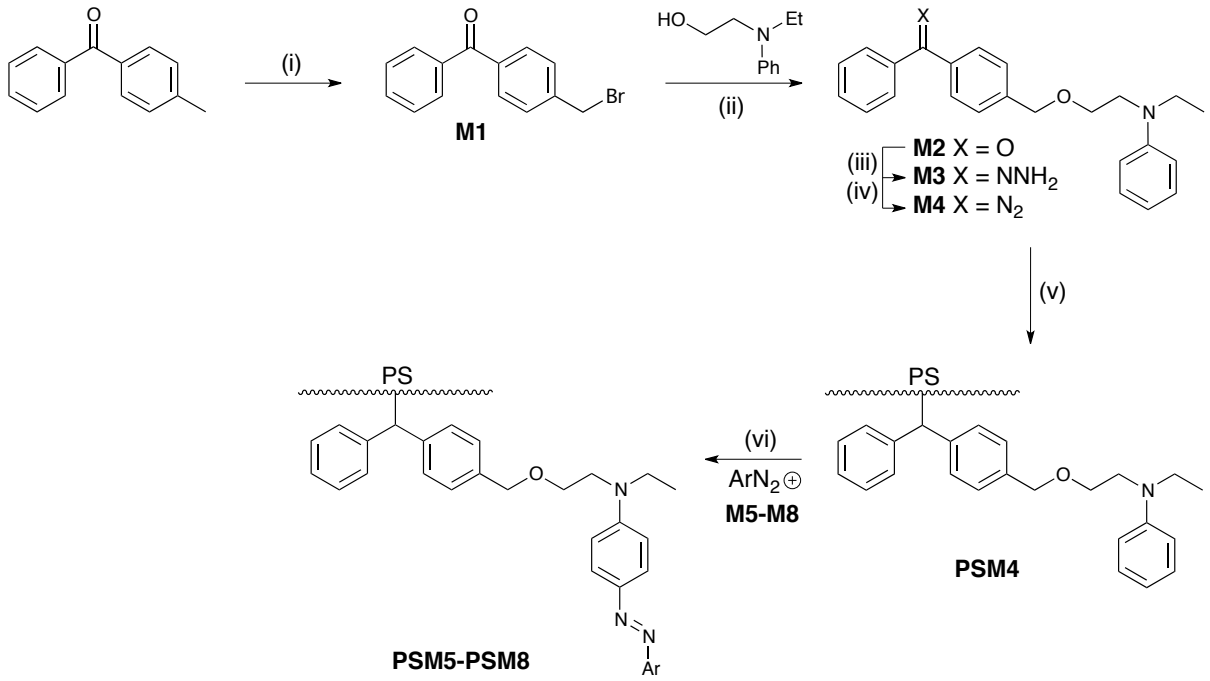

Scheme 1 Reactions and conditions
(i) NBS, $CHCl_3$, hv, heat under reflux, 54%; (ii) $PhN(Et)CH_2CH_2OH$, NaH, THF, room temperature, 67%; (iii) $H_2NNH_2.H_2O$, EtOH, heat under reflux, 90%;
(iv) MnO_2, KOH, MeOH, room temperature (dark), 91%; (v) 120°C; (vi) soak in THF/H_2O.

Colourless polystyrene beads were soaked with an ether solution of diazo compound **M4** and the solvent was slowly evaporated *in vacuo* in order to obtain polystyrene beads in which the diazo molecule was physisorbed on the surface. Thermal treatment of the beads by heating at 120°C led to decomposition of the diazo compound, *in situ* carbene formation, and consequently material insertion to generate very pale yellow pre-activated polystyrene beads **PSM4**.

Diazonium coupling of modified polymer **PSM4** with diazonium salts **M5-M8** (**Figure 6**) gave the derivatives **PSM5-PSM8**, accompanied by colouration of the materials. This colouration was a result of azo link formation, which visually indicated

successful post-modification of polymer **PSM4**. The colours of modified **PSM5-PSM8** were determined by the structure and substituents of diazonium salts **M5-M8**, and the intensities of colouration were associated with degrees of loading.

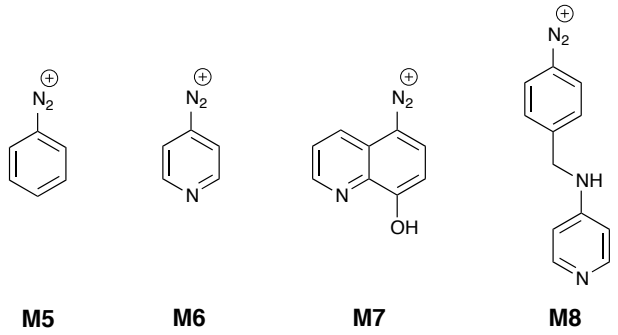

M5 **M6** **M7** **M8**

Figure 6 Structures of diazonium salts

Diazonium salts **M5-M7** were prepared from the corresponding commercially available amines, by reacting the amines with sodium nitrite in aqueous hydrochloric acid (**Scheme 2**). The formation of diazonium salts was confirmed by H-acid test, and the products were immediately used without further purification to avoid degradation. Diazonium ion **M6** contains a pyridine ring, which is the preferred functional group that would be used to coordinate with metal ions/complexes, while the cation **M5** consists of only a phenyl ring and would be experimented as a control. The structure of diazonium salt **M7** was chosen because the compound also has a hydroxyl group in addition to the pyridine moiety and both functions are in close proximity i.e. on the same side of the naphthalene backbone. It was anticipated that this would affect the ability to bind with metal ions/complexes.

The production of diazonium salts **M5-M7** was rapidly accessible as it required only one step; however, these molecules do not have the preferred structure in which the pyridine or DMAP unit is isolated from conjugation system and does not have resonance contribution from the azo link as in the case of compound **M5-M7**.

Therefore, the structure of diazonium salt **M8** was selected so that the diazonium phenyl group is separated from the aminopyridine ring by a saturated carbon atom.

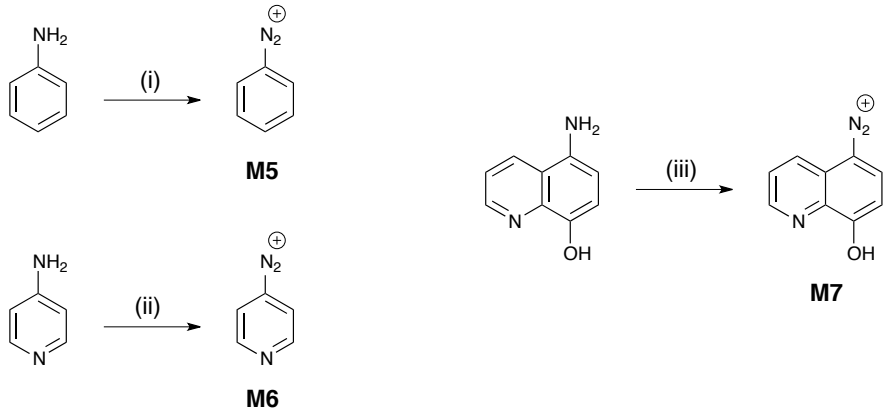

Scheme 2 Reactions and conditions
(i)-(iii) $NaNO_2$, HCl, THF/water, 0°C.

It was envisaged that compound **M8** would be synthesised from a four-step process (**Scheme 3**). Firstly, condensation of 4-nitrobenzaldehyde and 4-aminopyridine generated the imine **M9** with excellent yield. The formation of the product was confirmed by the ^{1}H NMR spectroscopic data, with the IR spectrum showing an absorption peak at 1638 cm^{-1} corresponding to C=N stretching mode, and the MS spectra displaying a peak at 228($[M+H]^+$). The imine group was then reduced by $NaBH_4$ in anhydrous MeOH to give the amine **M10**, with low yield, confirmed by the ^{1}H NMR data and a peak at 230($[M+H]^+$) in the MS spectra. Reduction of the nitro group of compound **M10** by $SnCl_2$ and reflux generated the intermediate **M11** as an orange solid with poor solubility due to high polarity of the molecule. The terminal amino group of intermediate **M11** was then converted to a diazonium group by reaction with sodium nitrite in aqueous hydrochloric acid to produce the diazonium salt **M8**, confirmed by H-acid test and immediately used without further purification.

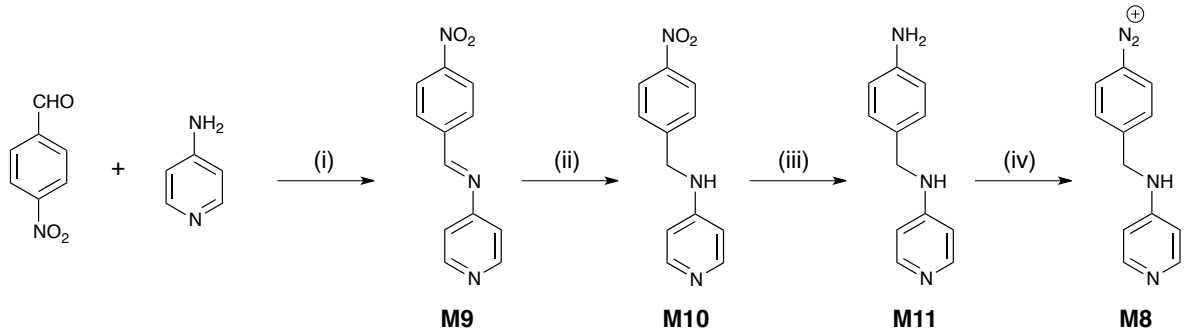

Scheme 3 Reactions and conditions
(i) PPTS, toluene, heat under reflux, 90%; (ii) $NaBH_4$, MeOH, room temperature, 29%, (iii) $SnCl_2.2H_2O$, MeOH, heat under reflux; (iv) $NaNO_2$, HCl, THF/water, 0°C.

Attempts to synthesise other preferred diazonium salts were also made as illustrated in **Scheme 4**. It was envisaged that diazonium salt **M15** would be made starting from commercially available 4-aminophenol. The amino group of the alcohol was initially protected with a *tert*-butyl carbamate (Boc) group by treatment with Boc_2O in water to obtain the amide **M12** with excellent yield, confirmed by the ^1H NMR data, with the IR spectrum exhibiting an absorption peak around 1700 cm^{-1} corresponding to C=O stretching mode of the carbamate group, and the MS spectra showing the base peak at 208($[M-H]^-$). The phenol group of the Boc-protected **M12** was then reacted with bromoacetyl bromide in the presence of Et_3N to produce the bromide ester **M13** in excellent yield. The structure of this compound was confirmed by the base peak at 352($[M+Na]^+$) in the MS spectra, an absorption peak at 1758 cm^{-1} in the IR spectrum as a result of C=O stretching mode of the generated ester group, and the ^1H NMR data. Coupling of bromide **M13** with 4-(methylamino)pyridine in the presence of proton sponge (**Figure 7**), which acted as a strong non-nucleophilic base, was conducted at low temperature, giving a black precipitate which was unidentifiable by ^1H NMR spectroscopy. This might have been due to attack by the pyridyl nitrogen rather than the side chain amine. In any event, this approach was clearly unproductive.

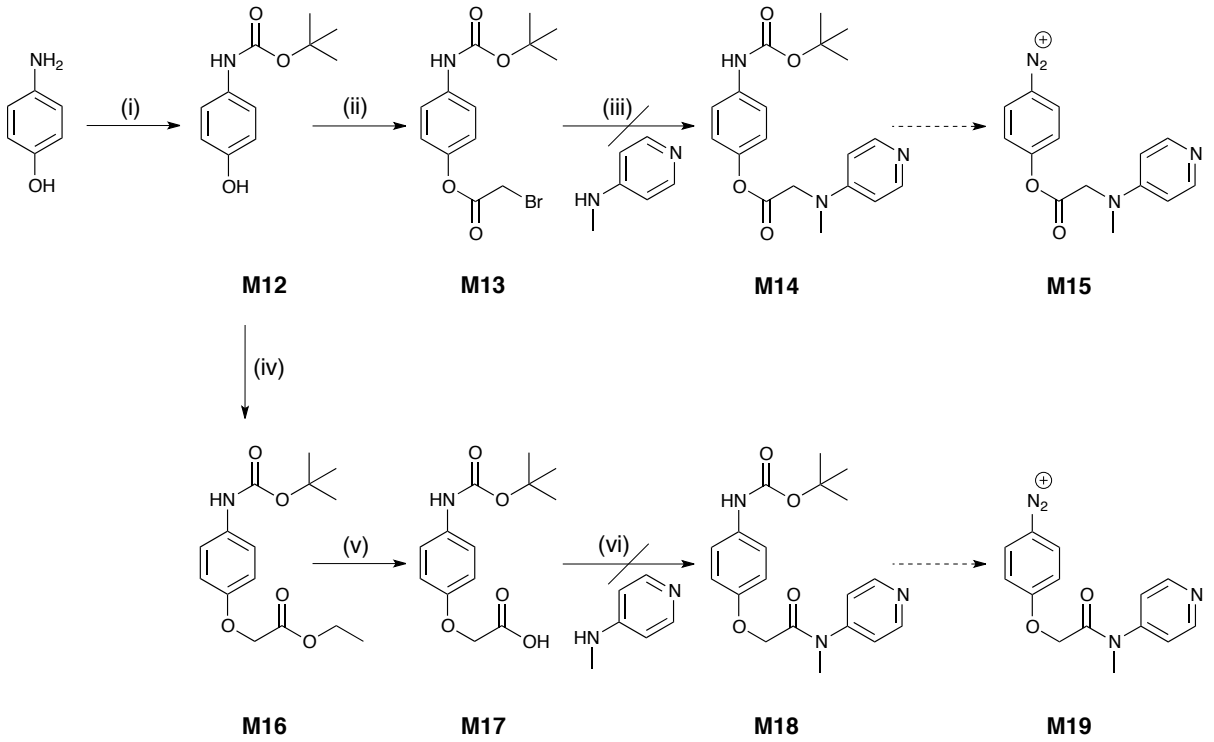

Scheme 4 Reactions and conditions
(i) $(Boc)_2O$, water, room temperature, 96%; (ii) bromoacetyl bromide, Et_3N, DCM, 0°C, 100%; (iii) proton sponge, $CHCl_3$, 0°C; (iv) ethyl bromoacetate, K_2CO_3, KI, acetone, room temperature, 76%; (v) KOH, MeOH, room temperature; (vi) DCC, DMAP, DCM, room temperature.

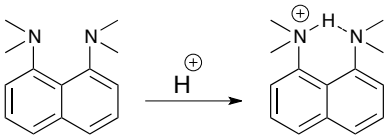

Figure 7 Protonation of 1,8-bis(dimethylamino)naphthalene (proton sponge)

It was suggested that the key step involving conjugation with 4-(methylamino)pyridine could be alternatively carried out via coupling with a carboxylic acid activated with a carbodiimide, in order to generate the diazonium **M19**. The N-protected alcohol **M12** was consequently treated with ethyl bromoacetate, K_2CO_3, and KI to give the ether ester **M16**, confirmed by the ^1H NMR data, the IR spectrum exhibiting an absorption peak around 1600 cm^{-1} corresponding to C=O stretching mode of the ester group, and the MS spectra showing the base peak at 318($[M+Na]^+$). Hydrolysis of the ester **M16** was done in basic conditions to

produce the carboxylic acid **M17**. The structure of this acid was confirmed by the ^{1}H NMR data, the base peak at 290($[M+Na]^{+}$) in the MS spectra, and an absorption peak at 1692 cm^{-1} in the IR spectrum corresponding to the C=O stretching mode of the carboxylic group, however, the compound could not sufficiently well purified for ^{13}C NMR analysis. Conjugation of this acid **M17** with 4-(methylamino)pyridine in the presence of DCC and DMAP was attempted, but unfortunately, the product was again not identifiable by ^{1}H NMR spectroscopy. It was decided that alternative derivatisations of polymers tethered with pyridine/DMAP-containing molecules would be demonstrated by direct modification technique.

2.2.2 Direct Modification

It was envisaged that the diazo compound **M22** which contains a pyridine unit would be made from a three-step sequence (**Scheme 5**). The corresponding ketone **M20** was obtained from the reaction between previously made bromide **M1**, pyridin-4-ylmethanol, and NaH with moderate yield. The ^{1}H NMR data confirmed the structure of the product and the MS spectra showed the base peak at 326($[M+Na]^{+}$). The synthetic route then proceeded by the standard methodology for diazo preparation. Addition of hydrazine monohydrate to the carbonyl **M20** gave the hydrazone intermediate **M21**. The observed MS spectra displayed a peak at 340 ($[M-H+Na]^{+}$). Oxidation of the condensed product **M21** was achieved by MnO_2 in anhydrous basic solution of MeOH in the dark, generating benzophenone diazo compound **M22**. The presence of the diazo group was confirmed by the IR spectrum, showing an absorption peak around 2040 cm^{-1} corresponding to N≡N stretching mode. This diazo molecule **M22** was then dissolved in ether and mixed with polystyrene beads, followed by evaporation of the solvent to allow physisorption of

the compound on the surface. Thermal treatment at 120°C yielded surface functionalised polystyrene **PSM22** by carbene formation preceding bond insertion.

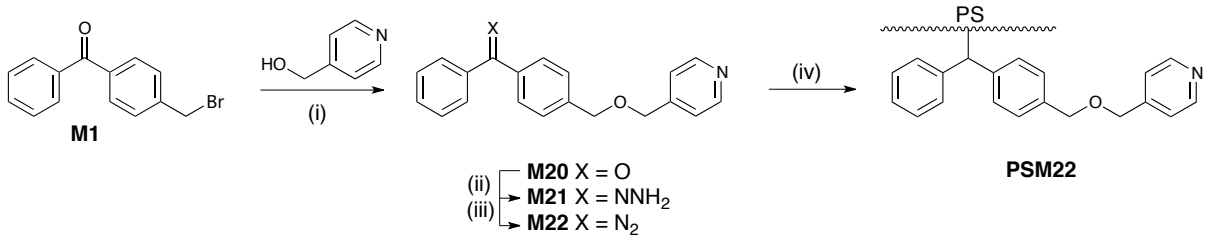

Scheme 5 Reactions and conditions
(i) NaH, THF, room temperature, 55%; (ii) $H_2NNH_2.H_2O$, EtOH, heat under reflux, 100%; (iii) MnO_2, KOH, MeOH, room temperature (dark), 100%; (iv) 120°C.

Another compound containing a DMAP derivative was also synthesised via a similar synthetic scheme that was used to make the amine **M10** (**Scheme 6**). A mixture of 4-hydroxybenzaldehyde, 4-aminopyridine, and PPTS in toluene was heated under reflux to generate the imine **M23**. Its structure was confirmed by ^{1}H NMR data, with the IR spectrum showing a peak at 1651 cm^{-1} for the imine absorbance, and the MS spectra displaying the base peak at 197($[M-H]^-$). Reduction of the imine **M23** by $NaBH_4$ was performed to produce the amine **M24**, confirmed by ^{1}H NMR data and the base peak at 201($[M+H]^+$) in the MS spectra, with overall moderate yield.

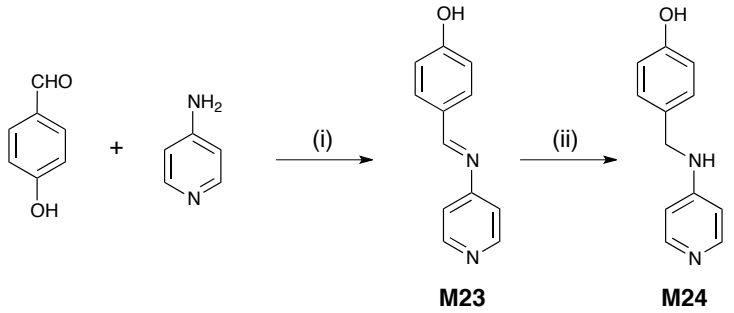

Scheme 6 Reactions and conditions
(i) PPTS, toluene, heat under reflux, 68%; (ii) $NaBH_4$, MeOH, room temperature, 49%.

Similarly, this alcohol **M24** was coupled with previously synthesised bromo molecule **M1**, giving the carbonyl compound **M25** in excellent yield (**Scheme 7**). The ^{1}H NMR data confirmed the structure of the product and the MS spectra exhibited the base peak at 395($[M+H]^+$). Addition of hydrazine monohydrate to the carbonyl **M25** and reflux provided the hydrazone intermediate **M26**. The MS spectra showed the base peak at 409($[M+H]^+$). Oxidation of the intermediate **M26** was done by MnO_2 in anhydrous basic MeOH solution in the absence of light, producing diazo compound **M27**. The presence of the diazo group was confirmed by an absorption peak at 2039 cm^{-1} in the IR spectrum corresponding to N≡N stretching mode. Surface modification of polystyrene beads by diazo compound **M27** was conducted by standard procedure to generate functionalised material **PSM27**.

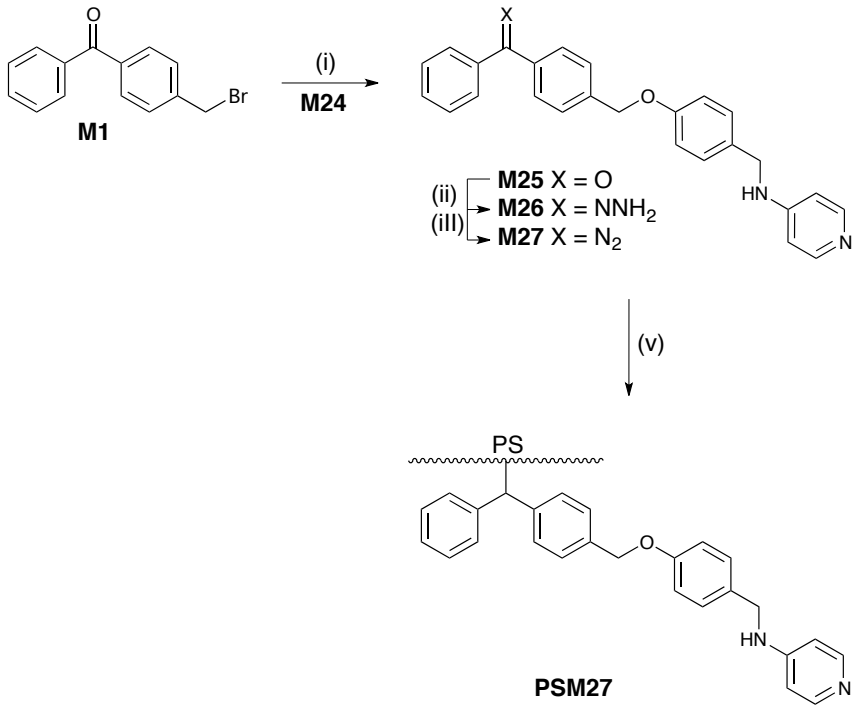

Scheme 7 Reactions and conditions
(i) NaH, THF, room temperature, 100%; (ii) $H_2NNH_2.H_2O$, EtOH, heat under reflux, 88%; (iii) MnO_2, KOH, MeOH, room temperature (dark), 76%; (iv) 120°C;

2.2.3 Visual Observations

All the samples showed colours that can be distinguished from the original white polystyrene beads, although material **PSM4** displayed a very pale yellow colour while polymer **PSM22** was plain white (**Table 1**). The mechanism of surface modification by decomposition of diazo functional groups followed by carbene insertion was demonstrated as the change in colour of the physisorbed polymers upon formation of materials **PSM4**, **PSM22**, and **PSM27** by heat as a result of structural changes, while diazonium coupling was indicated by colouration of pre-activated polymer **PSM4** to generate material **PSM5-PSM8** as azo links were developed.

Polymer	Structure	Appearance
PSM4	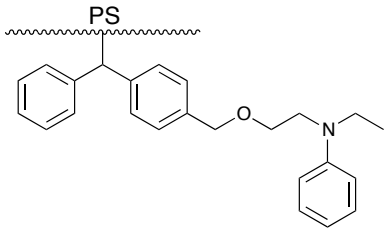	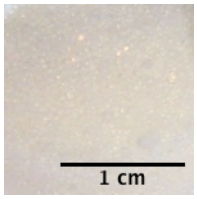
PSM5	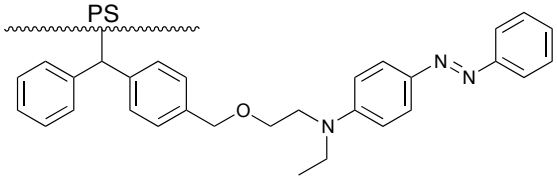	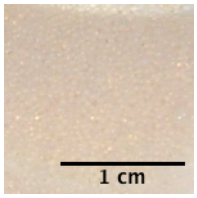
PSM6	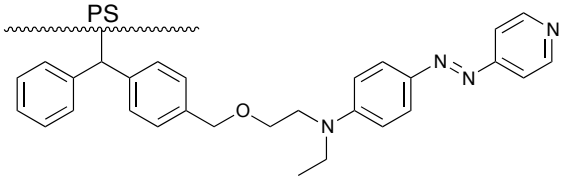	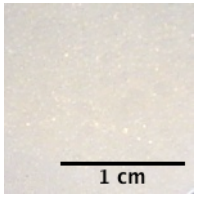
PSM7	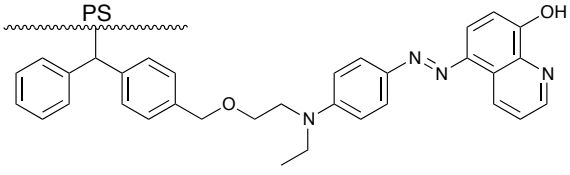	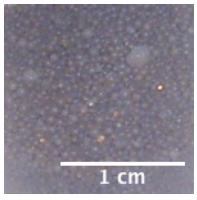

Polymer	Structure	Appearance
PSM8	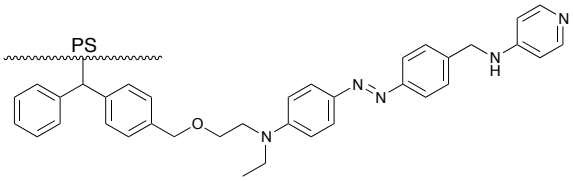	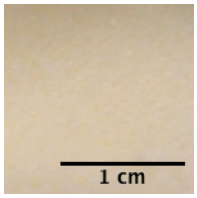
PSM22	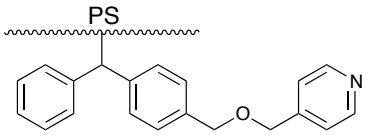	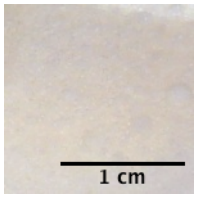
PSM27	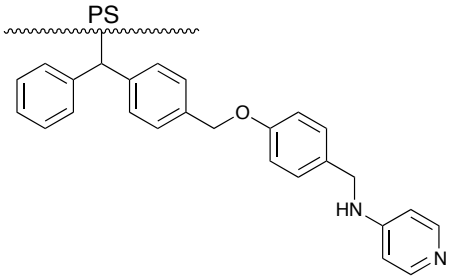	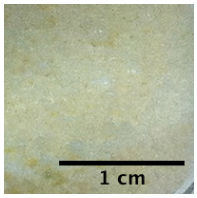

⁎The average diameter of polystyrene beads is 1 mm (manufacturer's data).

Table 1 Visual observation

2.2.4 Characterisation of Modified Polymers

2.2.4.1 Elemental Analysis

All samples were submitted to Elemental Analysis Service of London Metropolitan University[39] and analysed for C,H,N composition. The error of combustion analysis within a batch was estimated by submitting all of blank PS XAD, **PSM27** (Chapter 2), and **PSP19** (Chapter 3) for duplicate analysis and the data is presented in **Table 2**. This data shows good reproducibility, and on this basis a typical value of ±10% is assumed in the following analysis. It should be noted that the error rises to ±20% nearer the detection limit.

Sample	%N (duplicate)	%N (average)	error	% error
PS XAD	0.06, 0.04	0.05	±0.01	20
PSM27	0.11, 0.13	0.12	±0.01	8
PSP19	0.14, 0.19	0.17	±0.02	12

Table 2 Duplicate elemental analysis of blank PS XAD, **PSM27**, and **PSP19**

The results of this analysis and calculated loading data are summarised in **Table 3**. The elemental analysis proved the existence of nitrogen, ranging from 0.22% to 0.49% for functionalised PS materials, which was consistent with the presence of amino group and/or azo link and/or pyridine moiety on the surface, showing a loading level of 0.048-0.25 mmol/g or 4.0×10^{12}-21×10^{12} molecules/cm^2, assuming a surface area of 725 m^2/g (from manufacturer's data) with assumed error estimates of ±5% or ±36 m^2/g. The percentages of area coverage were calculated on an assumption that the side chain of a diphenylmethane unit is folded away from the surface (**Table 4**), and the projected surface area of the inserted carbene is approximately equivalent to the limiting area (A^o) of anthracene (0.46 nm^2/molecule).[40] This represents a minimum value for the system **PSM4-PSM27**, since it does not take account of the steric effect of the side chain. The error estimates from this rough approximation are assumed to be ±10% for each sample. The data from **Table 3** indicated a surface coverage of approximately 2-10%.

Polymer	Elemental Analysis of N (%)	Loading (mmol/g)	Loading (molecules/cm^2)†	Surface Coverage (%)‡	N*
PSM4	C 85.65±0.01, H 7.54±0.01, N 0.22±0.02	0.16±0.02	(13±2) x 10^{12}	6.0±1.5	57±6
PSM5	C 90.71±0.01, H 8.10±0.01, N 0.22±0.02	0.052±0.005	(4.4±0.7) x 10^{12}	2.0±0.5	180±20

Polymer	Elemental Analysis of N (%)	Loading (mmol/g)	Loading (molecules/cm^2)†	Surface Coverage (%)‡	N*
PSM6	C 91.11±0.01, H 7.84±0.01, N 0.27±0.03	0.048±0.005	(4.0±0.6) x 10^{12}	1.8±0.5	190±20
PSM7	C 90.10±0.01, H 8.08±0.01, N 0.49±0.05	0.088±0.009	(7±1) x 10^{12}	3.4±0.9	100±10
PSM8	C 90.12±0.01, H 8.03±0.01, N 0.35±0.04	0.050±0.005	(4.2±0.6) x 10^{12}	1.9±0.5	190±20
PSM22	C 91.10±0.01, H 7.90±0.01, N 0.35±0.04	0.25±0.03	(21±3) x 10^{12}	10±2	35±4
PSM27	C 83.86±0.01, H 6.99±0.01, N 0.24±0.02	0.086±0.009	(7±1) x 10^{12}	3.3±0.8	110±10

Table 3 Elemental analysis and loading data of modified polymers
† Assumes surface area of 725 m^2/g (manufacturer's data);
‡ Assumes limiting area (A^o) for monolayer formation is 0.46 nm^2/molecule;
* N represents the ratio of unmodified styrene monomers to functionalised units.

The theoretical yields for diazo modification of **PSM4**, **PSM22**, and **PSM27** are 0.136, 0.159, and 0.123 mmol/g, respectively, assuming that the carbene insertion process onto the polymer surface is fully efficient. However, the nitrogen incorporation from this diazo modification as determined by combustion analysis indicates efficiencies of 118%, 157%, and 70% for **PSM4**, **PSM22**, and **PSM27** respectively. It was suggested that diazo molecules could be trapped inside polymer beads or reacted with the surface without extrusion of nitrogen gas, leading to the efficiencies of higher than 100% of samples **PSM4** and **PSM22**.

Polymer	Structure	Polymer	Structure
PSM4	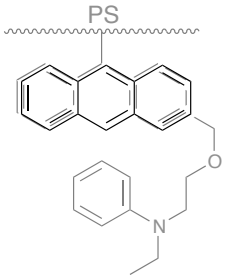	**PSM7**	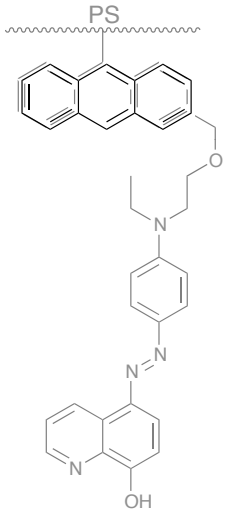
PSM5	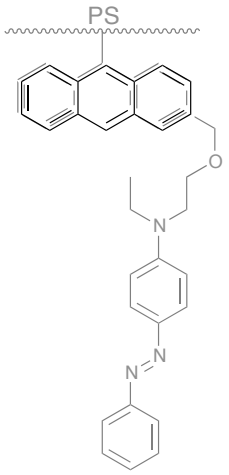		
PSM6	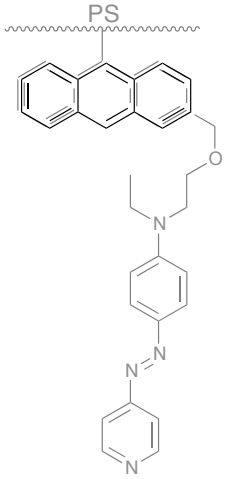	**PSM8**	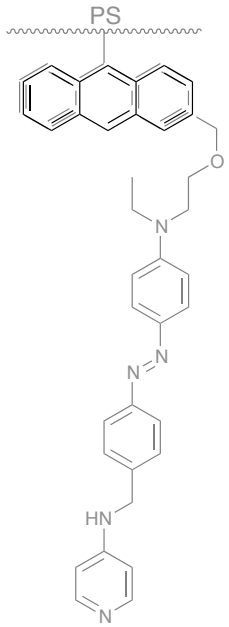

Polymer	Structure	Polymer	Structure
PSM22	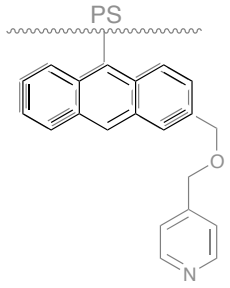	**PSM27**	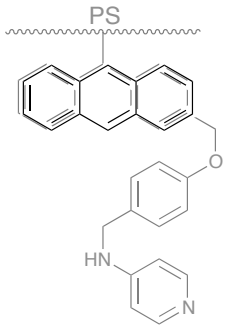

Table 4 Structures for calculations of limiting areas

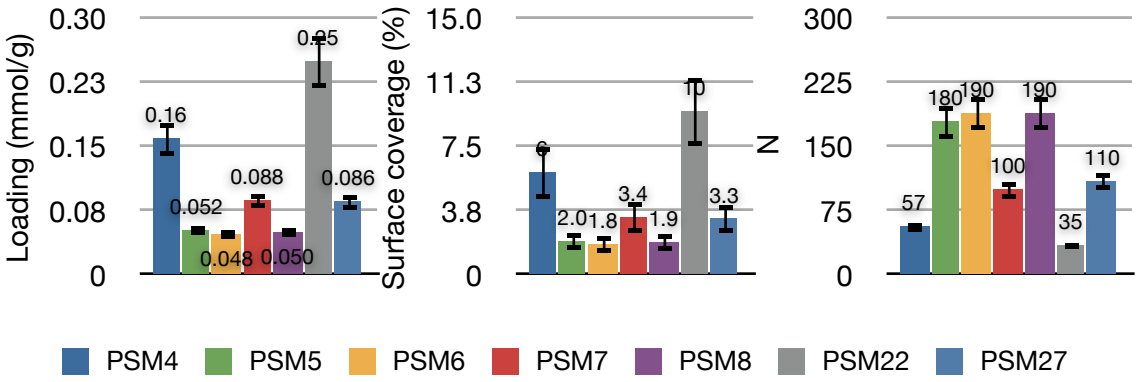

Figure 8 Loading data of modified polymers

The N values represent the ratio of unmodified styrene monomers to functionalised monomer units, ranging from 35 to 190. The relatively low N value of **PSM4** and **PSM22** implied a high degree of surface modification, meaning that for each functionalised monostyrene unit, there were 57 and 35 unmodified monomers, respectively. **PSM7** and **PSM27** showed moderate values of N around 100, and **PSM5**, **PSM6**, and **PSM8** displayed high N values of around 200.

In addition, from this loading data the number of pyridine units on the surface was calculated, ranging from 0.012 to 0.60 mmol/g (**Table 5**). Material **PSM22** revealed the highest number of pyridine groups, while sample **PSM6** had the lowest. The calculation for polymers **PSM4** and **PSM5** was ignored and the values were

assumed to be zero as the structures of both materials do not contain a pyridine moiety.

Polymer	pyr units (mmol/g)	% diazonium coupling
PSM4	0	-
PSM5	0	5±1
PSM6	0.012±0.001	9±2
PSM7	0.060±0.006	47±9
PSM8	0.023±0.002	17±3
PSM22	0.16±0.02	-
PSM27	0.09±0.01	-

Table 5 Loading data of modified polymers

Based on the theoretical yield for diazo modification by compound **M4** which is 0.136 mmol/g, the efficiency in diazonium coupling to produce polymer **PSM5-PSM8** was evaluated. The yield of the process for **PSM7** was exceptionally high at 47%, while the calculated values for the other samples ranged from 5 to 17%. These data reflected the loading levels as obtained from elemental analysis.

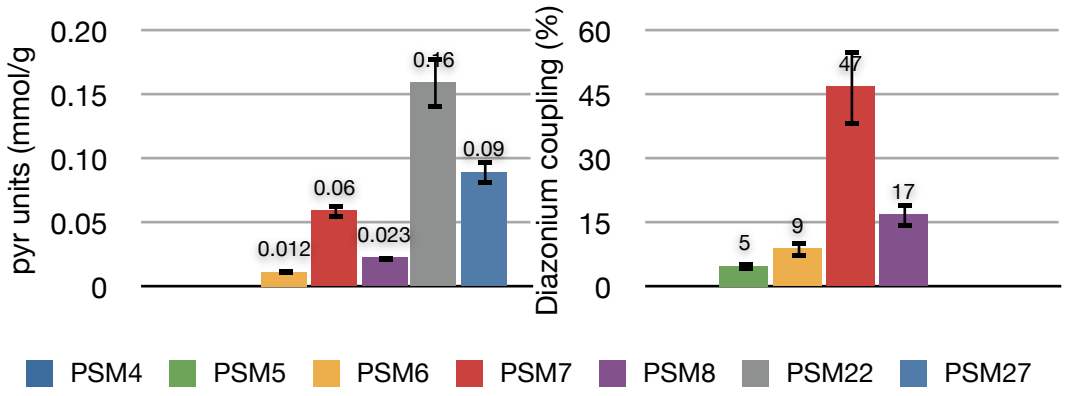

Figure 9 Loading data of modified polymers

2.2.4.2 ATR-IR

Attenuated Total Reflectance (ATR) is a non-destructive technique for material analysis which can be used in conjunction with infrared spectroscopy in order to examine samples in the solid state. In ATR, the beam of the spectrometer is introduced into a suitable prism at an angle exceeding the critical angle for internal reflection to take place and therefore leads to generation of an evanescent wave. This evanescent wave, whose intensity decays exponentially with the distance from the boundary, extends beyond the reflecting surface of the crystal into a sample, which must be mechanically pressed into direct contact with the crystal to achieve optical contact, allowing the sample to absorb IR energy, and the transmitted light is then examined.[41]

Prior to investigation of the polymer samples by ATR-IR spectroscopy, a background IR spectrum was collected in order to record characteristic absorptions of the atmosphere and diamond window, which would then be used to normalise the sample data. The spectrum of blank PS XAD beads was also collected, so that it could be subtracted from the sample spectra, in order to allow identification of peaks that are present only as a result of surface modification (**Figure 10**).

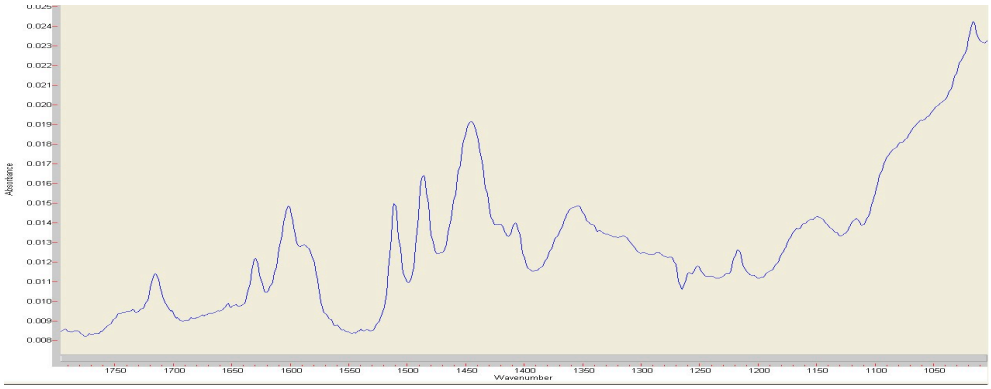

Figure 10 ATR-IR spectrum of unmodified PS XAD

This approach has different limits of detection which varies with the specific technique.[42] ATR-IR can be used for the detection of films on various surfaces with high sensitivity of 0.025 μg/cm^2; however, the samples routinely prepared in the work presented in this thesis have a typical loading level of approximately 10^{13} molecules/cm^2 and assuming a MW of some 400 g/mol for most of the benzophenone-derived systems, the surface loading can be approximated to be 0.0066 μg/cm^2 (**Equation 1**) i.e. about 3.8 times under the lower detection limit (**Equation 2**). As a result, weak signals would be expected in the ATR-IR spectrum. In addition to this, as spectra are obtained by subtraction of the blank spectrum, interpretation of the results needs to be made carefully.

$$\text{Surface loading} = \left(\frac{10^{13}\text{molecules/cm}^2}{6.02\text{x}10^{23}\text{molecules/mol}}\right) \text{x } (400 \text{ g/mol}) \text{ x } (10^6 \text{ µg/g}) = 0.0066 \text{ µg/cm}^2$$

Equation 1

$$\text{Detection ratio} = \frac{0.025 \text{ µg/cm}^2 \text{ (detection limit)}}{0.0066 \text{ µg/cm}^2 \text{ (surface loading)}} = 3.8$$

Equation 2

Full spectral data are available in **Appendix I**. The main region of interest at 1800-1000 cm^{-1} will be discussed in this section. It was noted that the absorption maxima at 1715, 1630, 1602, 1511, 1486, 1445, 1354, 1286, 1150, and 1017 cm^{-1} could be assigned to strong absorbances in the spectrum of unmodified PS XAD beads.[43] Unfortunately, good quality IR spectra which would have confirmed surface modification by the presence of a C-O-C signal at 1090 cm^{-1} and a C-N signal at 1350 cm^{-1} could not be obtained for sample **PSM8**. However, absorbances of samples **PSM4**, **PSM5**, **PSM6**, **PSM7**, **PSM22**, and **PSM27** were observed in the ATR-IR spectra and these are summarised in **Table 6**.

Polymer	ATR-IR (cm^{-1})	Spectrum
PSM4	1087 (C-O-C)	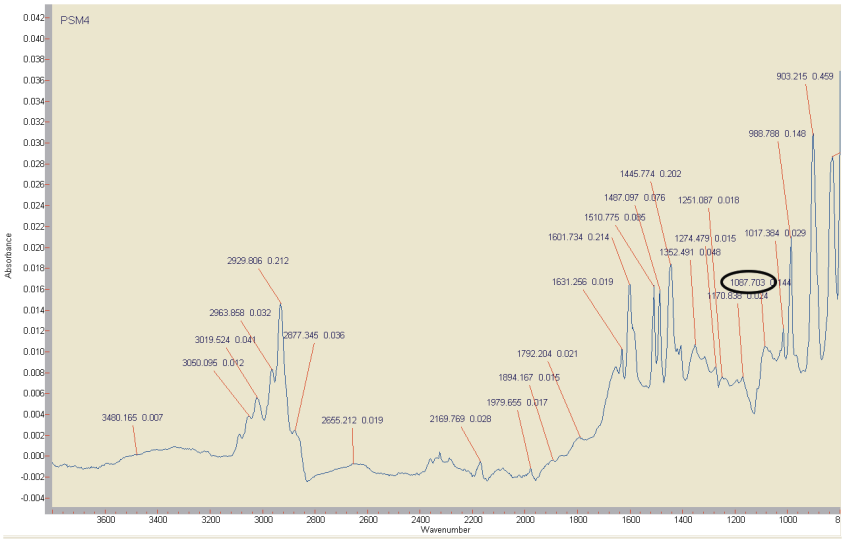
PSM5	1352 (C-N), 1087 (C-O-C)	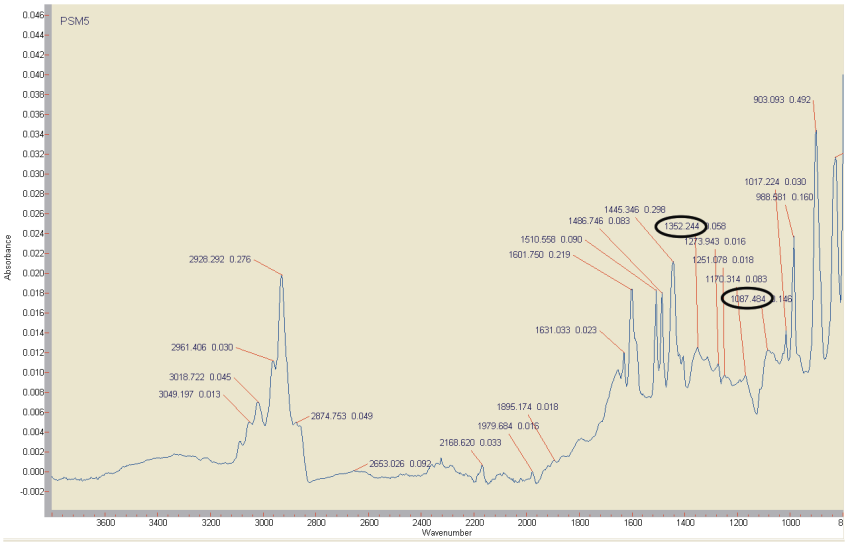
PSM6	1352 (C-N), 1087 (C-O-C)	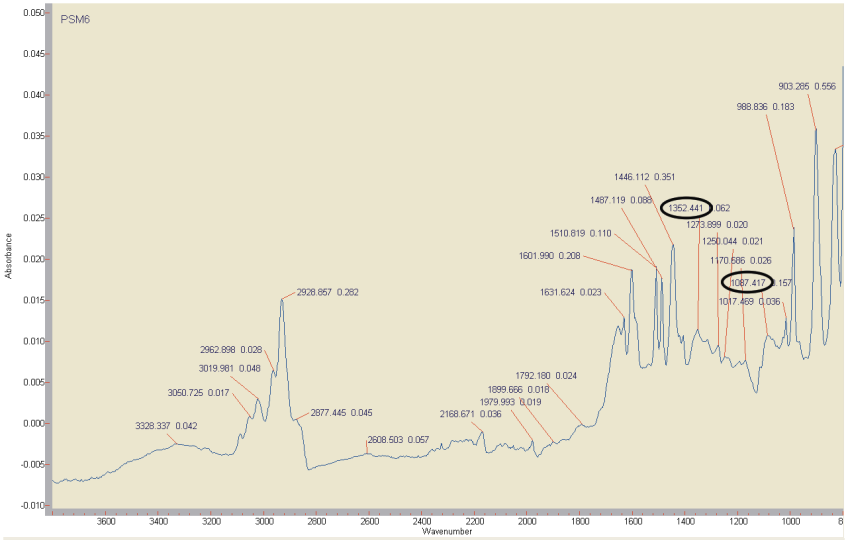

Polymer	ATR-IR (cm^{-1})	Spectrum
PSM7	1350 (C-N), 1081 (C-O-C)	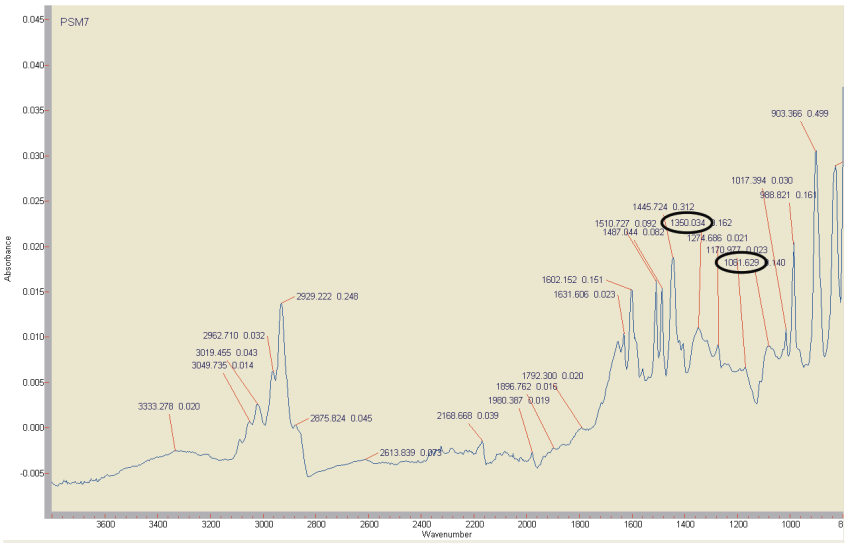
PSM22	1350 (C-N), 1082 (C-O-C)	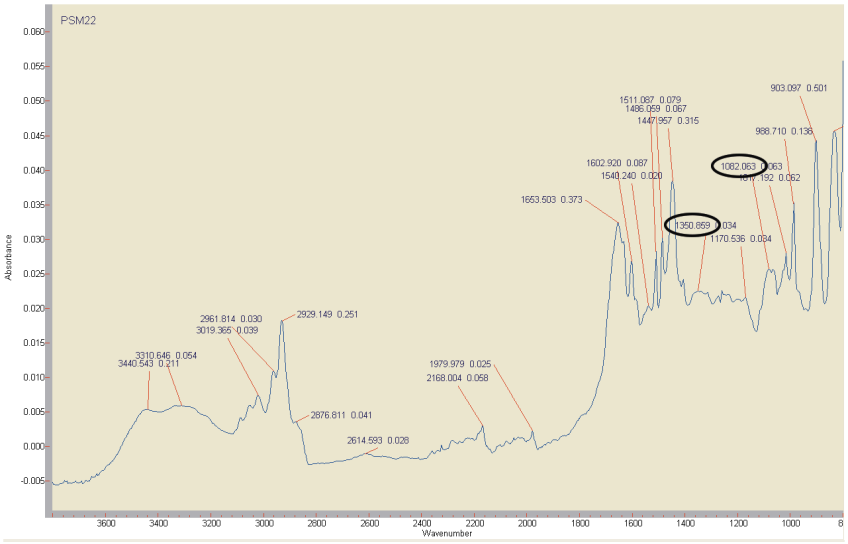
PSM27	1350 (C-N), 1063 (C-O-C)	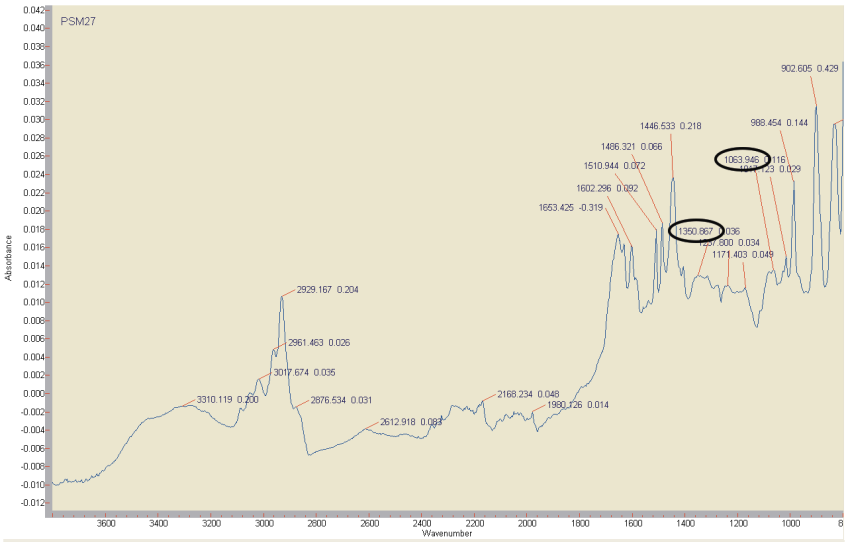

Table 6 ATR-IR data of modified PS beads

The ATR-IR spectra of samples **PSM4**, **PSM5**, **PSM6**, **PSM7**, **PSM22**, and **PSM27** exhibited absorbances around 1060-1090 cm^{-1} corresponding to the ether group (C-O-C stretching) which does not exist on the blank polystyrene. In addition, modified polymers **PSM5**, **PSM6**, **PSM7**, **PSM22**, and **PSM27** also revealed absorptions around 1350 cm^{-1} responsible for the C-N stretching mode. However, an absorbance around 1429 cm^{-1} contributing to the N=N azo resonance is generally weak and was not observed in these ATR-IR spectra.[44] Together with the results from combustion analysis that showed the existence of nitrogen, this ATR-IR spectra confirmed the presence of relevant functional groups, at least in some cases.

2.2.4.3 XPS

All samples were submitted to Cardiff University[45] for XPS analysis. Full spectral data are available in **Appendix II**, including the quantitative data. Expected N/C ratios were calculated from an assumption that monolayer of diazo compounds **M4**, **M22**, and **M27** was formed on the surface of polymers prior to generation of corresponding carbenes, and each monostyrene unit was reacted with only one molecule of carbene. With polymers **PSM5-PSM8**, it was also assumed that each modified monostyrene was reacted with only one molecule of diazonium. Examples of the structure of modified monostyrenes are shown in **Table 7**.

It is assumed that the area integrate software calculates areas with an error of ±5% (by analogy with NMR) and the error of the N/C ratio is ±10%. It was found that the XPS results confirmed the incorporation of the diaryldiazo units into the polymer surfaces and the successful diazonium coupling step. All modified polymers showed the presence of nitrogen-type species from N1s signals at binding energies of 399 eV.

Polymer	Structure	The number of nitrogen atoms	The number of carbon atoms
PSM4	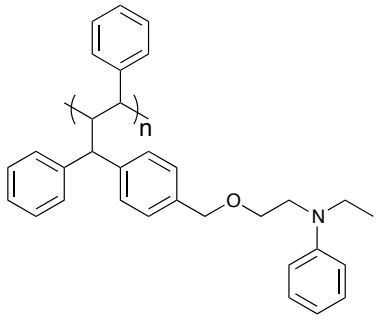	1	32
PSM5	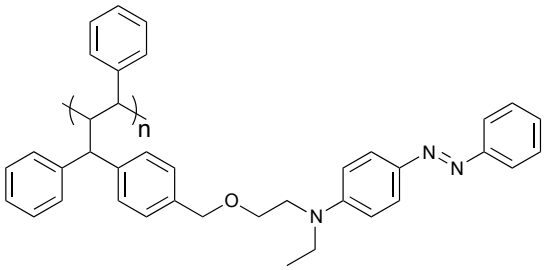	3	38
PSM6	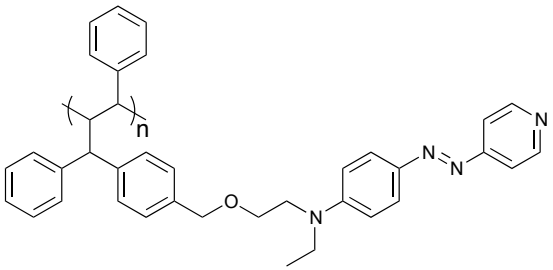	4	37
PSM7	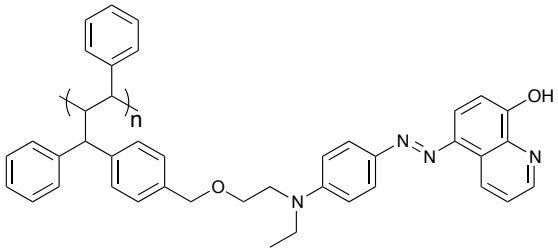	4	41
PSM8	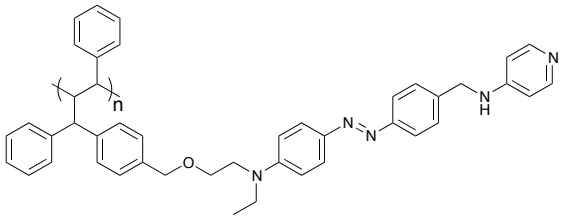	5	44
PSM22	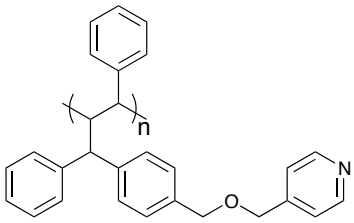	1	28

Polymer	Structure	The number of nitrogen atoms	The number of carbon atoms
PSM27	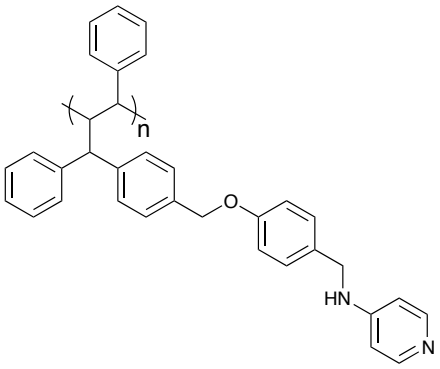	2	34

Table 7 Examples of the structure of modified monostyrenes

Polymer	Structure	Expected N/C	Found N/C
PSM4	$C_{32}H_{33}NO$	0.031	0.034±0.003
PSM5	$C_{38}H_{37}N_3O$	0.079	0.054±0.005
PSM6	$C_{37}H_{36}N_4O$	0.108	0.105±0.011
PSM7	$C_{41}H_{38}N_4O_2$	0.098	0.084±0.008
PSM8	$C_{44}H_{43}N_5O$	0.114	0.048±0.005
PSM22	$C_{28}H_{25}NO$	0.036	0.088±0.009
PSM27	$C_{34}H_{30}N_2O$	0.059	0.035±0.004

Table 8 XPS data of modified polymers

From **Table 8**, it can be seen that the observed N/C atomic ratios of modified substrates ranged from 0.034 to 0.105. However, the expected N/C ratios of materials **PSM4** and **PSM22** were lower than the found values. This most likely results from contamination, but could be also due to multiple carbene insertions leading to a higher than expected N/C ratios.

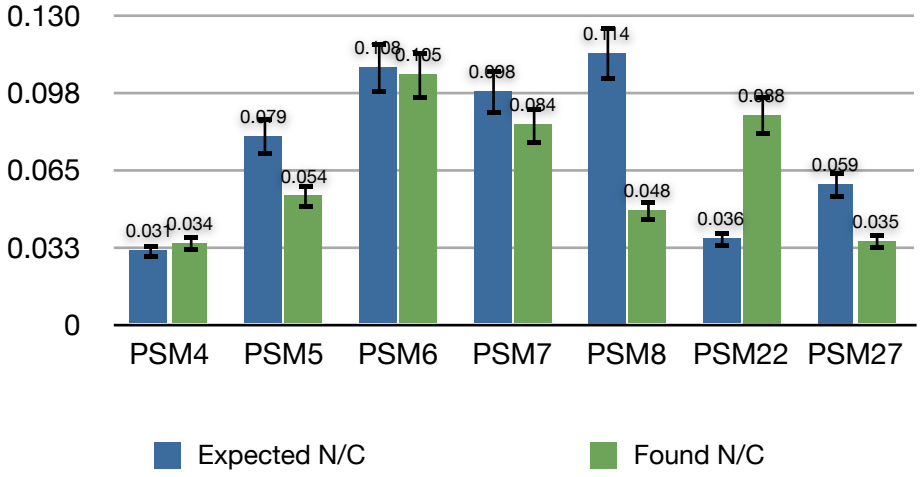

Figure 11 Expected and found N/C values

2.2.5 Metal Binding and Transmetallation

The capability of modified polymers to bind with Zn^{2+} ions was investigated by soaking the samples in $ZnSO_4$ solution and washing with an excess of water and acetone to remove excess unbound zinc ions (**Scheme 8**).

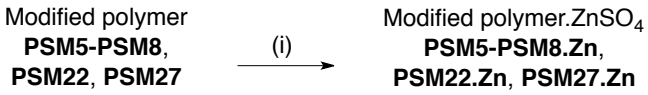

Scheme 8 Reactions and conditions
(i) $ZnSO_4$.

All samples were submitted to Cardiff University[45] for XPS analysis. Full spectral data are available in **Appendix II**, including the quantitative data. It was found that the the presence of Zn^{2+} ions was confirmed by XPS results. Except material **PSM8.Zn** which its XPS data were not obtained, all modified polymers exhibited the presence of zinc species from the Zn2p signal at binding energies of 1021 eV. Polymers **PSM22.Zn** and **PSM27.Zn**, which were produced from direct modification, displayed substantially high percentages of zinc at 15% and 11%, respectively (**Figure 12**). Disappointedly, samples **PSM6.Zn** and **PSM7.Zn**, generated from pre-activation of polymers followed by reaction with diazonium salts,

showed low degrees of binding, which were relatively lower than that of the control **PSM4.Zn** and **PSM5.Zn**.

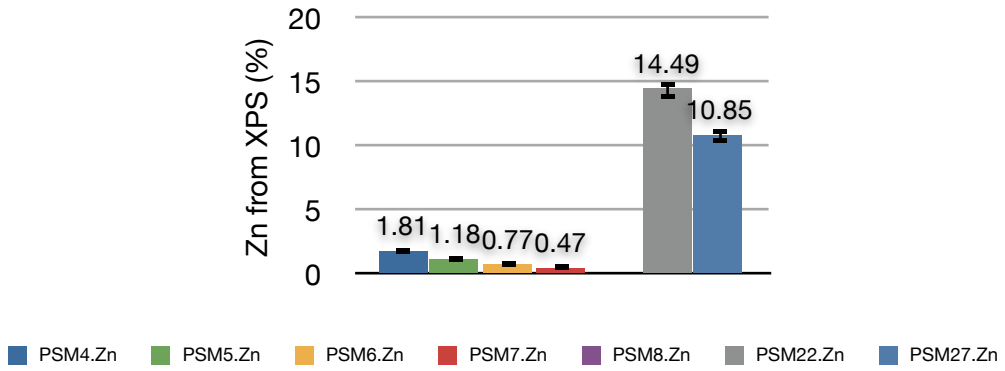

Figure 12 Loading data of modified polymers

Three samples were further analysed by inductively coupled plasma optical emission (ICP-OES) by Medac Ltd. ICP-OES is an analytical technique which uses inductively coupled plasma to generate atoms or ions in their excited states that emit electromagnetic radiation at wavelengths characteristic of a particular element.[46,47] The wavelength characteristic of zinc is at 213.86 nm and that of copper is at 327.395 nm.[48] In order to run the analysis, the ICP plasma torch (**Figure 13**), which consists of 3 concentric quartz glass tubes, is turned on to create an intense electromagnetic field within a coil of the high power radio frequency generator located around the quartz glass tubes. Argon gas, a typical atom used to create the plasma, flows through the ICP torch and ionisation of the argon flow is initiated by ignition in the intense electromagnetic field. This ionised argon gas then flows towards the magnetic field of the radio frequency coil to create a high temperature plasma of around 7000-10000 K as a result of inelastic collisions between the ionised species and neutral argon atoms.

Figure 13 ICP plasma torch[49]

A sample in either aqueous or organic solution is then delivered into an analytical nebuliser by a peristaltic pump to produce a fine spray which is introduced directly inside the plasma flame. The sample particles then collide with the electrons and charged particles in the plasma and are broken down from molecules to charged ions. These ions then repeatedly lose and recombine with electrons and generate radiation at the characteristic wavelengths of the involved elements. The emitted radiation is deflected to enter the optical chamber where the light is detected and its intensity is measured with a semiconductor photodetector for each wavelength. By comparison with the calibration lines obtained from intensities of known concentrations of each elements, the concentration of the sample can then be interpret from its intensity measured from ICP analysis. The model of the machine used by Medac Ltd is Varian Vista MPX.

Polymer **PSM7.Zn** was chosen for analysis as its quinoline system was found to effectively bind with transition metal ions, while material **PSM8.Zn** and **PSM27.Zn** were selected as their structures are more similar to DMAP system which bind efficiently with metal complexes.[50] It is assumed that the error estimates of this technique were ±5%. It was found that polymer **PSM7** bound Zn^{2+} ions poorly at 41 ppm or 0.63 μmol/g, however, polymers **PSM8** and **PSM27** were significantly more effective, with the binding of zinc at 117 and 340 ppm or 1.79 and 5.1 μmol/g, respectively (**Table 9**).

Polymer	Zn^{2+} (ppm)	Zn^{2+} (μmol/g)	Coordination (%)
PSM7.Zn	41±2	0.63±0.03	1.0±0.2
PSM8.Zn	117±6	1.79±0.09	8±1
PSM27.Zn	(3.4±0.2) x 10^2	5.1±0.3	6±1

Table 9 Analysis of zinc contents on modified polymers

Based on the number of pyridine units on the surface of polymers as previously investigated, the efficiency in metal coordination was evaluated. Material **PSM7.Zn** showed a binding level of only 1.0%, as compared to considerably higher binding levels of 8% and 6% for samples **PSM8.Zn** and **PSM27.Zn**, respectively. This implied that the quinoline ring of **PSM7** was a weaker zinc chelating ligand, while more coordination sites of **PSM8** and **PSM27** were able to tether with zinc ions via pyridine-containing residues.

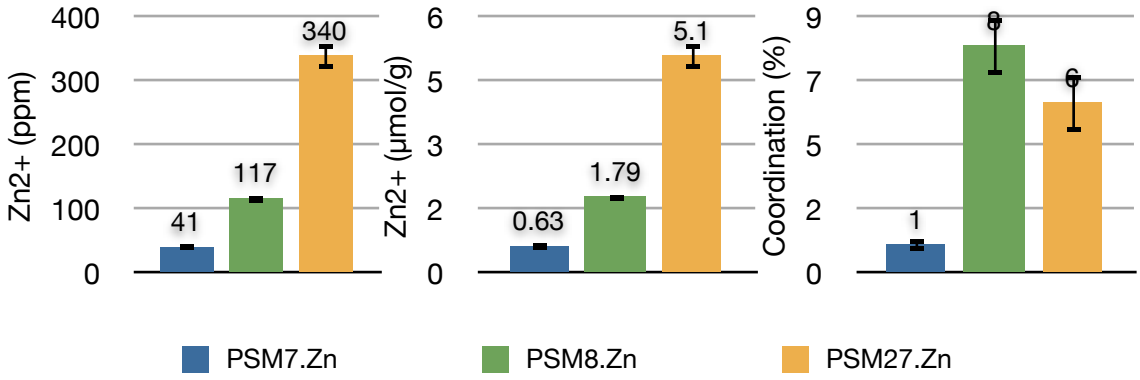

Figure 14 Loading data of modified polymers

Although polymer **PSM8** was slightly more efficient for binding of zinc ions than polymer **PSM27** in terms of percentages of coordination, the synthesis of the latter material required fewer steps, and hence, was more readily accessible. It was of interest to us to examine the ability of polymer **PSM27** to bind with zinc ATSMA/ ATSM complexes for the purpose of performing transmetallation.

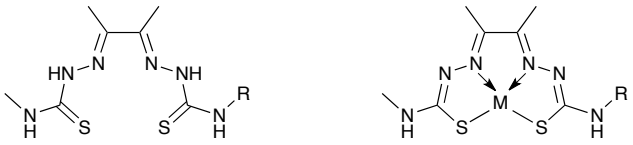

ATSMA: R=NH_2
ATSM: R=Me

M28a R=NH_2, M=Zn^{2+}
M28b R=NH_2, M=Cu^{2+}
M28c R=Me, M=Zn^{2+}
M28d R=Me, M=Cu^{2+}

Figure 15 Structures of ATSMA, ATSM, and metal complexes

The complex ZnATSMA **M28a** was obtained from the Gray Institute for Radiation Oncology & Biology Laboratory, University of Oxford. The complex ZnATSM **M28c** was synthesised by a two-step process (**Scheme 9**). Condensation of butane-2,3-dione with two equivalents of 4-methylthiosemicarbazide in the presence of concentrated H_2SO_4 was carried out at room temperature to generate the ATSM ligand or $ATSMH_2$ molecule as a white solid with moderate yield. The ^1H NMR data confirmed the structure of the condensed product and the observed MS spectra showed the base peak at 259($[M-H]^-$). The $ATSMH_2$ compound was then suspended in MeOH and $Zn(OAc)_2.2H_2O$ was added to give the desired ZnATSM complex **M28c**, confirmed by the the ^1H NMR data and the MS spectra displayed a peak at 323($[M+H]^+$).

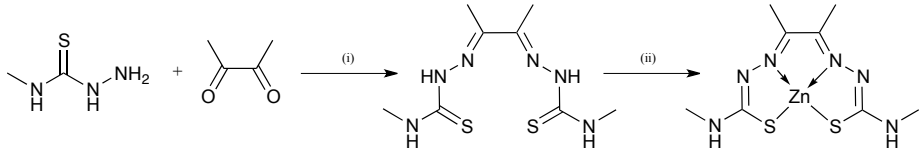

Scheme 9 Reactions and conditions
(i) conc H_2SO_4, EtOH, room temperature, 48%; (ii) $Zn(OAc)_2.2H_2O$, MeOH, room temperature, 27%.

With these zinc complexes in hand, polymer **PSM27** beads were soaked with a solution of ZnATSMA and ZnATSM, then washed thoroughly with an excess of

water and acetone to give material **PSM27.ZnATSMA** and **PSM27.ZnATSM**, respectively (**Scheme 10**).

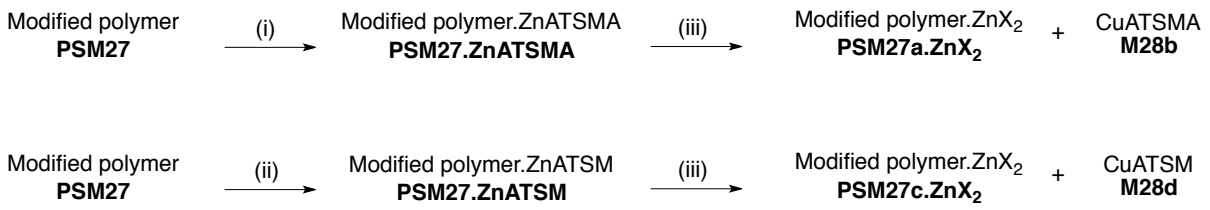

Scheme 10 Reactions and conditions
(i) ZnATSMA; (ii) ZnATSM (iii) $CuCl_2$.

The existence of the ATSMA and ATSM ligands on the surface of both samples was demonstrated by combustion analysis, showing a loading level of sulphur at 0.1%, and XPS analysis confirming the presence of N, S, and Zn at binding energies of 400, 169, and 1022 eV. The elemental analysis was carried out once for each sample and the percentage of nitrogen was measured with an error estimate of ±0.01%. It was noted that the percentages of sulphur were found to be at the lower detection limit of 0.1%. The ATR-IR spectra of sample **PSM27.ZnATSM** revealed absorption peaks at 1631 and 1259 cm^{-1} corresponding to the C=N and CSNH stretching modes, however, good quality IR spectra of sample **PSM27.ZnATSMA** could not be obtained. ICP analysis of polymers **PSM27.ZnATSMA** and **PSM27.ZnATSM** showed zinc contents at 540 and 200 ppm or 8.2 and 3.1 μmol/g, respectively. This gave rise to the efficiency in metal-complex binding at 10% for **PSM27.ZnATSMA** and 3.6% for **PSM27.ZnATSM** (**Table 10**).

It was noted that polymer **PSM27.ZnATSM** was yellow corresponding to the yellow solution of ZnATSM, while the yellow solution of ZnATSMA produced brown sample **PSM27.ZnATSMA** upon coordination with modified polymer **PSM27**. It has been reported that the axial coordination site of a ZnATSMA molecule could be occupied by the terminal amino group from an adjacent ZnATSMA molecule (**Figure**

16),[51] although no spectrometric characterisation was included and this may be responsible for the enhanced colouration in the ZnATSMA system, however, this was not examined in any detail.

Polymer	Appearance	Elemental Analysis (%)	Zn^{2+} (ppm)	Zn^{2+} (μmol/g)	% coordination
PSM27.ZnATSMA	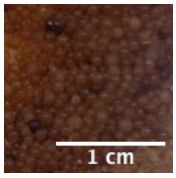	C 91.09±0.09, H 8.01±0.08, N 0.42±0.04, S 0.10‡	(5.4±3) x 10^2	8.2±0.4	10±1
PSM27.ZnATSM	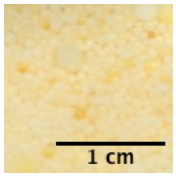	C 87.32±0.09, H 8.32±0.08, N 0.10±0.01, S 0.10‡	(2.0±0.1) x 10^2	3.1±0.2	3.6±0.5

‡ The percentages of sulphur were found to be at the lower detection limit of 0.1%.

Table 10 Analysis of zinc contents

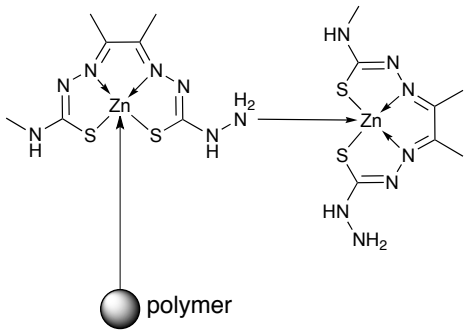

Figure 16 Possible structural change of sample **PSM27.ZnATSMA**

From **Scheme 10**, transmetallation of polymers **PSM27.ZnATSMA** and **PSM27.ZnATSM** was carried out by soaking the polymers with a solution of $CuCl_2$ and extracting the copper complexes by DMF to give a solution containing Cu[ATSMA] as **M28b** and a solution containing Cu[ATSM] as **M28d**, leaving residual polymers **PSM27a.ZnX$_2$** and **PSM27c.ZnX$_2$**, where X = Cl and X_2 = ATSMA or ATSM. ICP analysis of polymers **PSM27a.ZnX$_2$** and **PSM27.cZnX$_2$** exhibited zinc contents at 30 and 77 ppm or 0.45 and 1.2 μmol/g, respectively (**Table 11**). The loss of zinc

contents from the previously determined values from polymers **PSM27.ZnATSMA** and **PSM27.ZnATSM** suggested that the metal complexes ZnATSMA and ZnATSM have higher affinity to bind with modified polymer **PSM27** than Zn^{2+} ions.

Polymer	Appearance	Elemental Analysis (%)†	Zn^{2+} (ppm)	Zn^{2+} (μmol/g)
PSM27a.ZnX2	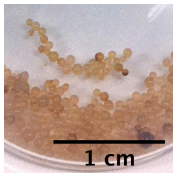	C 91.04±0.09, H 7.94±0.08, N 0.41±0.04	30±2	0.45±0.02
PSM27c.ZnX2	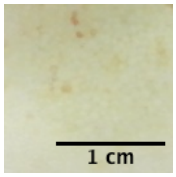	C 89.77±0.09, H 8.43±0.08, N 0.10±0.01	77±4	1.2±0.1

Table 11 Analysis of zinc contents

The eluant solutions of **M28b** containing Cu[ATSMA] and **M28d** containing Cu[ATSM] were analysed by ICP-OES, displaying copper contents at 103 and 24 ppm or 1.62 and 0.38 μmol/g, respectively. By comparison with the zinc loading levels, this lead to the efficiency in metal exchange at 20% for **PSM27.ZnATSMA** and 12% for **PSM27.ZnATSM** (**Table 12**).

Sample	Cu (ppm)	Cu2+ (μmol/g)	Metal exchange (%)
M28b	103±5	1.62±0.08	20±2
M28d	24±1	0.38±0.02	12±1

Table 12 Analysis of copper contents

The presence of the ATSMA and ATSM complexes in the eluant solutions **M28b** and **M28d** was also confirmed by other techniques: elemental analysis showed a loading level of sulphur at 0.1%, HPLC/MS analysis (**Figure 17**) revealed the existence of Cu[ATSM] (retention time = 4.33 min, m/z at 322/324), which was

essentially consistent with a reference sample (retention time = 4.53 min, m/z at 322/324) with the difference in retention times of 5% within experimental errors range, UV/visible spectrophotometry (**Figure 18**) exhibited absorption maxima at 294 and 439 nm for Cu[ATSMA] and at 290, 364, and 475 nm for Cu[ATSM] as compared to absorptions at 314, 355, and 476 nm from literature,[51] and EPR spectroscopy (**Figure 19**) confirmed the presence of copper complexes with B_0 values at around 325 mT; and.

Although modified polymers were not used on metal binding/exchange experiments for multiple cycles, it was expected that these materials could reverse to the original conditions by washing with proper solvents to release any coordinated species, and therefore, could be reused if desired.

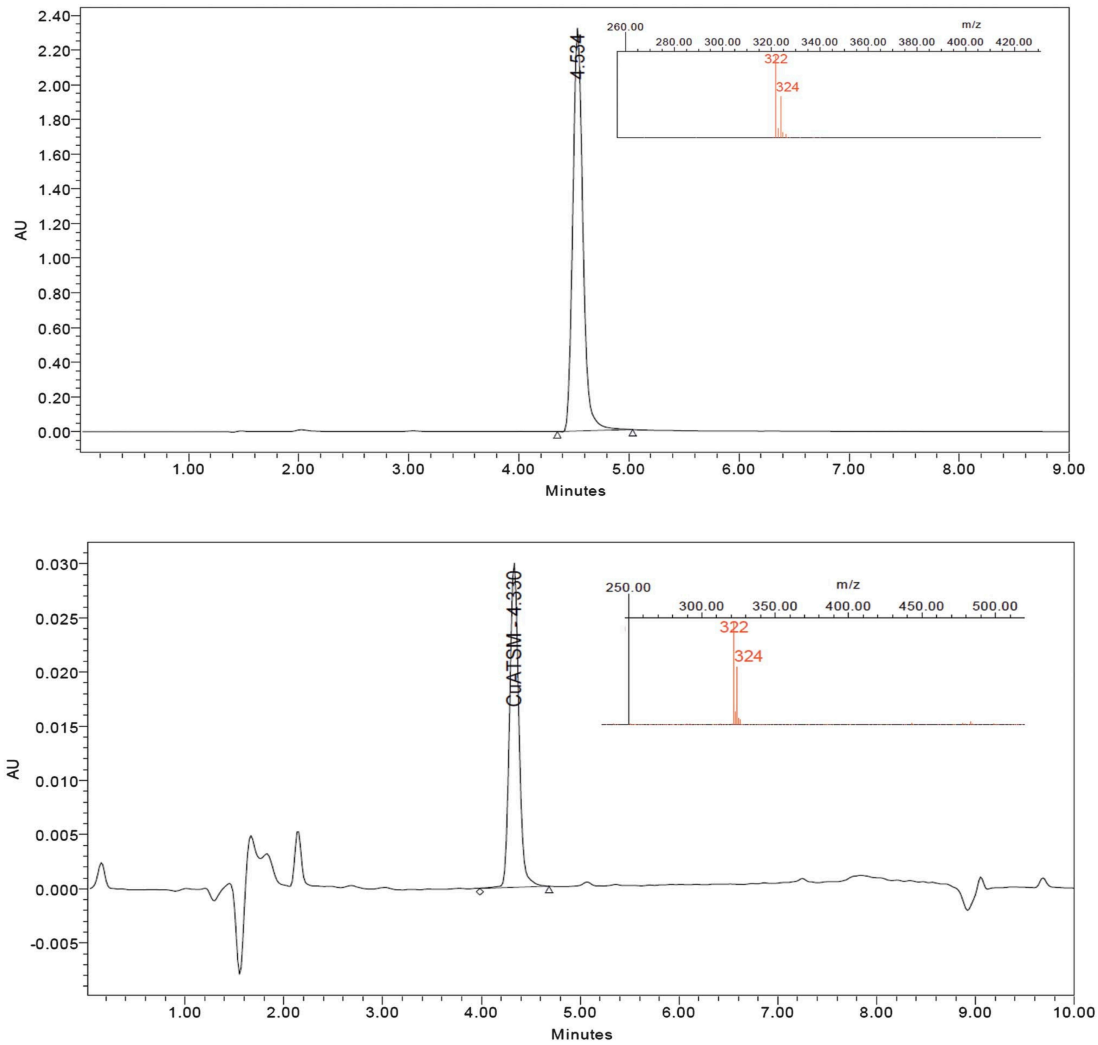

Figure 17 HPLC/MS of solutions of authentic CuATSM and released CuATSM
Column Phenomenex Luna Phe-Hex, 150 3 mm 3 mm/30 C;
20% MeCN/MeCN, 30–90%, 50/0.5 ml/min/PDA/ZQ; channel 307 nm.

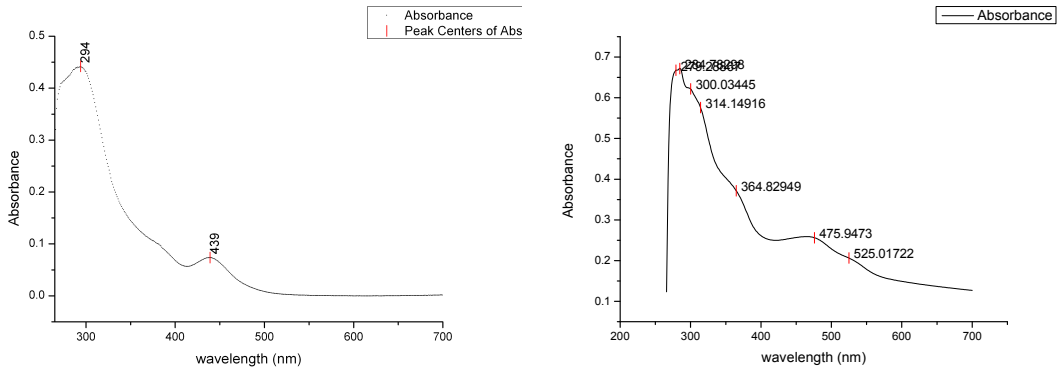

Figure 18 Solution UV-Vis spectra of CuATSMA and CuATSM
Scan Speed: 960.00 nm/min, Slit Width: 1.0000 nm, Smooth Bandwidth: 0.00 nm,
Instrument Model: Lambda 25, Data Interval: 1.0000 nm.

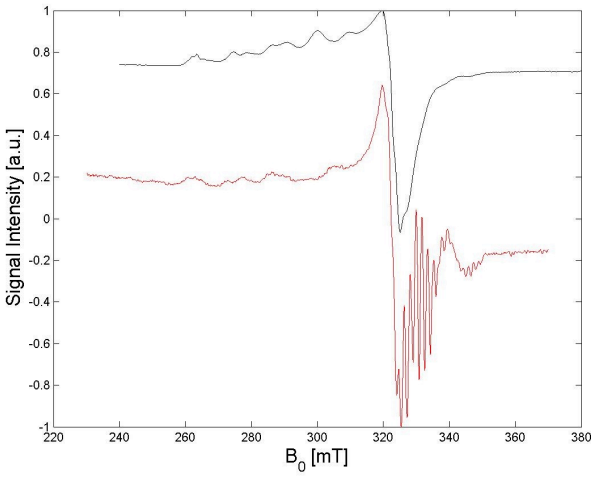

Figure 19 Solution EPR spectra of CuATSMA (black) and CuATSM (red)
X-band CW EPR 9.389378 GHz at 55 K, modulation amplitude 0.3 mT,
modulation frequency 100 kHz, microwave power 3.17 mW.

2.2.6 Affinity Chromatography

The above work showed the feasibility of reversible bindings of metals on a polystyrene substrate and this is similar to the affinity chromatography technique which has been widely used to identify and purify proteins from a mixture. The technique is based on reversible biological interactions between a protein and a

specific ligand that is covalently attached to a physically and chemically inert chromatography matrix. These interactions result from a combination of electrostatic attraction, hydrophobic interaction, van der Waals force, and hydrogen bonding between the protein and the ligand. The method is suitable for ligands such as enzyme and substrate, antibody and antigen, lectin and polysaccharide, nucleic acid and complementary base, hormone and receptor, glutathione and glutathione-S-transferase, and metal ions and proteins with histidine/cysteine/tryptophan residues on their surfaces.[52] Work described in this chapter is related to interactions between proteins and metals, known as immobilised metal ion affinity chromatography (IMAC). This specific system has been reported for separation and identification of proteins such as nucleic acids,[53] human serums,[54] and bacteria.[55] The general process involves preparation of affinity medium by equilibration in binding buffer, followed by treatment of the medium with a sample under specific conditions that favour binding of a target substance to the stationary medium whereas other mobile molecules do not bind with the matrix due to a lack of specific interactions and will be easily removed by washing. Then the target substance can be collected via elution in different conditions that reverse the binding (**Figure 20**). The elution process can be achieved either by using a competitive ligand or by changing the pH, ionic strength, or polarity. The affinity medium can also be re-equilibrated for reuse.

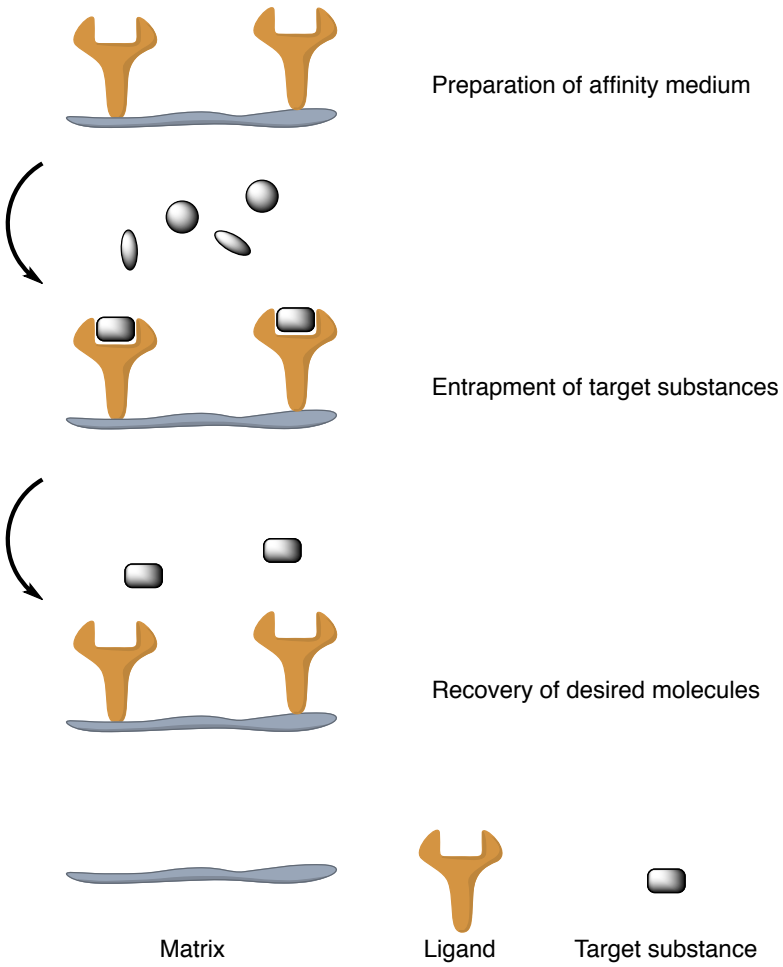

Figure 20 Affinity purification

Common terms in affinity chromatography	Analogy from metal coordination work
Matrix	Polystyrene beads
Ligand	Pyridine or DMAP groups
Ligand attachment	Surface modification using diaryl carbenes and/or diazonium salts
Binding	Coordination bonds
Competitive elution	Extraction via transmetallation

Table 13 Analogy of common terms in affinity chromatography

By analogy, polystyrene beads could be regarded as an inert matrix. The attachment of ligands was achieved by either direct modification via diazo compounds containing a pyridyl system or by diazonium coupling with pre-activated materials. This pyridine or DMAP unit would bind reversibly to target metal complexes (**Table 13**). When soaked with a solution of Zn[ATSMA]/Zn[ATSM complexes, the pyridyl groups trapped the metal complexes by coordination bonds, and the stationary phase of polymers was separated. Then a solution of copper ions which acted as a competitive agent and competed for binding to the ATSMA/ATSM pro-ligands was added. Metal exchange produced Cu[ATSMA]/Cu[ATSM] complexes and Jahn-Teller effect led to a weaker coordination bond between the pyridine/DMAP groups and the copper molecules, hence, the target copper substances were eluted from the affinity medium (**Figure 21**).

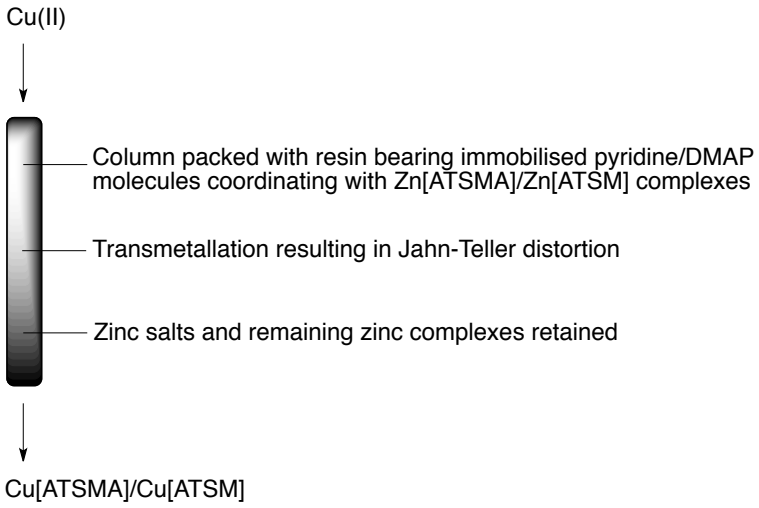

Figure 21 Generation of Cu[ATSMA]/Cu[ATSM] complexes

2.2.7 Conclusions

We have demonstrated surface modification of polymers using diazo compounds and diazonium salts to build a library of functionalised materials containing pyridine rings. Elemental analysis, ATR-IR, and XPS data of the modified

polymers confirmed the presence of nitrogen and important functional groups on polystyrenes. These polymers were capable of binding with Zn^{2+} ions and Zn[ATSMA]/Zn[ATSM] complexes. Upon transmetallation with Cu^{2+} ions, the materials showed the ability to release the generated Cu[ATSMA]/Cu[ATSM] complexes. The existence of these copper species was proved by ICP-OES, XPS, UV/visible, EPR, and HPLC/MS analysis. This project has established an approach to introduce a pyridyl system onto the surface of polymers and demonstrated the feasibility of reversible metal binding. However, when the solutions of Cu[ATSMA]/ Cu[ATSM] complexes were obtained by transmetallation and extraction from the modified polymers tethered with Zn[ATSMA]/Zn[ATSM] complexes, these solutions contained Zn^{2+} ions as impurities. Although only a trace amount of Zn^{2+} ions was observed, for clinical use the existence of these ions can be regarded as a contaminant in the radiolabelled solution of Cu(II) complexes. Therefore, this technique needs to be further developed so that extracted solutions with high purities of Cu[ATSMA]/Cu[ATSM] complexes can be produced without complicated purifications. For future work different systems of functionalised materials with improved capability of metal coordination would need to be synthesised.

Chapter 3 Photochromophores

3.1 Introduction

3.1.1 Photochromophores

Photochromic compounds are molecules which can be interconverted between two states upon irradiation at different wavelengths. This behaviour generally is the result of cis/trans photoisomerization and/or photocyclisation. Photochromic molecules can be categorised as spirobenzopyrans, spironaphthooxazines, naphthopyrans, furylfulgides, dithienylethenes, and azobenzenes (**Figure 1**).[56-58]

The reversible phototransformation between the two states is light-induced and is accompanied by a change in various properties such as molecular geometry, absorption spectra, refractive index, and polarity. In some cases, the metastable form of photochromophores can be relaxed thermally to the original isomer in the dark.[56-60]

3.1.2 Spiropyrans and their Properties

Spiropyrans are an important type of photochromic switches and have been widely studied and used due to their stability, rapid response, high sensitivity, dramatic change in physical properties upon photoisomerisation, and reversibility.[56,57,61] The photochromic transformation occurs via C-O cleavage at the spiro moiety and cis/trans isomerisation by UV irradiation at 365 nm to convert the ring-closed spiropyran form to the ring-opened meta-stable merocyanine isomer, which inturn can revert to the original closed form either thermally or by irradiation with visible light (**Figure 2**).[58,62,63] This cycle of transformation can also be accompanied by thermal

equilibration via single-bond rotation in the merocyanine form which can exist as any of four conformers with trans configuration at the methine bridge (**Figure 3**).[64,65]

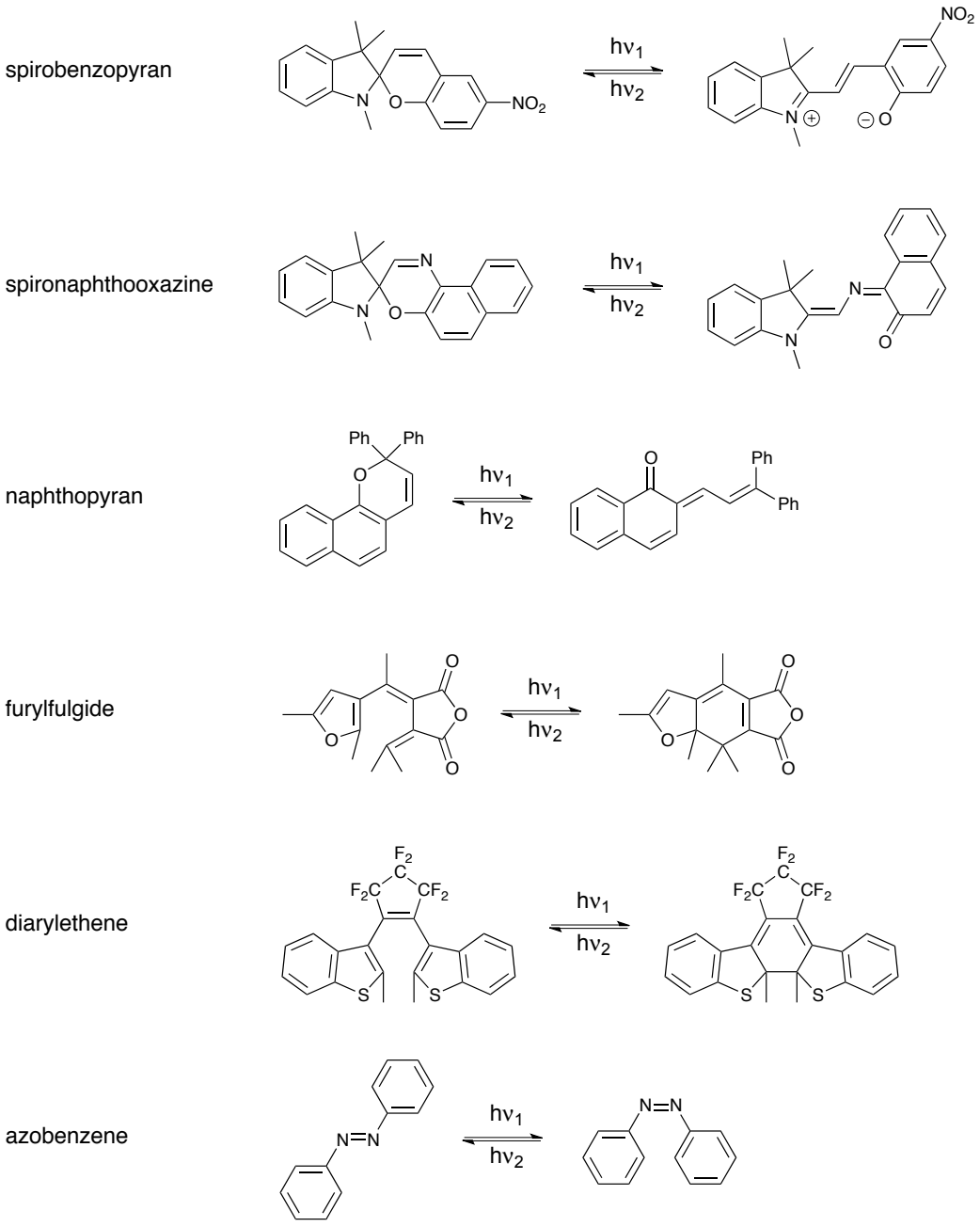

Figure 1 Examples of photochromophores

In addition, the spiropyran isomer can be transformed to the merocyanine form by mechanical forces[66] or addition of strong acids (**Figure 4**).[67] The photochromicity of spiropyran can also be inhibited in the presence of an amidine base such as

1,8-diazabicyclo[5.4.0]undec-7-ene (DBU), and the effect can also be reversibly reactivated/deactivated by the addition/removal of carbon dioxide to the solution.[68]

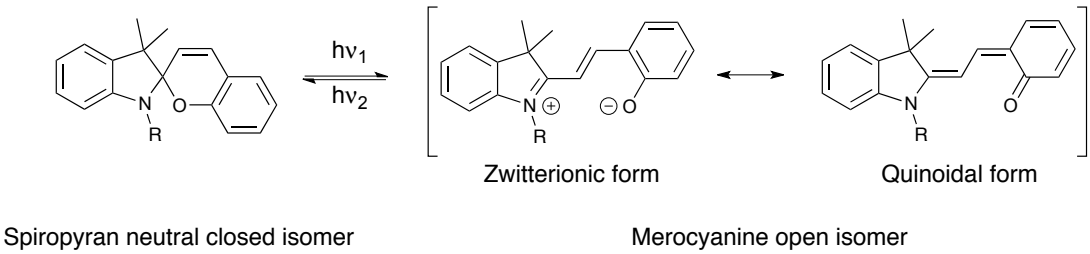

Figure 2 Photoisomerisation of spiropyran

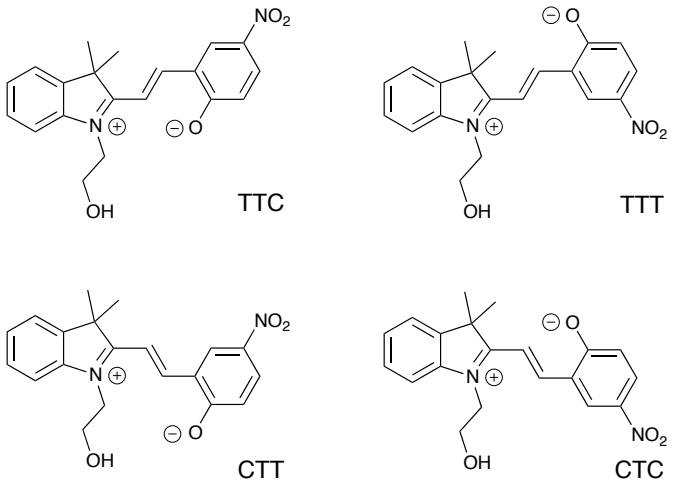

Figure 3 Possible conformers of merocyanine

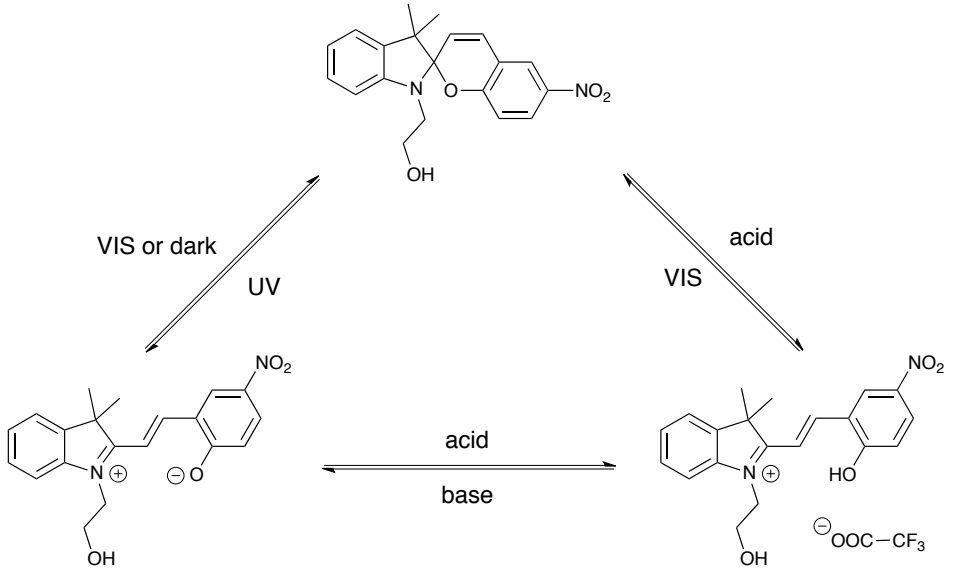

Figure 4 Transformation of spiropyran in acidic/basic conditions

The position of this equilibrium or the stability of the closed/opened form depends on the nature of the medium and/or environmental conditions. In polar solvents, the open merocyanine form is the more stable while in non-polar matrices the closed spiropyran is more favourable. This affects the rate the thermal conversion in that the rate of change from the merocyanine isomer to the spiropyran form in a non-polar solvent, typically with a half-life of ten minutes at room temperature, is higher than that in polar media.[57,58,64,69,70] Thermally-induced conversion of the spiropyran to merocyanine forms is also possible in aqueous media as the ground state energy of the merocyanine form is decreased, leading to an increase in the stability of the merocyanine isomer. This effect can be enhanced when spiropyrans are substituted with carboxylic or sulfonic groups.[71]

The spiropyran isomer is colourless and relatively more hydrophobic than the merocyanine form, which exists as a zwitterionic or quinoidal form (**Figure 2**), and has a much larger dipole moment and is intensely coloured due to its extensive conjugation system.[57] The colour of the merocyanine form also depends on the pattern of aggregation or dipole arrangement in solid phase.[72] When protonated, the merocyanine becomes yellow, exhibiting strong absorptions at 400-500 nm as compared to the purple neutral form, which shows strong absorptions at 500-700 nm. Nonetheless, they are in equilibrium and the observed colour of the mixture is determined by the ratio of the two molecules.[73]

3.1.3 Spiropyrans and its Applications

3.1.3.1 Chemical and Optical Sensors

Many applications have been reported using spiropyrans, and all of these arise from the reversibility of phototransformation and the difference in the properties between the spiropyran form and the merocyanine isomer. As charge separation

accompanies the formation of merocyanine isomer, an electrophile becomes available at the C=N+ site which is susceptible to an attack by a nucleophile anion such as a cyanide ion (**Figure 5**). The spiropyran then behaves as a selective cyanide ion receptor which can reverse the equilibrium in the presence of visible light. This allows sensitive detection of cyanide ion at the lower limit of 1.7 μM.[74] The spiropyran can also be used to indirectly detect other anions by incorporating the system with silica-based nanoparticles functionalised with thiourea molecules which act as a chemical sensor. As a carboxylate anion interacts with a thiourea unit and consequently tethers with the surface of nanoparticles, the structure of merocyanine is then affected by polarity change from surrounding environment and is induced to convert to the spiropyran form, leading to decolouration of the material and demonstrating optical chemical sensor property.[75]

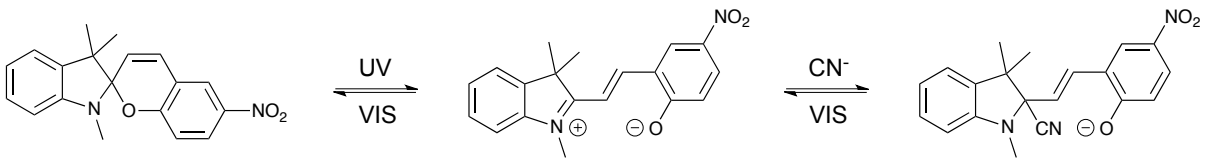

Figure 5 Transformation of spiropyran in cyanide solution

Similarly, the negatively charged oxygen atom of the merocyanine isomer is sensitive to chelation with cations such as zinc, copper, and aluminium with a fast response and is fully reversible by controlling the wavelength of irradiation.[63,76] The stability of aluminium complexes with the phenoxide group is further enhanced when the spiropyran compound has a pyridine ring in proximity to metal complexes capable of coordination (**Figure 6**).[76] Another example of an anion sensor is a fluorescent spiropyran which is bound with zinc ions and capable of detection of pyrophosphate anions, resulting in a change of fluorescent emission.[77]

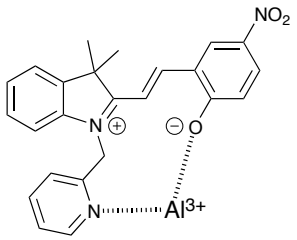

Figure 6 Chelation of an aluminium ion with a spiropyran containing a pyridine ring

As the equilibrium between the spiropyran and merocyanine isomers can be affected by pH adjustment of the medium,[67] a combination of this effect and UV/ visible irradiation as input stimulations can then be used to make acid/base and optical sensors by trapping spiropyran compounds within solid matrices such as a rigid silica monolith.[78] Most importantly, with high sensitivity of spiropyrans to irradiation at certain wavelengths, it is possible to form specific patterns on solid surfaces doped with spiropyran molecules, for example quartz and colloidal silica particles, which are derived from a poly(methyl methacrylate) copolymer and chemically bonded with spirobenzopyran compounds. This can be used to create distinct patterns with precise placement.[73] This application was also extended to flexible materials such as fabricating rubbers embedded with spiropyran for patterning regions with various shapes and colours,[79] while the simplest pattern of spiropyran coating for optical sensors is found in photochromic sunglasses which can absorb solar radiation resulting in colouration on the glasses and reversion back to transparencies in room light.[80]

3.1.3.2 Switch, Wettability, and Logic Gate Modulation

Generally, the ground state of the spiropyran form is lower in energy than that of the merocyanine form and thermal relaxation drives the system towards the ring-closed form in equilibrium.[71] Upon UV irradiation, the system can ‘switch’ to the other

state, change its properties, and affect the environments in many ways. The reverse process can be rapidly achieved by visible light. This on-and-off phenomenon is useful in controlling physical properties via variation of applied wavelengths, enabling wide application. Examples include a light-controlled nanoporous alumina membrane acting as a burst valve and electrical switch for the transport of water and ions across the membrane,[81] a photosensitive layer on a capillary tube or microchannel controlling photocapillarity or the microfluidic actuation of water,[82] amphiphilic core-shell nanoparticles and triblock copolymer micelles containing spiropyran units for accommodation of dye molecules, enhancement of fluorescence emission, and fluorescence modulation by energy transfer through spiropyran moiety,[83,84] photon-modulated control of DNA-binding affinity to inhibit DNA-associated processes by photoswitches,[85] and a photoresponsive culture surface for *in situ* reversible photocontrol of cell adhesion and cell detachment by regional photoirradiation and temperature change of a polymer material and copolymer membranes.[86,87]

In addition, the on/off switch behaviour can be considered as 0 and 1 in binary strings for data storage or data encoder/decoder applications. If the system produces a single logic output in any form from a performed logical operation on one or more logic inputs or irradiation at certain wavelengths, then the system can be used to construct Boolean function(s). This can be done in either solution phase, for example, a molecular switch that responds to three inputs namely UV irradiation, visible light, and acidity of the solution and generates two outputs as UV-VIS absorption,[67] or in solid materials such as a photosensitive switch that operates in a rigid silica monolith.[78] A spiropyran molecule can also be combined with another type of photochromic compounds such as quinoline-derived dihydroindolizines via chemical links to generate molecular operators based on the absorption properties of the molecule or on/off responses (**Figure 7**).[88]

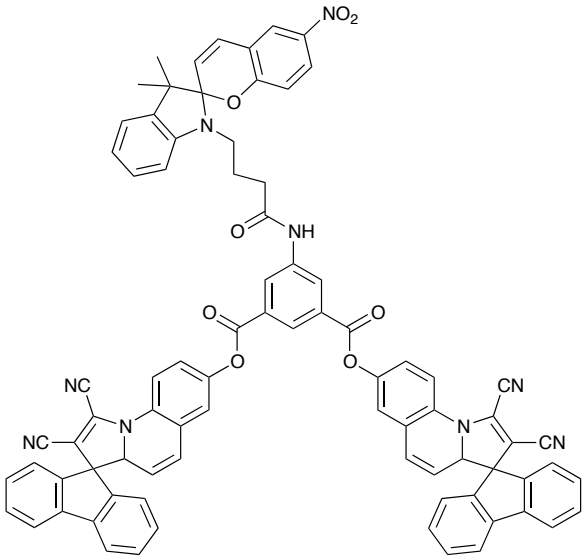

Figure 7 An example of Boolean-functional molecule

With literature precedent suggesting that spiropyrans are robust, synthetically readily accessible, and suitable for attachment of materials as photochromophores, it was of interest therefore to study the behaviour and properties of spiropyrans in the context of material modification, and using the carbene derivatisation approach developed within the Moloney group.

3.1.4 Proposed Strategy and Aims of the Project

It was envisaged that a spiropyran compound would be linked to a diaryldiazo molecule in order to introduce the photochrome onto the surface of polymers. Previous work[19] has shown that the spiropyran system is susceptible to a nucleophilic attack by hydrazine monohydrate. As a result, the carbonyl group of a benzophenone would have to be converted to the corresponding diazo group prior to conjugation with a spiropyran molecule which would be independently made at a late synthetic stage (**Figure 8**).

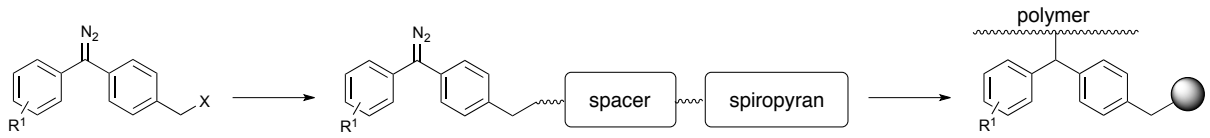

Figure 8 Proposed strategy

The general structure of preferred spiropyran compounds contains a nitro group in the 6-position of the pyran as illustrated in **Figure 9**. This is because an absence of a strong electron withdrawing group at that position tends to decrease the stability and hence the population of the merocyanine state.[69]

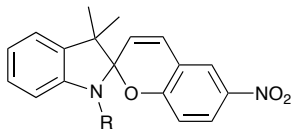

Figure 9 General structure of desired spiropyrans

The formation of spiropyran benzophenone diazo compounds would be followed by surface modification of polystyrene (PS) beads and polyethylene terephthalate (PET) sheets. Polystyrenes were selected as an example of non-polar hydrocarbon polymers in the form of beads with large surface areas to facilitate the diazo modification process and increase degrees of loading, while the PET sheets were chosen in order to observe the effect of environmental polarity on the equilibrium between the spiropyran and the merocyanine states and contact angle measurements on the flat surface upon irradiation as a result of a change in dipole moments. It was intended that modified polymeric materials would be characterised by standard methods namely elemental analysis, ATR-IR, and XPS and the effects of photochromicity of the polymers determined from both colour change and contact angle change.

3.2 Results and Discussion

3.2.1 Synthesis and Characterisation of Diazo Compounds

Friedel-Crafts acylation was performed by the reaction between 4-nitrobenzoyl chloride and toluene, which also acted as the solvent, in the presence of the Lewis acid ($AlCl_3$) to yield diaryl ketone **P1** with moderate yield and excellent purity, confirmed by the ^1H NMR data and the MS spectra showing the base peaks at 279($[M-H+K]^+$) (**Scheme 1**). The methyl group was then modified by radical bromination using NBS in the presence of light giving bromide **P2**, followed by hydroxylation with aqueous $CaCO_3$ to produce alcohol **P3**. The overall yield of these two steps was higher than 90%, with the benzophenone **P3** exhibiting the base peak at 256($[M-H]^-$) in the MS spectra. The synthetic route then proceeded by the standard methodology for diazo preparation.[8,16]

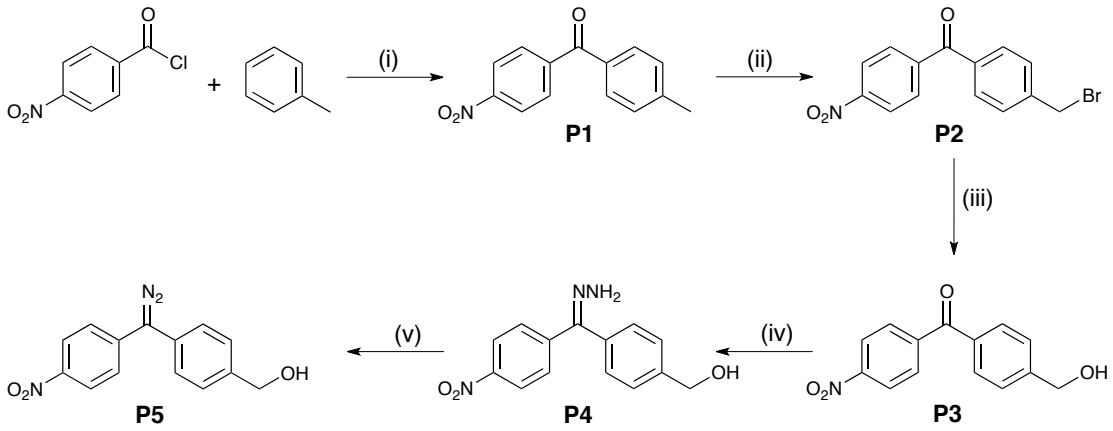

Scheme 1 Reactions and conditions
(i) $AlCl_3$, toluene, room temperature, 45%; (ii) NBS, $CHCl_3$, hv, heat under reflux, 100%; (iii) $CaCO_3$, 1,4-dioxane/water, heat under reflux, 91%; (iv) $H_2NNH_2.H_2O$, EtOH, heat under reflux, 96%; (v) MnO_2, Na_2SO_4, KOH, MeOH, room temperature (dark), 89%.

Addition of hydrazine monohydrate to the carbonyl **P3** gave the hydrazone intermediate **P4**. The observed MS spectra displayed the base peak at 270($[M-H]^-$), and aromatic region of the ^1H NMR spectrum became more complicated upon formation of C=N bonds as a result of non-equivalence resulting from the existence

of both *syn* and *anti* isomers. Oxidation of the condensed product **P4** was achieved by MnO_2 in anhydrous basic solution of MeOH in the dark, generating the benzophenone diazo compound **P5**. We have previously used a mercuric oxide system, which is very reliable, but the manganese oxide method was used here for its better environmental credentials. The presence of diazo groups was confirmed by the IR spectra, showing an absorption peak around 2040 cm^{-1} corresponding to N≡N stretching mode.

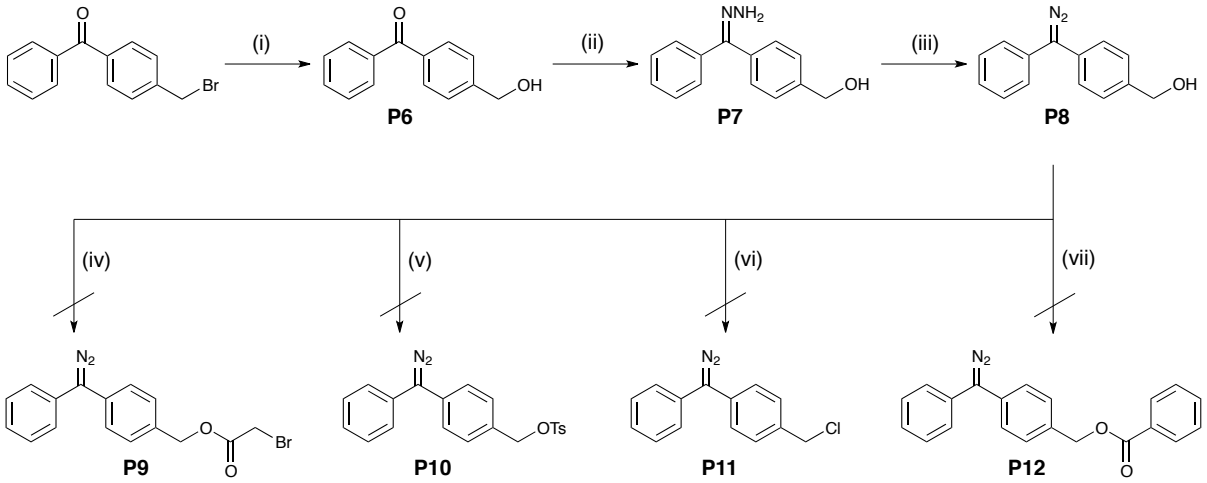

Scheme 2 Reactions and conditions
(i) $CaCO_3$, 1,4-dioxane/water, heat under reflux, 75%; (ii) $H_2NNH_2.H_2O$, EtOH, heat under reflux, 100%; (iii) HgO, Na_2SO_4, saturated KOH/EtOH, THF, dark, room temperature, 100%; (iv) Bromoacetyl bromide, Et_3N, DCM, 0°C; (v) TsCl, pyridine, DCM, room temperature; (vi) PPh_3, CCl_4, 50°C; (vii) benzoic acid, DCC, DMAP, DCM, room temperature.

The structure of these ketones and hence corresponding diazo molecule was chosen due to its expected greatest stability upon conversion to diazo **P5**. Previous work has shown that a lack of the nitro group as an electron withdrawing function had a deleterious effect on the stability of the diazo moiety.[14,17-20] For example, in spite of the successful synthetic route to benzophenone diazo compound **P8**, the diazo functional group did not survive through reaction conditions that could be utilised to couple it with spiropyran systems (**Scheme 2**). It was found that the diazo compound **P8** was sensitive to reactions with bromoacetyl bromide in the presence of Et_3N, TsCl

with pyridine, PPh_3 in CCl_4, and benzoic acid with DCC and DMAP. The decomposition involved loss of N_2 and was indicated by fast decolouration.

3.2.2 Synthesis and Characterisation of Spiropyrans

A spiropyran compound is generally synthesised by coupling between a 2-hydroxybenzaldehyde derivative and an indolium salt, and it was anticipated that ready replication of literature chemistry would be possible.[89] Therefore, it was envisaged that spiropyran **P14** would be made from a reaction between 5-nitrosalicylaldehyde and indolium **P13** (**Scheme 3**). A commercially available 2,3,3-trimethylindolenine was reacted with 5-bromovaleric acid in chlorobenzene at high temperature to produce a highly coloured indolium salt **P13** with excellent yield and its structure was confirmed by the ^1H NMR data and the MS spectra, showing a peak at 260($[M\text{-}Br]^+$). This organic salt was then treated with 5-nitrosalicylaldehyde by a standard method,[89] however, the product of the reaction was not identifiable by ^1H NMR spectroscopy. It was found that, in general, although spiropyrans are widely reported, experimental details are frequently lacking, and in any case, functional group variation limited.

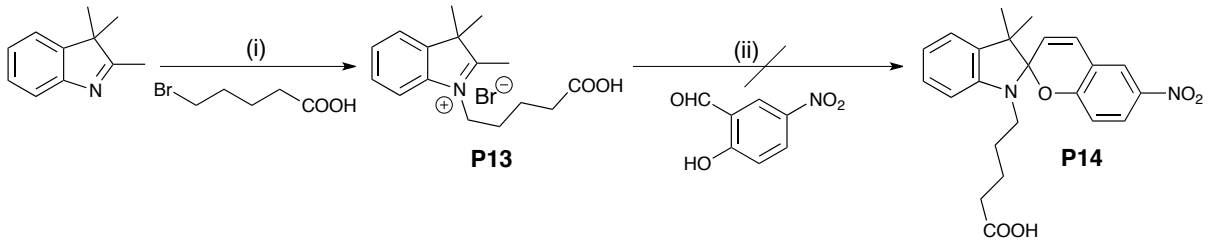

Scheme 3 Reactions and conditions
(i) C_6H_5Cl, 140°C, 100%; (ii) THF, 80°C.

After extensive literature searching, the synthesis of a spiropyran in a three-step process was identified; after investigation, this proved to be very reliable.[90]

Firstly, substitution of 3-iodopropanol by 2,3,3-trimethylindolenine generated a dark-red indolium **P15** with excellent yield. The formation of the indolium salt was confirmed by the ^{1}H NMR data and the MS spectra, displaying the base peak at 218([M-I]$^+$) (**Scheme 4**).

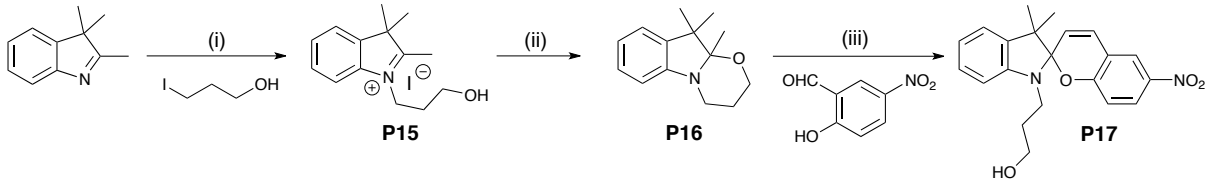

Scheme 4 Reactions and conditions
(i) $CHCl_3$, room temperature 100%; (ii) KOH, H_2O, room temperature, 41%;
(iii) EtOH, room temperature, 10%.

Deprotonation of indolium **P15** with KOH led to cyclisation and production of indole **P16**, which was then treated with 5-nitrosalicylaldehyde to construct the spiro system, giving the desired photochromic molecule **P17**. Unfortunately, the yield of the last condensation step was low, only at 10%. This might be because purification of spiropyran **P17** involved flash column chromatography that trapped a significant amount of the merocyanine form, in equilibrium with the spiropyran isomer, within the column.

3.2.3 Conjugation of Diazo and Spiropyran Units

The terminal hydroxyl group of compound **P5** was converted to bromoester **P18** by reaction with bromoacetyl bromide in the presence of Et_3N. Without further purification this ester **P18** was then coupled with spiropyran **P17** to produce a red brown solid of diazo spiropyran **P19** (**Scheme 5**).

The diazo groups of both compound **P18** and **P19** were present as confirmed by the IR spectra, showing absorption peaks around 2045 cm^{-1}, however, purification of diazo **P5**, and hence **P18** and **P19**, proved to be extremely difficult due to the

instability and sensitivity of the diazo part, even with the presence of the electron withdrawing nitro group.[14,17,18,20] As the diazo compound decomposed on TLC plates as indicated by rapid decolouration and streaking of sample, column chromatography was not an option, and the material had to be used in crude form. It was noted that purification by column chromatography with either silica gel or alumina as a stationary phase was not attempted.

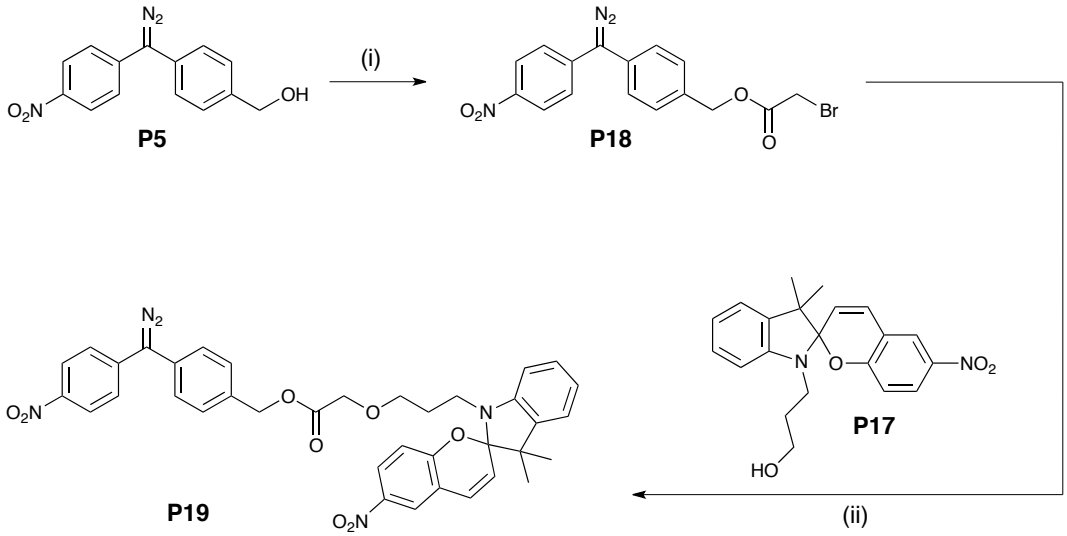

Scheme 5 Reactions and conditions
(i) Bromoacetyl bromide, Et_3N, DCM, 94%; (ii) Et_3N, DCM, room temperature, 100%.

3.2.4 Surface Modification of Polymers

With the desired diazo compound **P19** in hand, investigation of its suitability for surface functionalisation of polystyrene beads (PS) and polyethylene terephthalate sheets (PET) was made. Thus, each polymer was treated with the diazo compound **P5**, as a control, and **P19** in ether solution. The solvent was then removed *in vacuo* at 40°C and each sample was carefully heated at 120°C to facilitate decomposition until no colour from diazo groups was observable. The corresponding highly reactive carbenes which were generated *in situ* were assumed to have reacted with the surface of the appropriate substrates. The materials were allowed to cool to room

temperature, washed thoroughly with excess acetone and left to dry under suction. This gave surface-modified polymers **PSP5**, **PSP19**, **PETP5**, and **PETP19**.

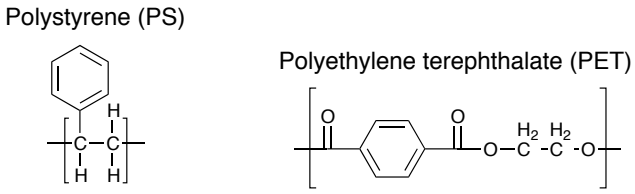

Figure 10 Structures of PS and PET polymers

Similar treatment was also applied with spiropyran **P17**, to give coloured materials **PSP17** and **PETP17** via physical adsorption of the spiropyran only at the surface; this provides a useful control for the lack of diazo group. This experiment was performed in order to compare and contrast the efficiency and hence degree of surface modification between chemically modified materials and physically adsorbed polymers at ambient temperature (120^{o}C).

3.2.5 Visual Observations

All the samples could be distinguished from their colour, which was invariably different from the purple colour of the physisorbed material, prior to heating. Although a slight physical adsorption was observed as can be seen from the colour of polymer **PSP17** and **PETP17**, which indicated that a trace amount of spiropyran **P17** was coated on the surface, the mechanism of functionalisation by carbene insertion was demonstrated by the change in colour of the coated polymer beads and sheet upon activation by heat as a result of structural changes. In addition, all materials were evenly modified at the surface, except polymer **PETP17**.

Polymer	Structure	Appearance
PSP5	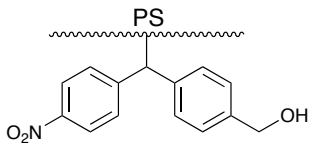	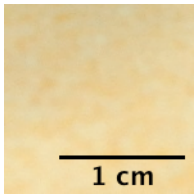
PSP17	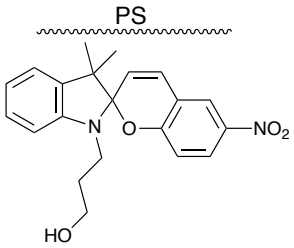	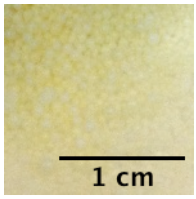
PSP19	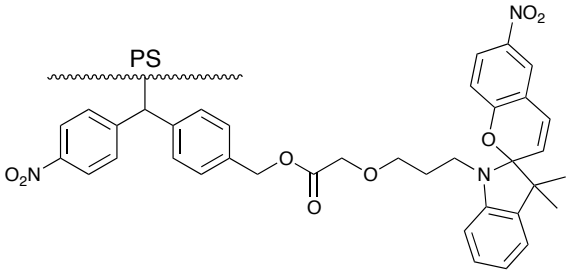	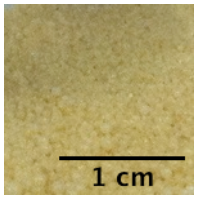
PETP5	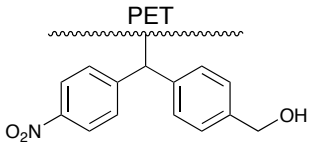	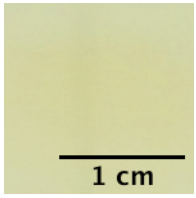
PETP17	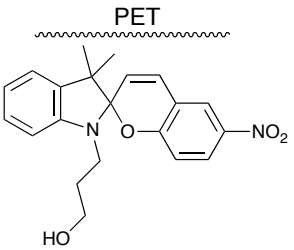	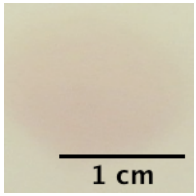
PETP19	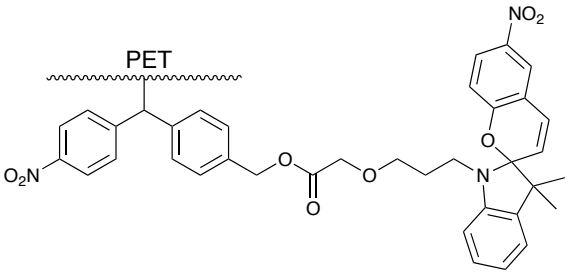	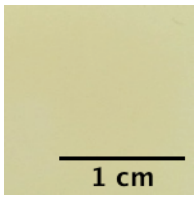

⁎The average diameter of polystyrene beads is 1 mm (manufacturer's data).

Table 1 Visual observation

3.2.6 Characterisation of Modified Polymers

3.2.6.1 Elemental Analysis

All samples were submitted to Elemental Analysis Service of London Metropolitan University[39] and analysed for C,H,N composition. The error estimates were assumed to be ±10% The results of this analysis and calculated loading data are summarised in **Table 2**.

Polymer	Elemental Analysis of N (%)	Loading (mmol/g)	Loading (molecules/cm^2)†	Surface Coverage (%)‡	N*
PSP5	C 85.71±0.01, H 6.80±0.01, N 0.21±0.01	0.15±0.02	(13±2) x 10^{12}	9±2	61±6
PSP17	C 86.44±0.01, H 7.35±0.01, N 0.14±0.01	0.050±0.005	(4.2±0.6) x 10^{12}	3.0±0.8	190±20
PSP19	C 87.41±0.01, H 7.91±0.01, N 0.11±0.01	0.026±0.003	(2.2±0.3) x 10^{12}	1.5±0.4	400±40
PETP5	C 61.69±0.01, H 4.21±0.01, N <0.10⁕	<0.071	<5.9 x 10^{12}	<4.0	>68
PETP17	C 60.84±0.01, H 3.75±0.01, N <0.10⁕	<0.036	<3.0 x 10^{12}	<2.1	>141
PETP19	C 61.45±0.01, H 4.16±0.01, N <0.10⁕	<0.024	<1.9 x 10^{12}	<3.8	>214

Table 2 Elemental analysis and loading data of modified polymers
† Assumes surface area of 725 m^2/g (manufacturer's data);
‡ Assumes limiting area (A^o) for monolayer formation is 0.70 nm^2/molecule;
* N represents the ratio of unmodified styrene monomers to functionalised units.
⁕ The percentages of nitrogen were found to be less than the lower detection limit of 0.1%, and no error estimate was calculated.

The elemental analysis proved the existence of nitrogen, ranging from 0.11 to 0.21% for functionalised PS materials, which was consistent with the presence of nitro group and/or spiropyran moiety on the surface, showing a loading level of

0.026-0.15 mmol/g or $2.2x10^{12}$-$13x10^{12}$ molecules/cm^2, assuming a surface area of 725 m^2/g (from manufacturer's data) with assumed error estimates of ±5% or ±36 m^2/g. The percentages of area coverage were calculated on an assumption that the side chain of a diphenylmethane unit is folded away from the surface (**Table 3**), and the projected surface area of the inserted carbene is approximately equivalent to the limiting area (A^o) of 1.5 molecules of anthracene (0.70 nm^2/molecule).[40] This represents a minimum value for the system **PSP5-PSP19**, since it does not take account of the steric effect of the side chain. The error estimates from this rough approximation are assumed to be ±10% for each sample. The data from **Table 2** indicated a surface coverage of approximately 2-9%.

Polymer	Structure	Polymer	Structure
PSP5/PETP5	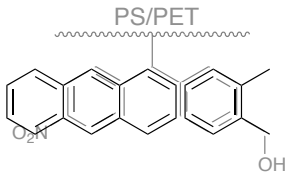	**PSP19/PETP19**	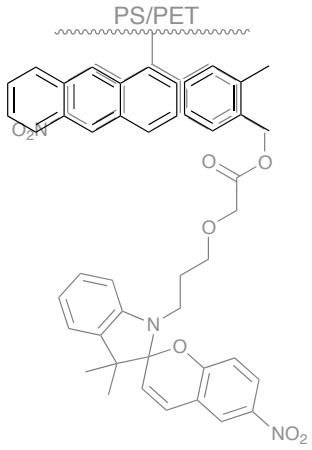
PSP17/PETP17	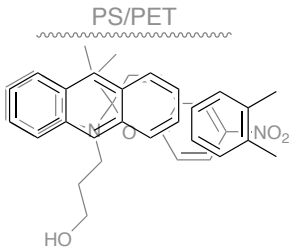		

Table 3 Structures for calculations of limiting areas

The theoretical yields for diazo modification of **PSP5** and **PSP19** are 0.074 and 0.186 mmol/g, respectively. These were calculated from 5% loading of the corresponding diazo compounds to polystyrene beads in the procedure, yielding the efficiency in diazo modification to be 32% and 81% for **PSP5** and **PSP19**, respectively.

The N values represent the ratio of unmodified styrene monomers to functionalised monomer units. The relatively low N value of **PSP5** implied a high degree of surface modification, meaning that for each functionalised monostyrene unit, there were 61 unmodified monomers. The high N value of around 400 from **PSP19** indicated low loadings, and this is likely to be due to steric effects as a result of the large limiting areas of spiropyran diazo benzophenone **P19**.

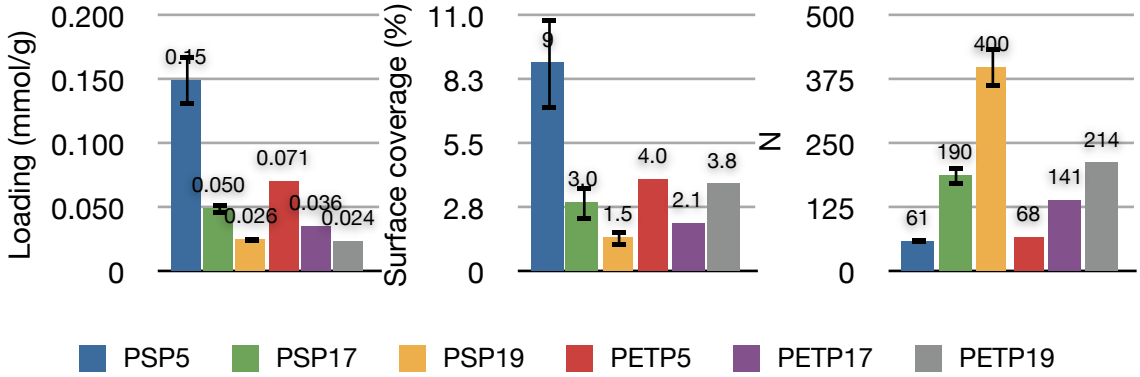

Figure 11 Loading data of modified polymers

Disappointingly, the level of nitrogen on all of PET surfaces was less than 0.1%, implying that the material is less receptive to the approach due to smaller surface area of PET sheet as compared to highly adsorbent porous PS beads. Consequently, the loading data of modified PET sheets, namely loading (mmol/g), loading (molecules/cm^2), % surface coverage, and the N values, were calculated by assuming the percentages of N to be 0.10, and thus, give maximum loading levels.

3.2.6.2 ATR-IR

Full spectral data is available in **Appendix III**. The ATR-IR spectra of sample **PSP5** and **PSP19** displayed absorbances around 1345 and 1510 cm^{-1} which were attributed to the nitro group (**Table 4**); however, polymer **PSP19** did not display an absorption around 1730 cm^{-1} corresponding to the ester resonance.

Unfortunately, good quality IR spectra of sample **PSP17** could not be obtained, and modified PET sheets did not give observable ATR-IR spectra, probably owing to low degree of loading as indicated by the data from the combustion analysis.

Polymer	ATR-IR (cm^{-1})	Spectrum
PSP5	1346 and 1511 (NO_2)	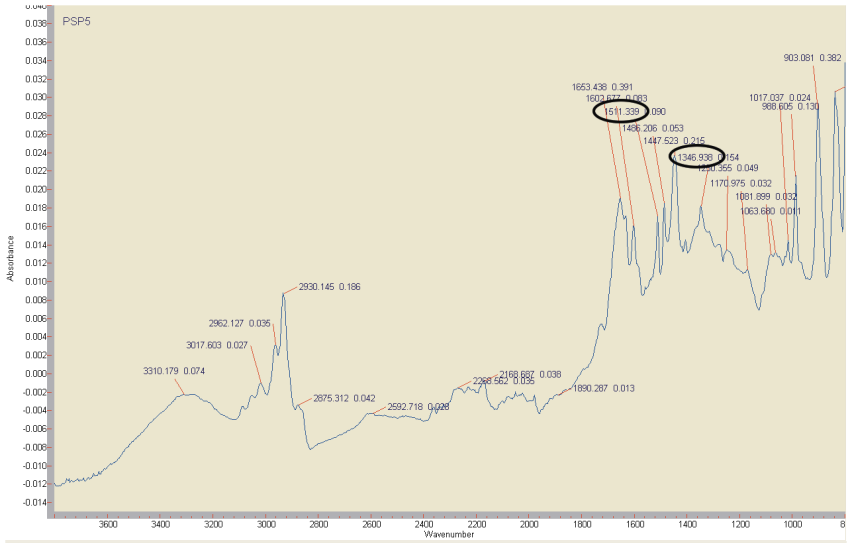
PSP19	1347 and 1511 (NO_2)	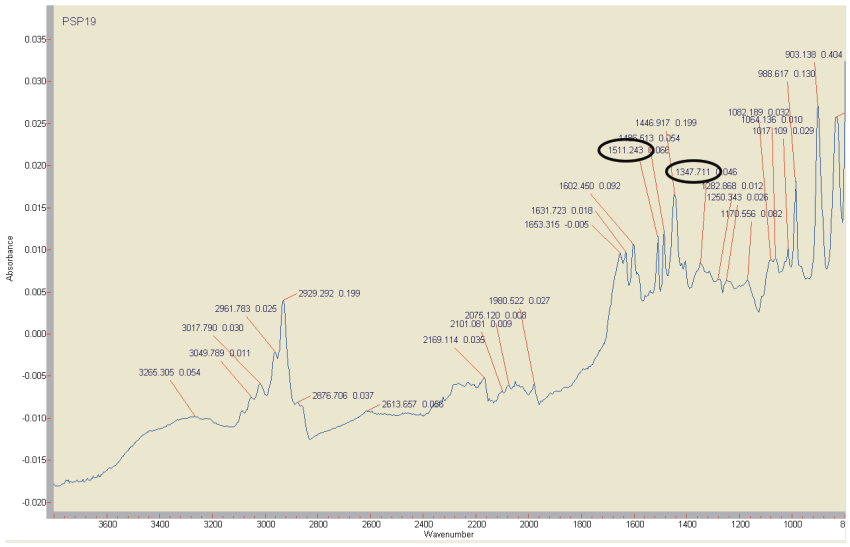

Table 4 ATR-IR data of modified PS beads

3.2.6.3 XPS

All samples were submitted to Cardiff University[45] for XPS analysis. Full spectral data are available in **Appendix IV**, including the quantitative data. Expected N/C ratios were calculated from an assumption that monolayer of diazo compounds

P5 and **P19** and spiropyran **P17** was formed on polymers prior to surface modificaion, and each monomer unit was reacted with only one molecule of carbene or physisorbed only one molecule of spiropyran. Examples of the structure of modified monostyrenes are shown in **Table 5**.

Polymer	Structure	The number of nitrogen atoms	The number of carbon atoms
PSP5	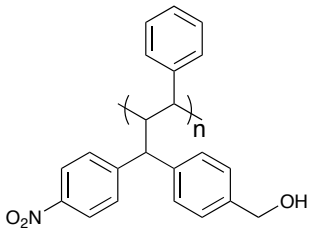	1	22
PSP17	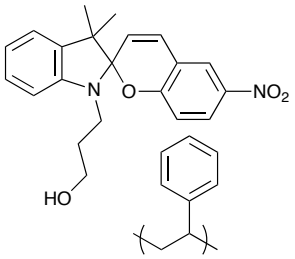	2	29
PSP19	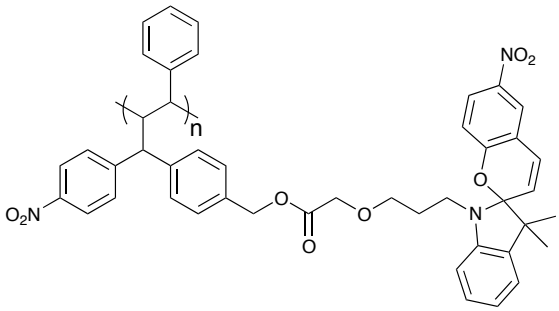	3	45
PETP5	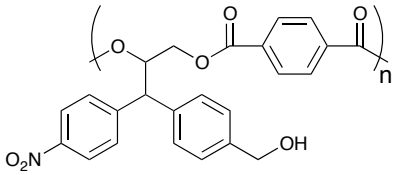	1	24
PETP17	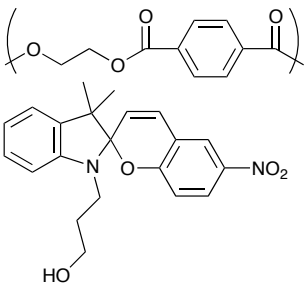	2	31

Polymer	Structure	The number of nitrogen atoms	The number of carbon atoms
PETP19	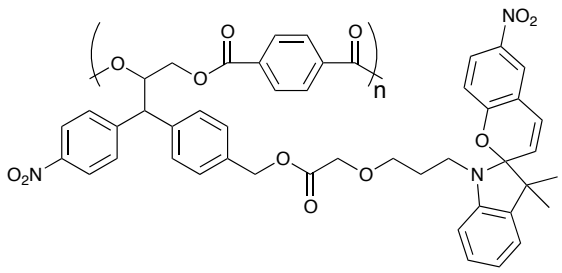	3	47

Table 5 Examples of the structure of modified monostyrenes

It is assumed that the area integrate software calculates areas with an error of ±5% (by analogy with NMR) and the error of the N/C ratio is ±10%. It was found that the XPS results confirmed the incorporation of the diaryldiazo units into the polymer surfaces. All chemically-improved samples showed the presence of nitrogen-type species from N1s signals at binding energies of 399 eV. The percentages of nitrogen on the surface of polystyrene **PSP5** and **PSP19** were 8.67 and 7.30, respectively.

From **Table 6**, It can be noted that the expected N/C atomic ratios of both modified substrates were lower than the found values. It was suggested that diazo molecules could be trapped inside polymer beads or reacted with the surface without extrusion of nitrogen gas. By contrast, polyethylene terephthalate **PETP5** and **PETP19** showed low percentages of nitrogen at 0.39% and 0.45%, respectively, indicating a poor level of modification of the polymeric sheet, which was consistent with the elemental analysis data. The XPS experiments of both **PSP17** and **PETP17** materials did not produce spectra that could be processed to calculate the amount of nitrogen on the surface.

Polymer	Structure	Expected N/C	Found N/C
PSP5	$C_{22}H_{19}NO_3$	0.045	0.122±0.012
PSP17	$C_{29}H_{30}N_2O_4$	0.069	not found
PSP19	$C_{45}H_{41}N_3O_8$	0.067	0.103±0.010
PETP5	$C_{24}H_{19}NO_7$	0.042	0.005±0.001
PETP17	$C_{31}H_{30}N_2O_8$	0.065	not found
PETP19	$C_{47}H_{41}N_3O_{12}$	0.064	0.005±0.001

Table 6 XPS data of modified polymers

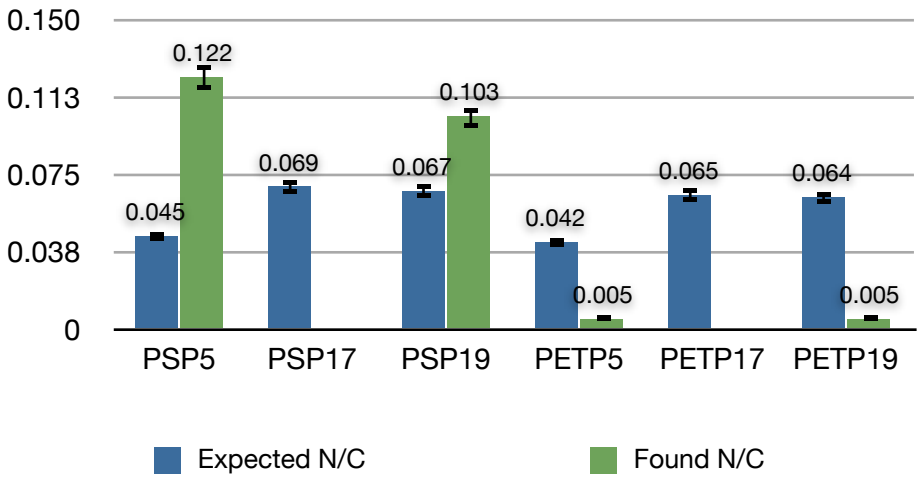

Figure 13 Expected and found N/C values

3.2.7 Photochromicity

As previous discussed, spiropyrans are molecular heterocyclic switches that can undergo reversible photoisomerisation between a spiropyran form and a merocyanine isomer upon irradiation with UV and/or visible light. The thermally stable spiropyran closed form is relatively hydrophobic and formed favourably in non-polar media,[57] whereas the metastable merocyanine opened form, which is either a zwitterionic ion at high pH or protonated and positively charged at neutral pH[91], has a much larger dipole moment that is highly hydrophilic and stabilised in polar

environments.[81] In addition, the merocyanine photoisomer, which has a characteristic absorption band in the visible wavelength region (500-700 nm),[92] shows an intense colouration as a result of the extended conjugation of the π-electronic delocalisation system, compared to the colourless spiropyran form with an orthogonal geometry between the two planar heterocycles, which prevents the extension of conjugation of the π-electronic systems, resulting in the lowest electronic transition in the near-UV wavelength region (λ<400 nm).[92]

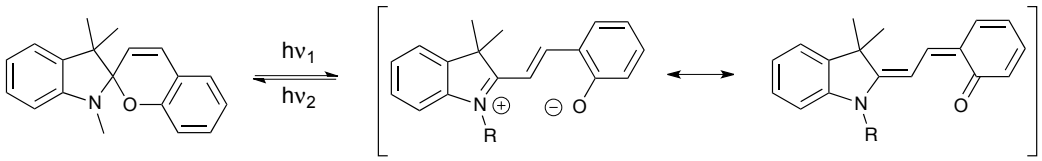

Figure 14 Light-induced spiropyran-merocyanine transformation

Previous work[57,81,85,87,92-95] has shown that the spirocyclic isomer can be interconverted to the merocyanine form by exposure to UV light, and when the irradiation stops, the system can convert reversibly to its ring-closed spiropyran form either thermally in the dark or via visible irradiation (**Figure 14**). In the case of thermal equilibration, typical reaction times are 2-3 hours,[94] while for photochemical isomerisation, reactions take place on a faster timescale.[85]

3.2.7.1 Colour Changes

Oxidative decomposition of photochromes during exposure to UV light results from oxygen in both free radical and singlet form.[96,97] Hence, the **PSP19** beads were placed in a sealed cuvette under nitrogen and were irradiated by a 365 nm portable source (**Figure 15**). However, the experiment with **PETP19** sheet was carried out under open atmosphere with the same light source.

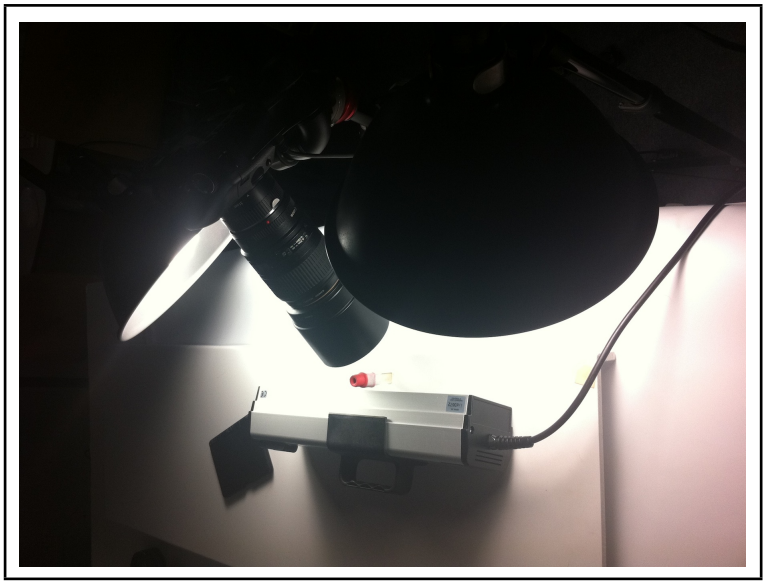

Figure 15 Photochromicity experiment set up

Both materials were kept in the dark, before being irradiated with UV light for 5 minutes, followed by visible light for 5 minutes. The effects of UV light are shown in **Table 7**, which shows how the polymers changed their colour when irradiated with different light sources.

When **PSP19** sample, whose initial colour was yellow under normal light or when kept inside an aluminium foil package, was irradiated with UV light, the material changed its colour to pale blue-green. This was then subsequently irradiated with visible light and the beads changed their colour back to 'original-yellow' as anticipated. The observation of colour was also quantified by a Digitalcolor Meter (Apple Inc, version 4.1) to determine the value of each colour component. The blue component was not significantly adjusted either by UV or visible light, while the red and green components marginally increased by around 15/255 units upon visible light irradiation, and were reset by UV light (**Figure 16**).

Polymer	Under normal light	Kept in the dark	At the end of UV irradiation for 5 minutes	At the end of visible irradiation for 5 minutes
PSP19	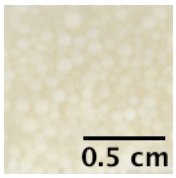	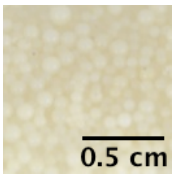	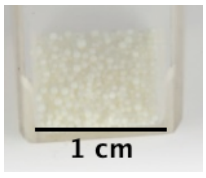	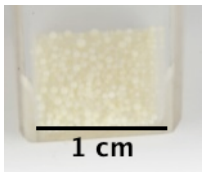
PETP19	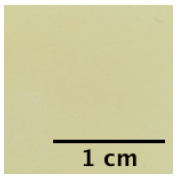	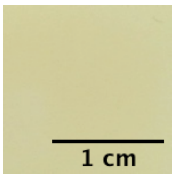	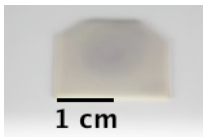	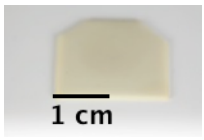

Table 7 Visual observation

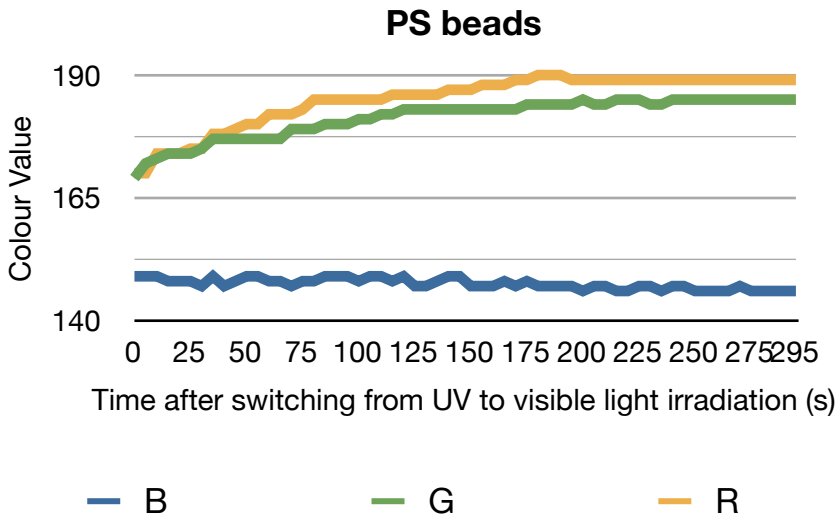

Figure 16 Colour components of **PSP19** beads.

With **PETP19** polymer, as can be seen from **Table 7**, the sheet was yellow under normal light; however, after being kept in the dark the material changed to pale orange, indicating partial isomerisation from the colourless spiropyran form to the intensely coloured merocyanine state. As the structure of the polyethylene terephtalate sheet is polar due to the presence of ester groups, it can then induce structural change of spiropyran moiety on the surface to the more polar merocyanine

or quinoidal isomers, and thereby, colouration.[58] After irradiation with UV light, the **PETP19** sample changed its colour to purple, which was then changed to yellow following visible light irradiation. Similar to **PSP19** material, the blue component of **PETP19** polymer was also not considerably adjusted either by UV or visible light as shown in **Figure 17**, while there was an increase in the red and green components by around 20/255 units upon visible light irradiation, which were reset by UV source.

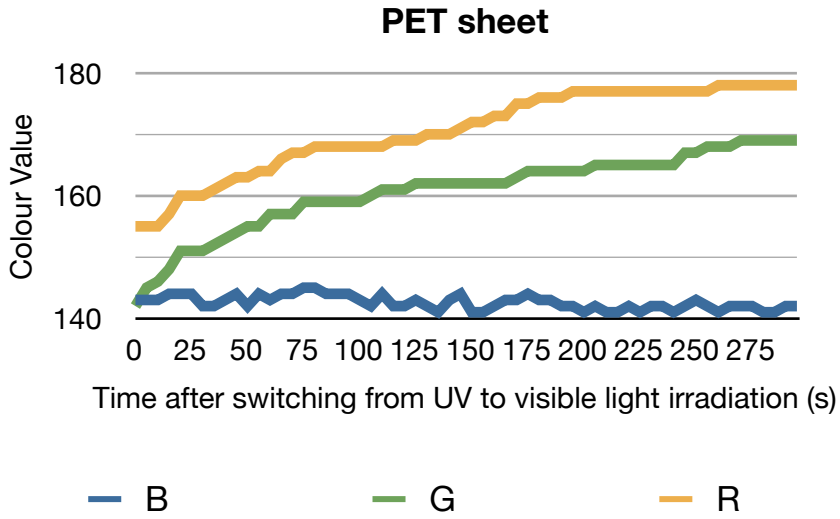

Figure 17 Colour components of **PETP19** sheet.

It was noted that from these experiments the colours of photochromic materials were faded due to highly intense light from the two visible light sources that were used in order to exclude environmental lights. When photochromic polymers were investigated for colour changes by using the same UV light source but with normal light in the laboratory as a visible light source, the colour changes of both **PSP19** and **PETP19** samples were more obvious as can be seen from **Table 8**.

These photoisomerisation processes could be repeated and the polymers still showed observable colour change. This colour alteration is consistent with the presence of spiropyran based systems on the surface of the polymers.

Polymer	At the end of UV irradiation for 5 minutes	At the end of visible irradiation for 5 minutes
PSP19	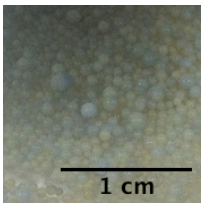	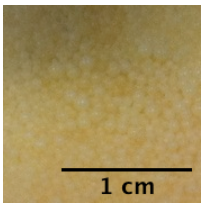
PETP19	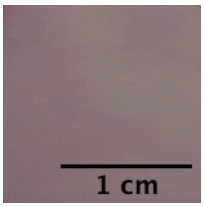	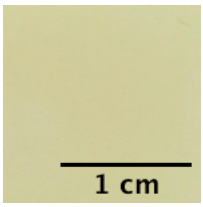

Table 8 Visual observation

3.2.7.2 Contact Angles

The contact angle is the angle between a solid surface and a droplet of liquid that settles on the surface. It can be used to quantify the wetability of a solid surface by a liquid. In order to determine the degree of hydrophilicity or hydrophobicity of the surface of modified polymers, water contact angles were measured.

The size and shape of modified polyethylene terephthalate sheets allowed direct investigation of contact angles, and gave the results shown in **Table 9**. Polymer **PETP5**, **PETP17**, **PETP19**, and blank PET sheet were treated with water droplets, with and without UV lamp irradiation. The contact angles were measured three times and the average values were recorded with standard deviations. It was found that the blank and **PETP5** materials, which were not modified with spiropyran-containing molecules, showed a slight change in contact angle of 0.30^{o} and 0.44^{o}, respectively, equal to 0.40% and 0.57% changes. However, although polymer **PETP17** was only physically coated at a low loading level, it showed relatively higher contact angle change of 1.48^{o} or 1.87%, and the effect of structural change of

photochromophores was significantly greater with polymeric **PETP19** sheet, with 3.61° or 4.45% change in contact angle after UV irradiation.

Polymer	Contact angle	After UV	Angle change	% Change
blank PET	80.70±0.05	80.38±0.02	0.30±0.07	0.40±0.09
PETP5	76.76±0.03	77.20±0.03	0.44±0.06	0.57±0.08
PETP17	79.04±0.02	77.56±0.04	1.48±0.06	1.87±0.08
PETP19	81.17±0.04	77.56±0.03	3.61±0.07	4.45±0.07

Table 9 Drop Shape analysis

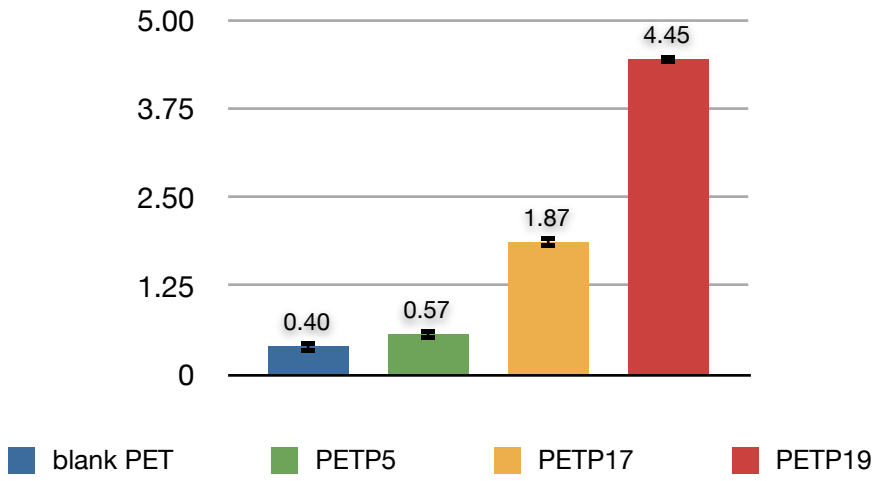

Figure 18 %Change of contact angles

This can be explained in terms of polarity change when the structure of the less polar closed spiropyran form was switched to more polar zwitterionic open merocyanine isomer upon UV photoconversion. As the polarity of the surface increased, the attraction between water molecules and modified PET surface becomes stronger, resulting in a change in shape of water droplets as the contact angles decreased.[82]

Polymer	Contact angle	After UV
blank PET	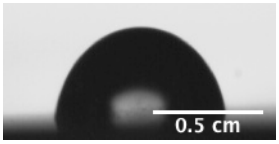	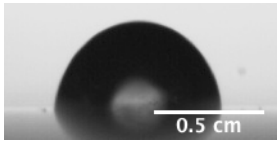
PETP5	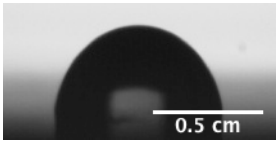	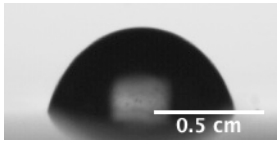
PETP17	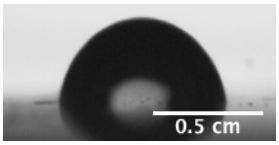	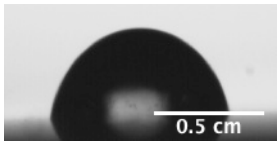
PETP19	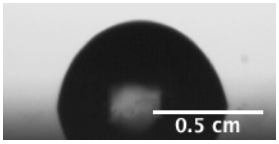	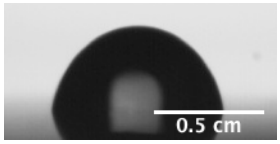

Table 10 Drop shape analysis

3.2.8 Conclusions

We have managed to chemically incorporate the desired spiropyran unit on the surface of polystyrene and polyethylene terephthalate by means of diaryldiazo modification via reactive carbenes. Elemental analysis and XPS data of the modified polymers confirmed the presence of nitrogen at a significant level, implying successful surface modification of polymeric materials, and ATR-IR spectroscopy revealed the existence of important functional groups on polystyrenes that were traced back to the corresponding diazo substances. The switchability of colours and hence structures of modified polymers was demonstrated to prove photochromicity. In addition, drop shape analysis exhibited contact angle and wettability changes upon phototransformation. This method of introduction of spiropyrans on the surface of polymers have several advantages over other techniques. Firstly, as demonstrated that the method could be apply on polymers which are inert or have low surface energy (e.g. polystyrenes), it was envisaged that the same procedure would be

capable of modifying a variety of materials. In addition, this technique does not required harsh reaction conditions to generate carbenes for the modification step, and the reactive intermediates could react with polymers without requirements for specific groups on the surface. This would be needed for other techniques such as self-assembled monolayers (SAMs) by chemisorption.[98,99] When spiropyran carbenes interacted with polymers and form covalent bonds, the spiropyran groups were be tethered with the surface, and thus, would be more resistant to degradation by extensive contacts with aqueous or organic solvents as compared to spiropyran films obtained via solution coatings. However, several drawbacks of this approach have been observed. The synthesis of spiropyran diazo compound involved many steps with low overall yield, and the product could not be easily purified as soon as a diazo functional group was formed. Furthermore, in order to assume monolayer formation on the surface of polymers by solution coating prior to generation of carbenes, a dilute solution of spiropyran diazo compound was needed. And this led to low loading levels of spiropyran on the polymers, especially when materials with small surface areas such as PET sheets were used. Nonetheless, the photochromicity of both modified polystyrene beads and PET sheets synthesised by this method was illustrated with observable colouration/decolouration and contact angle changes. It was noted that other techniques for investigation of photochromic properties should be performed for future work in order to quantify the observations as a result of structural change of spiropyrans upon irradiation.

Chapter 4 Bioactivity

4.1 Introduction

4.1.1 Bactericidal Activity and Immobilisation

In recent years, the construction and study of antimicrobial polymers has been of interest, not least to help control the spread of infection. Such materials need to be stable, non-corrosive, reusable, resistant to water and common organic solvents, and able to be fabricated by various techniques.[100,101] Examples are biocidal photocatalytic anti-infective TiO_2 nanoparticles embedded within a polyvinyl shell,[102] an amino-functionalised polynorbornene film used as a bactericide against *Escherichia coli* and *Staphylococcus aureus*,[103] a thermally-stable antimicrobial alkylated/protonated cysteamine polyisoprene,[104] a polysiloxane-based polyurethane film having quaternary ammonium groups as bioactive pendants active against *Escherichia coli*,[105] a biocidal polystyrene containing *N*-halamine residues for treatment of contaminated water and air,[106] and a halogenated uramil-derived polyurethane with an *N*-halamine moiety for use in water filters.[107,108]

The work outlined in **Chapter 2** indicated that modified polystyrenes tethered with a pyridine ring are capable of coordinating and releasing metal complex molecules, and also in **Chapter 3** indicated that spiropyran derivatives in their merocyanine form can act as chemical sensors to detect free ions and reversibly unbind these ions upon irradiation, it was envisaged that polystyrenes functionalised with either pyridine moiety or spiropyran units might be suitable for immobilisation and delivery of bioactive species.

Generally, techniques to immobilise free particles to the surface of polymeric materials are via covalent bonds, ionic attractions, and receptor links (**Figure 1**).

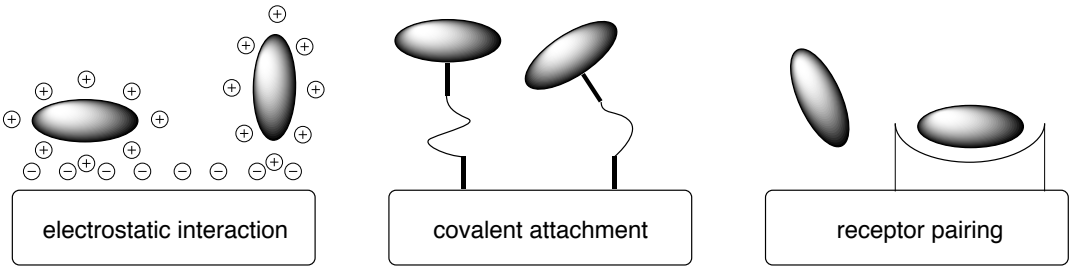

Figure 1 Immobilisation mechanisms

The pairing of ligand-receptor requires specific structures in both units, requiring careful design and construction, while covalent attachments might be expected to have the advantage of providing more stable and stronger bonds between antimicrobial agents and the polymer surface, leading to maximisation of loading levels on the surface. Electrostatic interactions are beneficial for drug delivery applications, offering rapid trapping and transfer of bioactive fragments.[1,2,9,15] Of interest to us was the use of a combination of these interactions i.e. covalent bonds, coordinations/chelations, electrostatic attractions, and van der Waals forces to 'tether' bioactive ions/molecules on the surface of pre-activated polymers containing functional groups suitable for attachment processes. The application of the carbene surface modification protocol for the introduction of such functionality in the context of drug delivery forms the basis of the work described in this chapter, with a focus on the degrees of activities rather than the mechanisms of immobilisation.

4.1.2 Aims of the Project

Modified polymers **PSM4**, **PSM27**, and **PSP19** were chosen to assess their ability to carry and release bioactive molecules, thereby imparting bioactivity to the polymer in bioassay experiments. Their structures are shown in **Figure 2**.

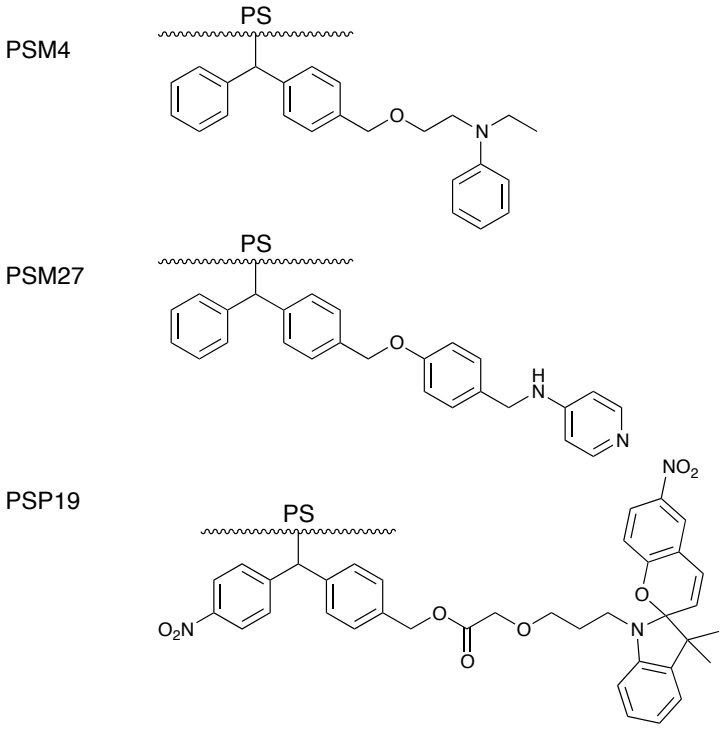

Figure 2 Structures of modified polymers

Bioactive species that were chosen for deposition on the surface of polymers were penicillin V and silver ions, well known for their antibacterial activity, In addition, some selected organic molecules recently made within the group that showed high antibacterial activities, namely B066 (MW 407.50 g/mol, made by Benjamin Tan), G243 and G503 (MW 477.63 and 346.42 g/mol respectively, synthesised by Yongchul Jeong), were examined. The structures of these organic compounds are shown in **Figure 3**.

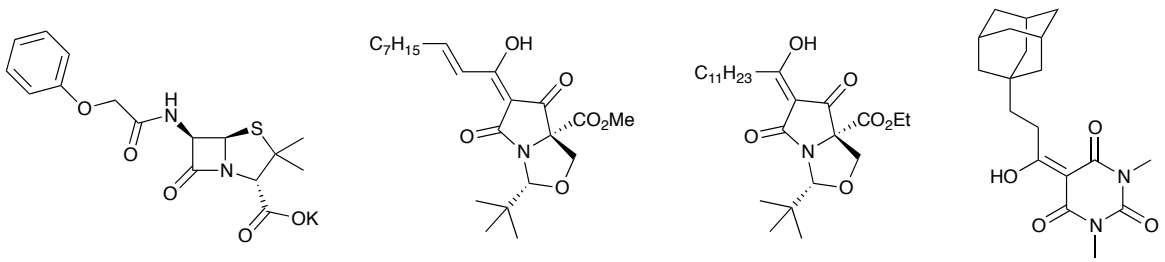

Penicillin V B066 G243 G503

Figure 3 Structures of bioactive organic molecules

Penicillin V was chosen due to its highly effective antimicrobial activity especially against Gram-positive *Straphylococcus aureus* bacteria.[109,110] Silver ions were selected as an example of inorganic salts which has been extensively studied and used as antimicrobial reagent for a range of Gram-negative and Gram-positive organisms, for instance, silver-coated medical devices,[111-114] chitosan-based silver-loaded wound dressing,[115] and silver-catalysed polymerisation for bactericidal wound-healing gels.[116] Functionalised materials coated with bioactive species would be examined for the ability to inhibit Gram-positive *Staphylococcus aureus* and Gram-negative *Escherichia coli*, both available within Department of Chemistry, University of Oxford. The bioactive polymers would also be characterised by elemental analysis in order to calculate the amount of bioactive species that display activities and hence the efficiency, and ATR-IR to confirm the presence of bioactive organic molecules.

4.2 Results and Discussion

4.2.1 Experiment 1: Tests

Modified polymers **PSM4** and **PSM27**, prepared as described in **Chapters 2**, together with blank polystyrene were treated with a solution of silver nitrate (2 equivalents) to give the corresponding adducts **PSM4Ag+**, **PSM27Ag+**, and **PS XAD Ag+**. Half of materials **PSM27Ag+** was reacted with benzaldehyde (2 equivalents) in the presence of ammonia (10 equivalents) at 70^{o}C to reduce the metal ion to a solid silver coating on the surface, giving the beads **PSM27Ag**.

To polymers **PSP19**, prepared as described in **Chapters 3**, were added silver ions by the same procedure, however, as two separate batches, one being irradiated with UV and the other under normal fluorescent light, in order to observe the effect of

light-induced polarity change, generating materials **PSP19Ag+UV** and **PSP19Ag +VIS**. Polymers **PSP19** were also tested with a Dulbecco's phosphate buffered saline (PBS) solution of penicillin V (2 equivalents) to produce polymer **PSP19PenV**.

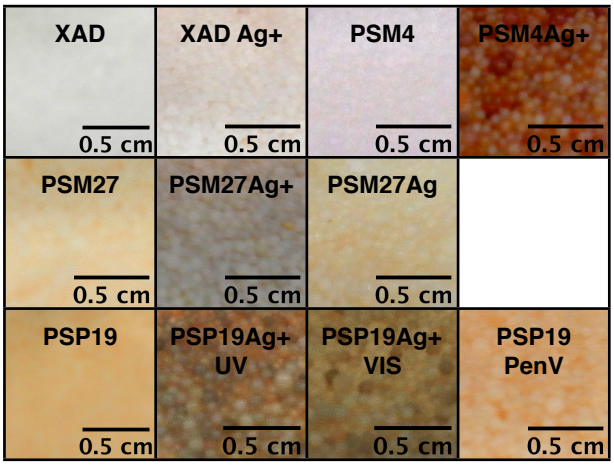

Figure 4 Visual polymer appearance

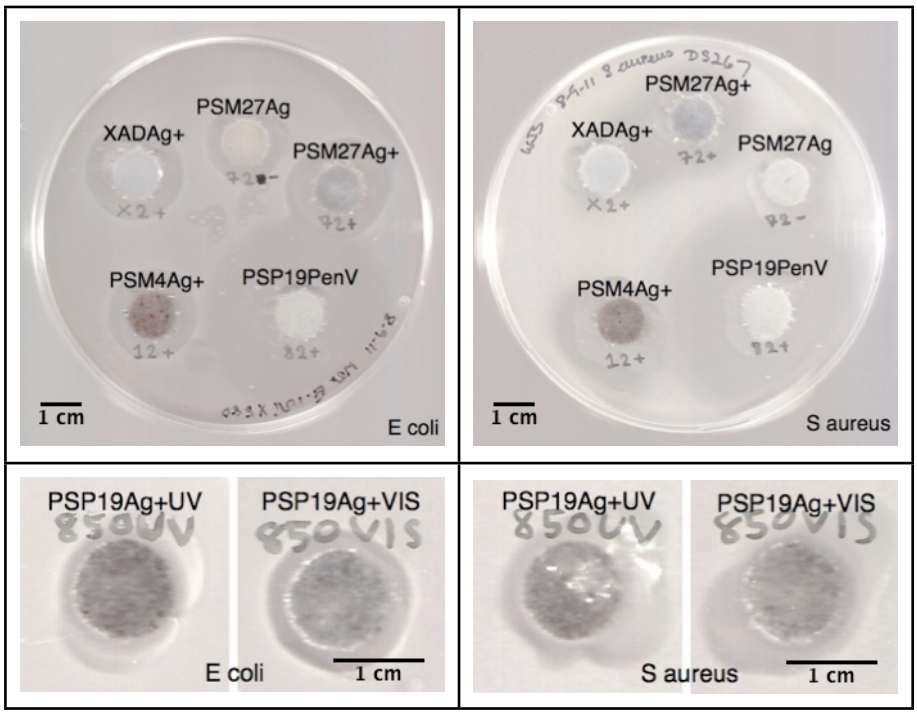

Figure 5 Bioassay plates of Experiment 1

The antibacterial activity against *S. aureus* and *E. coli* was determined with 50 mg of each sample; the appearance of the incubation plates are shown in **Figure 5**

and the values of the inhibition zones are given in **Table 1**. All modified polymers with silver ions on the surface including the blank PS XAD exhibited bioactivity against *S. aureus* and *E. coli*, in terms of inhibition zone ranging from 10-20 mm and 12-23 mm, respectively. Calibration of these plates against Cephalosporin C gave a linear concentration-activity plot, and enabled calculation of the equivalent activity of Cephalosporin C for a given zone size. The calibration plot was assumed to have ±5% error estimates and the inhibition zone size was measured to the nearest 0.5 mm. As the diameter of the antimicrobial clear zones around each well was measured twice, the average values were recorded with an error estimate of ±1 mm.

S. aureus	Inhibition zone diameter (mm)	Ceph C (nmol)	E. coli	Inhibition zone diameter (mm)	Ceph C (nmol)
XADAg+	19±1	$(2.6\pm0.3)\times10^2$	**XADAg+**	21±1	1.3±0.1
PSM4Ag+	18±1	$(2.1\pm0.2)\times10^2$	**PSM4Ag+**	19±1	1.0±0.1
PSM27Ag+	20±1	$(3.1\pm0.3)\times10^2$	**PSM27Ag+**	23±1	1.8±0.2
PSM27Ag	15±1	$(1.2\pm0.1)\times10^2$	**PSM27Ag**	16±1	0.6±0.1
PSP19Ag+VIS	10±1	34±5	**PSP19Ag+VIS**	12±1	0.9±0.1
PSP19Ag+UV	11±1	40±6	**PSP19Ag+UV**	14±1	1.1±0.1
PSP19penV	41±1	$(8.4\pm0.6)\times10^3$	**PSP19penV**	39±1	32±2

Table 1 Bioassay results of Experiment 1

Against *S. aureus,* the bioactivity of **PSM27Ag+** was the highest except for sample **PSP19penV**, equivalent to 310 nmol of Ceph C as compared to 260 nmol and 210 nmol of Ceph C from the blank PS XAD and the control **PSM4Ag+**, respectively. Unfortunately, **PSM27Ag** showed a relatively low activity equal to 120 nmol of Ceph C which was less than half of that of the same material before reduction by benzaldehyde. Reasons for this lower activity might be because of the low mobility of silver metal as compared to silver ions, as well as the coating the surface with heavy metal resulting in a blockage of active species inside porous polystyrene beads. Noteworthy was that **PSP19Ag+UV** and **PSP19Ag+VIS**

displayed considerably lower activity at 34 nmol and 40 nmol of Ceph C, respectively.

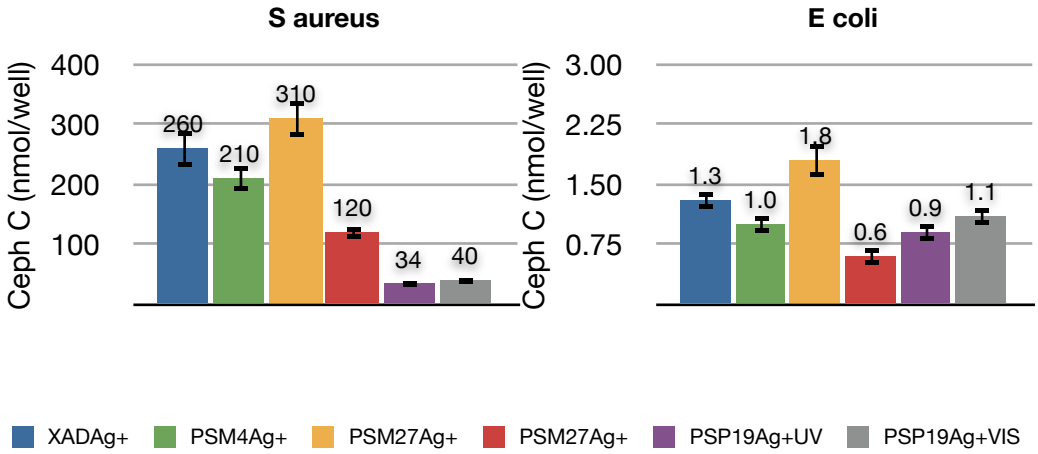

Figure 6 Bioassay results of Experiment 1

With *E. coli*, except for sample **PSP19penV**, incubation experiments **PSM27Ag+** also showed the highest bioactivity of 1.8 nmol of Ceph C, slightly higher than the blank PS XAD and moderately higher than the control **PSM4Ag+**. Similarly, **PSM27Ag** was observed to yield a relatively low activity of 0.6 nmol of Ceph C. **PSP19Ag+UV** and **PSP19Ag+VIS**, however, exhibited significant bioactivities of 0.9 nmol and 1.1 nmol of Ceph C, similar to 1.0 nmol of Ceph C from **PSM4Ag+** beads.

Regarding polymers with penicillin V as bactericidal materials, the bioactivity of **PSP19penV** was found to be exceptionally higher than those of polymers modified with silver ions. The activities against *S. aureus* and *E. coli* of **PSP19penV** were 41 mm and 39 mm in zone of inhibition, equivalent to 8.6×10^4 nmol and 32 nmol of Ceph C, respectively. This suggested that modified polymers **PSP19**, although displaying low activity when coated with silver species, were capable of showing significant results after the introduction of potent bioactive molecules. Thus, other organic compounds were chosen to extend this study. The large zone sizes of these results were obtained as the upper limit of diffusion rate in the bioassay, therefore, dilutions were needed in the following experiments.

4.2.2 Experiment 2: Organic Molecules

The antibacterial activities against *S. aureus* and *E. coli* were demonstrated with 50 mg of each polymer sample. Functionalised polymers **PSM27** and blank PS XAD were separately soaked with 1 equivalent (4.3 mmol) of bioactive compounds, namely penicillin V, B066, G243, and G503. Modified materials **PSP19** and blank PS XAD were also separately soaked with 1 equivalent (1.2 mmol) of these bioactive compounds. The calibration plot was assumed to have ±5% error estimates and the diameter of the antimicrobial clear zones was measured twice. The average values were recorded with an error estimate of ±1 mm. The values obtained are given in **Table 2**.

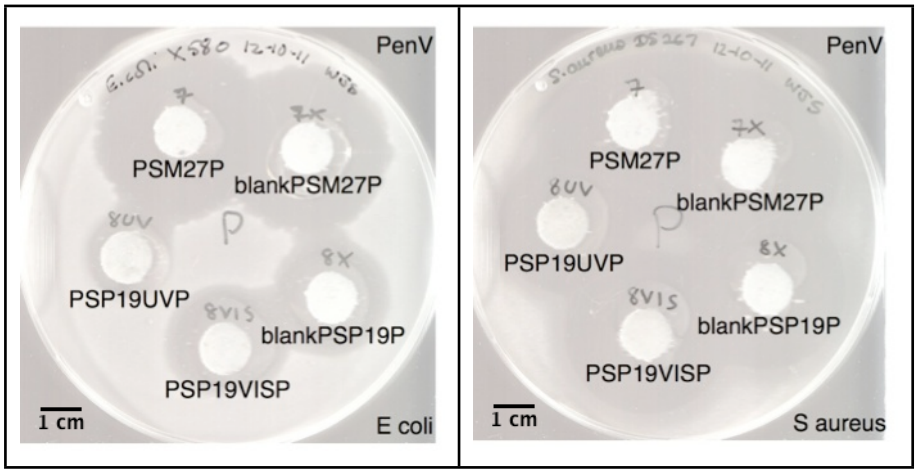

Figure 7 Bioassay plates of Experiment 2

Except for modified materials treated with penicillin V (**PSM27P**, **PSP19UVP**, and **PSP19VISP**) for which the scans of incubated plates are shown in **Figure 7**, all the others did not display bioactivity against either *S. aureus* or *E. coli*. This could be the result from low loading levels on the surface of PS beads and/or low activities of each individual molecules. However, earlier work had shown each of these compounds to be highly active in solution; the minimum inhibitory concentration

(MIC) against *S. aureus* is 8 μg/ml (B066), 1 μg/ml (G243), and 2 μg/ml (G503), and the MIC against *E. coli* is >64 μg/ml for all three compounds.

S. aureus	Inhibition zone diameter (mm)	Ceph C (nmol)	E. coli	Inhibition zone diameter (mm)	Ceph C (nmol)
PSP19UVP	24±1	$(4.1\pm0.4)\times10^2$	**PSP19UVP**	13±1	1.0±0.1
PSP19VISP	32±1	$(1.7\pm0.1)\times10^3$	**PSP19VISP**	21±1	2.9±0.3
blankPSP19P	31±1	$(1.4\pm0.1)\times10^3$	**blankPSP19P**	21±1	2.9±0.3
PSM27P	37±1	$(4.1\pm0.3)\times10^3$	**PSM27P**	34±1	16±1
blankPSM27P	37±1	$(4.0\pm0.3)\times10^3$	**blankPSM27P**	34±1	16±1

Table 2 Bioassay results of Experiment 2

From **Table 2,** it can be seen that in general **PSM27P** beads exhibited substantially higher activities against *S. aureus* (4100 nmol of Ceph C) and *E. coli* (16 nmol of Ceph C) than both **PSP19UVP** and **PSP19VISP**. Nonetheless, the bioactivities of **PSM27P** were close to samples **blankPSM27P** against *S. aureus* (4000 nmol of Ceph C) and *E. coli* (16 nmol of Ceph C). This suggested that the amount of penicillin V on **PSM27P** was still too high to obtain reliable data, hence, more dilutions will be needed in future experiments.

By comparison between the activities of **PSP19UVP** and **PSP19VISP**, it was shown that **PSP19UVP** gave considerably lower activities against *S. aureus* (410 nmol of Ceph C) and *E. coli* (1.0 nmol of Ceph C) than those of **PSP19VISP** (1700 nmol and 2.9 nmol of Ceph C, respectively), and also lower activity than sample **blankPSP19P**. This might be due to the fact that the structure of **PSP19**, as it becomes interchanged from the more hydrophobic spiropyran form to the more hydrophilic merocyanine state upon UV irradiation, has weaker interactions with

penicillin V molecules, thus, **PSP19** in its highly polar form is less efficient in adsorbing penicillin V units.

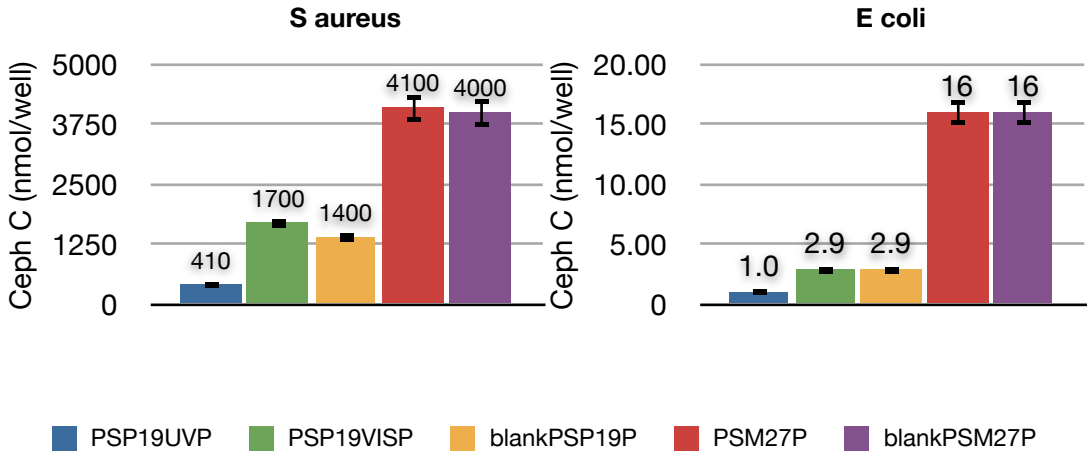

Figure 8 Bioassay results of Experiment 2

It was noted that sample **blankPSM27P** showed much higher activity than that of sample **blankPSP19P**, resulting from the different ligand and penicillin V loading levels on the different polymers.

Modified **PET163** sheets and blank PET were also treated with bioactive organic molecules by a similar approach. However, none of these samples displayed activity against either *S. aureus* or *E. coli*, possibly due to small surface areas on the sheets and hence low degree of adsorption, as compared to the much higher activities shown by the PS XAD systems.

4.2.3 Experiment 3: Concentrations

As previously mentioned, the activities of modified PS beads with penicillin V were too high, causing the inhibition zone sizes in bioassay experiments to be off the diffusion limit. In order to attenuate this activity, experiments in which bioactive **PSM27P** and **PSP19P** beads were mixed with blank PS XAD in the ratio 1:4, giving

PSM27P5, **PSP19UVP5**, and **PSP19VISP5**. Then 50 mg of the mixture of each sample were used. Sample **PSM27P5** and blank PS XAD were soaked with 1 equivalent (0.86 mmol) of penicillin V while sample **PSP19UV5**, **PSPVISP5**, and blank PS XAD were soaked with 1 equivalent (0.24 mmol) of penicillin V. The calibration plot was assumed to have ±5% error estimates and the diameter of the antimicrobial clear zones was measured twice. The average values were recorded with an error estimate of ±1 mm. The results are demonstrated in **Table 3**.

The activities against *S. aureus* showed that **PSM27P5** still exhibited a large inhibition zone of 36 mm even at lower concentration, equivalent to 3400 nmol of Ceph C which is significantly higher than the value of 1700 nmol of Ceph C for sample **blankPSM27P5**. This implies that the structure of PS XAD tethered with a molecule containing a pyridine moiety has a higher efficiency in catching and releasing bioactive molecules than blank PS XAD. This was also confirmed from the activities against *E. coli*, for which **PSM27P5** displayed bioactivity at 3.3 nmol of Ceph C while sample **blankPSM27P5** showed activity at 1.3 nmol of Ceph C, less than half of that of **PSM27P5**.

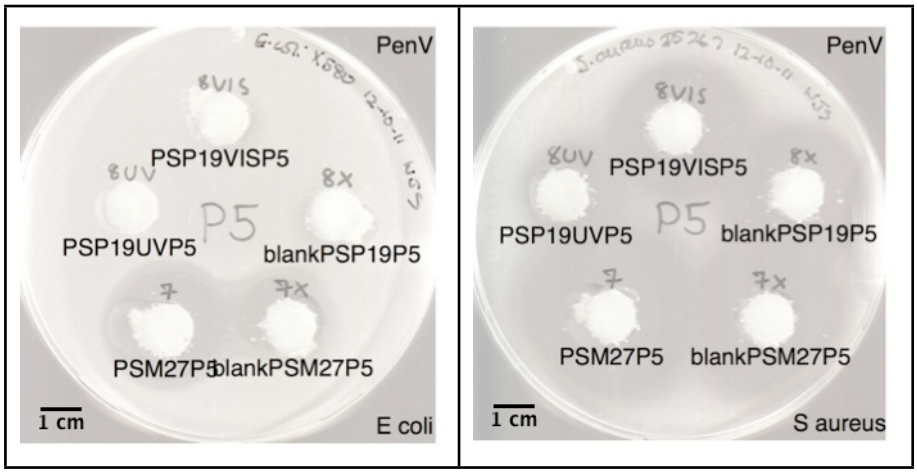

Figure 9 Bioassay plates of Experiment 3

S. aureus	Inhibition zone diameter (mm)	Ceph C (nmol)	E. coli	Inhibition zone diameter (mm)	Ceph C (nmol)
PSP19UVP5	20±1	$(2.0\pm0.2)\times10^2$	**PSP19UVP5**	n/a	n/a
PSP19VISP5	27±1	$(6.9\pm0.6)\times10^2$	**PSP19VISP5**	n/a	n/a
blankPSP19P5	28±1	$(8.3\pm0.7)\times10^2$	**blankPSP19P5**	n/a	n/a
PSM27P5	36±1	$(3.4\pm0.3)\times10^3$	**PSM27P5**	22±1	3.3±0.3
blankPSM27P5	32±1	$(1.7\pm0.1)\times10^3$	**blankPSM27P5**	15±1	1.3±0.2

Table 3 Bioassay results of Experiment 3

With **PSP19** materials, similar to Experiment 2, **PSP19UVP5** and **PSP19VISP5** exhibited much lower activities against *S.aureus*, at 200 nmol and 690 nmol of Ceph C respectively, than **PSM27P5** at 3400 nmol of Ceph C. This also confirmed the result in Experiment 2 that **PSP19** in its merocyanine form after UV irradiation was less capable of trapping penicillin V than the more hydrophobic spiropyran isomer. It was noted that samples **PSP19UVP5**, **PSP19VISP5**, and **blankPSP19P5** showed no activities against *E. coli*.

It was noted that sample **blankPSM27P5** showed much higher activity than that of **blankPSP19P5**, resulting from the different ligand and penicillin V loading levels on the different polymers.

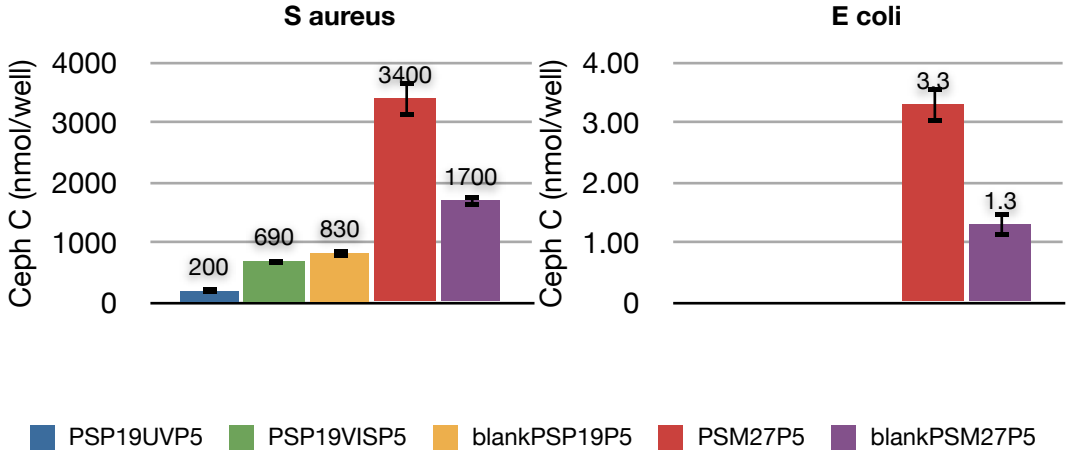

Figure 10 Bioassay results of Experiment 3

4.2.4 Experiment 4: Solvents

From all of the previous experiments, molten agar was used to seal the polymer into the wells of bioassay plates. This was to ensure that the polymeric beads were fully immobilised inside the wells so that the bioactive species resting on the surface of modified polymers were able to diffuse through the medium to bacteria-seeded agar. It was envisaged that using an aqueous/organic solvent would provide the same effect.

The antibacterial activities against *S. aureus* and *E. coli* were demonstrated with 25 mg of each polymer sample suspended in a mixture of DMSO and water (7:3), which was used as a medium to carry out the same experiment with compound B066. Functionalised polymers **PSM27** and blank PS XAD were separately soaked with 1 equivalent (2.2 mmol) of penicillin V, B066, G243, and G503. Modified materials **PSP19** and blank PS XAD were also separately soaked with 1 equivalent (0.6 mmol) of these bioactive compounds. The calibration plot was assumed to have ±5% error estimates and the diameter of the antimicrobial clear zones was measured twice. The average values were recorded with an error estimate of ±1 mm.

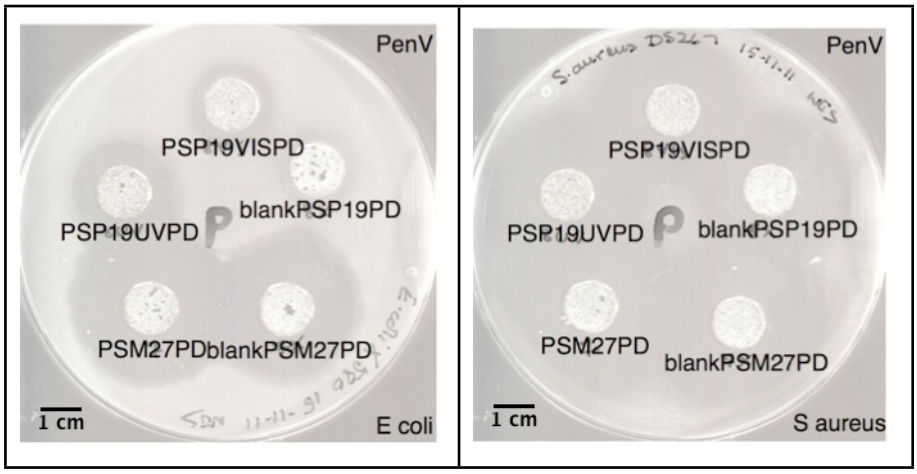

Figure 11 Bioassay plates of Experiment 4

The results observed were similar to those from Experiment 2 that only modified materials treated with penicillin V (**PSM27PD**, **PSP19UVPD**, and **PSP19VISPD**), showed activity, with all the others being inactive against either *S. aureus* or *E. coli*. The values obtained are given in **Table 4**.

S. aureus	Inhibition zone diameter (mm)	Ceph C (nmol)	E. coli	Inhibition zone diameter (mm)	Ceph C (nmol)
PSP19UVPD	32±1	(1.4±0.1)x10^3	**PSP19UVPD**	20±1	2.6±0.3
PSP19VISPD	32±1	(1.4±0.1)x10^3	**PSP19VISPD**	17±1	1.6±0.2
blankPSP19PD	30±1	(1.1±0.1)x10^3	**blankPSP19PD**	15±1	1.2±0.1
PSM27PD	37±1	(3.0±0.2)x10^3	**PSM27PD**	32±1	17±1
blankPSM27PD	36±1	(2.6±0.2)x10^3	**blankPSM27PD**	28±1	9.1±0.8

Table 4 Bioassay results of Experiment 4

PSM27PD exhibited the highest activities at 3000 nmol of Ceph C against *S. aureus* and at 17 nmol of Ceph C against *E. coli*, higher than sample **blankPSM27PD** at 2600 nmol (8% error) and 9.1 nmol of Ceph C, respectively. Both **PSP19UVPD** and **PSP19VISPD** displayed bioactivities at 1400 nmol of Ceph C against *S. aureus* and around 1.6-2.6 nmol of Ceph C against *E. coli*, substantially lower than those of **PSM27PD** samples.

It was noted that sample **blankPSM27PD** showed much higher activity than that of sample **blankPSP19PD**, resulting from the different ligand and penicillin V loading levels on the different polymers.

This experiment confirmed that both molten agar and DMSO/water could be used as media for bioactive molecules to diffuse from the surface of the polymeric solids outwards. Moreover, both media could also be conveniently applied to the bioassay wells for the purpose of handling the polymer. Comparison of diffusion rates

and efficiency could be achieved by controlling the amount of functionalised polymers and concentrations of bioactive compounds.

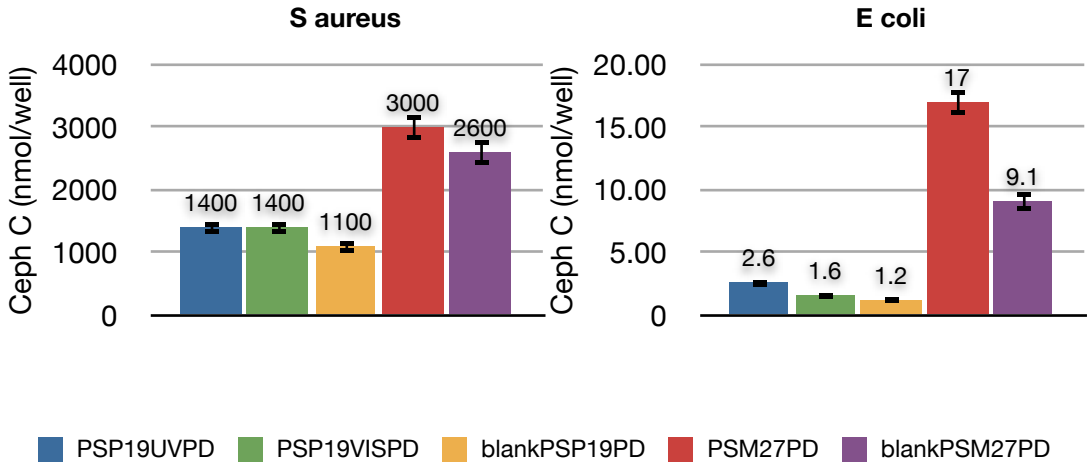

Figure 12 Bioassay results of Experiment 4

4.2.5 Experiment 5: Penicillin V

In order to calculate the amount of penicillin V that was released from modified polymers in previous experiments, solutions of penicillin V in both PBS and DMSO/ water were prepared for bioassay tests against *S. aureus* and *E. coli*, with concentrations of 4.0, 2.0, 1.0, 0.5, 0.25, 0.125, 6.25×10^{-2}, 3.125×10^{-2}, 1.56×10^{-2}, 7.81×10^{-3}, 5.86×10^{-3}, 4.88×10^{-3}, 3.91×10^{-3}, 2.93×10^{-3}, and 1.95×10^{-3} mg/mL. The calibration plot was assumed to have ±5% error estimates and the diameter of the antimicrobial clear zones was measured twice. The average values were recorded with an error estimate of ±1 mm.

From **Figure 13**, it can be seen that penicillin V had extremely high activity against *S. aureus*. With the most diluted solutions of penicillin V, the zones of inhibition were still at the diffusion limit, hence, reliable inhibition zone diameters could not be measured. However, the treatments against *E. coli* produced readable

results in which the data were obtained from samples with concentrations equal to and less than 7.81×10^{-3} mg/mL as shown in **Table 5**.

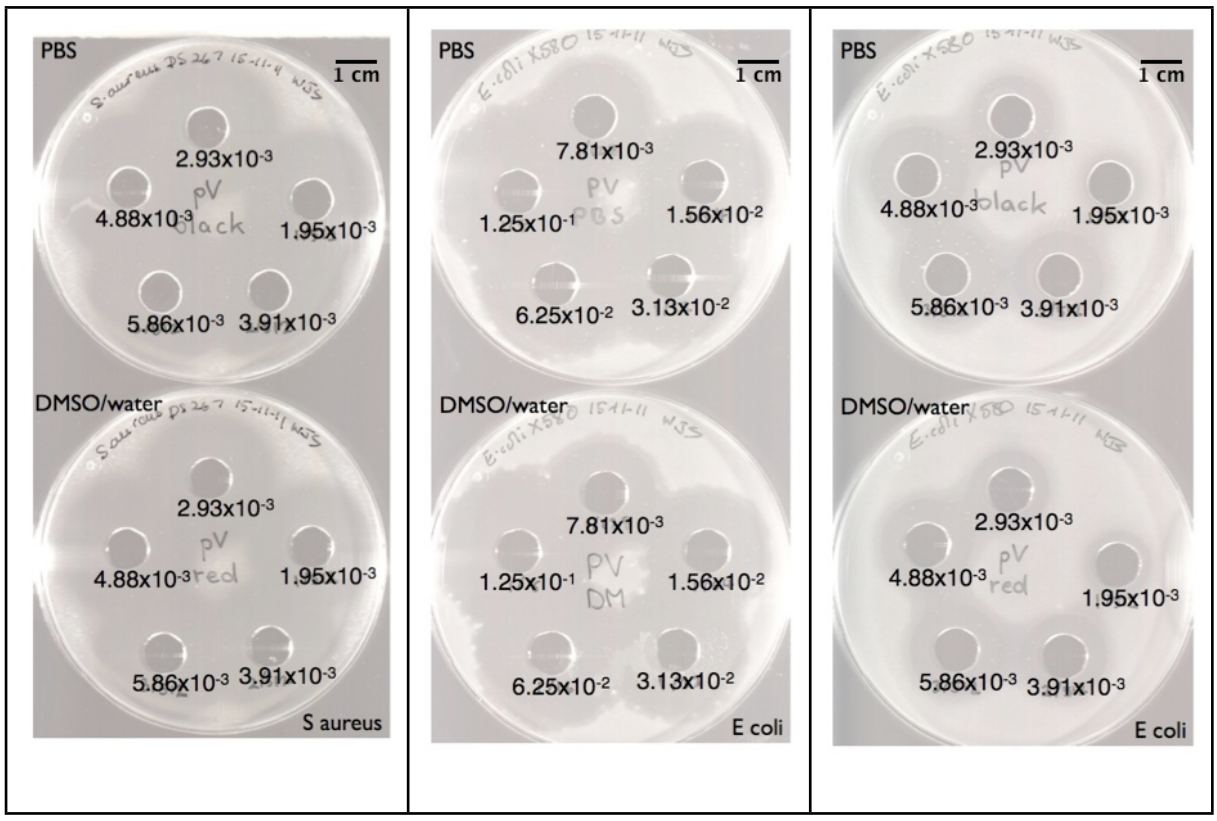

Figure 13 Bioassay plates of Experiment 5

Concentrations (mg/mL)	From PBS solutions			From DMSO/water solutions		
	Inhibition zone diameter (mm)	log Ceph C	Ceph C (nmol)	Inhibition zone diameter (mm)	log Ceph C	Ceph C (nmol)
7.81×10^{-3}	27±1	0.89±0.08	7.8±0.7	25±1	0.76±0.07	5.7±0.5
5.86×10^{-3}	23±1	0.62±0.06	4.2±0.4	22±1	0.55±0.05	3.6±0.3
4.88×10^{-3}	23±1	0.62±0.06	4.2±0.4	21±1	0.48±0.05	3.0±0.3
3.91×10^{-3}	20±1	0.42±0.04	2.6±0.3	20±1	0.42±0.04	2.6±0.3
2.93×10^{-3}	19±1	0.35±0.04	2.2±0.2	18±1	0.28±0.03	1.9±0.2
1.95×10^{-3}	13±1	-0.06±0.01	0.9±0.1	15±1	0.08±0.01	1.2±0.1

Table 5 Bioassay against *E. coli* of Experiment 5

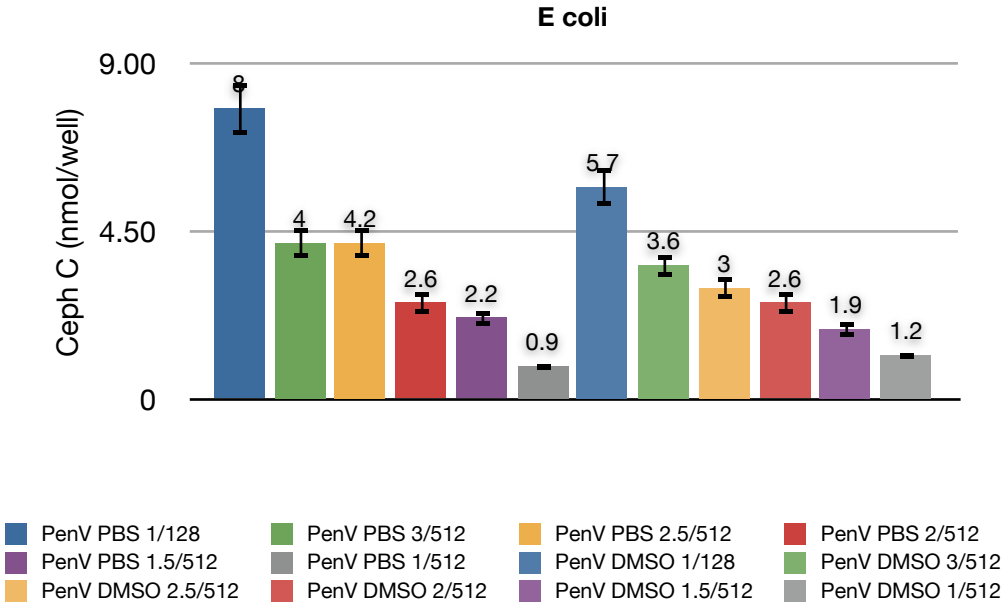

Figure 14 Bioassay against *E coli* of Experiment 5

Plots of concentrations of penicillin V solutions against concentrations of Ceph C were performed, generating linear correlations between the two variables. The equations derived from the experiments with PBS solutions and DMSO/water mixtures were (y) = 1105.9(x) - 1.39 and (y) = 732.89(x) - 0.34, respectively (**Figure 15**).

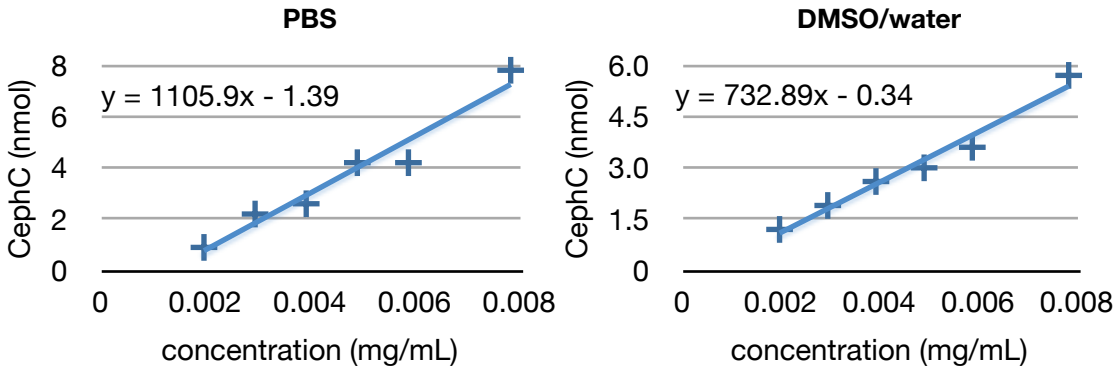

Figure 15 Linear correlations between concentrations of penicillin V and concentrations of Ceph C from Bioassay against *E coli*

The bioactivities from Experiment 2, 3, and 4 were transformed from nmol of Ceph C to nmol of Ceph C per mg of PS that was used in each well. The equation obtained from the experiment with PBS solutions was chosen as an example to calculate the equivalents of penicillin V that inhibited bacteria cell growth upon incubation, and the results were shown in **Table 6**.

Data from experiment	Samples	Ceph C (nmol/mgPS)	PenV (mg/mL)
2	**PSP19UVP**	$(2.0\pm0.3)\times10^{-2}$	$(1.3\pm0.2)\times10^{-3}$
	PSP19VISP	$(5.8\pm0.6)\times10^{-2}$	$(1.3\pm0.1)\times10^{-3}$
	blankPSP19P	$(5.8\pm0.6)\times10^{-2}$	$(1.3\pm0.1)\times10^{-3}$
	PSM27P	$(3.3\pm0.3)\times10^{-1}$	$(1.6\pm0.1)\times10^{-3}$
	blankPSM27P	$(3.3\pm0.3)\times10^{-1}$	$(1.6\pm0.1)\times10^{-3}$
3	**PSP19UVP5**	n/a	n/a
	PSP19VISP5	n/a	n/a
	blankPSP19P5	n/a	n/a
	PSM27P5	$(3.3\pm0.3)\times10^{-1}$	$(1.6\pm0.1)\times10^{-3}$
	blankPSM27P5	$(1.3\pm0.2)\times10^{-1}$	$(1.4\pm0.2)\times10^{-3}$
4	**PSP19UVPD**	$(1.0\pm0.1)\times10^{-1}$	$(1.4\pm0.1)\times10^{-3}$
	PSP19VISPD	$(6.5\pm0.7)\times10^{-2}$	$(1.3\pm0.2)\times10^{-3}$
	blankPSP19PD	$(4.8\pm0.6)\times10^{-2}$	$(1.3\pm0.2)\times10^{-3}$
	PSM27PD	$(6.8\pm0.6)\times10^{-1}$	$(1.9\pm0.2)\times10^{-3}$
	blankPSM27PD	$(3.7\pm0.3)\times10^{-1}$	$(1.6\pm0.1)\times10^{-3}$

Table 6 Equivalents of penicillin V that inhibited *E coli* cell growth

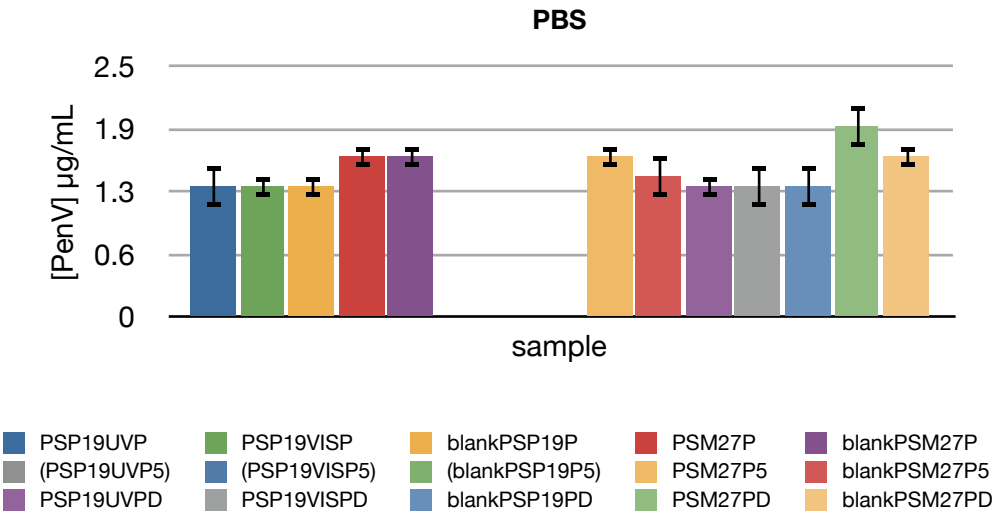

Figure 16 Equivalents of penicillin V that inhibited *E coli* cell growth

It was shown that the amounts of penicillin V displaying activities on **PSP19UV** and **PSP19VIS** materials were approximately at 1.3 μg/mL, while those on the surface of **PSM27** polymers were slightly higher, at 1.6 μg/mL. It was noted that **PSM27PD**, from Experiment 4 applying DMSO/water as a medium for diffusion, exhibited highest bioactivity, equivalent to 19 μg of penicillin V per mg of modified PS beads. Three samples, namely **PSP19UVP5**, **PSP19VISP5**, blank for **PSP19P5** from Experiment 3, did not provide observable data as previously discussed.

4.2.6 Efficiency

In order to calculate the efficiency of modified polymers in performing bioactivity against bacteria, the total amounts of active species on the surface of functionalised materials were needed. Not only samples treated with penicillin V but also samples soaked with compounds B066, G503, and G243 were characterised by elemental analysis to acquire the loading data as summarised in **Table 7**.

Samples	% N	Loading (mmol/g)	Samples	% N	Loading (mmol/g)
PSP19UVPenV	0.32±0.03	0.046±0.005	PSP19UVG243	0.34±0.03	0.049±0.005
PSP19VISPenV	0.35±0.04	0.050±0.005	PSP19VISG243	0.35±0.04	0.050±0.005
blankPSP19PenV	0.28±0.03	0.10±0.01	blankPSP19G243	0.31±0.03	0.11±0.01
PSM27PenV	0.43±0.04	0.077±0.008	PSM27G243	0.32±0.03	0.057±0.006
blankPSM27PenV	0.33±0.03	0.12±0.01	blankPSM27G243	0.26±0.03	0.093±0.009
PSP19UVB066	0.32±0.03	0.057±0.006	PSP19UVG503	0.36±0.04	0.064±0.006
PSP19VISB066	0.32±0.03	0.057±0.006	PSP19VISG503	0.32±0.03	0.057±0.006
blankPSP19B066	0.26±0.03	0.19±0.02	blankPSP19G503	0.10±0.02	0.07±0.01
PSM27B066	0.35±0.04	0.083±0.008	PSM27G503	0.32±0.03	0.076±0.008
blankPSM27B066	0.27±0.03	0.19±0.02	blankPSM27G503	0.31±0.03	0.22±0.02

Table 7 Elemental analysis and loading data of bioactive polymers

Combustion analysis proved the existence of nitrogen, ranging from 0.10-0.43%, giving rise to loading levels of 0.046-0.22 mmol/g. This was consistent with the presence of nitrogen atoms from modified materials and amide and/or

lactam groups from bioactive molecules on the surface of the polymers. However, the loading levels of B066, G503 and G243 were all sufficiently low that no activity was observed, although activity with penicillin V was found.

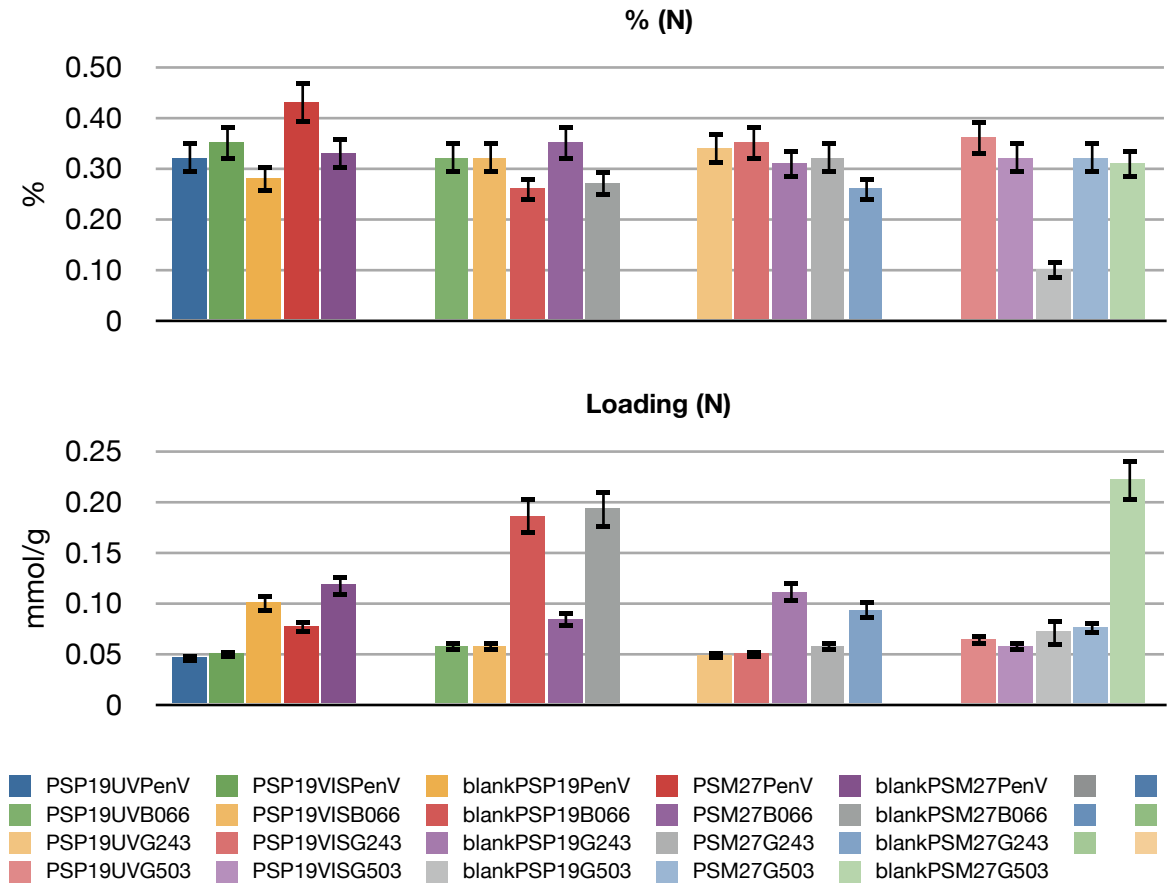

Figure 17 Percentages of nitrogen and loading data of bioactive polymers

Samples	% S	Loading (mmol/g)
PSP19UVPenV	0.34±0.03	0.10±0.01
PSP19VISPenV	0.35±0.04	0.11±0.01
blankPSP19PenV	0.31±0.03	0.10±0.01
PSM27PenV	0.32±0.03	0.10±0.01
blankPSM27PenV	0.26±0.03	0.081±0.008

Table 8 Percentages of sulphur and loading data of bioactive polymers

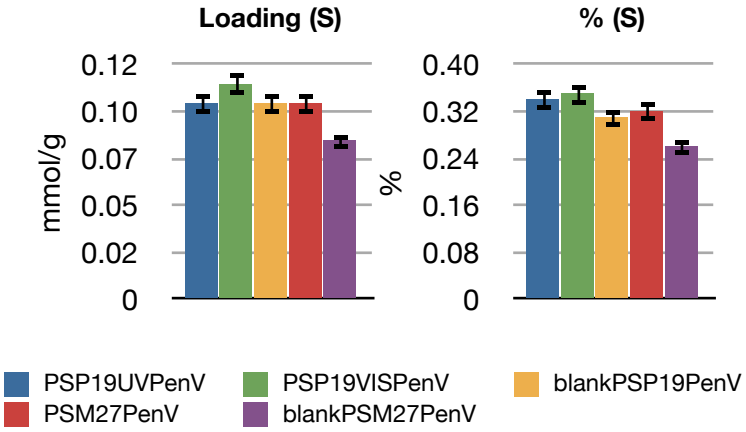

Figure 18 Percentages of sulphur and loading data of bioactive polymers

Samples coated with penicillin V were also analysed for percentages of sulphur, and gave values ranging from 0.26-0.34% or 0.081-0.11 mmol/g, clearly indicating the presence of sulphur atoms from penicillin V moiety (**Table 8**). However, the loadings calculated from percentages of sulphur were different from those from percentages of nitrogen. It was decided that the loadings from analysis of nitrogen would be used so that it could be compared with results from modified polymers with compounds B066, G243, and G503 for future work.

Samples	Active PenV (mg/mL)	Active PenV (mmol/g)	Loading (mmol/g)	% Bioactive
PSP19UVP	$(1.3\pm0.2)\times10^{-3}$	$(3.3\pm0.4)\times10^{-7}$	0.046±0.005	$(7\pm2)\times10^{-4}$
PSP19VISP	$(1.3\pm0.1)\times10^{-3}$	$(3.4\pm0.3)\times10^{-7}$	0.050±0.005	$(7\pm1)\times10^{-4}$
blankPSP19P	$(1.3\pm0.1)\times10^{-3}$	$(3.4\pm0.3)\times10^{-7}$	0.10±0.01	$(3.4\pm0.7)\times10^{-4}$
PSM27P	$(1.6\pm0.1)\times10^{-3}$	$(4.0\pm0.3)\times10^{-7}$	0.077±0.008	$(5.2\pm0.9)\times10^{-4}$
blankPSM27P	$(1.6\pm0.1)\times10^{-3}$	$(4.0\pm0.3)\times10^{-7}$	0.12±0.01	$(3.3\pm0.6)\times10^{-4}$
PSP19UVPD	$(10.1\pm0.3)\times10^{-3}$	$(3.5\pm0.3)\times10^{-7}$	0.046±0.005	$(8\pm2)\times10^{-4}$
PSP19VISPD	$(9.3\pm0.3)\times10^{-3}$	$(3.4\pm0.4)\times10^{-7}$	0.050±0.005	$(7\pm1)\times10^{-4}$
blankPSP19PD	$(9.1\pm0.3)\times10^{-3}$	$(3.4\pm0.4)\times10^{-7}$	0.10±0.01	$(3.4\pm0.7)\times10^{-4}$
PSM27PD	$(31.0\pm0.6)\times10^{-3}$	$(4.8\pm0.4)\times10^{-7}$	0.077±0.008	$(6\pm1)\times10^{-4}$
blankPSM27PD	$(16\pm1)\times10^{-3}$	$(4.1\pm0.4)\times10^{-7}$	0.12±0.01	$(3.4\pm0.6)\times10^{-4}$

Table 9 Efficiency of modified polymers in Bioactivity experiments against *E coli*

With the loading data in hand, the efficiency of polymeric beads in generating bioactivity on bacteria-seeded agar was then calculated. The results from Experiment

2 and 4 together with the loading levels obtained from percentages of nitrogen were used to calculate the efficiency presented as % bioactive and the values obtained are shown in **Table 9**.

$$\% \text{ Bioactive} = \frac{\text{moles of active penicillin V}}{\text{total moles of penicillin V}} \text{ x } 100$$

Figure 19 Definition of % Bioactive

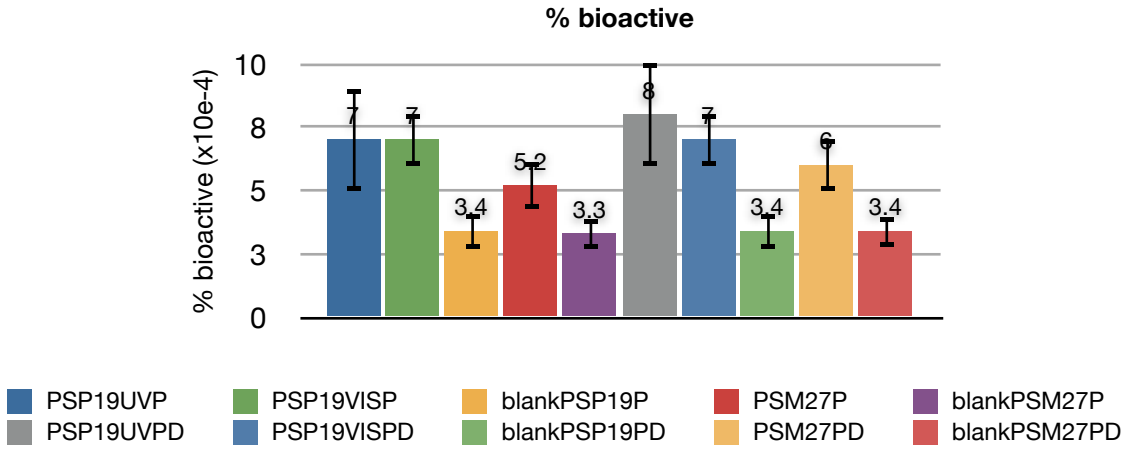

Figure 20 Efficiency of modified polymers in bioactivity experiments against *E coli*

All blank samples, namely **blankPSP19P**, **blankPSM27P**, **blankPSP19PD**, and **blankPSM27PD**, expressed relatively lower bioactivities at (3.3-3.4)x10^{-4}% efficiency. The other materials showed activities in a range of (5.2-8.0)x10^{-4}% efficiency. This implied that from **Figure 17**, although the blank samples could catch bioactive molecules at higher loading levels, they performed less efficiently in releasing these active species in bioassay experiments, compared to polymers **PSP19** and **PSM27**.

4.2.7 ATR-IR

Major absorbances observed in the ATR-IR spectra of some modified polymers treated with bioactive compounds are summarised in **Table 10**. Full spectral data is available in **Appendix V**. The main region of interest is at 1800-1500 cm^{-1}.

Polymer	ATR-IR (cm^{-1})	Spectrum
PSP19 UVPenV	1602 (carboxylate), 1656 (amide)	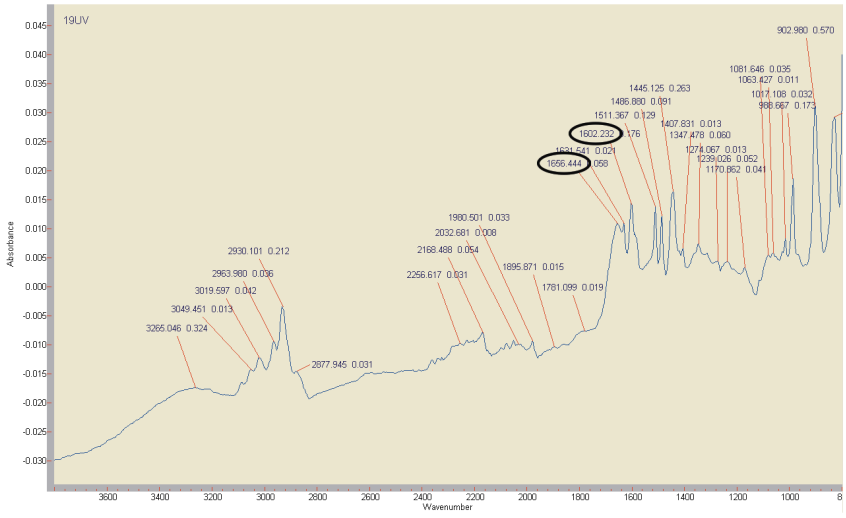
PSP19 VISPenV	1602 (carboxylate), 1657 (amide)	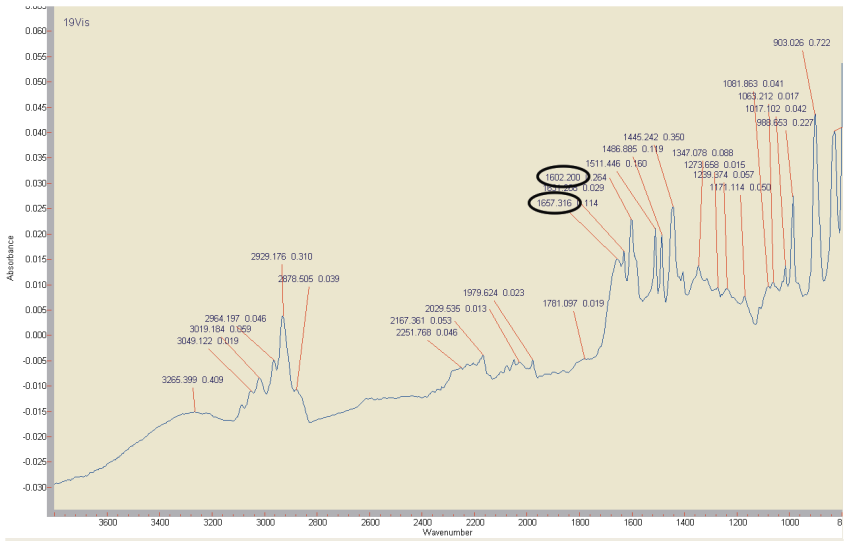

Polymer	ATR-IR (cm^{-1})	Spectrum
blank PSP19 PenV	1601 (carboxylate), 1657 (amide)	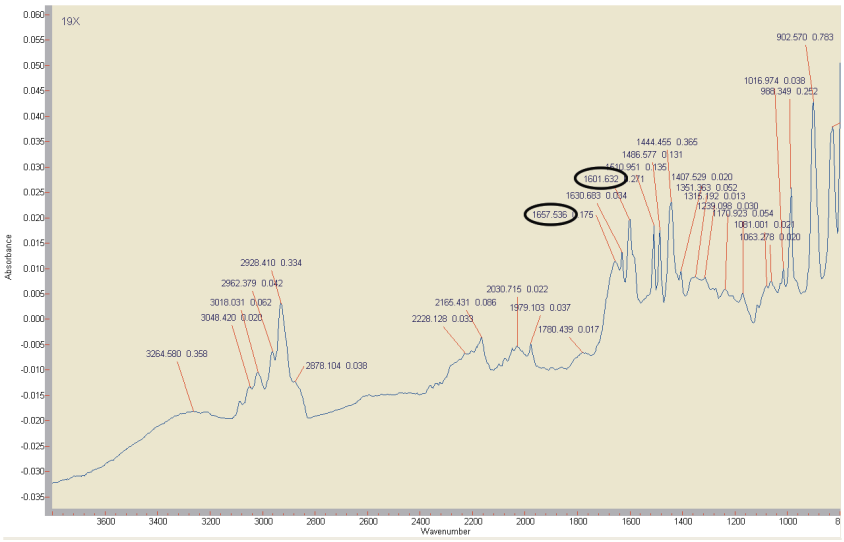
PSM27 PenV	1601 (carboxylate), 1653 (amide)	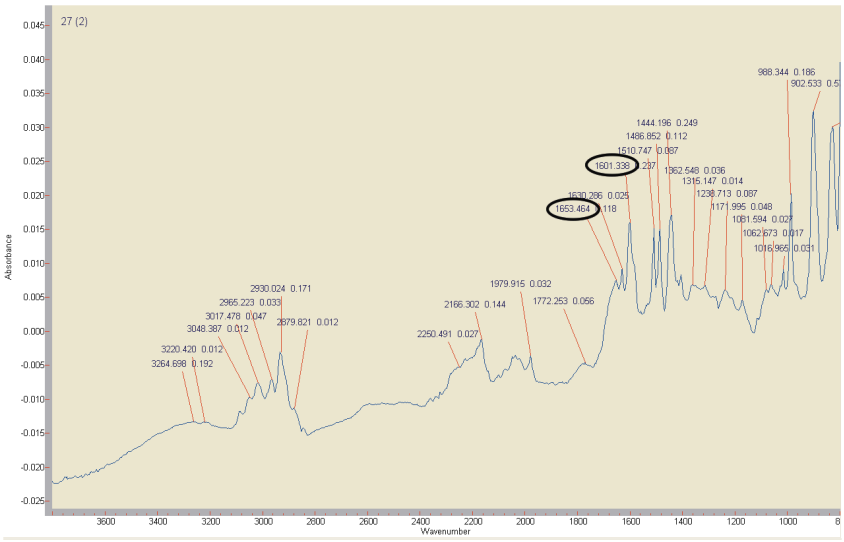
blank PSM27 PenV	1601 (carboxylate), 1654 (amide)	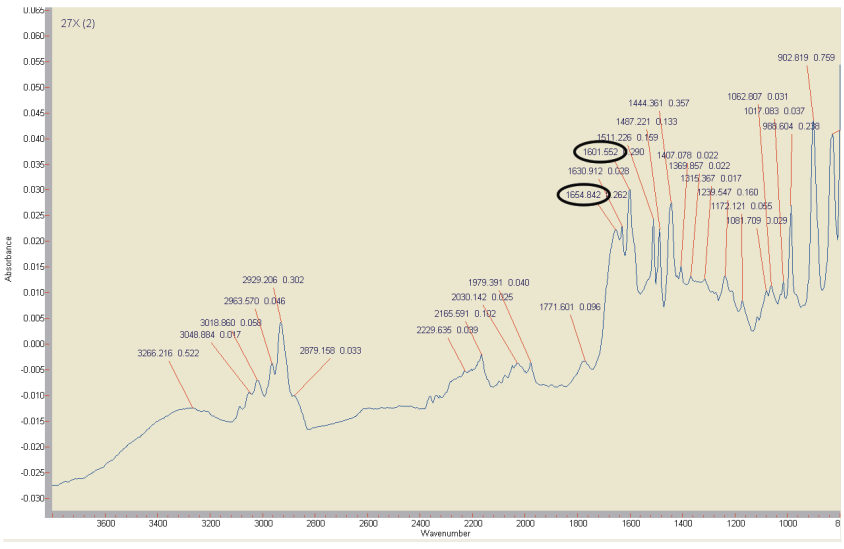

Table 10 ATR-IR data of bioactive polymers

All samples treated with penicillin V, namely **PSP19UVPenV**, **PSP19VISPenV**, **blankPSP19PenV**, **PSM27PenV**, and **blankPSM27**, displayed absorbances around 1600 and 1650 cm^{-1} which were attributed to the carboxylate and amide groups, respectively. However, these samples only showed a weak signal around 1770-1780 cm^{-1} corresponding to the lactam group. Other related work in the group has clearly indicated that the lactam group can be observed, and this suggests that, for these samples, lactam hydrolysis by water must have occurred by the time ATR-IR spectra were obtained.[117] Nonetheless, since these samples exhibited bioactivities in **Experiments 1-4**, hydrolysis of the lactam group was clearly not the case when the samples were fresh.

Unfortunately, for other samples, namely **PSP19UVB066**, **PSP19VISB066**, **blankPSP19B066**, **PSM27B066**, **blankPSM27B066**, **PSP19UVG243**, **PSP19VISG243**, **blankPSP19G243**, **PSM27G243**, **blankPSM27G243**, **PSP19UVG503**, **PSP19VISG503**, **blankPSP19G503**, **PSM27G503**, and **blankPSM27G503**, good quality IR spectra which would have confirmed adsorption of bioactive compounds at the surface by the presence of C=O signals (lactam, ester, and β-keto groups) around 1750-1550 cm^{-1} could not be obtained.

The samples prepared in this work have a surface loading level of $(0.38\text{-}1.8)\times10^{13}$ molecules/cm^2 or 0.0025-0.011 $\mu g/cm^2$ as determined by combustion analysis, which are 2.4-10 times under the lower detection limit for ATR-IR. As a result, only weak or non-observable signals would be expected in the ATR-IR spectra.

4.2.8 Reproducibility

Polymers **PSM27** (loading 0.10 mmol/g) and **PSP19** (loading 0.028 mmol/g) were used to repeat experiment 4 where the antibacterial activities against *S. aureus*

and *E. coli* were demonstrated with 25 mg of each polymer sample suspended in a mixture of DMSO and water (7:3). Sample **PSM27** and blank PS XAD were separately soaked with 1 equivalent (2.5 mmol) of penicillin V, while sample **PSP19** and blank PS XAD were also separately soaked with 1 equivalent (0.70 mmol) of penicillin V, and this procedure for the preparation of these samples were repeated 10 times in order to obtain information on the reproducibility and standard deviation of the experiment. The diameter of the antimicrobial clear zones was measured twice and the average values were recorded. The results from bioactivity experiments against *S aureus* and *E coli* are shown in **Table 11** and **Table 12**, respectively.

Samples	Inhibition zone diameter (mm)									
	Sample number									
	1	2	3	4	5	6	7	8	9	10
PSP19UVrepeat	36	37	36	36	37	38	37	36	36	36
PSP19VISrepeat	38	40	39	40	40	40	40	38	40	39
blankPSP19repeat	39	38	40	38	38	38	39	39	38	40
PSM27repeat	42	43	43	42	44	42	44	43	42	41
blankPSM27repeat	42	42	44	44	44	43	44	43	42	42

Table 11 Bioassay results against *S aureus*

Samples	Inhibition zone diameter (mm)									
	Sample number									
	1	2	3	4	5	6	7	8	9	10
PSP19UVrepeat	22	23	22	21	21	21	21	22	21	23
PSP19VISrepeat	28	26	28	28	27	26	28	27	28	28
blankPSP19repeat	27	26	28	28	26	28	26	28	28	27
PSM27repeat	35	35	34	34	34	36	35	35	36	34
blankPSM27repeat	33	32	33	34	33	32	34	34	34	32

Table 12 Bioassay results against *E coli*

The average values of the inhibition zone diameters and the antibacterial activities were calculated with standard deviation as error estimates. The calibration plot was assumed to have ±5% error estimates. The results are demonstrated in **Table 13**.

S. aureus	Inhibition zone diameter (mm)	Ceph C (nmol)	E. coli	Inhibition zone diameter (mm)	Ceph C (nmol)
PSP19UVrepeat	37±5	(5.0±0.8)x10^3	**PSP19UVrepeat**	22±6	1.2±0.4
PSP19VISrepeat	39±6	(7±1)x10^3	**PSP19VISrepeat**	27±6	2.9±0.8
blankPSP19repeat	39±6	(7±1)x10^3	**blankPSP19repeat**	27±8	3±1
PSM27repeat	43±8	(15±4)x10^3	**PSM27repeat**	35±6	11±2
blankPSM27repeat	43±8	(15±4)x10^3	**blankPSM27repeat**	33±7	8±2

Table 13 Bioassay results of repeated experiments.

It was noted that sample **blankPSM27PD** showed much higher activity than that of sample **blankPSP19PD**, resulting from the different ligand and penicillin V loading levels on the different polymers.

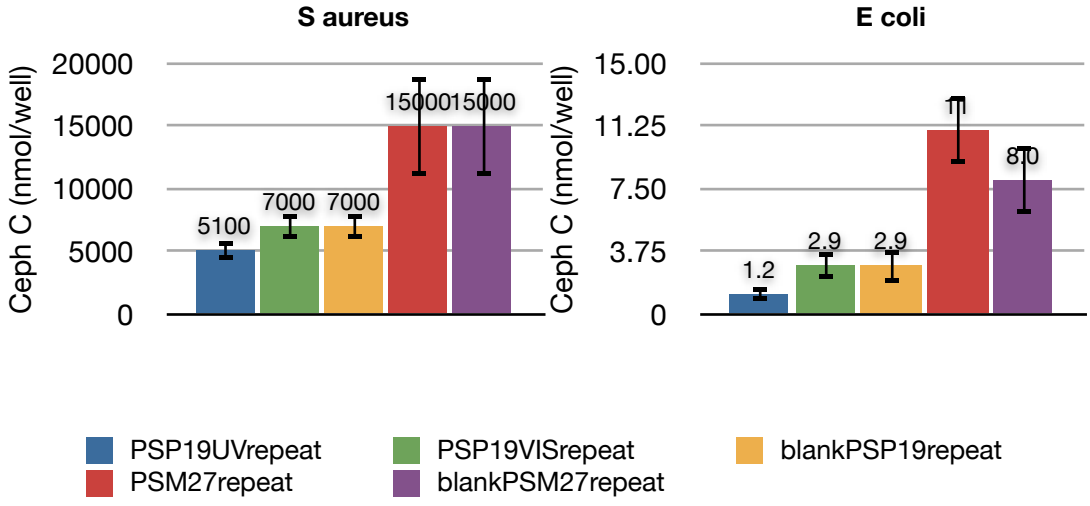

Figure 21 Bioassay results of Experiment X

With the activities against **S aureus**, samples **PSP19UVrepeat**, **PSP19VISrepeat**, and **blankPSP19repeat** showed large inhibition zones of 37, 39, and 39 mm, equivalent to 5100, 7000, and 7000 nmol of Ceph C, respectively. Similarly, large zones of inhibition of polymers **PSM27repeat** and **blankPSM27repeat** were equivalent to 15000 nmol of Ceph C for both samples. This was similar to the results from Experiment 4 in that the activities against *S aureus* of sample **PSP19UVrepeat** and **PSP19VISrepeat** did not show substantial differences from that of **blankPSP19repeat**, and the activity of sample **PSM27repeat** was in fact the same as that of **blankPSM27**. It should be noted that because the loading density of polymers used in this experiment was higher than that used in experiment 4, the absolute assay zone sizes in this experiment were also higher.

However, the activities against *E coli* provided a more obvious comparison between these samples. **PSM27repeat** exhibited the highest activities at 11 nmol of Ceph C, moderately higher than **blankPSM27repeat** at 8.0 nmol of Ceph C. Nonetheless, samples **PSP19UVrepeat** displayed bioactivities at 1.2 nmol of Ceph C, moderately lower than those of **PSP19VISrepeat** and **blankPSP19**. Simlilarly, the large errors of 24-33% were assumed to be from experimental errors. It was noted that polymer **blankPSM27repeat** showed much higher activity than that of **blankPSP19repeat**, implying an effect of different concentrations of penicillin V solutions that were used to prepare the samples.

With regards to reproducibility, this experiment has shown that the method to deposit penicillin V as a bioactive species on the surface of modified polymers and to use these polymers in bioassay experiments against *E coli* and *S aureus* could be repeated to produce consistent results. Given the uncertainty in the chemical preparation of the polymers, its loading with penicillin V, and the bioassay procedure, the level of reproducibility is remarkable.

4.2.9 Conclusions

The ability of modified polymers to catch and release silver ions and penicillin V has been demonstrated in preliminary investigations. The bioassay experiments were carried out on bacteria-seeded agar against *E coli* and *S aureus* as a example of Gram-negative and Gram-positive bacteria, respectively. Modified polymers with silver ions on the surface showed significant inhibition zones which would need further investigation to confirm reproducibility. Materials coated with penicillin V displayed high degrees of bioactivity even at low concentrations and the antibacterial molecule could diffuse through either molten agar or DMSO/water mixture as a medium. Elemental analysis proved the existence of nitrogen of these samples and revealed the total amount of penicillin V on the surface. From the data, the efficiency of modified polymers with penicillin V film in suppressing bacteria cell growth could be calculated. This activity appears to be due to only a small amount of penicillin V released through the media. Duan et al. reported that when antibiotics were immobilised onto implant surfaces by either covalent, ionic, or coordination bonds and the release of the antibiotics were conducted in PBS, the loading ratios affected the release time.[118] It was found that gentamicin, which is an antibiotic, was completely released in PBS with an hour when it was loaded with <5 nmol/mg, whereas cephalothin, another type of antibiotic, was loaded at 30 nmol/mg and displayed a 50% release within the same length of time, followed by another 20% release after 16 hours. It was envisaged that the materials that were examined in this thesis might be able to provide a continuous delivery of penicillin V. The difference in activities of blank polystyrenes which were soaked with different amounts of penicillin V implied that the degrees of bioactivities from materials with the same structure could be controlled by varying the amount or concentration of penicillin V in the preparation of samples prior to bioassay experiments. Reproducibility of the binding

experiment was demonstrated. A drawback from this method of adsorption on modified polymers **PSP19** and **PSM27** was that compounds with low activities, namely molecules B066, G243, and G503, did not exhibit bioactivity in the same conditions. However, the results could be improved by increasing the concentration of organic bioactive solutions when soaking with the polymers, or by using materials with different structures that would have higher affinity to these molecules but also be able to release the species to inhibit bacteria cell growth.

Chapter 5 Stable Diazo Compounds

5.1 Introduction

As mentioned in **Chapter 1**, indirect modification via a pre-activation step followed by diazonium coupling suffers from several limitations. From **Figure 1**, the electron-rich aromatic rings i.e. 4-methoxyphenyl groups, which are essential for the diazonium coupling step, in fact decrease the stability of the diazo functional group. Although the use of remote high electron density units such as arylamino residues solves this issue, the need for diazonium formation limits the choice of substituents on the diazonium ions that must survive through reaction conditions and allows only a narrow range of structures of aliphatic or aromatic diazonium compounds.

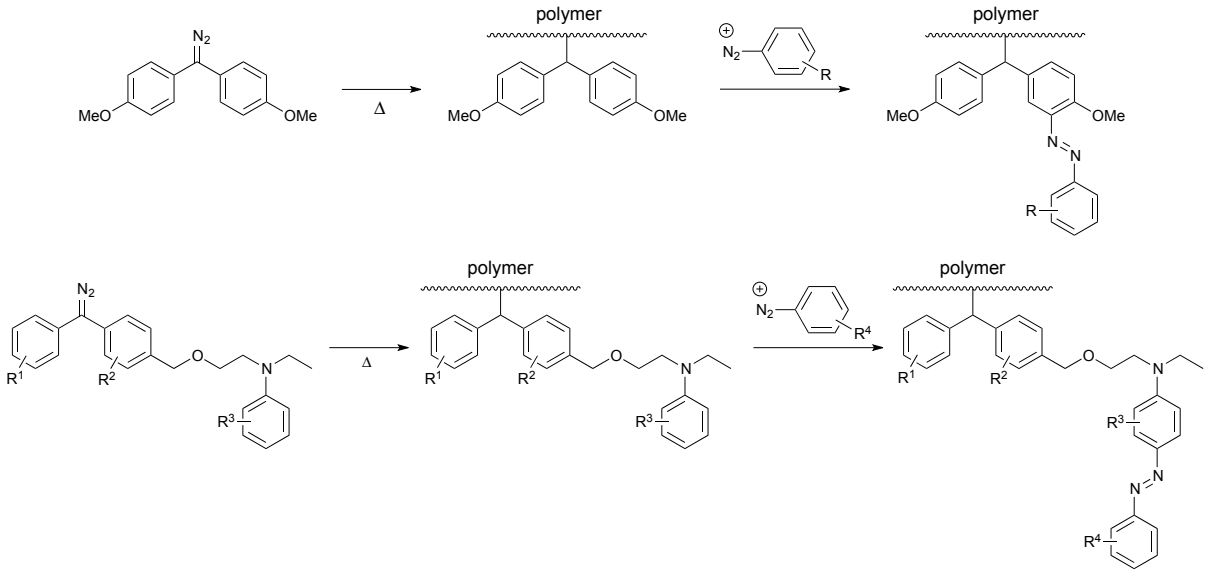

Figure 1 Indirect modification

Fortunately, these problems might be avoided by a direct modification technique using molecules with functional groups that are conjugated with a pre-synthesised diazo compound prior to surface modification sequence. This however requires the synthesis of diazo compounds with balanced reactivity towards

surface activation of polymers and improved stability or capability of conjugation with other fragments. Details of synthesis and properties of such proposed diazo molecules will be discussed in this chapter.

Earlier work in the group showed that substituted diaryldiazomethanes and diazofluorenes exhibited variation in stability depending on the substitution pattern.[14] For example, the decomposition temperature of non-substituted diphenyl diazomethane of 130°C (with heat of decomposition of 124 kJ/mol)[119] was reduced for the unstable bis-4-(methoxyphenyl) diazomethane containing electron-donating groups, which was much less stable and decomposed at 120°C, while bis-4-(nitrophenyl)diazomethane with electron-withdrawing substituents was stable at significantly higher temperature up to 160°C (**Table 1**). This confirms the ability of electron-withdrawing groups to stabilise diazo compounds, whereas electron-donating substituents facilitate decomposition relative to diphenyldiazomethane.[17,18]

Diazo compound	Structure	Onset temperature (°C)
diphenyldiazomethane	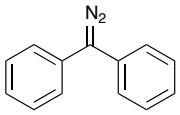	130
bis-4-(methoxyphenyl)diazomethane	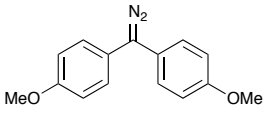	120
bis-4-(nitrophenyl)diazomethane	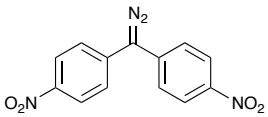	160

Table 1 Decomposition temperatures of diaryldiazo compounds

In addition, diazofluorenone derivatives were found to generally exhibit higher decomposition temperatures than the diaryl systems (**Table 2**).[14] With this

background in mind, an investigation of such stabilising effects and their relevance to surface modification was made.

Diazo compound	Structure	Onset temperature (°C)
9-diazo-9H-fluorene	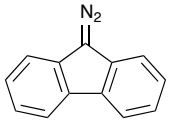	165
4-aza-9-diazofluorene	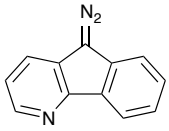	165
4,5-diaza-9-diazofluorene	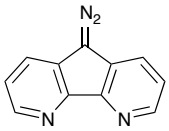	165
9-diazo-4-hydroxymethyl-9H-fluorene	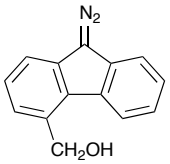	170
2,7-dibromo-9-diazo-9H-fluorene	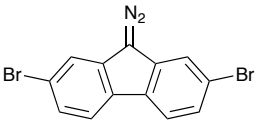	188

Table 2 Decomposition temperatures of diazofluorenones

A previous worker in the group (L, Harris, 2009) found that except for 9-diazo-9H-fluorene, rapid decolouration of diaryldiazo compounds shown in **Table 1** and **Table 2** was observed on TLC plates, giving severe streaking. When column chromatography of bis-4-(nitrophenyl)diazomethane, 2,7-dibromo-9-diazo-9H-fluorene, and 4,5-diaza-9-diazofluorene was attempted, this gave a large exothermic binding to silica gel. However, only 9-diazo-4-hydroxymethyl-9H-fluorene, 4-aza-9-diazofluorene, and 2-bromo-9-diazo-9H-fluorene could be purified by column

chromatography. This is because silica gel is weakly acidic and diaryldiazo compounds are highly acid sensitive.

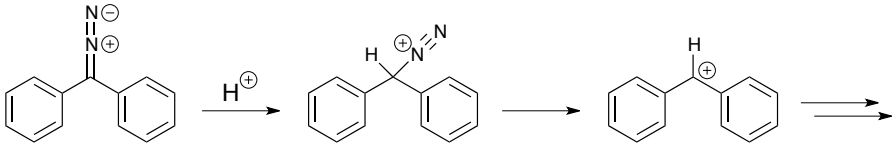

Figure 2 Decomposition of diphenyldiazo compound in acid

It was reported that although decomposition of crystalline diphenyldiazo methane occurs at temperatures higher than 10 °C, only around 9% has decomposed after 100 hours at room temperature.[120] At temperatures above 30 °C, however, the diazo compound melts and decomposes much more rapidly. 13% decomposition was observed after 20 hours at 30 °C and 90% decomposition was found after 20 hours at 50 °C. As a result, all synthesised diazo compounds mentioned in this thesis were handled at room temperature, stored in a freezer (-18 °C), or immediately used. In addition, all reactions were conducted in the dark by wrapping reaction flasks with aluminium foil since diazo compounds are also light sensitive, and column chromatography was not performed.

5.2 Results and Discussion

5.2.1 Fluorene System

Previous work has shown that the diazofluorenone system is an excellent alternative to non-polycyclic aromatic diazo compounds in terms of its greater stability compared to corresponding diaryldiazo molecules with the same substituents.[14,121] This is because the two aromatic rings of diaryldiazo compounds are not coplanar due to a steric clash between the ortho-substituents. This steric

repulsion is relieved by rotation of the aromatic rings around the C(=N)-C(Ar) bond, increasing the interplanar angle, rather than widening the C(Ar)-C(=N)-C(Ar) angle.[122] Although this geometry shields the diazo group more effectively as a result of steric hindrance from substituents on the rotated aromatic rings, the diazofluorenone structure is necessarily planar and can benefit from the resonance stabilisation of an extended π-delocalised system.

Figure 3 General structures of benzophenone and fluorenone diazo compounds

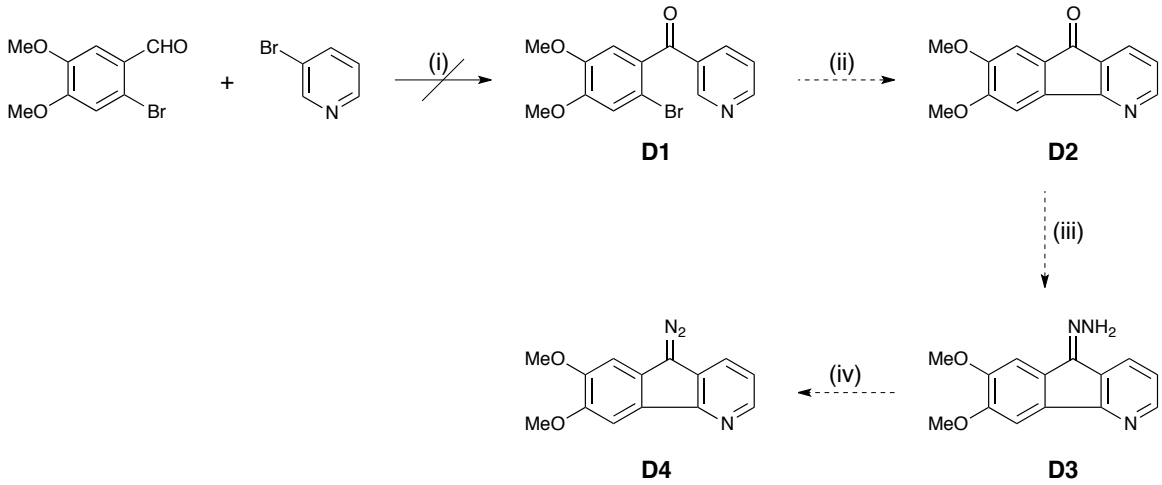

Scheme 1 Reactions and conditions
(i) n-BuLi, THF, -100°C then -78°C, 2h then room temperature, 8h then MnO_2, benzene, reflux.

It was envisaged that the fluorenone diazo compound **D4** would be synthesised from a four-step sequence (**Scheme 1**). The pyridine ring would be needed in the second step for the formation of the fluorene ring, and the two methoxy groups were selected as potential linkers after deprotection. Lithiation of commercially available 3-bromopyridine was carried out at low temperature before being added to a solution of 6-bromoveratraldehyde. However, only the starting

aldehyde was recovered and no alcohol intermediate was formed, therefore the oxidation step by MnO_2 was not carried out. It was decided that an alternative system would be employed to make stable diazo molecules.

5.2.2 Carbonyl Stabilisation

Studies have shown that diazo dienone compounds are accessible via a oxidation of hydrazones by heavy metals or deprotonation of azo salts.[123-126] These diazo dienones are stabilised by resonance through conjugated alkene and carbonyl double bonds.

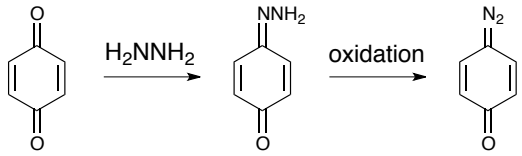

Figure 4 Formation of a diazo dienone via hydrazonisation

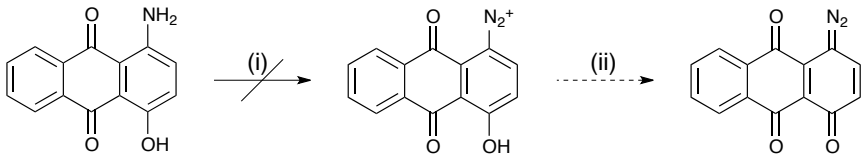

D5 **D6** **D7**

Scheme 2 Reactions and conditions
(i) Isopentyl nitrite, MeCN, room temperauture.

It was envisaged that the diazonium salt **D6** and the diazo **D7** would subsequently be made from commercially available 1-amino-4-hydroxy-anthraquinone (**Scheme 2**). The two carbonyl groups would stabilise the diazo moiety, with the phenyl group acting as a spacer. The anthraquinone **D5** was treated with isopentyl nitrite at room temperature to convert the amino group to the diazonium salt. It was observed that the red solution mixture turned to yellow after 20

minutes, however, the product of the reaction was not identifiable by ^{1}H NMR spectroscopy.

It was found that another system in which the diazo group is adjacent to a carbonyl moiety could be synthesised (**Scheme 3**).[127-130] The alpha-diazo ketone **D10** was successfully made starting from benzil **D8** by a standard method.[8,16] Addition of hydrazine monohydrate to the alpha diketone **D8** and reflux produced the intermediate **D9** with good yield. The observed MS spectra displayed a peak at 247([M+Na]$^+$), and the aromatic region of the ^{1}H NMR spectrum became more complicated.

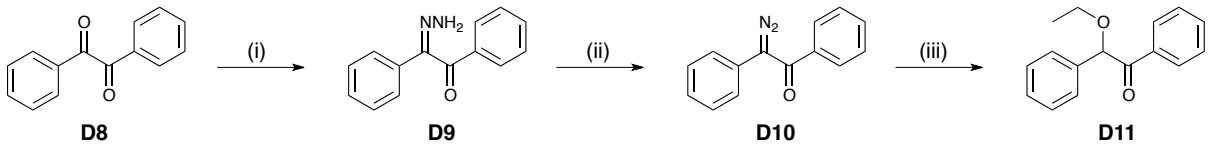

Scheme 3 Reactions and conditions
(i) $H_2NNH_2.H_2O$, EtOH, reflux, 89%; (ii) MnO_2, $CHCl_3$, room temperature, 54%;
(iii) EtOH, reflux, 61%.

This hydrazone was then oxidised by MnO_2 in anhydrous chloroform and neutral conditions in the dark to generate the alpha-carbonyl diazo molecule **D10** with moderate yield and the presence of the diazo group was confirmed by the IR spectrum, showing an absorption peak around 2070 cm^{-1} corresponding to N≡N stretching mode. This diazo compound was then heated under reflux in EtOH in order to test the ability to decompose and react with other organic functional groups. It was found that this conversion gave a product corresponding to the structure of ether **D11** as confirmed by the ^{1}H NMR data and a peaks at 263([M+Na]$^+$) in the MS spectra.

After demonstrating that the alpha-diazo ketone **D10** could be synthesised and was able to decompose to react with EtOH at ambient temperature, it was suggested

that a derivative of **D10** with linker groups could also be made by similar methods. The desired diketone **D13** was chosen as it has two methoxy groups which might act as linking groups after deprotection and the structure is symmetrical so that complications in purifications could be avoided. It was envisaged that the corresponding diazo compound could be made from a four-step process (**Scheme 4**).

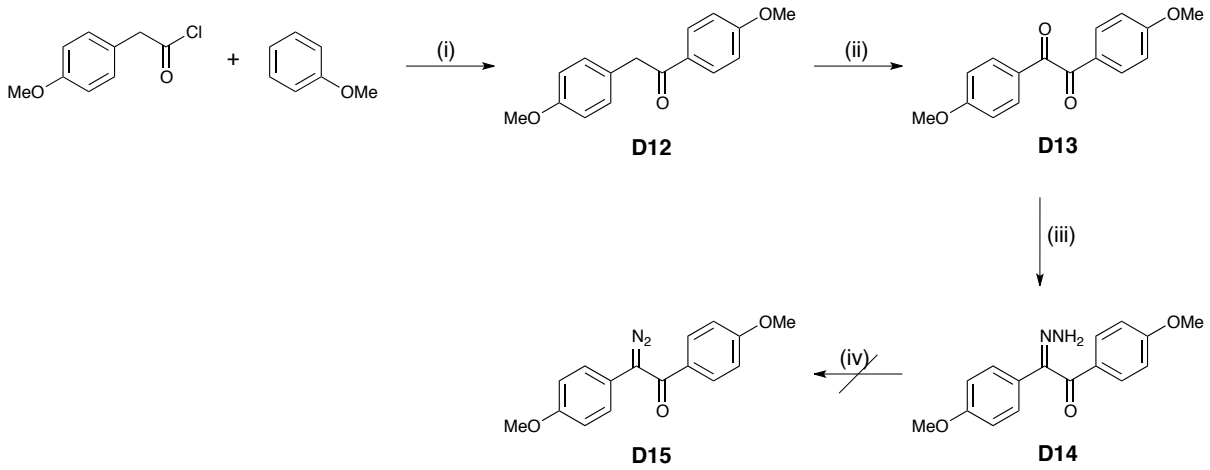

Scheme 4 Reactions and conditions
(i) $AlCl_3$, DCM, room temperature, 100%; (ii) NBS, DMSO, room temperature, 60%; (iii) $H_2NNH_2.H_2O$, EtOH, reflux; 57%; (iv) MnO_2, $CHCl_3$, room temperature.

Fridel-Craft acylation of anisole and 4-methoxyphenylacetyl chloride was performed in the presence of $AlCl_3$, giving the ketone **D12** with excellent yield and purity as confirmed by the ^1H NMR, the MS spectra exhibiting a peak at 279 ($[M+Na]^+$), and the IR spectrum showing an absorption peak at 1680 cm^{-1} corresponding to C=O stretching mode. Conversion of the ketone **D12** to diketone **D13** was achieved by treatment with NBS in anhydrous DMSO at room temperature, generating the product with moderate yield and the expected ^1H NMR spectrum, displaying a clear double doublet at 7.94-7.97 and 6.96-6.99 ppm, and the base peak at 293($[M+Na]^+$) in the MS spectra.

Hydrazonisation of diketone **D13** was carried out with reasonable yield and the observed MS spectra showed a peak at 307 corresponding to the ($[M+Na]^+$) fragment. To this intermediate was then added the oxidising agent MnO_2 in order to convert the hydrazone **D14** to the diazo compound **D15**, however, the IR spectrum of the product did not show important absorbances around 2000 cm^{-1} for the N≡N stretching. This implied that either the diazo functional group of **D15** was not formed or the group was destabilised by electron donating methoxy groups, leading to decomposition by carbene formation followed by Wolff rearrangement. It was decided that synthesis of other diazo systems would have to be examined.

5.2.3 Substituted Benzophenones

As previous discussed in **Chapter 3**, the presence of an electron withdrawing group such as NO_2 would be expected to stabilise the diazo group of diaryldiazo system.[14,17,18] It was then suggested that a fluorine substituent, which has the highest electronegativity and the ability to withdraw electrons from aromatic rings of benzophenone compounds, would be suitable as an substituent on the benzene rings.

From **Scheme 5**, it was envisaged that the diazo compound **D20** would be synthesised from a five-step sequence, starting from commercially available 4-fluorobenzaldehyde. A mixture of n-butyllithium and 4-bromotoluene was added to this benzaldehyde at low temperature to produce an alcohol intermediate, which was then oxidised by I_2 in basic conditions to give the benzophenone **D16** with moderate yield. Its structure was confirmed by ^1H NMR displaying double doublets corresponding to the aromatic region, IR spectrum showing an absorbance at 1655 cm^{-1} for the carbonyl group, and the MS spectra exhibiting the base peak at 237 ($[M+Na]^+$).

Bromination of the ketone **D16** was carried out by treating it with NBS and benzoyl peroxide and irradiation with UV light, giving bromo substituted intermediate **D17**. Without further purification, hydroxylation by $CaCO_3$ in a mixture of dioxane and water was performed at reflux to provide the alcohol **D18**, whose structure was confirmed by ^1H NMR analysis and the base peak at 253($[M+Na]^+$) in the observed MS spectra. However, the overall yield was disappointingly low.

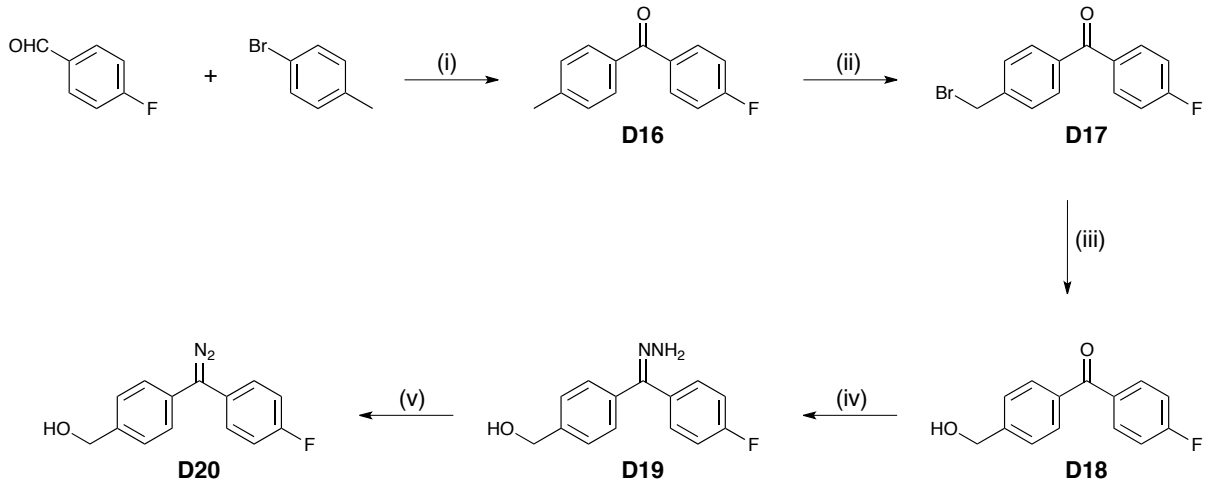

Scheme 5 Reactions and conditions
(i) 4-Bromotoluene, n-BuLi, THF, -78°C, then aldehyde, -78°C, room temperature, then I_2, K_2CO_3, *t*-BuOH, reflux, 38%; (ii) NBS, benzoyl peroxide, $CHCl_3$, reflux, UV;
(iii) $CaCO_3$, 1,4-dioxane/water, reflux, 12%; (iv) $H_2NNH_2.H_2O$, EtOH, reflux, 85%;
(v) MnO_2, Na_2SO_4, KOH, MeOH, room temperature, dark, 60%.

The synthetic route then proceeded by the standard methodology for diazo preparation.[10,15] Addition of hydrazine monohydrate to the carbonyl **D18** gave the hydrazone intermediate **D19**. The observed MS spectra displayed the base peak at 285($[M+MeCN]^+$). Oxidation of the condensed product **D19** was achieved by MnO_2 in anhydrous MeOH in the dark, generating benzophenone diazo compound **D20**. The presence of the diazo group was confirmed by the IR spectrum, which showed an absorption peak around 2040 cm^{-1} corresponding to N≡N stretching mode.

As a result of this successful synthetic scheme, it was envisaged that the diazo compound **D25**, which consists of CF_3 on an aromatic ring acting as an electron withdrawing unit, would be made by the same procedure (**Scheme 6**).

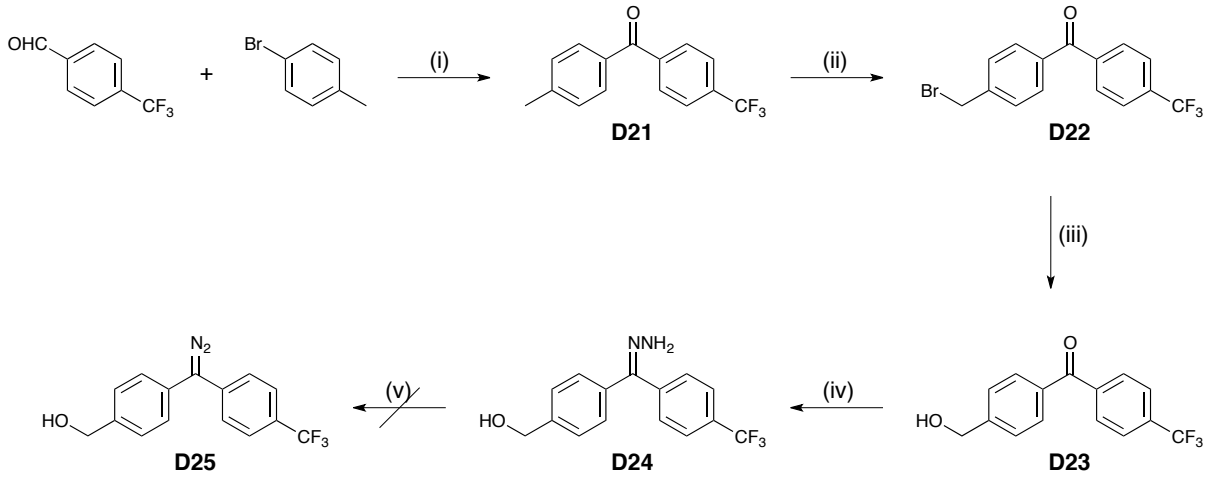

Scheme 6 Reactions and conditions
(i) 4-Bromotoluene, n-BuLi, THF, -78°C, then aldehyde, -78°C, room temperature, then I_2, K_2CO_3, *t*-BuOH, reflux, 64%; (ii) NBS, benzoyl peroxide, $CHCl_3$, reflux, UV;
(iii) $CaCO_3$, 1,4-dioxane/water, reflux, 10%; (iv) $H_2NNH_2.H_2O$, EtOH, reflux, 93%;
(v) MnO_2, Na_2SO_4, KOH, MeOH, room temperature, dark.

4-(Trifluoromethyl)benzaldehyde was added to a mixture of n-butyllithium and 4-bromotoluene at -78°C to produce an alcohol intermediate. Oxidation of this alcohol with I_2 and K_2CO_3 gave the ketone **D21** with moderate yield. Its IR spectrum showed an absorbance at 1647 cm^{-1} corresponding to the carbonyl structure, while the MS spectra exhibited a peak at 287($[M+Na]^+$), and the ^1H NMR displayed expected double doublets in the aromatic region.

Benzophenone **D21** was consequently brominated by NBS in the presence of benzoyl peroxide and UV lamp, generating the bromo intermediate **D22** which was then hydroxylated without further purification using $CaCO_3$ in dioxane/water at reflux, to provide the alcohol **D23**, again in considerably low yield. The formation of the product was confirmed by ^1H NMR and MS spectra, the latter showing the base peak at 279($[M-H]^-$).

To the ketone **D23** was then added hydrazine monohydrate to give the hydrazone **D24**, with MS spectra displaying the base peak at 335([M+MeCN]$^+$). This intermediate was then oxidised by MnO_2 in a solution of anhydrous MeOH in the dark, however, the IR spectrum of the product did not show important absorbances around 2000 cm^{-1} for the N≡N stretching. This indicated that either the diazo functional group of **D25** was not formed or the compound was unstable and decomposed prior to characterisation.

With the successful synthesis of compound **D20** containing a fluorine atom as a substituent, the synthesis was extended to chloro-substituted benzophenone by the same approach. It was envisaged that the diazo compound **D30** would be synthesised from a five-step process, starting from commercially available 3-chlorobenzaldehyde (**Scheme 7**).

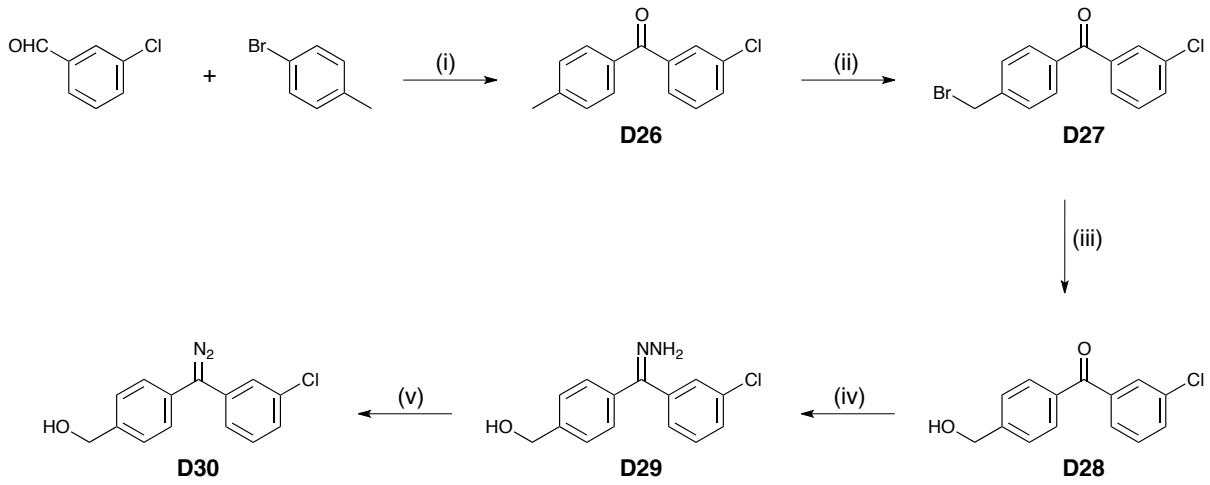

Scheme 7 Reactions and conditions
(i) 4-Bromotoluene, n-BuLi, THF, -78^{o}C, then aldehyde, -78^{o}C, room temperature, then I_2, K_2CO_3, *t*-BuOH, reflux, 29%; (ii) NBS, benzoyl peroxide, $CHCl_3$, reflux, UV;
(iii) $CaCO_3$, 1,4-dioxane/water, reflux, 37%; (iv) $H_2NNH_2.H_2O$, EtOH, reflux, 91%;
(v) MnO_2, Na_2SO_4, KOH, MeOH, room temperature, dark, 77%.

It was noted that the desired diazo compound had a chloro substituent at the meta position, unlike compound **D20** which has a fluorine atom at the para position. The structure of molecule **D20** was selected so that the fluorine atom was further

away from the carbonyl moiety and thus did not hinder reactions that took place at the C=O part, while they were still able to withdraw electrons from the rings as a result of strong electron attraction from fluorine atoms. In the case of compound **D30**, the chloro substituent was chosen to be at the meta position or nearer to the carbonyl group in order to increase the degree of inductive effect

A mixture of 4-bromotoluene and n-butyllithium was added to 3-chlorobenzaldehyde at low temperature to generate an alcohol which was then oxidised by I_2 in basic conditions to give the benzophenone **D26** in a slightly low yield. The structure of this product was confirmed by ^{1}H NMR and IR analysis, the latter spectrum showing a peak at 1649 cm^{-1} for the carbonyl absorbance, and the MS spectra displaying the base peak at 253($[M+Na]^+$) and a peak at 231($[M+H]^+$).

Bromination of the ketone **D26** was achieved by reacting it with NBS and benzoyl peroxide while irradiated with UV light, and the bromo-substituted intermediate **D27** was formed. Without further purification, hydroxylation by $CaCO_3$ in a mixture of dioxane and water was carried out at reflux to give the alcohol **D28**, whose structure was confirmed by ^{1}H NMR analysis and the base peak at 245 ($[M-H]^-$) in the observed MS spectra, with moderate overall yield which was relatively higher than those from the production of compound **D18** and **D23**.

Then addition of hydrazine monohydrate to the carbonyl **D28** and reflux provided the hydrazone intermediate **D29**. The MS spectra showed the base peak at 283($[M+Na]^+$) and a peak at 261($[M+H]^+$). Oxidation of the intermediate **D29** was done by MnO_2 in anhydrous MeOH solution in the absence of light, producing diaryldiazo compound **D30**. The presence of the diazo group was confirmed by an absorption peak at 2041 cm^{-1} in the IR spectrum corresponding to N≡N stretching mode.

An attempt to make another chloro substituted benzophenone diazo compound was made. It was envisaged that the trichloro diazo compound **D35** would be synthesised as outline in **Scheme 8**.

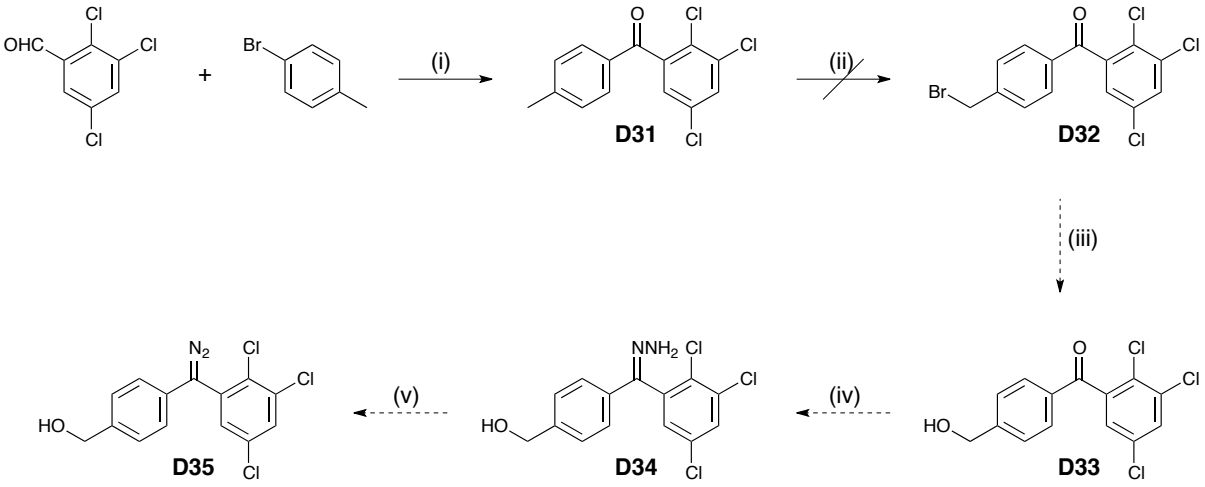

Scheme 8 Reactions and conditions
(i) 4-Bromotoluene, n-BuLi, THF, -78°C, then aldehyde, -78°C, room temperature, then I_2, K_2CO_3, *t*-BuOH, reflux, 16%; (ii) NBS, benzoyl peroxide, $CHCl_3$, reflux, UV.

2,3,5-Trichlorobenzaldehyde was added to a solution of n-butyllithium and 4-bromotoluene at -78°C. Then oxidation of the alcohol intermediate with I_2 and K_2CO_3 gave the ketone **D31** in low yield. Its IR spectrum showed an absorbance at 1670 cm^{-1} corresponding the carbonyl group, the MS spectra exhibiting a peak at 321 ($[M+Na]^+$). The benzophenone **D31** was then treated with NBS in the presence of benzoyl peroxide and UV lamp, and consequently hydroxylated without further purification by $CaCO_3$ in dioxane/water at reflux, however, the product of the reaction was not identifiable by ^1H NMR spectroscopy.

It can be seen above that the syntheses of the two diaryldiazo compounds containing halogen atoms/groups were successfully achieved. Of interest was to synthesise and examine the stability of other diazo derivatives with different core systems.

5.2.4 Heteroaromatic Diazo Compounds

As the diazo group of diaryldiazo compounds can be stabilised by delocalisation of electrons into the aromatic rings, it was suggested that diaryldiazo molecules consisting of heterocyclic rings could also be made and the heteroaromatic units would increase the stability of the diazo group. Thiophene was selected because of its aromaticity or the ability to delocalise electrons in the π-electron system. It was envisaged that the diazo compound **D40** would be synthesised from a five-step sequence starting from commercially available 2-thiophenecarboxaldehyde (**Scheme 9**).

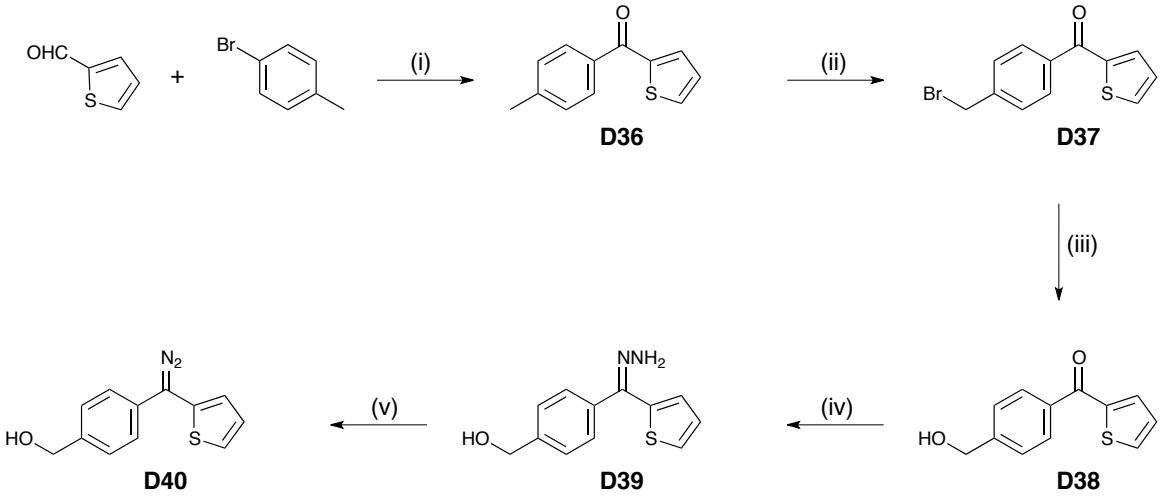

Scheme 9 Reactions and conditions
(i) 4-Bromotoluene, n-BuLi, THF, -78°C, then aldehyde, -78°C, room temperature, then I_2, K_2CO_3, *t*-BuOH, reflux, 50%; (ii) NBS, benzoyl peroxide, $CHCl_3$, reflux, UV;
(iii) $CaCO_3$, 1,4-dioxane/water, reflux, 10%; (iv) $H_2NNH_2.H_2O$, EtOH, reflux, 74%;
(v) MnO_2, Na_2SO_4, KOH, MeOH, room temperature, dark, 51%.

A mixture of n-butyllithium and 4-bromotoluene was added to 2-thiophenecarboxaldehyde to produce an alcohol intermediate which was then oxidised by I_2 in basic condition to give the benzophenone **D36** with moderate yield. Its structure was confirmed by ^1H NMR analysis, with the IR spectrum showing an absorbance at 1628 cm^{-1} for the carbonyl group, and the MS spectra exhibiting the base peak at 225($[M+Na]^+$) and a peak at 203($[M+H]^+$).

Bromination of the ketone **D36** was carried out by treating it with NBS and benzoyl peroxide and irradiated with UV light, the bromo-substituted intermediate **D37** was obtained. Without further purification, hydroxylation by $CaCO_3$ in a mixture of dioxane and water was performed at reflux to provide the alcohol **D38**, confirmed by ^1H NMR and a peak at 219($[M+Na]^+$) in the observed MS spectra. Unfortunately, the yield of this step was considerably low, similar to the synthesis of compound **D18** and **D23**.

To the ketone **D38** was then added hydrazine monohydrate to give the hydrazone **D39**, with MS spectra displaying a peak at 273($[M+MeCN]^+$). This intermediate was then oxidised by MnO_2 in basic solution of anhydrous MeOH in the dark to provide diaryldiazo compound **D40**, exhibiting an absorption peak at 2040 cm^{-1} in IR spectrum corresponding to N≡N stretching mode.

This particular isomer of the starting material was chosen because upon formation of the diazo group **D40** the electrons from the diazo moiety could then resonate through the whole thiophene ring, giving rise to a greater increase in stability as compared to the other isomer **D40*** made from 3-thiophene carboxaldehyde as illustrated in **Figure 5**.

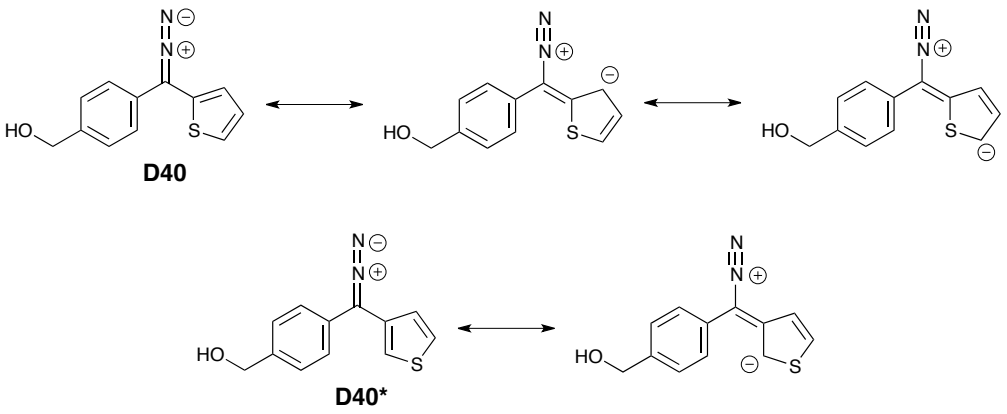

Figure 5 Resonance contributors of diazo **D40** and its isomer **D40***.

Another heteroaromatic system of interest was pyridine ring as the molecule is electron deficient due to the electronegative nitrogen in the ring. Therefore, the presence of a pyridine ring in the structure of diazo compounds would help stabilising the diazo functional group. In addition, the lone pair electrons on the nitrogen atom would be suitable for metal coordination after being introduced onto the surface of polymers. It was envisaged that the diazo molecule **D45** would be synthesised as shown in **Scheme 10**.

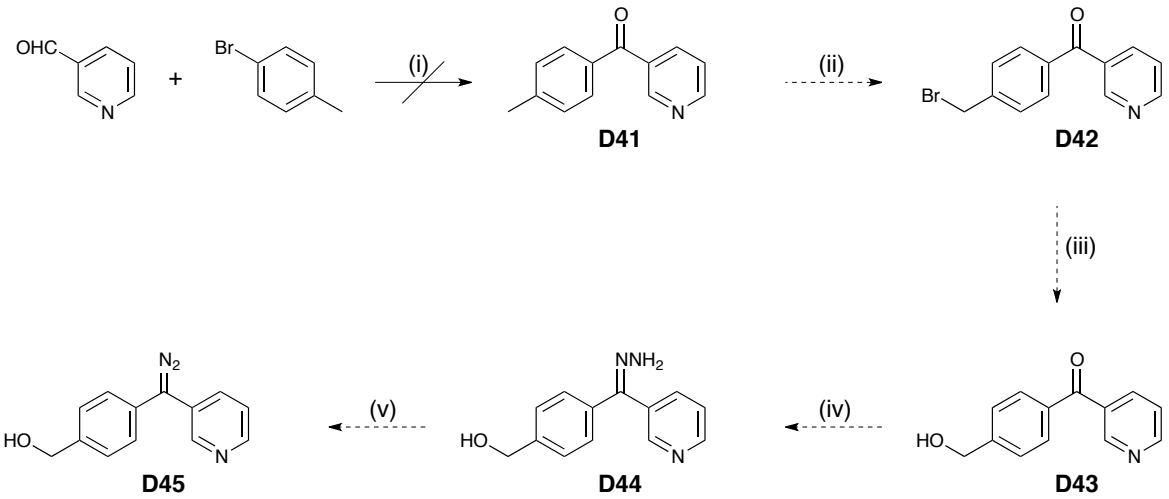

Scheme 10 Reactions and conditions
(i) 4-Bromotoluene, n-BuLi, THF, -78°C, then aldehyde, -78°C, room temperature, then I_2, K_2CO_3, *t*-BuOH, reflux.

3-Pyridinecarboxaldehyde was added to a mixture of titrated n-butyllithium and 4-bromotoluene at -78°C, then the solution mixture was treated with I_2 and K_2CO_3. After work up, however, the ^1H NMR spectrum of the product revealed that only the starting material 3-pyridinecarboxaldehyde (75%) was obtained instead of the desired ketone **D41**, and this reaction was not pursued any further.

5.2.5 DSC Study of Diazo Compounds

Differential scanning calorimetry (DSC) is a thermoanalytical technique which measures the heat of a sample relative to a reference while heating the sample with

a linear temperature ramp. It provides quantitative and qualitative information about physical and chemical changes that involve endothermic or exothermic processes. Of interest to us was the investigation of thermal stabilities of diazo compounds as determined from DSC thermograms, along with decomposition temperatures or the onset temperature and heat of decomposition. Diazo compounds **P19** (spiropyran diazo molecule from **Chaper 3**), **D10**, **D20**, **D30**, and **D40** were submitted to the Oxford Advanced Surfaces group and analysed for DSC, with a heating rate of 5^{o}C/min. The results of this analysis are summarised in **Table 3**. Full spectral data are available in **Appendix VI**.

Diazo compound	Structure	Onset temperature (^{o}C)	ΔH (kJ/mol)
P19	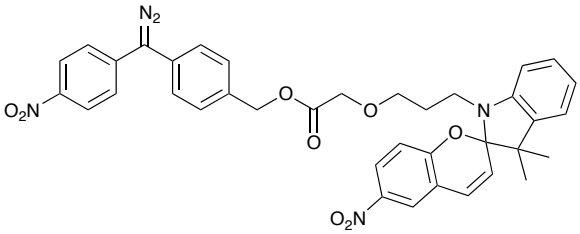	93.4	-118.4
D10	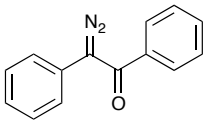	62.3	-86.0
D20	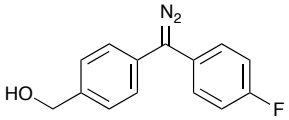	73.4	-20.1
D30	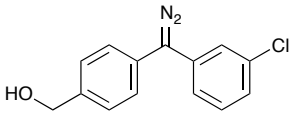	56.2	-12.1
diphenyl diazo methane	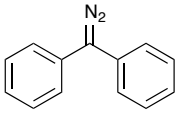	130	-124

Table 3 Results from DSC curves of diazo compounds

From the DSC data, **P19** showed the highest onset temperature at 93°C, consistent with the greatest stability derived from the presence of strong electron withdrawing nitro group on the phenyl ring, and its biggest magnitude of exotherm implied high purity of the sample. The thermal decomposition temperatures of **D10**, **D20**, and **D30** were unexpectedly low, at 62, 73, and 56°C, respectively. In addition, the fact that diazo compound **D10** decomposed at relatively low temperature was perhaps because of a tendency to form a ketene as the generated carbene can react with the adjacent carbonyl group. It was noted that all samples showed low onset temperatures as compared to the onset temperature of diphenyldiazomethane at 130 °C.[14] This indicated that the aim to synthesise more stable diazo compounds was not achieved, however, compound **P19** proved the ability of a diazo compound with a nitro substituent on an aromatic ring to couple with other molecules without complete decomposition. Moreover, the successful synthesis of compound **D10**, **D20**, and **D30** confirmed that a carbonyl group or electron withdrawing atoms can be tolerated in stabilise diazo compounds, which can be handled at room temperature. The stabilities of compounds **D20** and **D30** with a hydroxymethyl group is noteworthy.

By comparison between diazo compounds **D20** and **D30**, the onset temperatures revealed that the higher electronegative fluorine atom provided greater stabilisation even though the para-fluorine is further away from the diazo group than the meta-chlorine. However, this is in contrast with the Hammett equation and substituent constants that a meta-chloro substituent (σ=0.373) would be able to withdraw more electrons from the aromatic ring and hence stabilise the diazo group better than a para-fluoro substituent (σ=0.062).

All samples showed relatively low values of heat of decomposition as compared to that of diphenyldiazomethane of 124 kJ/mol.[119] This indicated low purities of the samples especially compounds **D20** and **D30** which showed only 20

and 12 kJ/mol on heat of decomposition, respectively, while the values for samples **P19** and **D10** are 118 and 86 kJ/mol, respectively.

Diazo compound **D40**, unfortunately, exhibited no thermal event. It was suggested that the sample went off before the measurements as confirmed by the IR spectra displaying only a small residual diazo stretching (**Figure 6**). This is possibly due to the fact that even though the π-system of the thiophene ring was expected to stabilise the diazo group by resonance effect, the presence of the sulphur atom increased the electron density of the ring and hence the ability to donate electrons to the diazo moiety. As a result of this, the thiophene ring would facilitate decomposition of the diazo group.[17,18]

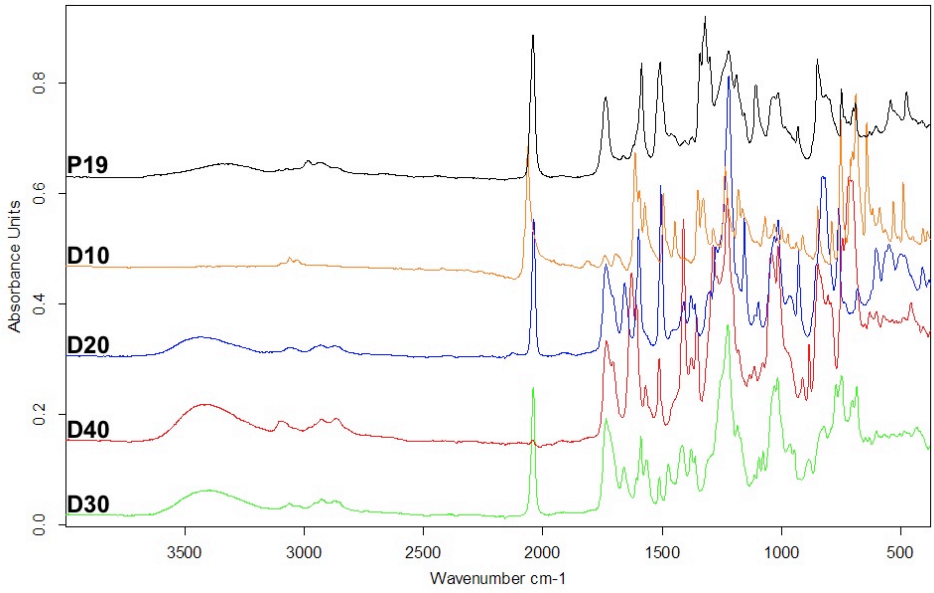

Figure 6 IR spectra of diazo compounds

5.2.6 Conclusions

We have managed to synthesise diazo compounds with different substitution systems, namely fluorenone, alpha-carbonyl, benzophenone, and heteroaromatic diazo compounds, indicating that these diazo compounds can be made and handled at room temperature as a result of stabilisation from a carbonyl group and

substituents capable of withdrawing electrons from the diazo group. Together with a nitro-containing diazo compound previously made for the investigation of photochromicity, all samples were analysed by DSC technique to assess their thermal stabilities. The DSC thermogram of thiophene-derivatived diazo compound indicated that decomposition of the compound prior to the measurement had occurred. The nitro diazo compound was found to be the most stable molecule, while the fluorenone, alpha-carbonyl, and diaryldiazo samples exhibited similar onset temperatures ranging from 56-73^{o}C. Unfortunately, the DSC results revealed that the onset temperatures of these compounds were lower that that of diphenyldiazomethane as a reference. Although this implied failure in syntheses of more stable diazo compounds, the structures of these diazo molecules contain a hydroxy group which could be used to couple with other molecules for synthetic purpose, as demonstrated from the synthesis of spiropyran diazo compound **P19**. Low values of heat of decomposition from DSC results reflected low purities and difficulty in purification of diaryldiazo compounds. According to this, diazo compounds with different functional groups or substituents that could stabilise the diazo moiety need to be identified in future work.

Chapter 6 Experimental

6.1 General procedures and equipment

^{1}H NMR spectra were recorded on Bruker DPX200 (200 MHz) or Bruker DQX400 (400 MHz) spectrometers. Chemical shifts (δ_H) are reported in parts per million (ppm) and are referenced to the residual protonated solvent peak. The abbreviations used to describe multiplicities are as follows: s (singlet), ds (double singlet), d (doublet), t (triplet), q (quartet), m (multiplet) and br (broad). Coupling constants (J) are given in Hertz (Hz). Two-dimensional COSY (correlation spectroscopy) spectra were obtained on a Bruker DQX400 spectrometer at 400 MHz.

^{13}C NMR spectra were recorded on a Bruker DQX400 spectrometer at 101 MHz with proton decoupling. Chemical shifts (δ_C) are reported in parts per million (ppm) and are referenced to the residual protonated solvent peak. Assignment was aided by the use of DEPT editing, HSQC, and HMQC.

^{19}F NMR spectra were recorded on a Bruker AVN400 spectrometer at 376 MHz with proton decoupling. Chemical shifts (δ_F) are reported in parts per million (ppm) and are referenced to the residual protonated solvent peak.

Infrared (IR) spectra were recorded on a Bruker Tensor 27 FT-IR spectrometer. Absorption maxima (ν_{max}) are reported in wavenumbers (cm^{-1}).

Melting points were recorded using a Stuart Scientific SMP1 melting point apparatus in open capillaries and are uncorrected.

Low resolution mass spectra (*m/z*) were recorded on a Fisons Platform spectrometer using electrospray ionisation (ESI). High resolution mass spectra (HRMS) were recorded on a Bruker microTOF (ESI). The *m/z* values of major peaks are reported in Daltons and their intensities given as percentages of the base peak.

Thin layer chromatography (TLC) was performed using Merck aluminium foil backed sheets precoated with 0.2 mm Kieselgel 60 F_{254}. Product spots were visualised by quenching of UV fluorescence (λ_{max} 254 nm), iodine vapour, or by staining with an aqueous solution of $KMnO_4$ or a solution of 5% (w/v) phosphomolybdic acid in ethanol, followed by heating. Both dips were prepared according to J. Leonard, B. Lygo and G. Procter, "Advanced Practical Organic Chemistry", Second Edition, Blackie A & P, 1995.

All reactions were carried out in oven-dried reaction flasks. 'Petrol' refers to that fraction of light petroleum ether boiling at 40-60°C and was used as received. Solvents were evaporated at 40°C or below under reduced pressure on a Buchi RE111 Rotavapor attached to a Vacuubrand CVC2 pump and pressure control system.

All reagents were obtained either from Sigma-Aldrich Chemicals Ltd or Lancaster Chemicals Ltd or Alfa Aesar Chemicals Ltd and used as supplied. NBS was purified according to Dauben, H. J.; McCoy, L. L. *Journal of the American Chemical Society* **1959**, *81*, 4863-4873. Polystyrene (PS) beads were purchased from Sigma-Aldrich Chemicals Ltd, Amberlite® XAD4 (20-60 mesh, surface area 725 m^2/g). Polyethylene terephthalate (PET) sheets were purchased from GoodFellow Cambridge Ltd, ES301485 (thickness 0.50 mm, biaxially oriented).

Surface analysis by Attenuated Total Reflectance Infrared (ATR-IR) was carried out using a Bio-RAD FTS-6000 FT-IR Spectrometer fitted with DuraSamp1IR Diamond ATR. All spectra were recorded at room temperature.

Drop shape analysis was carried out using a combination of surface tensiometer and contact angle goniometer. The results were recorded at room temperature.

Reaction times are recorded in hours (h) and minutes (min). Temperatures below 25°C were obtained using ice/water, dry ice/acetone, and dry ice/diethyl ether baths.

UV experiments were performed using a UVP UVGL-25 mineralight® lamp, multiband UV - 254/365 nm.

General method (I): Functionalisation of polystyrene beads[12]

The appropriate diaryldiazomethane (5mg) was dissolved in ether or THF (5ml) in 50 mL flask. The Amberlite XAD-4 polymer (100mg) was then placed in the solution and the solvent removed *in vacuo* at room temperature. This sample was carefully heated within oil bath at 120°C in their flasks. When no pink colour, due to diaryldiazomethane, was observable on the appropriate sample, heating was stopped and the sample was washed with excess of acetone until no colour was seen to be washed out and final samples were kept for analysis.

General Method(II): H-Acid test for presence of diazonium functionality[9,12]

H-acid (4-amino-5-hydroxynaphthalene-2,7-disulfonic acid) was dissolved in water to achieve a beige opaque solution (approximately 1:2 H-acid:water, v/v). The pH of a sample of the diazonium salt solution was adjusted to 4 using NaOAc. The solution was then added to the H-acid solution which was then agitated to ensure thorough mixing. The solution was left for 5min for the colour to develop. A positive H-acid test was observed as a significant colour change from beige to purple resulting from surface reaction of the diazonium compound.

General method (III): Coupling of diazonium compounds on modified polystyrene beads[12]

Each portion of functionalised Amberlite (100mg) was placed in a separate flask and a suspension of diazonium salt (12mg) in water was added and left overnight to stand. Each sample was then carefully washed with water and acetone by filtration through sintered funnel. This process was repeated until no colour was seen to be washed out and final samples were kept for analysis.

General method (IV): Metal ion coordination on modified polystyrene beads[12]

Each portion of functionalised Amberlite (100mg) was placed in a separate flask and a solution of $ZnSO_4.7H_2O$ (0.5 mg of Zn^{2+}/mL, 2 eq) in 1:1 water:acetone was added and left overnight to stand. Each sample was then carefully washed with water and acetone by filtration through sintered funnel.

General method (V): Metal complex coordination on modified polystyrene beads

Each portion of functionalised Amberlite **PSM27** (100mg) was placed in a separate flask and a solution of ZnATSMA or ZnATSM (8 mg/mL, 2 eq) in DMF was added and left overnight to stand. Each sample was then carefully washed with DMF, 1:1 EtOH:saline (0.9% w/v solution), and acetone by filtration through sintered funnel.

General method (VI): Transmetallation on modified polystyrene beads

Each portion of metal complex-coordinated Amberlite (100mg) was placed in a separate flask and a solution of $CuCl_2.2H_2O$ (4 mg/mL, 1 eq) in DMF was added and left for 72h to stand.

6.2 Experimental for Chapter 2

Synthesis of (4-(bromomethyl)phenyl)(phenyl)methanone (M1)[8]

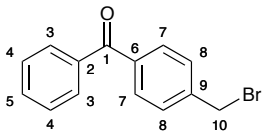

A stirred mixture of 4-methylbenzophenone (6.30 g, 32.11 mmol) and NBS (5.76 g, 32.36 mmol) in $CHCl_3$ (150 mL) was heated under reflux for 18h with a 100W bulb shining 2 cm from the flask. The reaction mixture was washed with water, dried ($MgSO_4$), and solvent was removed *in vacuo*. The resulting solid was then washed with Et_2O to give **M1** (4.74 g, 54%) as a white solid: mp 106-111 ^oC; ν_{max}(film)/cm^{-1} 2924, 2854, 1650(C=O), 1462, 1278, 923, 700; δ_H(200 MHz; $CDCl_3$; Me_4Si) 7.80(4H, m, H-3 and H-7), 7.61(1H, t, J=7.3 Hz, H-5), 7.50(4H, m, H-4 and H-8), 4.55(2H, s, H-10); δ_C(101 MHz; $CDCl_3$; Me_4Si) 196(C-1), 142.1, 137.4, 133.1, 132.8, 130.5, 130.0, 128.4, 126.5, 32.3(C-10); m/z (ESI) 258($[M-O]^+$, 100%), 262(52), 102(47), 195($[M-Br]^+$, 42).

Synthesis of (4-((2-(ethyl(phenyl)amino)ethoxy)methyl)phenyl)(phenyl) methanone (M2)[8]

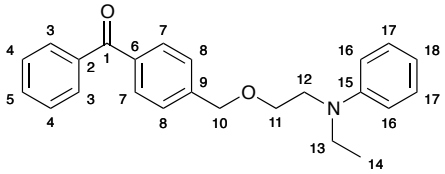

2-(N-Ethylanilino)ethanol (0.07 mL, 0.44 mmol) in dry THF (5 mL) was treated with NaH (60% dispersion in oil, 55.8 mg, 1.40 mmol) and stirred at 20°C for 1h. The bromide **M1** (104.2 mg, 0.38 mmol) was then added and stirring continued for 72h. Excess solvent was removed *in vacuo* and the residue diluted with DCM, washed

with water and $NaHCO_3$ solution (sat.), dried ($MgSO_4$) and solvent removed under vacuum. The resulting oil was purified by flash chromatography, eluting with petroleum (bp 40-60˚C):EtOAc (9:1), to give **M2** (91.0 mg, 67%) as a yellow oil: ν_{max}(film)/cm^{-1} 2867, 1657(C=O), 1598, 1505, 1446, 1353, 1315, 1276, 1193, 1102, 1036, 923, 787, 746, 701; δ_H(200 MHz; $CDCl_3$; Me_4Si) 7.81(4H, m, H-3 and H-7), 7.61(1H, m, H-5), 7.44(4H, m, H-4 and H-8), 7.24(2H, m, H-17), 6.71(3H, m, H-16 and H-18), 4.63(2H, s, H-10), 3.71(2H, t, J=6.3 Hz, H-11), 3.59(2H, t, J=6.3 Hz, H-12), 3.46(2H, q, J=7.1 Hz, H-13), 1.15(3H, t, J=7.1 Hz, H-14); δ_C(101 MHz; $CDCl_3$; Me_4Si) 196.4(C-1), 147.7, 143.1, 137.6, 136.8, 132.4, 130.2, 129.3, 127.0, 111.8, 72.7(C-10), 68.4(C-11), 50.0(C-12), 45.4(C-13), 12.1(C-14); m/z (ESI) 741([2M+Na]$^+$, 100%), 382([M+Na]$^+$, 80), 360([M+H]$^+$, 79), 398([M+K]$^+$, 44); HRMS $C_{24}H_{26}O_2N$ requires 360.1963, found 360.1963.[8]

Synthesis of (Z)/(E)-N-ethyl-N-(2-((4-(hydrazono(phenyl)methyl)benzyl) oxy)ethyl) aniline (M3)[8]

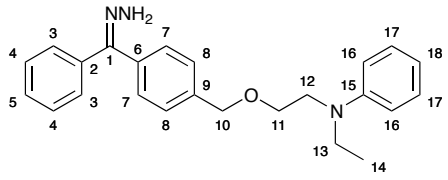

The benzophenone **M2** (691.5 mg, 1.92 mmol) was refluxed in EtOH and hydrazine hydrate (0.47 mL, 9.69 mmol) overnight. The solvent was removed *in vacuo* and the residue dissolved in DCM, washed with water, dried and concentrated under vacuum to give **M3** (646.6 mg, 90%) as a yellow oil. The hydrazone, which was obtained as inseparable mixtures of the *syn*- and *anti*- isomers, was then used without further purification: ν_{max}(film)/cm^{-1} 3405, 3025, 2968, 2865, 1598, 1505, 1444, 1353, 1271, 1193, 1099, 1036, 954, 825, 769, 747, 694; δ_H(200 MHz; $CDCl_3$; Me_4Si) 7.47-7.62(4H, m, H-3 and H-7), 7.21-7.37(7H, m, H-4, H-5, H-7, H-8, and H-17),

6.66-6.76(3H, m, H-16 and H-18), 5.45(2H, br s, NH_2), 4.63 and 4.54(2H, ds, H-10), 3.75(2H, t, J=6.06 Hz, H-11), 3.61(2H, t, J=6.06 Hz, H-12), 3.49(2H, q, J=7.08 Hz, H-13), 1.18(3H, t, J=7.08 Hz, H-14); δ_C(101 MHz; $CDCl_3$; Me_4Si) 149.0(C-1), 148.9, 139.1, 137.8, 132.9, 129.4, 128.8, 128.1, 127.4, 126.4, 115.6, 111.8, 73.1 and 73.0(C-10), 68.3(C-11), 50.1(C-12), 45.5(C-13), 12.2(C-14); m/z (ESI) 374($[M+H]^+$, 100%), 396($[M+Na]^+$, 83).

Synthesis of N-(2-((4-(diazo(phenyl)methyl)benzyl)oxy)ethyl)-N-ethylaniline (M4)[131,132]

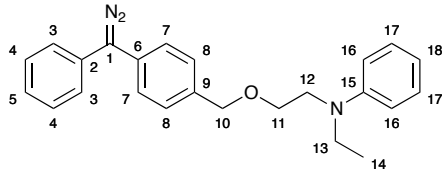

To a mixture of MnO_2 (423.8 mg, 4.87 mmol), Na_2SO_4 (368.4 mg, 2.59 mmol), and KOH (95.1 mg, 1.69 mmol) in MeOH (10 mL) was added a solution of the hydrazone **M3** (589.4 mg, 1.58 mmol) in MeOH (10 mL). The mixture was stirred in the dark for 3h then filtered through a celite pad, and concentrated *in vacuo*. The mixture was extracted with EtOAc, washed with water, dried ($MgSO_4$), and then concentrated *in vacuo* to give **M4** (538.6 mg, 91%) as a red oil: ν_{max}(film)/cm^{-1} 3025, 2864, 2038(C=N_2), 1597, 1506, 1447, 1353, 1273, 1193, 1100, 1036, 813, 747, 694; δ_H(200 MHz; $CDCl_3$; Me_4Si) 7.19-7.52(11H, m, H-3, H-4, H-5, H-7, H-8, and H-17), 6.69(3H, m, H-16 and H-18), 4.56(2H, s, H-10), 3.69(2H, m, H-11), 3.56(2H, m, H-12), 3.44(2H, m, H-13), 1.17(3H, m, H-14); δ_C(101 MHz; $CDCl_3$; Me_4Si) 147.7(C-1), 135.7, 130.2, 129.5, 128.8, 128.5, 128.0, 127.8, 127.2, 126.8, 125.6, 115.7, 111.7, 73.0(C-10), 68.0(C-11), 50.0(C-12), 45.4(C-13), 12.1(C-14); m/z (ESI) 372($[M+H]^+$, 100%), 344($[M-N_2+H]^+$, 92).

Synthesis of benzenediazonium chloride (M5)[50,132,133]

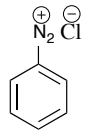

To a stirring solution of aniline (50.0 mg, 0.54 mmol) in THF/water (1:1) at 0 °C, a mixture of $NaNO_2$ (37.0 mg, 0.54 mmol) and HCl 3M (0.36 mL) in water was added. The reaction was stirred at 0 °C and consumption of the amine was tracked by TLC. The red solution was used reacted on straight after completion.

Synthesis of pyridine-4-diazonium chloride (M6)[50,132,133]

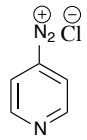

To a stirring colourless solution of 4-aminopyridine (52.2 mg, 0.53 mmol) in THF/water (1:1) at 0 °C, a mixture of $NaNO_2$ (37.0 mg, 0.54 mmol) and HCl 3M (0.35 mL) in water was added. The reaction was stirred at 0 °C and consumption of the amine was tracked by TLC. The yellow solution was used reacted on straight after completion.

Synthesis of 8-hydroxyquinoline-5-diazonium chloride (M7)[50,132,133]

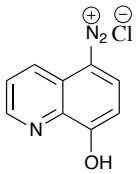

To a stirring red solution of 5-amino-8-hydroxyquinoline dihydrochloride (50.0 mg, 0.21 mmol) in THF/water (1:1) at 0 °C, a mixture of $NaNO_2$ (15.0 mg, 0.22 mmol) and HCl 3M (0.14 mL) in water was added. The reaction was stirred at 0 °C and

consumption of the amine was tracked by TLC. The brown solution was used reacted on straight after completion.

Synthesis of 4-((pyridin-4-ylamino)methyl)benzenediazonium chloride (M8)[50,132,133]

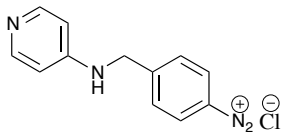

To a stirring yellow solution of N-(4-aminobenzyl)pyridin-4-amine **M11** (111.6 mg) in THF/water (1:1) at 0 °C, a mixture of $NaNO_2$ (38.6 mg, 0.56 mmol) and HCl 3M (0.37 mL) in water was added. The reaction was stirred at 0 °C and consumption of the amine was tracked by TLC. The brown solution was used reacted on straight after completion.

Synthesis of N-(4-nitrobenzylidene)pyridin-4-amine (M9)[134]

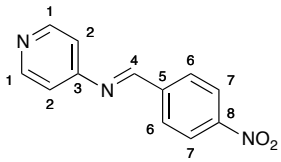

A mixture of 4-aminopyridine (366.7 mg, 3.90 mmol), 4-nitrobenzaldehyde (587.1 mg, 3.88 mmol), and PPTS (1.20 g, 4.78 mmol) was refluxed in toluene (25 mL) for 18h, during which period water was removed periodically by using a Dean-Stark apparatus. The solution was allowed to cool before being concentrated *in vacuo*. The mixture was extracted with DCM, washed with water, dried ($MgSO_4$), and then concentrated *in vacuo* to give **M9** (793 mg, 90%) as a yellow solid: mp 110-112 ^oC; v_{max}(film)/cm^{-1} 3091, 1638(C=N), 1519(NO_2), 1344(NO_2), 1204, 1122, 1034, 1011, 816, 681; δ_H(200 MHz; CD_3OD; Me_4Si) 8.31(2H, d, J=8.6 Hz, H-7), 8.25(1H, s, H-4),

7.86(2H, d, J=8.6 Hz, H-6), 7.68(2H, d, J=8.1 Hz, H-1), 7.22(2H, d, J=8.1 Hz, H-2); δ_C(101 MHz; CD_3OD; Me_4Si) 157.9, 147.2, 140.7, 128.8(C-2), 128.7(C-6), 125.9(C-1), 124.4(C-7), 123.2(C-4); m/z (ESI) 322(100%), 260($[M+H+MeOH]^+$, 89), 228($[M+H]^+$, 39).

Synthesis of N-(4-nitrobenzyl)pyridin-4-amine (M10)[135]

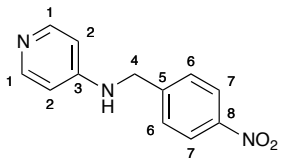

To a solution of the imine **M9** (518.0 mg, 2.28 mmol) in dry MeOH (20 mL), was added powdered $NaBH_4$ (646.8 g, 17.10 mol). The mixture was kept at room temperature for 18h. After completion of the reaction, water was added, and the inorganic precipitate was filtered off and washed with DCM. The organic solution was dried (Na_2SO_4) and removed *in vacuo* to give **M10** (118 mg, 29%) as a yellow oil: ν_{max}(film)/cm^{-1} 1600, 1579, 1521(NO_2), 1461, 1418, 1341(NO_2), 1265, 1208, 1107, 996, 826, 735; δ_H(200 MHz; CD_3OD; Me_4Si) 8.25(2H, d, J=8.1 Hz, H-7), 8.05 (2H, d, J=5.6 Hz, H-1), 7.79 (2H, d, J=8.1 Hz, H-6), 6.66 (2H, d, J=5.6 Hz, H-2), 4.5(2H, s, H-4); δ_C(101 MHz; CD_3OD; Me_4Si) 153.2, 148.7(C-1), 147.1, 146.6, 128.4(C-6), 123.7(C-7), 109.3(C-2), 45.4(C-4); m/z (ESI) 335(100%), 263(68), 230($[M+H]^+$, 30).

Synthesis of N-(4-aminobenzyl)pyridin-4-amine (M11)[136]

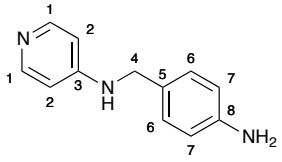

To a stirred solution of the nitro **M10** (129.1 mg, 0.56 mmol in MeOH (20 mL) at room temperature was added $SnCl_2.2H_2O$ (676.7 mg, 3.00 mmol) in portions,

following by the addition of conc HCl (0.23 mL). The reaction mixture was heated for 2h under reflux, cooled down to room temperature and adjusted to pH 8–9 by the addition of 1M NaOH to give a red precipitate which was washed with water and the solvent was evaporated to give an orange solid which was used without further purification.

Synthesis of tert-butyl (4-hydroxyphenyl)carbamate (M12)[137]

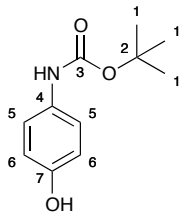

To a magnetically stirred suspension of 4-aminophenol (565.2 mg, 5.18 mmol) in water (20 mL) was added $(Boc)_2O$ (1.31 g, 6.01 mmol) at room temperature. A clear solution was formed with concomitant slow effervescence. After stirring the reaction mixture for 18h, the reaction mixture was extracted with EtOAc, dried (Na_2SO_4) and evaporated to yield **M12** (650.3 mg, 96%) as a white solid: mp 140-142 ^oC; ν_{max}(film)/cm^{-1} 3361(O-H), 2985, 1697(C=O), 1531, 1437, 1370, 1311, 1233, 1167, 1059, 830, 803, 762, 734; δ_H(200 MHz; $CDCl_3$; Me_4Si) 7.19(2H, d, J=8.1 Hz, H-5), 6.75(2H, d, J=8.1 Hz, H-6), 6.34(1H, br s, NH), 5.05(1H, br s, OH), 1.52(9H, s, H-1); δ_C(101 MHz; $CDCl_3$; Me_4Si) 151.8, 147.8, 131.1, 121.1(C-5), 115.6(C-6), 80.3(C-2), 28.3(C-1); m/z (ESI) 208($[M-H]^-$, 100%), 367(64); HRMS $C_{11}H_{14}O_3N$ requires 208.0974, found 208.0977.

Synthesis of 4-((tert-butoxycarbonyl)amino)phenyl 2-bromoacetate (M13)[138]

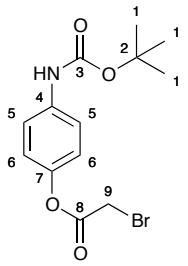

Bromoacetyl bromide (0.49 mL, 5.62 mmol) was dissolved in 3 mL of anhydrous DCM and cooled in an ice bath. Et_3N (0.99 mL, 7.10 mmol) was added, followed by phenol **M12** (594.0 mg, 2.84 mmol) dissolved in 10 mL of DCM. The resulting mixture was stirred for 1h at 0 ^oC. The ice bath was removed and the mixture was stirred for 1h at room temperature. Water (15 mL) was added and the aqueous layer was extracted with another potion of DCM. The combined organic layer was washed with saturated $NaHCO_3$, and brine. The organic layer was dried over $MgSO_4$ and concentrated to give **M13** (937.7 mg, 100%) as a dark brown oil: ν_{max}(film)/cm^{-1} 3321, 1758(C=O, ester), 1609(C=O, carbamate), 1508, 1409, 1367, 1263, 1194, 1159, 1054, 1015, 924, 837; δ_H(200 MHz; $CDCl_3$; Me_4Si) 7.39(2H, d, J=8.8 Hz, H-5), 7.06(2H, d, J=8.8 Hz, H-6), 4.04(2H, s, H-9), 1.41(9H, s, H-1); δ_C(101 MHz; $CDCl_3$; Me_4Si) 166.0(C-8), 152.7, 145.6, 136.5, 121.6(C-6), 121.4, 121.0, 119.3(C-5), 80.7(C-2), 28.3(C-1), 25.5(C-9); m/z (ESI) 352([M+Na]$^+$, 100%); HRMS $C_{13}H_{16}O_4NNaBr$ requires 352.0155, found 352.0159.

Attempted synthesis of 4-((tert-butoxycarbonyl)amino)phenyl 2-(methyl (pyridin-4-yl)amino)acetate (M14)[139]

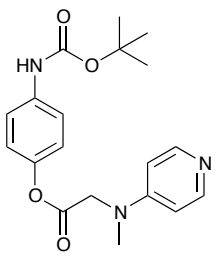

To a flame-dried flask was added 4-(methylamino)pyridine (330.0 mg, 3.05 mmol) and $CHCl_3$ (30.0 mL). The solution was cooled to 0 °C and proton sponge (2.36 g, 11.01 mmol) was added followed by the bromide **M13** (938.0 mg, 2.84 mmol). The mixture was stirred for 1h at 0 °C then warmed to ambient temperature where it was stirred for 24h to give a black precipitate which was unidentifiable by ^1H NMR spectroscopy.

Attempted synthesis of ethyl 2-(4-((tert-butoxycarbonyl)amino)phenoxy)acetate (M16)[140]

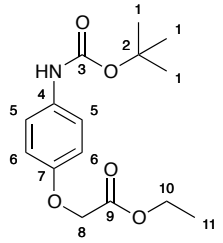

To a mixture of phenol **M12** (924.1 mg, 4.42 mmol), K_2CO_3 (3.06 g, 22.13 mmol), and KI (753.5 mg, 4.54 mmol) in acetone (50mL) was added ethyl bromoacetate (0.53 mL, 4.78 mmol). The mixture was stirred at room temperature for 18h, then concentrated *in vacuo*. The residue was dissolved in EtOAc, washed with water, dried ($MgSO_4$), and solvent was removed *in vacuo* to give **M16** (986.7 mg, 76%) as a pale brown oil: ν_{max}(film)/cm^{-1} 3356, 2979, 1723(C=O, ester), 1601(C=O, carbamate), 1515, 1412, 1367, 1161, 1086, 1053, 1027, 829; δ_H(200 MHz; $CDCl_3$; Me_4Si) 7.27(2H, d, J=9.1 Hz, H-5), 6.84(2H, d, J=9.1 Hz, H-6), 6.46(1H, br s, NH), 4.58(2H, s, H-8), 4.24(2H, q, J=7.08 Hz, H-10), 1.50(9H, s, H-1), 1.28(3H, t, J=7.08 Hz, H-11); the compound could not be sufficiently well purified for ^{13}C NMR analysis; m/z (ESI) 318($[M+Na)]^+$, 100%), 354(40); HRMS $C_{15}H_{21}O_5NNa$ requires 318.1312, found 318.1313.

Attempted synthesis of 2-(4-((tert-butoxycarbonyl)amino)phenoxy)acetic acid (M17)[141,142]

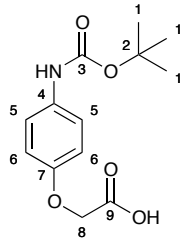

Powdered KOH (204.0 mg, 3.64 mmol) was added to the ester **M16** (431.7 mg, 1.46 mmol) and then dissolved in MeOH (10 mL). The resulting mixture was stirred for 24h. The solvent was evaporated under reduced pressure and the residue was dissolved in water and acidified to pH 4–5 with HCl 1M. The acidic phase was extracted with EtOAc, which was washed with water and brine over $MgSO_4$. The desiccant was filtered and the solvent was evaporated to give **M17** (390 mg) as a pale brown solid: mp 152-156 ^oC; ν_{max}(film)/cm^{-1} 3376, 2988, 1744(C=O, carboxylic), 1692(C=O, carbamate), 1524, 1411, 1310, 1259, 1227, 1158, 831, 430, 407; δ_H(200 MHz; $CDCl_3$; Me_4Si) 7.30(2H, d, J=8.6 Hz, H-5), 6.87(2H, d, J=8.6 Hz, H-6), 4.61(2H, s, H-8), 1.51(9H, s, H-1); the compound could not be sufficiently well purified for ^{13}C NMR analysis; m/z (ESI) 290($[M+Na]^+$, 100%), 266($[M-H]^-$, 95); HRMS $C_{13}H_{17}O_5NNa$ requires 290.0999, found 290.1000.

Attempted synthesis of tert-butyl (4-(2-(methyl(pyridin-4-yl)amino)-2-oxoethoxy)phenyl)carbamate (M18)[143]

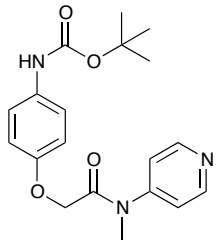

A mixture of the carboxylic acid **M17** (130.0 mg, 0.49 mmol), DCC (120.0 mg, 0.58 mmol), and DMAP (10.0 mg, 0.08 mmol) in DCM (5 mL) was added to a solution of 4-(methylamino)pyridine (70.0 mg, 0.65 mmol in DCM (5 mL) and stirred at room temperature for 18h. The solvent was removed *in vacuo* to give a brown semi-solid which was unidentifiable by ^{1}H NMR spectroscopy.

Synthesis of phenyl(4-((pyridin-4-ylmethoxy)methyl)phenyl)methanone (M20)[144]

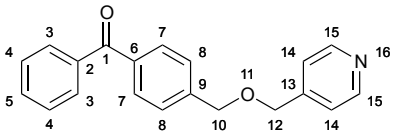

Pyridin-4-ylmethanol (195.0 mg, 1.79 mmol) and dry THF (5 mL) were added to a pre-purged reaction flask. NaH (122mg, 60% dispersion in oil, 3.05 mmol) was added to the reaction flask and the reaction mixture was stirred at 20˚C, for 1h until no more H_2 gas evolution was observed. The solution was heated until the THF boiled using a heat gun. The bromide **M1** (420.0 mg, 1.53 mmol) was dissolved in THF (5 mL) and was added dropwise to the boiling solution. The reaction mixture was stirred at 20˚C for 48h. The solvent was removed *in vacuo* and the residue was dissolved in DCM, washed with water, dried ($MgSO_4$) and the solvent removed *in vacuo*. The crude product was purified by flash column chromatography, eluting with DCM:MeOH (9.5:0.5). The product **M20** was obtained as a brown oil (255 mg, 55%): ν_{max}(film)/cm^{-1} 2924, 1656(C=O), 1606, 1446, 1413, 1278, 1102, 924, 795, 702; δ_H(200 MHz; $CDCl_3$; Me_4Si) 8.59(2H, d, J=5.6 Hz, H-15), 7.81(4H, m, H-3 and H-7), 7.61(1H, t, J=7.3 Hz, H-5), 7.46(4H, m, H-4 and H-8), 7.31(2H, d, J=5.6 Hz, H-14), 4.69(2H, s, H-10), 4.62(2H, s, H-12); δ_C(101 MHz; $CDCl_3$; Me_4Si) 196.3(C-1), 149.9, 147.1, 142.3, 137.5, 137.0, 132.4, 132.3, 132.1, 130.3, 128.2, 121.7, 72.1(C-10),

70.7(C-12); m/z (ESI) 326([M+Na]$^+$, 100%), 304([M+H]$^+$, 84); HRMS $C_{20}H_{18}NO_2$ requires 304.1338, found 304.1332.[144]

Synthesis of (Z)/(E)-4-(((4-(hydrazono(phenyl)methyl)benzyl)oxy)methyl) pyridine (M21)[144]

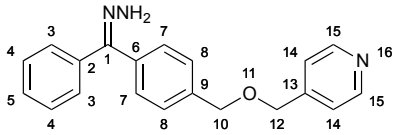

The benzophenone **M20** (235.0 mg, 0.77 mmol) was refluxed in EtOH and hydrazine hydrate (1.90 mL, 50.87 mmol) overnight. The solvent was removed *in vacuo* and the residue dissolved in DCM, washed with water, dried and concentrated under vacuum to give **M21** (244.4 mg, 100%) as a yellow oil. The hydrazone, which was obtained as inseparable mixtures of the *syn*- and *anti*- isomers, was then used without further purification: ν_{max}(film)/cm^{-1} 3384(N-H), 2851, 1606, 1492, 1451, 1416, 1362, 1260, 1099, 800, 699; δ_H(200 MHz; $CDCl_3$; Me_4Si) 8.49(2H, d, J=4.8 Hz, H-15), 7.25-7.55(11H, m, H-3, H-4, H-5, H-7, H-8, and H-14), 5.44(2H, br s, NH_2), 4.57(2H, s, H-12), 4.54(2H, ds, H-10); δ_C(101 MHz; $CDCl_3$; Me_4Si) 149.7(C-1), 148.8, 147.6, 138.4, 132.8, 132.5, 128.9, 128.6, 128.4, 128.1, 127.9, 127.4, 72.5(C-12), 72.4 and 70.2(C-10); m/z (ESI) 326(100%), 304(44), 328(41%), 340([M-H+Na]$^+$, 27).

Synthesis of 4-(((4-(diazo(phenyl)methyl)benzyl)oxy)methyl)pyridine (M22)[131,132]

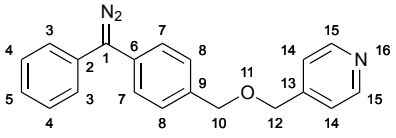

To a mixture of MnO_2 (156.0 mg, 1.80 mmol), Na_2SO_4 **M21** 143.0 mg, 1.01 mmol), and KOH (57.0 mg, 1.02 mmol) in MeOH (5 mL) was added a solution of the hydrazone (190.0 mg, 0.60 mmol) in MeOH (5 mL). The mixture was stirred in the

dark for 3h then filtered through a celite pad, and concentrated *in vacuo*. The mixture was extracted with EtOAc, washed with water, dried ($MgSO_4$), and then concentrated *in vacuo* to give **M22** (189.2 mg, 100%) as a red oil: ν_{max}(film)/cm^{-1} 2854, 2039(C=N_2), 1605, 1493, 1416, 1233, 1101, 799, 753, 698; δ_H(200 MHz; $CDCl_3$; Me_4Si) 8.51-8.55(2H, m, H-15), 7.19-7.42(11H, m, H-3, H-4, H-5, H-7, H-8, and H-14), 4.54-4.60(4H, m, H-10 and H-12); δ_C(101 MHz; $CDCl_3$; Me_4Si) 149.7(C-1), 144.0, 143.9, 136.7, 130.3, 129.3, 128.7, 127.2, 126.8, 125.7, 121.8, 121.8, 72.5(C-12), 70.3(C-10); m/z (ESI) 288(100%), 370(97), 328(71), 289([M-N_2+H]$^+$, 45).

Synthesis of (E)-4-((pyridin-4-ylimino)methyl)phenol (M23)[145]

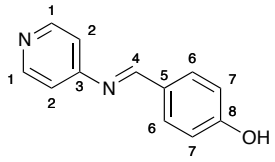

4-Aminopyridine (617 mg, 6.56 mmol) was added to 4-hydroxybenzaldehyde (803 mg, 6.58 mmol) in toluene (20 mL) and then refluxed for 18h. A Dean-Stark apparatus was used for continuous removal of the water that was produced in the reaction. The precipitates form were washed with hot toluene, dissolved in hot EtOH, then filtered while being hot. The solvent was then removed *in vacuo* to afford **M23** (885 mg, 68%) as a yellow solid: ν_{max}(film)/cm^{-1} 3418, 3005, 2918, 1437, 1407, 1316, 1021, 953, 707, 669, 573, 501, 465, 409; δ_H(200 MHz; DMSO-d_6; Me_4Si) 8.51(2H, d, J=3.03 Hz, H-1), 8.46(1H, s, H-4), 7.80(2H, d, J=8.59 Hz, H-6), 7.13(2H, d, J=3.03 Hz, H-2), 6.90(2H, d, J=8.59 Hz, H-7); δ_C(101 MHz; DMSO-d_6; Me_4Si) 162.3, 159.5, 151.3(C-1), 149.9(C-4), 132.1(C-6), 127.6, 116.8(C-7), 116.6(C-2); m/z (ESI) 197([M-H]$^-$, 100%), 198([M]$^-$, 34); HRMS $C_{12}H_9ON_2$ requires 197.0720, found 197.0719.

Synthesis of 4-((pyridin-4-ylamino)methyl)phenol (M24)[135]

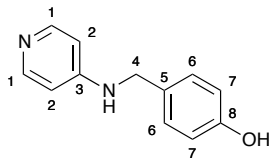

To a solution of the imine **M23** (789 mg, 3.98 mmol) in dry MeOH (20 mL), was added powdered $NaBH_4$ (1.506 g, 39.8 mol). The mixture was kept at room temperature for 18h. After completion of the reaction, the solvent was removed *in vacuo* and the residue was washed with DCM. Then water was added and adjusted to pH 8–9 by the addition of 3M HCl to give white precipitates which were washed with water and filtered to afford **M24** (390 mg, 49%) as a white solid: ν_{max}(film)/cm^{-1} 3417, 2255, 2128, 1026, 825, 764, 402; δ_H(200 MHz; DMSO-d_6; Me_4Si) 9.32(1H, br s, OH), 7.97(2H, d, J=5.31 Hz, H-1), 7.11(2H, d, J=8.34 Hz, H-6), 6.71(2H, d, J=8.34 Hz, H-7), 6.48(2H, d, J= 5.31 Hz, H-2), 4.16(2H, s, H-4); δ_C(101 MHz; DMSO-d_6; Me_4Si) 157.2, 154.4, 149.8(C-1), 129.7, 129.3(C-6), 115.9(C-7), 108.2(C-2), 45.8(C-4); m/z (ESI) 201($[M+H]^+$, 100%), HRMS $C_{12}H_{13}ON_2$ requires 201.1022, found 201.1017.

Synthesis of phenyl(4-((4-((pyridin-4-ylamino)methyl)phenoxy)methyl)phenyl) methanone (M25)[8]

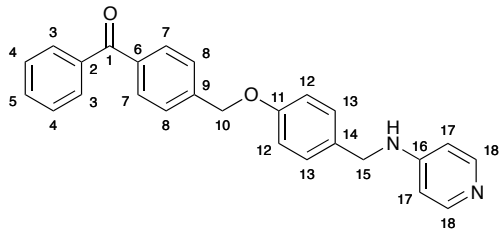

The phenol **M24** (177 mg, 0.88 mmol) in dry THF (10 mL) was treated with NaH (60% dispersion in oil, 110 mg, 2.75 mmol) and stirred at 20˚C for 1h. The bromide **M1** (261 mg, 0.94 mmol) was then added and stirring continued for 72h. Excess solvent was removed *in vacuo* and the residue diluted with DCM, washed

with water and $NaHCO_3$ solution (sat.), dried ($MgSO_4$) and solvent removed under vacuum to give **M25** as a dark brown semi-solid (347 mg, 100%): ν_{max}(film)/cm^{-1} 2923, 1655(C=O), 1603, 1510, 1446, 1315, 1277, 1175, 923, 701, 537, 501, 465, 405; δ_H(200 MHz; $CDCl_3$; Me_4Si) 8.19(2H, d, J=6.32 Hz, H-18), 7.78-7.84(4H, m, H-3 and H-7), 7.47-7.62(5H, m, H-4, H-5, and H-8), 7.26(2H, d, J=8.59 Hz, H-13), 6.97(2H, d, J=8.59 Hz, H-12), 6.46(2H, d, J=6.32 Hz, H-17), 5.16(2H, s, H-10), 4.29(2H, s, H-15); δ_C(101 MHz; $CDCl_3$; Me_4Si) 196.2(C-1), 157.9, 153.0, 150.0, 141.5, 137.5, 137.1, 132.5, 130.7, 130.4, 130.0, 128.7, 128.3, 126.9, 126.2, 115.1, 69.4(C-10), 46.2(C-15); m/z (ESI) 395($[M+H]^+$, 100%); HRMS $C_{26}H_{23}O_2N_2$ requires 395.1754, found 395.1746.

Synthesis of (Z)/(E)-N-(4-(4-(hydrazono(phenyl)methyl)benzyloxy)benzyl)aniline (M26)[8]

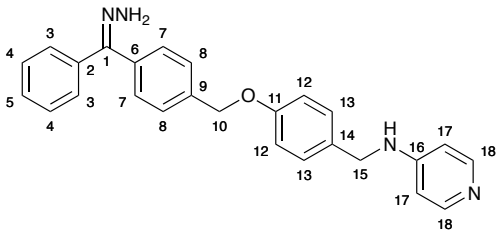

The benzophenone **M25** (810 mg, 2.05 mmol) was refluxed in EtOH and hydrazine hydrate (0.50 mL, 10.31 mmol) overnight. The solvent was removed *in vacuo* and the residue dissolved in DCM, washed with water, dried and concentrated under vacuum to give **M26** (737 mg, 88%) as a dark brown oil. The hydrazone, which was obtained as inseparable mixtures of the *syn*- and *anti*- isomers, was then used without further purification: ν_{max}(film)/cm^{-1} 3385, 2923, 1604, 1510, 1444, 1240, 1173, 813, 698; δ_H(200 MHz; $CDCl_3$; Me_4Si) 8.16(2H, m, H-18), 7.02-7.80(13H, m, H-3, H-4, H-5, H-7, H-8, H-12, and H-13), 6.46(2H, m, H-17), 5.46(2H, br s, NH_2), 5.13 and 5.03(2H, ds, H-10), 4.63(1H, br s, NH), 4.28(2H, s, H-15); δ_C(101 MHz; $CDCl_3$;

Me_4Si) 153.2(C-1), 149.9, 148.7, 136.6, 132.5, 130.4, 130.1, 129.4, 128.9, 128.6, 128.4, 128.1, 127.2, 126.9, 126.4, 115.1, 69.7 and 69.6(C-10), 46.3(C-15); m/z (ESI) 409($[M+H]^+$, 100%), 410(49), 441($[M+H+MeOH]^+$, 39); HRMS $C_{26}H_{25}ON_4$ requires 409.2023, found 409.2017.

Synthesis of N-(4-(4-(diazo(phenyl)methyl)benzyloxy)benzyl)aniline (M27)[131,132]

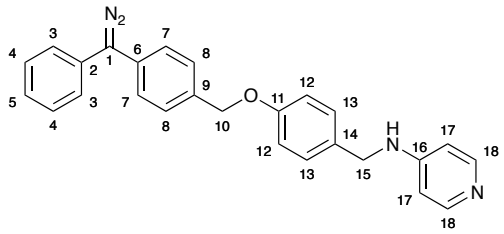

To a mixture of MnO_2 (474 mg, 5.45 mmol), Na_2SO_4 (442 mg, 3.11 mmol), and KOH (180 mg, 3.21 mmol) in MeOH (15 mL) was added a solution of the hydrazone **M26** (737 mg, 1.81 mmol) in MeOH (15 mL). The mixture was stirred in the dark for 18h then filtered through a celite pad, eluted with EtOAc/Et_3N, and concentrated *in vacuo*. The mixture was extracted with EtOAc, washed with water, dried ($MgSO_4$), and then concentrated *in vacuo* to give **M27** (560 mg, 76%) as a red oil: ν_{max}(film)/ cm^{-1} 2923, 2039(C=N_2), 1604, 1510, 1240, 1173, 988, 812, 732, 697; δ_H(200 MHz; $CDCl_3$; Me_4Si) 8.17(2H, m, H-18), 7.17-7.86(11H, m, H-3, H-4, H-5, H-7, H-8, and H-13), 6.97(2H, m, H-12), 6.46(2H, m, H-17), 5.06(2H, s, H-10), 4.68(1H, br s, NH), 4.29(2H, s, H-15); δ_C(101 MHz; $CDCl_3$; Me_4Si) 158.2(C-1), 153.3, 149.7, 134.0, 132.5, 130.4, 130.1, 129.5, 129.2, 128.7, 127.5, 126.9, 126.8, 125.7, 125.2, 115.1, 69.8(C-10), 46.3(C-15); m/z (ESI) 379($[M+H-N_2]^+$, 100%).

Synthesis of Diacetyl-bis(N-4-methyl-3-thiosemicarbazone) ($ATSMH_2$)[37]

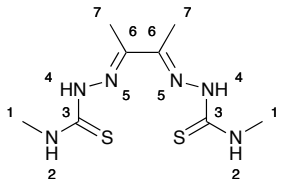

4-Methylthiosemicarbazide (573 mg, 5.45 mmol) was dissolved in ethanol (15 mL) and butane-2,3-dione (0.24 mL, 2.73 mmol), and conc H_2SO_4 (3 drops) were added. The reaction was stirred at room temperature for 16h. The white precipitate was filtered, rinsed with EtOH and Et_2O, then dried in vacuo to give $ATSMH_2$ as a white solid (344 mg, 48%); ν_{max}(film)/cm^{-1} 3442, 2250, 2125, 1662, 1053, 1024, 1005, 821, 758, 622; δ_H(200 MHz; DMSO-d_6; Me_4Si) 10.21(2H, s, H-4), 8.37(2H, s H-2), 3.02(6H, s, H-1), 2.20(6H, s, H-7); δ_C(101 MHz; DMSO-d_6; Me_4Si) 179.3(C-3), 148.8(C-6), 32.0(C-1), 12.5(C-7); m/z (ESI) 259($[M-H]^-$, 100%).

Synthesis of diacetyl-bis(N-4-methyl-3-thiosemicarbazonato) zinc(II) (ZnATSM/ M28c)[146]

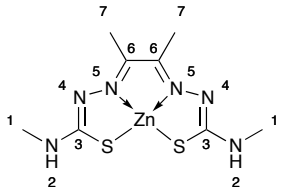

$ATSMH_2$ (344 mg, 1.32 mmol) was suspended in methanol (15 mL) and $Zn(OAc)_2.2H_2O$ (300 mg, 1.37 mmol) was added. The reaction stirred at room temperature for 16h. The yellow precipitate was filtered, rinsed with MeOH and Et_2O, then dried in vacuo to give **M28c** as a yellow solid (115 mg, 27%); ν_{max}(film)/cm^{-1} 3432, 2252, 2126, 1661, 1051, 1023, 1003, 859, 822, 614; δ_H(200 MHz; DMSO-d_6; Me_4Si) 7.18(2H, s, H-2), 2.82(6H, s, H-1), 2.20(6H, s, H-7); δ_C(101 MHz; DMSO-d_6; Me_4Si) 178.9(C-3), 145.2(C-6), 29.2(C-1), 13.8(C-7); m/z (ESI) 107(100%), 217(57), 323($[M+H]^+$, 41).

6.3 Experimental for Chapter 3

Synthesis of (4-nitrophenyl)(p-tolyl)methanone (P1)[147]

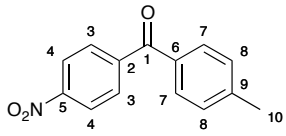

To a stirred solution of toluene (50 mL) and 4-nitrobenzoyl chloride (4.22 g, 24.61 mmol) was added $AlCl_3$ (3.40 g, 25.50 mmol). The resulting red solution was stirred at room temperature for 90min, and then 5 mL of water was added dropwise. The mixture was stirred for 20min, then washed with water and 10% $NaHCO_3$ and dried ($MgSO_4$). The solvent was removed *in vacuo* to give **P1** (2.58 g, 43%) as a pale yellow solid; mp 107-110 ^oC: ν_{max}(film)/cm^{-1} 3106, 2924, 1656(C=O), 1602, 1527(NO_2), 1352(NO_2), 1317, 1145, 1108, 931, 870, 852, 772, 731, 718, 703; δ_H(200 MHz; $CDCl_3$; Me_4Si) 8.33(2H, d, J=8.5 Hz, H-4), 7.91(2H, d, J=8.5 Hz, H-3), 7.71(2H, d, J=8.1 Hz, H-7), 7.32(2H, d, J=8.1 Hz, H-8), 2.46 (3H, s, H-10); δ_C(101 MHz; $CDCl_3$; Me_4Si) 194.5(C-1), 149.6, 144.5, 144.3, 133.6, 130.3(C-3 and C-7), 129.0(C-8), 123.2(C-4), 21.7(C-10); m/z (ESI) 279($[M-H+K]^+$, 100%), 281($[M+H+K]^+$, 42).

Synthesis of (4-(bromomethyl)phenyl)(4-nitrophenyl)methanone (P2)[8]

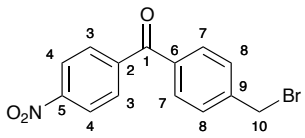

A stirred mixture of the benzophenone **P1** (2.56 g, 10.61 mmol) and NBS (3.10 g, 17.42 mmol) in $CHCl_3$ (50 mL) was heated under reflux for 18h with a 100W bulb shining 2 cm from the flask. The reaction mixture was washed with water, dried ($MgSO_4$), and solvent was removed *in vacuo*. The resulting solid was then washed

with Et_2O to remove any starting material to give **P2** (3.40 g, 100%) as a brown solid; mp 133-135 ^oC; ν_{max}(film)/cm^{-1} 2924, 1658(C=O), 1600, 1517(NO_2), 1410, 1354(NO_2), 1316, 1276, 931, 868, 852, 779, 748, 708, 601; δ_H(200 MHz; $CDCl_3$; Me_4Si) 8.35(2H, d, J=8.6 Hz, H-4), 7.94(2H, d, J=8.6 Hz, H-3), 7.80(2H, d, J=8.3 Hz, H-7), 7.54(2H, d, J=8.3 Hz, H-8), 4.55(2H, s, H-10); δ_C(101 MHz; $CDCl_3$; Me_4Si) 193.6(C-1), 149.8, 143.3, 142.2, 136.0, 130.5(C-3), 130.4(C-7), 129.3(C-8), 123.6(C-4), 31.9(C-10); m/z (ESI) 360($[M+MeCN+H]^+$, 100%).

Synthesis of (4-(hydroxymethyl)phenyl)(4-nitrophenyl)methanone (P3)[148]

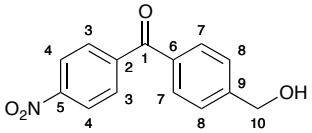

To a suspension of the bromide **P2** (1.73 g, 5.34 mmol) in a mixture of 1,4-dioxane (25 mL) and water (25 mL) was added $CaCO_3$ (3.12 g, 31.17 mmol). The mixture was heated under reflux for 18h, then allowed to cool before being concentrated *in vacuo*. Then 10% aqueous HCl solution (30 mL) was added. The mixture was extracted with DCM, washed with water, dried ($MgSO_4$), and then concentrated *in vacuo* to give **P3** (1.24 g, 90%) as a brown solid; mp 134-137 ^oC; ν_{max}(film)/cm^{-1} 3000-3500(OH), 2867, 1650(C=O), 1601, 1519(NO_2), 1347(NO_2), 1316, 1046, 932, 852, 772, 704; δ_H(200 MHz; $CDCl_3$; Me_4Si) 8.32(2H, d, J=6.3 Hz, H-4), 7.92(2H, d, J=6.3 Hz, H-3), 7.79(2H, d, J=7.6 Hz, H-7), 7.51(2H, d, J=7.6 Hz, H-8), 4.82(2H, s, H-10); δ_C(101 MHz; $CDCl_3$; Me_4Si) 194.5(C-1), 149.7, 142.9, 130.9, 130.6, 130.4, 129.7, 127.6, 126.9, 64.4(C-10); m/z (ESI) 256($[M-H]^-$, 100%), 240($[M-OH]^-$, 65); HRMS $C_{14}H_{10}NO_4$ requires 256.0615, found 256.0609.

Synthesis of (Z)/(E)-(4-(Hydrazono(4-nitrophenyl)methyl)phenyl)methanol (P4)[8]

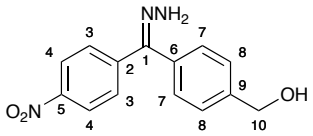

To a stirred solution of the benzophenone **P3** (4.67 g, 18.15 mmol) and EtOH (40 mL) was added hydrazine monohydrate (4.4 ml, 90.70 mmol). The mixture was heated under reflux for 18h, then allowed to cool before being concentrated *in vacuo*. The residue was dissolved in DCM, washed with water, dried ($MgSO_4$), and solvent was removed *in vacuo* to give **P4** (4.73 g, 96%) as an orange semi-solid; ν_{max}(film)/ cm^{-1} 3405(OH), 1596, 1554, 1511(NO_2), 1407, 1336(NO_2), 1190, 1109, 854, 700; δ_H(200 MHz; $CDCl_3$; Me_4Si) 8.07-8.36(2H, m, H-4), 7.13-7.78(6H, m, H-3, H-7, and H-8), 5.81(2H, br s, NH_2), 4.64(2H, ds, H-10); δ_C(101 MHz; $CDCl_3$; Me_4Si) 146.9(C-1), 145.9, 144.8, 142.5, 141.4, 139.5, 130.2, 128.4, 126.9, 64.6(C-10); m/z (ESI) 270([M-H]$^-$, 100%), 271(M^-, 21); HRMS $C_{14}H_{12}N_3O_3$ requires 270.0884, found 270.0883.

Synthesis of (4-(diazo(4-nitrophenyl)methyl)phenyl)methanol (P5)[131,132]

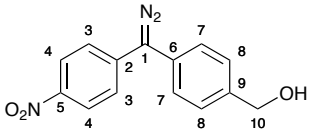

To a mixture of MnO_2 (124 mg, 1.42 mmol), Na_2SO_4 (130 mg, 0.92 mmol), and KOH (50 mg, 0.89 mmol) in MeOH (10 mL) was added a solution of the hydrazone **P4** (125 mg, 0.46 mmol) in MeOH (5 mL). The mixture was stirred in the dark for 3h then filtered through a celite pad, and concentrated *in vacuo*. The mixture was extracted with EtOAc, washed with water, dried ($MgSO_4$), and then concentrated *in vacuo* to give **P5** (110 mg, 89%) as a red oil: ν_{max}(film)/cm^{-1} 2918, 2043(C=N_2), 1587, 1508(NO_2), 1322(NO_2), 1260, 1111, 851, 749; δ_H(200 MHz; $CDCl_3$; Me_4Si) 8.16-8.23(2H, m, H-4), 7.19-7.51(6H, m, H-3, H-7, and H-8), 4.76(2H, s, H-10);

δ_C(101 MHz; $CDCl_3$; Me_4Si) 154.3(C-1), 140.5, 130.6, 129.4, 127.3, 127.0, 124.6, 123.5, 122.8, 64.7(C-10); m/z (ESI) 367(100%).

Synthesis of 1-(4-carboxybutyl)-2,3,3-trimethyl-3H-indol-1-ium bromide (P13)[89]

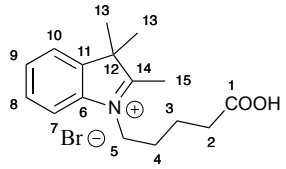

A solution of 2,3,3-trimethylindolenine (0.70 mL, 4.36 mmol) and 5-bromovaleric acid (800.0 mg, 4.42 mmol) in 5 mL of chlorobenzene was heated at 140 °C for 16h. After cooling to room temperature, the solvent was removed *in vacuo* to give **P13** (1.48 g, 100%) as a dark red semi-solid: ν_{max}(film)/cm^{-1} 2927, 1729(C=O), 1463, 1388, 1168, 862, 763, 650, 537, 501, 465, 429, 402; δ_H(200 MHz; $CDCl_3$; Me_4Si) 7.39-8.00(4H, m, H-7, H-8, H-9, and H-10), 4.50(2H, t, J=5.06 Hz, H-5), 2.86(3H, s, H-15), 2.31(2H, t, J=7.33 Hz, H-2), 1.86(2H, m, H-4), 1.65(2H, m, H-3), 1.54(6H, s, H-13); δ_C(101 MHz; $CDCl_3$; Me_4Si) 197.0(C-1), 151.1, 144.1, 142.9, 130.2, 129.2, 124.4, 117.4, 54.7(C-5), 40.9(C-12), 33.5, 32.4, 30.2(C-15), 22.8(C-3), 22.5(C-13); m/z (ESI) 470(100%), 260($[M-Br]^+$, 62), 160(58).

Attempted synthesis of 5-(3',3'-dimethyl-6-nitrospiro[chromene-2,2'-indolin]-1'-yl)pentanoic acid (P14)[89]

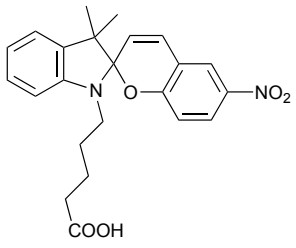

A solution of the iminium **P13** (227 mg, 0.67 mmol) and 5-nitrosalicylaldehyde (114 mg, 0.68 mmol) in 10 mL of THF was heated at 80 °C for 12h. After cooling to

room temperature, the solvent was removed *in vacuo* to give a dark red oil which was unidentifiable by ^{1}H NMR spectroscopy.

Synthesis of 1-(3-hydroxypropyl)-2,3,3-trimethyl-3H-indol-1-ium iodide (P15)[90]

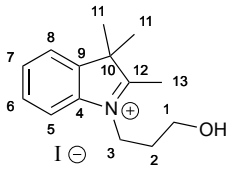

2,3,3-Trimethyl-3H-indole (0.17 mL, 1.06 mmol) was dissolved in $CHCl_3$ (5 mL) and degassed. 3-iodopropan-1-ol (0.10 mL, 1.00 mmol) was added and the solution was refluxed for 24h. The mixture was cooled to room temperature, the solvent was evaporated, and the oil was washed with petroleum ether and triturated with Et_2O to afford **P15** as a dark-red oil (359 mg, 100%): ν_{max}(film)/cm^{-1} 3374, 2929, 2873, 1625, 1606, 1478, 1460, 1367, 1183, 1070, 935, 765, 650, 572, 537, 501, 465, 430, 411; δ_H(200 MHz; DMSO-d_6; Me_4Si) 7.95(1H, d, J=7.33 Hz, H-5), 7.85(1H, d, J=7.08 Hz, H-8), 7.62(2H, m, H-6 and H-7), 4.55(2H, t, J=6.82 Hz, H-3), 3.84(1H, br s, OH), 3.54(2H, t, J=5.56 Hz, H-1), 2.85(3H, s, H-13), 2.03(2H, m, H-2), 1.53(6H, s, H-11); δ_C(101 MHz; DMSO-d_6; Me_4Si) 142.7, 141.9, 140.8, 130.1, 129.7, 124.3(C-8), 116.3(C-5), 58.7(C-1), 46.6(C-3), 41.0(C-10), 30.5(C-2), 22.7(C-11), 15.0(C-13); m/z (ESI) 218([M-I]$^+$, 100%), 198(98); HRMS $C_{14}H_{19}ON$ requires 217.1467, found 217.1472.[90]

Synthesis of 10,10,10a-trimethyl-3,4,10,10a-tetrahydro-2H-[1,3]oxazino[3,2-a]indole (P16)[90]

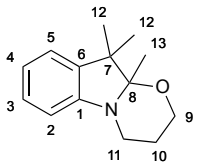

The indolium **P15** (541 mg, 1.57 mmol) was suspended in degassed water (10 mL), finely ground KOH (180 mg, 3.21 mmol) was added, and the mixture was stirred at room temperature for 2h. DCM (10 mL) was added and the mixture was stirred for 30min. The aqueous layer was separated and extracted with DCM. The combined organic layers were washed with brine and water, then dried over Na_2SO_4. The solvent was evaporaterd. The residue was dried under vacuum and purified by flash chromatography on silica gel (petroleum ether:EtOAc 4:1 to 1:1) to afford **P16** as a brown oil (140 mg, 41%): ν_{max}(film)/cm^{-1} 2923, 2853, 1606, 1481, 1372, 1266, 1073, 741; δ_H(200 MHz; $CDCl_3$; Me_4Si) 7.18(1H, t, J=7.71 Hz, H-3), 7.13(1H, d, J=7.33 Hz, H-5), 6.86 (1H, t, J=7.33 Hz, H-4), 6.64(1H, d, J=7.83 Hz, H-2), 4.13(1H, dt, J=2.53, 12.13 Hz, H-9), 3.71(1H, dd, J=5.30, 11.62 Hz, H-9), 3.68(1H, dd, J=4.80, 14.65 Hz, H-11), 3.54(1H, m, H-11), 1.98-2.07(1H, m, C-10), 1.60(3H, s, H-13), 1.35 and 1.12(6H, ds, C-12), 1.23(1H, d, J=13.39 Hz, C-10); δ_C(101 MHz; $CDCl_3$; Me_4Si) 148.0, 139.2, 127.2(C-3), 122.0(C-5), 119.2(C-4), 108.6(C-2), 98.3(C-8), 61.0(C-9), 48.0(C-7), 39.1(C-11), 21.7(C-10), 18.6(C-12) 13.0(C-13); m/z (ESI) 218([M+H]$^+$, 100%), 240([M+Na]$^+$, 98); HRMS $C_{14}H_{20}ON$ requires 218.1539, found 218.1545.

Synthesis of 3-(3',3'-dimethyl-6-nitrospiro[chromene-2,2'-indolin]-1'-yl)propan-1-ol (P17)[90]

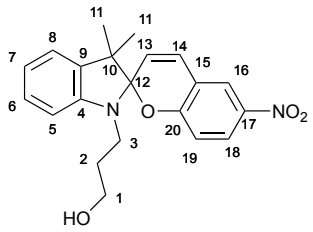

To a degassed solution of the indole **P16** (140 mg, 0.64 mmol) in dry EtOH (5 mL) was added 5-nitrosalicylaldehyde (115 mg, 0.69 mmol). The mixture was sonicated. EtOH was evaporated. The residue was taken up in DCM, washed with

water, and dried over Na_2SO_4. The solvent was evaporated and dried under vacuum. The crude product was purified by flash chromatography on silica gel (hexane:EtOAc 1:1) to afford **P17** (25 mg, 10%) as a pale purple solid: ν_{max}(film)/cm^{-1} 2963, 1610, 1516(NO_2), 1481, 1335(NO_2), 1089, 955, 910, 806, 746; δ_H(200 MHz; $CDCl_3$; Me_4Si) 8.00(2H, m, H-16 and H-18), 7.20(1H, m, H-7), 7.09(1H, d, J=7.07 Hz, H-5), 6.91(1H, d, J=6.06 Hz H-14), 6.88(1H, m, H-6), 6.75(1H, d, J=8.59 Hz, H-19), 6.65(1H, d, J=7.83, H-8), 5.88(1H, d, J=6.06 Hz, H-13), 3.71(2H, t, J=6.00 Hz, H-1), 3.23-3.40(2H, m, H-3), 1.77-1.98(2H, m, H-2), 1.19 and 1.29(6H, ds, H-11); δ_C(101 MHz; $CDCl_3$; Me_4Si) 159.6, 147.0, 141.0, 136.0, 128.2(C-5), 127.8(C-7), 125.9(C-16), 122.7(C-18), 121.8(C-14), 121.7(C-13), 119.6(C-6), 118.5, 115.5(C-19), 106.9(C-8), 60.7(C-1), 52.6(C-10), 40.67(C-3), 31.6(C-2), 19.9(C-11); m/z (ESI) 389([M+Na]$^+$, 100%), 367([M+H]$^+$, 52); HRMS $C_{21}H_{23}O_4N_2$ requires 367.1652, found 367.1653.

Synthesis of 4-(diazo(4-nitrophenyl)methyl)benzyl 2-bromoacetate (P18)[149]

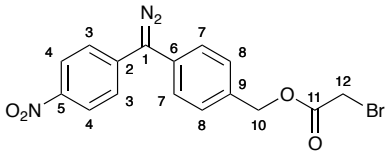

To a stirred solution of the diazo **P5** (110 mg, 0.41 mmol) and Et_3N (0.18 ml, 1.29 mmol)/DCM (5 ml) was added bromoacetyl bromide (0.04 ml, 0.46 mmol) dropwise over 5 min. The mixture was stirred at 0^{o}C for 4h, washed with water, dried ($MgSO_4$), and solvent was removed *in vacuo* to give **P18** (151 mg, 94%) as a red oil; ν_{max}(film)/cm^{-1} 2045(C=N_2), 1743(COO), 1622, 1587, 1509(NO_2), 1322(NO_2), 1301, 1256, 1227, 1190, 1111, 1018, 933, 851, 749; δ_H(200 MHz; $CDCl_3$; Me_4Si) 8.33(2H, d, J=8.7 Hz, H-4), 7.91(2H, d, J=8.7 Hz, H-3), 7.70(2H, d, J=8.3 Hz, H-7), 7.48(2H, d, J=8.3 Hz, H-8), 5.10(2H, s, H-10), 3.73(2H, s, H-12); δ_C(101 MHz; $CDCl_3$; Me_4Si)

167.4(C-11), 152.9(C-1), 138.2, 135.4, 131.2, 130.3, 129.4, 127.3, 126.9, 124.5, 65.6(C-10), 55.0(C-12); m/z (ESI) 240(100%), 242(62).

Synthesis of 4-(diazo(4-nitrophenyl)methyl)benzyl 2-(3-(3',3'-dimethyl-6-nitrospiro[chromene-2,2'-indoline]-1'-yl)propoxy)acetate (P19)

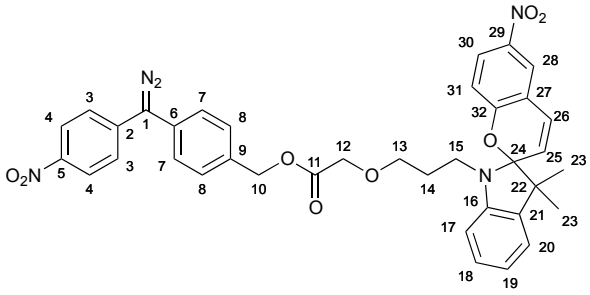

To a stirred solution of the spiropyran **P17** (23 mg, 0.063 mmol) and Et_3N (0.03 mL, 0.22 mmol)/DCM (5 ml) was added 4-(diazo(4-nitrophenyl)methyl)benzyl 2-bromoacetate **P18** (26 mg, 0.067 mmol). The mixture was stirred at room temperature for 18h, washed with water, dried ($MgSO_4$), and solvent was removed *in vacuo* to give **P19** (41 mg, 100%) as a red brown solid; ν_{max}(film)/cm^{-1} 2962, 2925, 2046(C=N_2), 1740(COO), 1609, 1588, 1514(NO_2), 1481, 1458, 1334(NO_2), 1330, 1275, 1230, 1160, 1110, 1089, 1026, 950, 911, 850, 805, 748; δ_H(200 MHz; $CDCl_3$; Me_4Si) 8.33(2H, m, H-4), 8.00(2H, m, H-28 and H-30), 7.92(2H, m, H-3), 7.71(2H, m, H-7), 7.48(2H, m, H-8), 7.20(1H, m, H-19), 7.09(1H, m, H-17), 6.91(1H, m, H-26), 6.88(1H, m, H-18), 6.74(1H, m, H-31), 6.65(1H, m, H-20), 5.88(1H, m, H-25), 5.14(2H, s, H-10), 4.42(2H, s, H-12), 3.68(2H, m, H-13), 3.23-3.40(1H, m, H-15), 1.77-1.96(1H, m, H-14), 1.28 and 1.18(6H, ds, H-23); δ_C(101 MHz; $CDCl_3$; Me_4Si) 167.7(C-11), 159.6(C-1), 147.0, 140.8, 135.9, 130.6, 130.3, 129.4, 128.1, 128.0, 127.7, 127.3, 127.1, 127.0, 125.8, 124.6, 124.5, 123.5, 123.4, 122.8, 122.6, 121.9, 121.6, 119.5, 118.5, 65.6(C-10), 60.3(C-13), 53.4(C-12), 52.6(C-22), 40.6(C-15), 31.9(C-14), 19.8(C-23); m/z (ESI) 365(100%), 289(79), 674([M-H]$^-$, 11), 675(M$^-$, 4).

6.4 Experimental for Chapter 4

Bioactive-molecule loading on the polymer samples

A sample of the functionalised polymer was suspended in solutions of bioactive compounds for 18h. The polymer was collected by filtration and washed with water and acetone, collected in a stoppered vial, and stored at room temperature in a darkened cupboard.

Bacteria-seeded agar plate preparation[15]

The microorganism was washed off a nutrient slope with sterile water (5 mL). The specific bacterial solution was diluted to 1:50 with sterile water and was added to cooled molten agar in a 1:100 ratio (bacterial solution (1:50): agar, v/v). The inoculated agar (17 mL) was pipetted into empty Petri dishes (90 mm), which were then swirled to ensure even agar thickness. The Petri dishes were allowed to set and were refrigerated until needed.

Polymer bioassay[15]

Using a sterile method, 10-mm-diameter circles were punched in the agar seeded with bacteria. The inner agar was removed to produce empty wells. The test polymer was accurately weighed and added to prepunched wells of the seeded agar plates. The well was then sealed with another 100 μL of molten agar so that a uniform layer of agar was produced. The agar plates were covered and incubated for 18h to encourage bacterial growth. The diameter of the antimicrobial clear zones around each well was measured twice and the average values were recorded. A blank polymer sample was taken as a reference. The equivalent activity of Cephalosporin

C for a given zone size was calculated from a calibration plot of zone size against the log of the molar concentration of Cephalosporin C.

PBS solution[150]

A PBS solution is isotonic to solutions in human body i.e. similar osmolarity and ion concentrations. 1 Litre of PBS solution contains 8 g of NaCl, 0.2 g of KCl, 1.44 g of Na_2HPO_4, 0.24 g of K_2HPO_4, and the pH of the solution is adjusted to 7.4.

6.5 Experimental for Chapter 5

Attempted synthesis of (2-bromo-4,5-dimethoxyphenyl)(pyridin-3-yl)methanone (D1)[151]

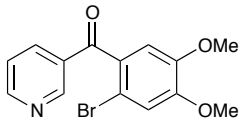

To a solution of 3-bromopyridine (0.13 mL, 1.35 mmol) in THF (0.05 M) was added n-BuLi (0.97 mL, 1.36 mmol) at -100 °C. The mixture was stirred at this temperature for 10 minutes followed by the addition of 6-bromoveratraldehyde (331 mg, 1.35 mmol) as a solution in THF. The reaction was warmed up to -78 °C for 2h and then stirred at room temperature for 8h. The reaction was quenched with water and extracted with EtOAc. The organic phase was then washed with brine, dried over $MgSO_4$, followed by filtration and concentration *in vacuo* to give a solid which was the starting material 6-bromoveratraldehyde.

Attempted synthesis of 4-hydroxy-9,10-dioxo-9,10-dihydroanthracene-1-diazonium (D6)[123]

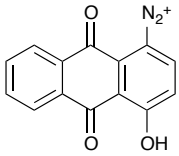

A solution of 1-amino-4-hydroxy-anthraquinone (2 mg, 8.36 *μ*mol) and isopentyl nitrite (0.1 mL, 0.744 mmol) in 5 mL of MeCN was stirred at room temperature for 20min. The red solution turned to yellow and solvent was removed *in vacuo* to give a yellow oil which was unidentifiable by ^{1}H NMR spectroscopy.

Synthesis of (Z)/(E)-2-hydrazono-1,2-diphenylethanone (D9)[8]

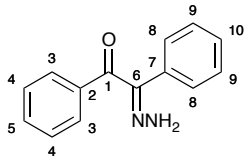

To a stirred solution of benzil (350 mg, 1.66 mmol) and EtOH (5 mL) was added hydrazine monohydrate (0.08 mL, 1.66 mmol). The mixture was heated under reflux for 18h, then allowed to cool before being concentrated *in vacuo*. The residue was dissolved in DCM, washed with water, dried ($MgSO_4$), and solvent was removed *in vacuo* to give **D9** (330 mg, 89%) as a yellow solid: ν_{max}(film)/cm^{-1} 3400, 1636(C=O), 1542, 1489, 1444, 1341, 1260, 1049, 1023, 1002, 867, 823, 799, 761, 701, 661; δ_H(200 MHz; $CDCl_3$; Me_4Si) 7.95-7.96(2H, m, H-3), 7.52-7.56(3H, m, H-5 and H-9), 7.44-7.47(3H, m, H-4 and H-10), 7.35-7.37(2H, m, H-8), 6.30(2H, s, NH_2); δ_C(101 MHz; $CDCl_3$; Me_4Si) 191.8(C-1), 145.5(C-6), 138.1, 131.5, 130.1, 129.7, 129.3, 129.2, 128.9, 127.7; m/z (ESI) 471(100%), 247([M+Na]$^+$, 59), 225(M$^+$, 16).

Synthesis of 2-diazo-1,2-diphenylethanone (D10)[8,127]

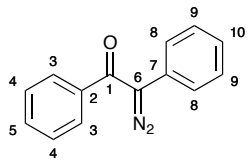

To a solution of the hydrazone **D9** (56 mg, 0.25 mmol) in $CHCl_3$ was added MnO_2 (57 mg, 0.66 mmol). The mixture was stirred in the dark for 1h then filtered through a celite pad, and concentrated *in vacuo* to give **D10** (30 mg, 54%) as a yellow semi-solid: ν_{max}(film)/cm^{-1} 2074(C=N_2), 1623(C=O), 1496, 1262, 755, 694; δ_H(200 MHz; $CDCl_3$; Me_4Si) 8.02-8.04(2H, m, H-3), 7.08-7.64(8H, m, H-4, H-5, H-8, H-9, and H-10); δ_C(101 MHz; $CDCl_3$; Me_4Si) 192.0(C-1), 151.8(C-6), 131.7, 129.2, 129.0, 128.6, 128.5, 127.7, 127.0, 126.0; m/z (ESI) 855(100%), 439(76), 388(64), 297(43).

Synthesis of 2-ethoxy-1,2-diphenylethanone (D11)

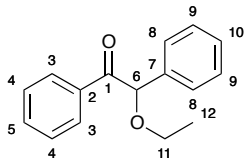

A solution of the diazo **D10** (496 mg, 2.23 mmol) in EtOH was heated under reflux for 1h, then allowed to cool before being concentrated *in vacuo* to give **D11** (205 mg, 61%) as a yellow oil: ν_{max}(film)/cm^{-1} 2981, 1682(C=O), 1496, 1452, 1368, 1276, 1189, 1150, 1027, 744, 700, 636; δ_H(200 MHz; $CDCl_3$; Me_4Si) 7.19-8.08(10H, m, H-3, H-4, H-5, H-8, H-9, H-10), 5.03(1H, s, H-6), 4.20-4.24(2H, q, J=7.12 Hz, H-11), 1.26-1.29(3H, t, J=7.12 Hz, H-12); δ_C(101 MHz; $CDCl_3$; Me_4Si) 172.2(C-1), 138.7, 132.7, 130.0, 129.5, 128.5, 128.3, 127.7, 127.2, 126.8, 61.1(C-11), 14.1(C-12); m/z (ESI) 979(100%), 263([M+Na]$^+$, 72), 241([M+H]$^+$, 27).

Synthesis of 1,2-bis(4-methoxyphenyl)ethanone (D12)[152]

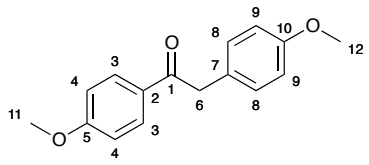

Anisole (0.44 mL, 3.68 mmol) and $AlCl_3$ (542 mg, 4.06 mmol) were dissolved in dry DCM. The mixture was cooled to 0°C and 4-methoxyphenylacetic acid chloride (0.56 mL, 3.66 mmol) was added dropwise. The reaction was stirred at room temperature for 1h and then poured into ice. The organic phase was extracted with DCM. The united organic phases were washed with water, 2% NaOH solution and again water, and dried ($MgSO_4$). The solvent was removed *in vacuo* to give **D12** (938 mg, 100%) as a cream white solid; mp 112-114 ^oC:[152] ν_{max}(film)/cm^{-1} 2957, 1680(C=O), 1604, 1578, 1516, 1467, 1418, 1336, 1250, 1203, 1174, 1106, 1031, 994, 828, 807, 781; δ_H(200 MHz; $CDCl_3$; Me_4Si) 8.00(2H, d, J=8.8 Hz, H-3), 7.19(2H, d, J=8.6 Hz, H-8), 6.93(2H, d, J=8.8 Hz, H-4), 6.87(2H, d, J=8.6 Hz, H-9), 4.18(2H, s, H-6), 3.87(3H, s, H-11), 3.79(3H, s, H-12); δ_C(101 MHz; $CDCl_3$; Me_4Si) 196.5(C-1), 163.4, 158.4, 130.9(C-3), 130.3(C-8), 129.6, 126.9, 114.0(C-9), 113.7(C-4), 55.4(C-12), 55.2(C-11), 44.3(C-6); m/z (ESI) 669(100%), 279($[M+Na]^+$, 85), 257($[M+H]^+$, 30).

Synthesis of 1,2-bis(4-methoxyphenyl)ethane-1,2-dione (D13)[153]

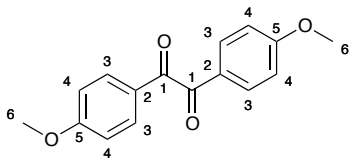

To a solution of the ketone **D12** (204 mg, 0.80 mmol) in anhydrous DMSO (10 mL) was added NBS (460 mg, 2.58 mmol). The mixture was stirred at room temperature for 72h, then quenched with water and extracted with DCM. The organic phase was then washed with water, dried over $MgSO_4$, followed by filtration and

concentration *in vacuo*. The crude product was purified by flash column chromatography, eluting with petrol:EtOAc (20:1) to give **D13** (130 mg, 60%) as a pale green solid; mp 122-124 ^{o}C: ν_{max}(film)/cm^{-1} 1655(C=O), 1598, 1572, 1509, 1424, 1312, 1262, 1225, 1162, 1016, 879, 831, 799, 746, 700, 642, 609; δ_H(200 MHz; $CDCl_3$; Me_4Si) 7.94-7.97(4H, d, J=8.84 Hz, H-3), 6.96-6.99 (4H, d, J=8.84 Hz, H-4), 3.89(6H, s, H-6); δ_C(101 MHz; $CDCl_3$; Me_4Si) 193.4(C-1), 164.8(C-5), 132.3(C-3), 126.2(C-2), 114.2(C-4), 55.6(C-6); m/z (ESI) 293([M+Na]$^+$, 100%), 294(25); HRMS $C_{16}H_{14}O_4Na$ requires 293.0784, found 293.0787.

Synthesis of (Z)/(E)-2-hydrazono-1,2-bis(4-methoxyphenyl)ethanone (D14)[8]

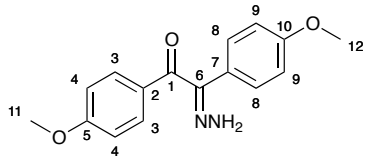

To a stirred solution of the diketone **D13** (892 mg, 3.30 mmol) and EtOH (30 mL) was added hydrazine monohydrate (0.16 mL, 3.30 mmol). The mixture was heated under reflux for 18h, then allowed to cool before being concentrated *in vacuo*. The residue was dissolved in DCM, washed with water, dried ($MgSO_4$), and solvent was removed *in vacuo*. The crude product was purified by flash column chromatography, eluting with petrol:EtOAc (3:1) to give **D14** (530 mg, 57%) as a yellow oil. The hydrazone, which was obtained as inseparable mixtures of the *syn*- and *anti*- isomers, was then used without further purification: ν_{max}(film)/cm^{-1} 3399, 1638(C=O), 1509, 1462, 1303, 1250, 1173, 1030, 879, 833, 617; δ_H(200 MHz; $CDCl_3$; Me_4Si) 6.68-7.58(8H, m, H-3, H-4, H-8, and H-9), 3.87(2H, s, H-11), 3.85(2H, s, H-12); δ_C(101 MHz; $CDCl_3$; Me_4Si) 190.4(C-1), 162.6(C-6), 159.7, 149.2, 132.5, 130.5, 128.8, 126.6, 121.9, 114.3, 113.8, 55.3(C-11 and C-12); m/z (ESI) 591(100%),

307([M+Na]$^+$, 80), 285 ([M+H]$^+$, 36); HRMS $C_{16}H_{16}O_3N_2Na$ requires 307.1057, found 307.1053.

Attempted synthesis of 2-diazo-1,2-bis(4-methoxyphenyl)ethanone (D15)[127]

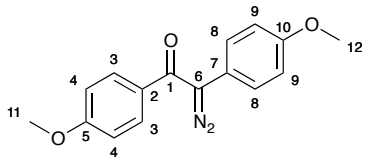

To a solution of the hydrazone **D14** (56 mg, 0.25 mmol) in $CHCl_3$ was added MnO_2 (57 mg, 0.66 mmol). The mixture was stirred in the dark for 1h then filtered through a celite pad, and concentrated *in vacuo* to give a yellow semi-solid which was unidentifiable.

Synthesis of (4-fluorophenyl)(p-tolyl)methanone (D16)[154]

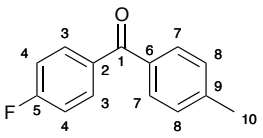

n-Butyllithium (1.4M solution in hexane, 3.55 mL, 4.97 mmol) was added dropwise to a solution of 4-bromotoluene (848 mg, 4.96 mmol) in THF (20 mL) at -78 ^oC for 30min. Then 4-fluorobenzaldehyde (0.54 mL, 5.03 mmol) was added to the mixture at -78 ^oC and the obtained mixture was stirred at room temperature for 1h. After removal of the solvent, I_2 (1.899 g, 7.48 mmol), K_2CO_3 (963 mg, 17.16 mmol), and ^tBuOH (30 mL) were added and the obtained mixture was stirred for 3h at refluxing conditions. The reaction mixture was quenched with sat aqueous Na_2SO_3 and was extracted with $CHCl_3$. The organic layer was washed with brine and dried over Na_2SO_4. The crude product was purified by a short flash column chromatography (petrol/EtOAc 20:1) to give **D16** (400 mg, 38%) as a yellow solid: mp

94-96 °C; ν_{max}(film)/cm^{-1} 3431, 2924, 1655(C=O), 1599, 1506, 1409, 1278, 1223, 1183, 1155, 1095, 1014, 928, 853, 818, 758, 679; δ_H(200 MHz; $CDCl_3$; Me_4Si) 7.82-7.85(2H, d, J=8.59 Hz, H-4), 7.70(2H, d, J=8.08 Hz, H-7), 7.30(2H, d, J=8.08 Hz, H-8), 7.14-7.18 (2H, d, J=8.59 Hz, H-3), 2.46(3H, s, H-10); δ_C(101 MHz; $CDCl_3$; Me_4Si) 195.1(C-1), 166.5(C-5), 143.3, 134.7, 132.5(C-4), 130.1(C-7), 129.0(C-8), 115.2(C-3), 21.7(C-10); δ_F(377 MHz; $CDCl_3$, Me_4Si) -106.4; m/z (ESI) 237([M+Na]$^+$, 100%); HRMS $C_{14}H_{11}FNaO$ requires 237.0686, found 237.0679.

Synthesis of (4-fluorophenyl)(4-(hydroxymethyl)phenyl)methanone (D18)[8,148]

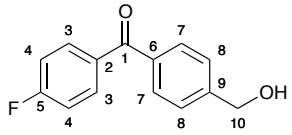

A stirred mixture of the ketone **D16** (4.09 g, 19.09 mmol), benzoyl peroxide (4.763 g, 19.66 mmol), and NBS (3.87 g, 21.74 mmol) in $CHCl_3$ (100 mL) was heated under reflux for 18h with a UV lamp (254 nm) shining 5 cm from the flask. The reaction mixture was washed with water, dried ($MgSO_4$), and solvent was removed *in vacuo* to give an brown oil which was suspended in a mixture of 1,4-dioxane (75 mL) and water (75 mL) and was added $CaCO_3$ (9.80 g, 97.94 mmol). The mixture was heated under reflux for 18h, then allowed to cool before being concentrated *in vacuo*. Then 10% aqueous HCl solution was added. The mixture was extracted with DCM, washed with water, dried ($MgSO_4$), and then concentrated *in vacuo*. The crude product was purified by a short flash column chromatography (petrol/EtOAc 20:1) to give **D18** (520 mg, 12%) as a brown solid: mp 84-86 °C; ν_{max}(film)/cm^{-1} 3425, 1655(C=O), 1598, 1503, 1410, 1308, 1279, 1231, 1156, 1015, 929, 855, 760, 732, 683; δ_H(200 MHz; $CDCl_3$; Me_4Si) 7.85(2H, d, J=8.59 Hz, H-4), 7.79(2H, d, J=8.08 Hz, H-7), 7.50(2H, d, J=8.08 Hz, H-8), 7.17 (2H, d, J=8.59, H-3), 4.82(2H, s, H-10);

δ_C(101 MHz; $CDCl_3$; Me_4Si) 194.9(C-1), 164.6(C-5), 145.5, 136.8, 132.6, 132.5(C-4), 130.2(C-7), 126.4(C-8), 115.5, 115.3(C-3), 64.6(C-10); δ_F(377 MHz; $CDCl_3$, Me_4Si) -105.9; m/z (ESI) 253($[M+Na]^+$, 100%), 229(M^-, 100%); HRMS $C_{14}H_{11}FNaO_2$ requires 253.0635, found 253.0636.

Synthesis of (Z)/(E)-(4-((4-fluorophenyl)(hydrazono)methyl)phenyl)methanol (D19)[8]

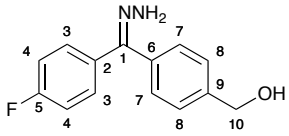

To a stirred solution of the benzophenone **D18** (500 mg, 2.17 mmol) and EtOH (10 mL) was added hydrazine monohydrate (0.60 mL, 12.37 mmol). The mixture was heated under reflux for 18h, then allowed to cool before being concentrated *in vacuo*. The residue was dissolved in DCM, washed with water, dried ($MgSO_4$), and solvent was removed *in vacuo*. The crude product was purified by a short flash column chromatography (petrol/EtOAc 20:1) to give **D19** (450 mg, 85%) as a brown oil: ν_{max}(film)/cm^{-1} 3361, 1602, 1506, 1411, 1365, 1314, 1223, 1156, 1014, 840; δ_H(200 MHz; $CDCl_3$; Me_4Si) 6.94-7.79(8H, m, H-3, H-4, H-7, and H-8), 4.63 and 4.74(2H, ds, H-10); δ_C(101 MHz; $CDCl_3$; Me_4Si) 165.0(C-5), 158.5(C-1), 143.1, 131.2, 130.3, 128.7, 127.1, 126.6, 116.4, 64.7(C-10); δ_F(377 MHz; $CDCl_3$, Me_4Si) -115.1; m/z (ESI) 285($[M+MeCN]^+$, 100%), 243($[M-H]^-$, 30).

Synthesis of (4-(diazo(4-fluorophenyl)methyl)phenyl)methanol (D20)[131,132]

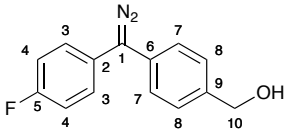

To a mixture of MnO_2 (402 mg, 4.62 mmol), Na_2SO_4 (277 mg, 1.95 mmol), and KOH (130 mg, 2.32 mmol) in MeOH (15 mL) was added a solution of the hydrazone **D19** (330 mg, 1.35 mmol) in MeOH (15 mL). The mixture was stirred in the dark for 18h then filtered through a celite pad, eluted with EtOAc, and concentrated *in vacuo*. The mixture was extracted with EtOAc, washed with water, dried ($MgSO_4$), and then concentrated *in vacuo* to give **D20** (60 mg, 18 %) as a red semi-solid: ν_{max}(film)/cm^{-1} 3416, 2043(C=N_2), 1597, 1508, 1307, 1224, 1169, 1014, 830; δ_H(200 MHz; CDCl3; Me_4Si) 6.84-7.98(8H, m, H-3, H-4, H-7, and H-8), 4.60(2H, s, H-10); δ_C(101 MHz; CDCl3; Me_4Si) 163.1(C-5), 150.6(C-1), 137.8, 132.7, 130.6, 126.8, 124.6, 122.9, 115.7, 65.9(C-10); δ_F(377 MHz; $CDCl_3$, Me_4Si) -115.7; m/z (ESI) 365(100%), 285(80).

Synthesis of p-tolyl(4-(trifluoromethyl)phenyl)methanone (D21)[154]

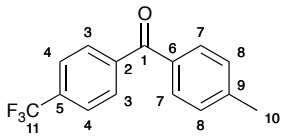

n-Butyllithium (1.4M solution in hexane, 11.37 mL, 15.92 mmol) was added dropwise to a solution of 4-bromotoluene (2.722 g, 15.92 mmol) in THF (25 mL) at -78 ^oC for 30min. Then 4-(trifluoromethyl)benzaldehyde (2.17 mL, 15.89 mmol) was added to the mixture at -78 ^oC and the obtained mixture was stirred at room temperature for 1h. After removal of the solvent, I_2 (6.024 g, 23.73 mmol), K_2CO_3 (2.713 mg, 48.35 mmol), and ^tBuOH (100 mL) were added and the obtained mixture was stirred for 3h at refluxing conditions. The reaction mixture was quenched with sat aqueous Na_2SO_3 and was extracted with $CHCl_3$. The organic layer was washed with brine and dried over Na_2SO_4. The crude product was purified by a short flash column chromatography (petrol/EtOAc 20:1) to give **D21** (2.704 g, 64%) as a yellow solid: mp 152-154 ^oC; ν_{max}(film)/cm^{-1} 2927, 1647(C=O), 1605, 1407, 1329, 1167, 1126, 1110,

1067, 1017, 860, 829, 762, 728, 682; δ_H(200 MHz; $CDCl_3$; Me_4Si) 7.88(2H, d, J=8.34 Hz, H-4), 7.75(2H, d, J=8.34 Hz, H-3), 7.71(2H, d, J=7.83 Hz, H-7), 7.31 (2H, d, J=7.83 Hz, H-8), 2.46(3H, s, H-10); δ_C(101 MHz; $CDCl_3$; Me_4Si) 195.2(C-1), 144.0, 141.1, 134.0, 130.3(C-7), 130.0(C-4), 129.2, 128.9(C-8), 125.2(q, C-11), 125.0(C-3), 21.7(C-10); δ_F(377 MHz; $CDCl_3$, Me_4Si) -62.9; m/z (ESI) 242(100%), 287($[M+Na]^+$, 40); HRMS $C_{15}H_{11}F_3NaO$ requires 287.0654, found 287.0657.

Synthesis of (4-(hydroxymethyl)phenyl)(4-(trifluoromethyl)phenyl)methanone (D23)[8,148]

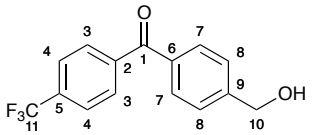

A stirred mixture of the ketone **D21** (1.898 g, 7.18 mmol), benzoyl peroxide (1.782 g, 7.36 mmol), and NBS (1.291 g, 7.25 mmol) in $CHCl_3$ (30 mL) was heated under reflux for 18h with a UV lamp (254 nm) shining 5 cm from the flask. The reaction mixture was washed with water, dried ($MgSO_4$), and solvent was removed *in vacuo* to give a brown solid which was suspended in a mixture of 1,4-dioxane (15 mL) and water (15 mL) and was added $CaCO_3$ (2.201 g, 21.99 mmol). The mixture was heated under reflux for 18h, then allowed to cool before being concentrated in vacuo. Then 10% aqueous HCl solution was added. The mixture was extracted with DCM, washed with water, dried ($MgSO_4$), and then concentrated *in vacuo*. The crude product was purified by a short flash column chromatography (petrol/EtOAc 20:1) to give **D23** (200 mg, 10%) as a white solid: mp 130-132 ^oC; ν_{max}(film)/cm^{-1} 1649(C=O), 1408, 1325, 1167, 1126, 1067, 1017, 932, 861, 764, 684; δ_H(200 MHz; $CDCl_3$; Me_4Si) 7.88(2H, d, J=8.08 Hz, H-4), 7.80(2H, d, J=8.08 Hz, H-3), 7.76(2H, d, J=8.34 Hz, H-7), 7.50(2H, d, J=8.34 Hz, H-8), 4.65(2H, s, H-10); δ_C(101 MHz; $CDCl_3$; Me_4Si)

195.2(C-1), 146.2, 140.7, 139.7, 135.8, 130.2(C-3), 129.7(C-4), 125.9(C-8), 125.2(C-7), 121.4(q, C-11), 64.5(C-10); δ_F(377 MHz; $CDCl_3$, Me_4Si) -62.9; m/z (ESI) 279($[M-H]^-$, 100%).

Synthesis of (Z)/(E)-(4-(hydrazono(4-(trifluoromethyl)phenyl)methyl)phenyl) methanol (D24)[8]

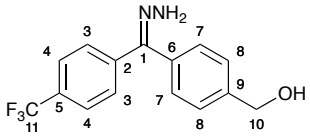

To a stirred solution of the benzophenone **D23** (160 mg, 0.57 mmol) and EtOH (10 mL) was added hydrazine monohydrate (0.14 mL, 2.89 mmol). The mixture was heated under reflux for 18h, then allowed to cool before being concentrated *in vacuo*. The residue was dissolved in DCM, washed with water, dried ($MgSO_4$), and solvent was removed *in vacuo* to give **D24** (157 mg, 93%) as a brown oil: ν_{max}(film)/cm^{-1} 3344, 2927, 1488, 1409, 1325, 1165, 1124, 1067, 1016, 842; δ_H(200 MHz; $CDCl_3$; Me_4Si) 7.17-7.76(8H, m, H-3, H-4, H-7, and H-8), 4.65 and 4.67(2H, ds, H-10); δ_C(101 MHz; $CDCl_3$; Me_4Si) 131.6, 129.4, 128.5, 127.3, 126.8, 126.7, 126.6, 125.4, 125.3(q, C-11), 64.8(C-10), the ^{13}C signal for C-1 was not observed; δ_F(377 MHz; $CDCl_3$, Me_4Si) -62.4; m/z (ESI) 130(100%), 335($[M+MeCN]^+$, 40).

Attempted synthesis of (4-(diazo(4-(trifluoromethyl)phenyl)methyl)phenyl) methanol (D25)[131,132]

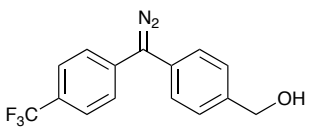

To a mixture of MnO_2 (152 mg, 1.75 mmol), Na_2SO_4 (144 mg, 1.01 mmol), and KOH (62 mg, 1.10 mmol) in MeOH (10 mL) was added a solution of the hydrazone

D24 (157 mg, 0.53 mmol) in MeOH (10 mL). The mixture was stirred in the dark for 18h then filtered through a celite pad, eluted with EtOAc, and concentrated *in vacuo*. The mixture was extracted with EtOAc, washed with water, dried ($MgSO_4$), and then concentrated *in vacuo* to give a brown oil which was unidentifiable.

Synthesis of (3-chlorophenyl)(p-tolyl)methanone (D26)[154]

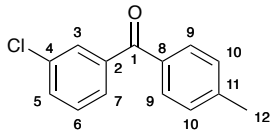

n-Butyllithium (1.56M solution in hexane, 7.35 mL, 15.92 mmol) was added dropwise to a solution of 4-bromotoluene (1.960 g, 11.46 mmol) in THF (25 mL) at -78 ^oC for 30min. Then 3-chlorobenzaldehyde (1.30 mL, 11.48 mmol) was added to the mixture at -78 ^oC and the obtained mixture was stirred at room temperature for 1h. After removal of the solvent, I_2 (4.380 g, 17.26 mmol), K_2CO_3 (1.975 mg, 35.20 mmol), and ^tBuOH (100 mL) were added and the obtained mixture was stirred for 3h at refluxing conditions. The reaction mixture was quenched with sat aqueous Na_2SO_3 and was extracted with $CHCl_3$. The organic layer was washed with brine and dried over Na_2SO_4. The crude product was purified by a short flash column chromatography (petrol/EtOAc 20:1) to give **D26** (756 mg, 29%) as a white solid: mp 108-110 ^oC; ν_{max}(film)/cm^{-1} 2919, 1649(C=O), 1606, 1566, 1421, 1311, 1281, 1184, 1077, 956, 907, 835, 797, 740, 705; δ_H(200 MHz; $CDCl_3$; Me_4Si) 7.76(1H, s, H-3), 7.71(2H, d, J=8.08 Hz, H-9), 7.65(1H, d, J=7.83 Hz, H-5), 7.55(2H, d, J=8.09 Hz, H-7), 7.42(1H, m, H-6), 7.30(2H, d, J=8.08 Hz, H-10), 2.46(2H, s, H-12); δ_C(101 MHz; $CDCl_3$; Me_4Si) 195.0(C-1), 143.7, 139.6, 134.4, 134.2, 131.9(C-7), 130.0(C-9), 129.8(C-3), 128.9(C-6), 128.8(C-10), 127.7(C-5), 21.6(C-12); m/z (ESI) 253($[M+Na]^+$, 100%), 231($[M+H]^+$, 27); HRMS $C_{14}H_{11}NaClO$ requires 253.0391, found 253.0385.

Synthesis of (3-chlorophenyl)(4-(hydroxymethyl)phenyl)methanone (D28)[8,148]

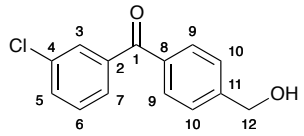

A stirred mixture of the ketone **D26** (719 mg, 3.12 mmol), benzoyl peroxide (772 mg, 3.19 mmol), and NBS (555 mg, 3.12 mmol) in $CHCl_3$ (25 mL) was heated under reflux for 18h with a UV lamp (254 nm) shining 5 cm from the flask. The reaction mixture was washed with water, dried ($MgSO_4$), and solvent was removed *in vacuo* to give an brown oil which was suspended in a mixture of 1,4-dioxane (15 mL) and water (15 mL) and was added $CaCO_3$ (939 mg, 9.38 mmol). The mixture was heated under reflux for 18h, then allowed to cool before being concentrated *in vacuo*. Then 10% aqueous HCl solution was added. The mixture was extracted with DCM, washed with water, dried ($MgSO_4$), and then concentrated *in vacuo*. The crude product was purified by a short flash column chromatography (petrol/EtOAc 20:1) to give **D28** (284 mg, 37%) as a white solid: mp 100-102 ^oC; ν_{max}(film)/cm^{-1} 3312, 2924, 1650(C=O), 1608, 1567, 1415, 1277, 1051, 800, 743, 712; δ_H(200 MHz; $CDCl_3$; Me_4Si) 7.80(2H, d, J=8.34 Hz, H-9), 7.77(1H, s, H-3), 7.67(1H, d, J=7.83 Hz, H-5), 7.58(1H, d, J=7.83 Hz, H-7), 7.51(2H, d, J=8.34 Hz, H-10), 7.44(1H, m, H-6), 4.82(2H, s, H-12); δ_C(101 MHz; $CDCl_3$; Me_4Si) 194.9(C-1), 145.9, 139.2, 136.0, 134.5, 132.9(C-7), 130.9(C-9), 130.0(C-6), 128.3(C-5), 126.4(C-10), 64.6(C-12); m/z (ESI) 166(100%), 345(92), 269($[M+Na]^+$, 73), 245($[M-H]^-$, 100%) 246(M^-, 38); HRMS $C_{14}H_{11}ClNaO_2$ requires 269.0340, found 269.0331.

Synthesis of (Z)/(E)-(4-((3-chlorophenyl)(hydrazono)methyl)phenyl)methanol (D29)[8]

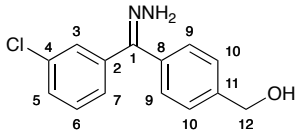

To a stirred solution of the benzophenone **D28** (271 mg, 1.10 mmol) and EtOH (10 mL) was added hydrazine monohydrate (0.27 mL, 5.57 mmol). The mixture was heated under reflux for 18h, then allowed to cool before being concentrated *in vacuo*. The residue was dissolved in DCM, washed with water, dried ($MgSO_4$), and solvent was removed *in vacuo* to give **D29** (261 mg, 91%) as a yellow oil: ν_{max}(film)/cm^{-1} 3359, 2921, 1567, 1470, 1414, 1277, 1185, 1015, 771, 702; δ_H(200 MHz; $CDCl_3$; Me_4Si) 7.18-7.81(8H, m, H-3, H-5, H-6, H-7, H-9, and H-10), 4.66(2H, s, H-12); δ_C(101 MHz; $CDCl_3$; Me_4Si) 145.7, 142.6, 134.3, 132.3, 131.4, 130.8, 129.8, 128.9, 128.0, 127.2, 126.9, 64.6(C-12) ; m/z (ESI) 283($[M+Na]^+$, 100%), 261($[M+H]^+$, 53), 259($[M-H]^-$, 53); HRMS $C_{14}H_{14}ClN_2O$ requires 261.0789, found 261.0790.

Synthesis of (4-((3-chlorophenyl)(diazo)methyl)phenyl)methanol (D30)[131,132]

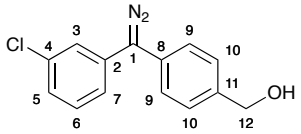

To a mixture of MnO_2 (272 mg, 3.13 mmol), Na_2SO_4 (248 mg, 1.75 mmol), and KOH (116 mg, 2.07 mmol) in MeOH (10 mL) was added a solution of the hydrazone **D29** (261 mg, 1.00 mmol) in MeOH (10 mL). The mixture was stirred in the dark for 18h then filtered through a celite pad, eluted with EtOAc, and concentrated *in vacuo*. The mixture was extracted with EtOAc, washed with water, dried ($MgSO_4$), and then concentrated *in vacuo* to give **D30** (199 mg, 77 %) as a red oil: ν_{max}(film)/cm^{-1} 3415, 2041($C=N_2$), 1736, 1660, 1590, 1513, 1477, 1418, 1379, 1229, 1031, 775, 686; δ_H(200 MHz; $CDCl_3$; Me_4Si) 6.69-7.88(8H, m, H-3, H-5, H-6, H-7, H-9 and H-10),

4.95(2H, s, H-12); δ_C(101 MHz; $CDCl_3$; Me_4Si) 150.0(C-1), 143.5, 139.0, 135.3, 133.7, 130.3, 128.5, 126.7, 125.4, 124.6, 122.6, 66.0(C-12); m/z (ESI) 283(100%).

Synthesis of p-tolyl(2,3,5-trichlorophenyl)methanone (D31)[154]

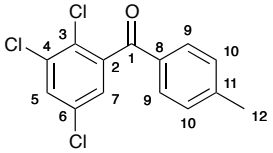

n-Butyllithium (1.56M solution in hexane, 6.33 mL, 9.87 mmol) was added dropwise to a solution of 4-bromotoluene (1.688 g, 9.87 mmol) in THF (25 mL) at -78 ^oC for 30min. Then 2,3,5-trichlorobenzaldehyde (2.070 g, 9.88 mmol) was added to the mixture at -78 ^oC and the obtained mixture was stirred at room temperature for 1h. After removal of the solvent, I_2 (3.759 g, 14.81 mmol), K_2CO_3 (1.660 mg, 29.58 mmol), and ^tBuOH (100 mL) were added and the obtained mixture was stirred for 3h at refluxing conditions. The reaction mixture was quenched with sat aqueous Na_2SO_3 and was extracted with $CHCl_3$. The organic layer was washed with brine and dried over Na_2SO_4. The crude product was purified by a short flash column chromatography (petrol/EtOAc 30:1) to give **D31** (475 mg, 16%) as a white solid: mp 114-116 ^oC; ν_{max}(film)/cm^{-1} 1670(C=O), 1604, 1554, 1409, 1386, 1312, 1279, 1250, 1172, 1121, 1057, 971, 868, 843, 763; δ_H(200 MHz; $CDCl_3$; Me_4Si) 7.70(2H, d, J=8.53 Hz, H-9), 7.61 and 7.59(1H, ds, H-5), 7.29(2H, d, J=8.53, H-10), 7.25 and 7.24(1H, ds, H-7), 2.45(3H, s, H-12); δ_C(101 MHz; $CDCl_3$; Me_4Si) 192.2(C-1), 145.6, 141.7, 134.6, 132.8, 131.1(C-5), 130.2(C-9), 129.6(C-10), 129.3, 127.5, 126.8(C-7), 21.8(C-12); m/z (ESI) 308(100%), 321($[M+Na]^+$, 77); HRMS $C_{14}H_9NaCl_3O$ requires 320.9609 and 322.9583, found 320.9611 and 322.9582.

Attempted synthesis of (4-(hydroxymethyl)phenyl)(2,3,5-trichlorophenyl) methanone (D32)[8,148]

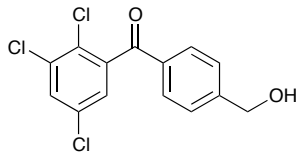

A stirred mixture of the ketone **D31** (421 mg, 1.41 mmol), benzoyl peroxide (345 mg, 1.42 mmol), and NBS (254 mg, 1.43 mmol) in $CHCl_3$ (20 mL) was heated under reflux for 18h with a UV lamp (254 nm) shining 5 cm from the flask. The reaction mixture was washed with water, dried ($MgSO_4$), and solvent was removed *in vacuo* to give a brown solid which was suspended in a mixture of 1,4-dioxane (10 mL) and water (10 mL) and was added $CaCO_3$ (447 mg, 4.47 mmol). The mixture was heated under reflux for 18h, then allowed to cool before being concentrated *in vacuo*. Then 10% aqueous HCl solution was added. The mixture was extracted with DCM, washed with water, dried ($MgSO_4$), and then concentrated *in vacuo* to give a yellow solid which was unidentifiable by ^{1}H NMR spectroscopy.

Synthesis of thiophen-2-yl(p-tolyl)methanone (D36)[154]

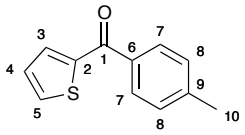

n-Butyllithium (1.56M solution in hexane, 4.17 mL, 6.51 mmol) was added dropwise to a solution of 4-bromotoluene (1.111 g, 6.50 mmol) in THF (20 mL) at -78 ^{o}C for 30min. Then 2-thiophenecarboxaldehyde (0.60 mL, 6.42 mmol) was added to the mixture at -78 ^{o}C and the obtained mixture was stirred at room temperature for 1h. After removal of the solvent, I_2 (2.600 g, 10.24 mmol), K_2CO_3 (1.100 g, 19.60 mmol), and ^{t}BuOH (50 mL) were added and the obtained mixture was stirred for 3h at

refluxing conditions. The reaction mixture was quenched with sat aqueous Na_2SO_3 and was extracted with $CHCl_3$. The organic layer was washed with brine and dried over Na_2SO_4. The crude product was purified by a short flash column chromatography (petrol/EtOAc 20:1) to give **D36** (653 mg, 50%) as a brown solid: mp 70-72 ^oC; ν_{max}(film)/cm^{-1} 1628(C=O), 1604, 1568, 1513, 1413, 1353, 1311, 1293, 1232, 1182, 1133, 1051, 883, 847, 784, 744, 723; δ_H(200 MHz; $CDCl_3$; Me_4Si) 7.79(2H, d, J=8.08 Hz, H-7), 7.70(1H, d, J=4.95 Hz, H-5), 7.65(1H, d, J=3.80 Hz, H-3), 7.30(2H, d, J=8.08 Hz, H-8), 7.15(1H, m, H-4), 2.44(3H, s, H-10); δ_C(101 MHz; $CDCl_3$; Me_4Si) 187.9(C-1), 143.7, 143.0, 135.4, 134.5(C-3), 133.8(C-5), 129.2(C-7), 129.1(C-8), 127.9(C-4), 21.6(C-10); m/z (ESI) 225($[M+Na]^+$, 100%), 203($[M+H]^+$, 10); HRMS $C_{12}H_{10}NaOS$ requires 225.0345, found 225.0343.

Synthesis of (4-(hydroxymethyl)phenyl)(thiophen-2-yl)methanone (D38)[8,148]

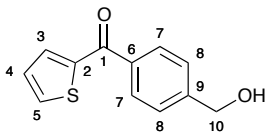

A stirred mixture of the ketone **D36** (602 mg, 3.05 mmol), benzoyl peroxide (738 mg, 3.05 mmol), and NBS (551 mg, 3.10 mmol) in $CHCl_3$ (25 mL) was heated under reflux for 18h with a UV lamp (254 nm) shining 5 cm from the flask. The reaction mixture was washed with water, dried ($MgSO_4$), and solvent was removed *in vacuo* to give a brown solid which was suspended in a mixture of 1,4-dioxane (15 mL) and water (15 mL) and was added $CaCO_3$ (953 mg, 9.52 mmol). The mixture was heated under reflux for 18h, then allowed to cool before being concentrated *in vacuo*. Then 10% aqueous HCl solution was added. The mixture was extracted with DCM, washed with water, dried ($MgSO_4$), and then concentrated *in vacuo*. The crude product was purified by a short flash column chromatography (petrol/EtOAc 20:1) to

give **D38** (201 mg, 10%) as a brown semi-solid: ν_{max}(film)/cm^{-1} 3415, 1629(C=O), 1514, 1414, 1354, 1290, 1052, 885, 849, 793, 714; δ_H(200 MHz; $CDCl_3$; Me_4Si) 7.79(2H, d, J=8.34 Hz, H-7), 7.70(1H, d, J=4.80 Hz, H-5), 7.65(1H, d, J=3.79 Hz, H-3), 7.49(2H, d, J=8.34 Hz, H-8), 7.15(1H, m, H-4), 4.81(2H, s, H-10); δ_C(101 MHz; $CDCl_3$; Me_4Si) 188.0(C-1), 145.3, 143.5, 137.2, 135.5(C-3), 134.6(C-5), 129.8(C-7), 128.4(C-4), 126.2(C-8), 64.6(C-10); m/z (ESI) 241(100%), 219([M+Na]$^+$, 28); HRMS $C_{12}H_{10}NaO_2S$ requires 241.0294, found 241.0291.

Synthesis of (Z)/(E)-(4-(hydrazono(thiophen-2-yl)methyl)phenyl)methanol (D39)[8]

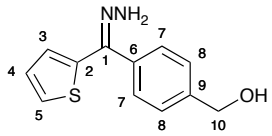

To a stirred solution of the ketone **D38** (162 mg, 0.74 mmol) and EtOH (10 mL) was added hydrazine monohydrate (0.18 mL, 3.71 mmol). The mixture was heated under reflux for 18h, then allowed to cool before being concentrated *in vacuo*. The residue was dissolved in DCM, washed with water, dried ($MgSO_4$), and solvent was removed *in vacuo* to give **D39** (128 mg, 74%) as a brown oil: ν_{max}(film)/cm^{-1} 3375, 2924, 1513, 1414, 1354, 1291, 1231, 1051, 1015, 885, 849, 792, 722; δ_H(200 MHz; $CDCl_3$; Me_4Si) 7.16-7.87(7H, m, H-3, H-4, H-5, H-7, and H-8), 4.80(2H, s, H-10); δ_C(101 MHz; $CDCl_3$; Me_4Si) 145.4(C-1), 143.5, 137.2, 134.8, 134.2, 129.5, 127.9, 126.9, 126.5, 64.6(C-10); m/z (ESI) 241(100%), 273([M+MeCN]$^+$, 64), 233([M+H]$^+$, 15).

Synthesis of (4-(diazo(thiophen-2-yl)methyl)phenyl)methanol (D40)[131,132]

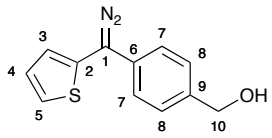

To a mixture of MnO_2 (143 mg, 1.64 mmol), Na_2SO_4 (123 mg, 0.87 mmol), and KOH (68 mg, 1.21 mmol) in MeOH (10 mL) was added a solution of the hydrazone **D39** (128 mg, 0.55 mmol) in MeOH (10 mL). The mixture was stirred in the dark for 18h then filtered through a celite pad, eluted with EtOAc, and concentrated *in vacuo*. The mixture was extracted with EtOAc, washed with water, dried ($MgSO_4$), and then concentrated *in vacuo* to give **D40** (64 mg, 51 %) as a red semi-solid: ν_{max}(film)/cm-1 3436, 2040(C=N_2), 1513, 1414, 1355, 1290, 1231, 1050, 885, 849, 725; δ_H(200 MHz; $CDCl_3$; Me_4Si) 6.76-7.95(7H, m, H-3, H-4, H-5, H-7, and H-8), 5.09(2H, s, H-10); δ_C(101 MHz; $CDCl_3$; Me_4Si) 148.3(C-1), 145.7, 143.5, 137.0, 135.0, 129.7, 126.5, 125.4, 124.7, 64.4(C-10); m/z (ESI) 393(100%).

Attempted synthesis of pyridin-3-yl(p-tolyl)methanone (D41)[154]

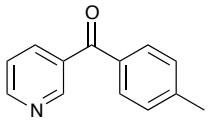

n-Butyllithium (1.5M solution in hexane, 0.91 mL, 1.37 mmol) was added dropwise to a solution of 4-bromotoluene (0.217 g, 1.27 mmol) in THF (5 mL) at -78 ^oC for 30min. Then 3-pyridinecarboxaldehyde (0.12 mL, 1.26 mmol) was added to the mixture at -78 ^oC and the obtained mixture was stirred at room temperature for 1h. After removal of the solvent, I_2 (488 mg, 1.93 mmol), K_2CO_3 (204 mg, 3.63 mmol), and ^tBuOH (10 mL) were added and the obtained mixture was stirred for 3h at refluxing conditions. The reaction mixture was quenched with sat aqueous Na_2SO_3 and was extracted with $CHCl_3$. The organic layer was washed with brine and dried over Na_2SO_4. The crude product was purified by a short flash column

chromatography (petrol/EtOAc 20:1) to give a colourless oil (101 mg) which was identified as the starting material 3-pyridinecarboxaldehyde by ^{1}H NMR spectroscopy.

Chapter 7 Bibliography

(1) Goddard, J. M.; Hotchkiss, J. H. *Prog Polym Sci* **2007**, *32*, 698.

(2) Kugel, A.; Stafslien, S.; Chisholm, B. J. *Prog Org Coat* **2011**, *72*, 222.

(3) Fourche, G. *Polym Eng Sci* **1995**, *35*, 968.

(4) Dhayal, M.; Awasthi, K.; Vijay, Y. K.; Avasthi, D. K. *Vacuum* **2006**, *80*, 643.

(5) Blencowe, A.; Cosstick, K.; Hayes, W. *New J Chem* **2006**, *30*, 53.

(6) Bentz, E. L.; Gibson, H.; Hudson, C.; Moloney, M. G.; Seldon, D. A.; Wearmouth, E. S. *Synlett* **2006**, 247.

(7) Baldwin, J. E.; Pratt, A. J.; Moloney, M. G. *Tetrahedron* **1987**, *43*, 2565.

(8) Awenat, K. M.; Davis, P. J.; Moloney, M. G.; Ebenezer, W. *Chem Commun* **2005**, 990.

(9) Choong, C.; Foord, J. S.; Griffiths, J. P.; Parker, E. M.; Luo, B. W.; Bora, M.; Moloney, M. G. *New J Chem* **2012**, *36*, 1187.

(10) Wang, H.; Griffiths, J. P.; Egdell, R. G.; Moloney, M. G.; Foord, J. S. *Langmuir* **2008**, *24*, 862.

(11) Moloney, M. G. *J Phys D Appl Phys* **2008**, *41*.

(12) Griffiths, J.-P.; Maliha, B.; Moloney, M. G.; Thompson, A. L.; Hussain, I. *Langmuir* **2010**, null.

(13) Choong, C.; Griffiths, J. P.; Moloney, M. G.; Triffitt, J.; Swallow, D. *React Funct Polym* **2009**, *69*, 77.

(14) Davis, P. J.; Harris, L.; Karim, A.; Thompson, A. L.; Gilpin, M.; Moloney, M. G.; Pound, M. J.; Thompson, C. *Tetrahedron Lett* **2011**, *52*, 1553.

(15) Griffiths, J. P.; Maliha, B.; Moloney, M. G.; Thompson, A. L.; Hussain, I. *Langmuir* **2010**, *26*, 14142.

(16) Leonard, D.; Moloney, M. G.; Thompson, C. *Tetrahedron Lett* **2009**, *50*, 3499.

(17) Miller, R. J.; Shechter, H. *J Am Chem Soc* **1978**, *100*, 7920.

(18) Miller, R. J.; Yang, L. S.; Shechter, H. *J Am Chem Soc* **1977**, *99*, 938.

(19) Aphaiwong, A. Part II, University of Oxford, 2009.

(20) Javed, M. I.; Brewer, M. *Org Lett* **2007**, *9*, 1789.

(21) http://www.sigmaaldrich.com.

(22) Clayden., J.; Greeves., N.; Warren., S. *Organic Chemistry*, 2012.

(23) Mieusset, J. L.; Brinker, U. H. *J Org Chem* **2008**, *73*, 1553.

(24) Skell, P. S.; Woodworth, R. C. *J Am Chem Soc* **1956**, *78*, 4496.

(25) Griller, D.; Hadel, L.; Nazran, A. S.; Platz, M. S.; Wong, P. C.; Savino, T. G.; Scaiano, J. C. *J Am Chem Soc* **1984**, *106*, 2227.

(26) Nazran, A. S.; Griller, D. *J Am Chem Soc* **1985**, *107*, 4613.

(27) Tomioka, H. *Res Chem Intermediat* **1994**, *20*, 605.

(28) Paterson, B. M.; Donnelly, P. S. *Chem Soc Rev* **2011**, *40*, 3005.

(29) Isa, A. Y.; Ward, T. H.; West, C. M. L.; Slevin, N. J.; Homer, J. J. *Brit J Radiol* **2006**, *79*, 791.

(30) Dearling, J. L. J.; Lewis, J. S.; McCarthy, D. W.; Welch, M. J.; Blower, P. J. *Chem Commun* **1998**, 2531.

(31) Krohn, K. A.; Link, J. M.; Mason, R. P. *J Nucl Med* **2008**, *49*, 129S.

(32) Hodgkiss, R. J. *Anti-Cancer Drug Des* **1998**, *13*, 687.

(33) Dubois, L.; Landuyt, W.; Haustermans, K.; Dupont, P.; Bormans, G.; Vermaelen, P.; Flamen, P.; Verbeken, E.; Mortelmans, L. *Brit J Cancer* **2004**, *91*, 1947.

(34) Troost, E. G. C.; Laverman, P.; Kaanders, J. H. A. M.; Philippens, M.; Lok, J.; Oyen, W. J. G.; van der Kogel, A. J.; Boerman, O. C.; Bussink, J. *Radiother Oncol* **2006**, *80*, 157.

(35) Yuan, H.; Schroeder, T.; Bowsher, J. E.; Hedlund, L. W.; Wong, T.; Dewhirst, M. W. *J Nucl Med* **2006**, *47*, 989.

(36) Hueting, R.; Christlieb, M.; Dilworth, J. R.; Garayoa, E. G.; Gouverneur, V.; Jones, M. W.; Maes, V.; Schibli, R.; Sun, X.; Tourwe, D. A. *Dalton T* **2010**, *39*, 3620.

(37) Christlieb, M.; Dilworth, J. R. *Chem-Eur J* **2006**, *12*, 6194.

(38) Betts, H. M.; Barnard, P. J.; Bayly, S. R.; Dilworth, J. R.; Gee, A. D.; Holland, J. P. *Angew Chem Int Edit* **2008**, *47*, 8416.

(39) Boyer, S. London Metropolitan University, Elemental Analysis Service.

(40) Birdi, K. S. *Self-Assembly Monolayer Structures of Lipids and Macromolecules at Interfaces*; Springer, 1999.

(41) Jacobs, R. University of Oxford, http://saf.chem.ox.ac.uk.

(42) http://www.ipfdd.de/fileadmin/user_upload/om/Mitarbeiter/IR_spek_ofl_2006_07_1c.pdf.

(43) Flores, K. O. V.; de Aguiar, A. P.; de Aguiar, M. R. M. P.; Maria, L. C. D. *Mater Lett* **2007**, *61*, 1190.

(44) Silverstein, R. M.; Webster, F. X.; Kiemle, D. *Spectrometric Identification of Organic Compounds*; 7 ed., 2005.

(45) Morgan, D. J. Cardiff University, the Kratos Ultra-DLD, http://www.cardiff.ac.uk/chemy/staffinfo/xpsaccess/analysis.html.

(46) Mermet, J. M. *J Anal Atom Spectrom* **2005**, *20*, 11.

(47) Stef√°nsson, A.; Gunnarsson, I.; Giroud, N. *Anal Chim Acta* **2007**, *582*, 69.

(48) http://www.colloidalsciencelab.com/fact_pages/Varian-MPX.pdf.

(49) http://www.medacltd.com.

(50) Ray, A.; Gupta, S. N. *J Appl Polym Sci* **1998**, *67*, 1215.

(51) Holland, J. P.; Aigbirhio, F. I.; Betts, H. M.; Bonnitcha, P. D.; Burke, P.; Christlieb, M.; Churchill, G. C.; Cowley, A. R.; Dilworth, J. R.; Donnelly, P. S.; Green, J. C.; Peach, J. M.; Vasudevan, S. R.; Warren, J. E. *Inorg Chem* **2007**, *46*, 465.

(52) http://www.med.unc.edu/pharm/sondeklab/Lab%20Resources/protein_purification_handbooks/Affinity%20chromatography.pdf.

(53) Murphy, J. C.; Jewell, D. L.; White, K. I.; Fox, G. E.; Willson, R. C. *Biotechnol Progr* **2003**, *19*, 982.

(54) Wang, F.; Chmil, C.; Pierce, F.; Ganapathy, K.; Gump, B. B.; Mackenzie, J. A.; Metchref, Y.; Bendinskas, K. *J Chromatogr B Analyt Technol Biomed Life Sci* **2013**, *934*, 26.

(55) Sun, X. S.; Xiao, C. L.; Ge, R. G.; Yin, X. F.; Li, H.; Li, N.; Yang, X. Y.; Zhu, Y.; He, X.; He, Q. Y. *Proteomics* **2011**, *11*, 3288.

(56) Kobatake, S.; Irie, M. *Annual Reports Section "C" (Physical Chemistry)* **2003**, *99*, 277.

(57) Katsonis, N.; Lubomska, M.; Pollard, M. M.; Feringa, B. L.; Rudolf, P. *Prog Surf Sci* **2007**, *82*, 407.

(58) Bossi, M. L.; Murgida, D. H.; Aramendia, P. F. *J Phys Chem B* **2006**, *110*, 13804.

(59) Samanta, S.; Locklin, J. *Langmuir* **2008**, *24*, 9558.

(60) Minkin, V. I. *Chem Rev* **2004**, *104*, 2751.

(61) Zhang, P.; Meng, J. B.; Li, X. L.; Matsuura, T.; Wang, Y. M. *Journal of Heterocyclic Chemistry* **2002**, *39*, 179.

(62) Sakata, T.; Yan, Y. L.; Marriott, G. *J Org Chem* **2005**, *70*, 2009.

(63) Natali, M.; Aakeroy, C.; Desper, J.; Giordani, S. *Dalton T* **2010**, *39*, 8269.

(64) Swansburg, S.; Buncel, E.; Lemieux, R. P. *J Am Chem Soc* **2000**, *122*, 6594.

(65) Hobley, J.; Malatesta, V.; Millini, R.; Montanari, L.; Parker, W. O. N. *Phys Chem Chem Phys* **1999**, *1*, 3259.

(66) Davis, D. A.; Hamilton, A.; Yang, J. L.; Cremar, L. D.; Van Gough, D.; Potisek, S. L.; Ong, M. T.; Braun, P. V.; Martinez, T. J.; White, S. R.; Moore, J. S.; Sottos, N. R. *Nature* **2009**, *459*, 68.

(67) Raymo, F. M.; Giordani, S. *J Am Chem Soc* **2001**, *123*, 4651.

(68) Darwish, T. A.; Evans, R. A.; James, M.; Malic, N.; Triani, G.; Hanley, T. L. *J Am Chem Soc* **2010**, *132*, 10748.

(69) Uznanski, P. *Langmuir* **2003**, *19*, 1919.

(70) Malatesta, V.; Neri, C.; Wis, M. L.; Montanari, L.; Millini, R. *J Am Chem Soc* **1997**, *119*, 3451.

(71) Shiraishi, Y.; Itoh, M.; Hirai, T. *Phys Chem Chem Phys* **2010**, *12*, 13737.

(72) Berkovic, G.; Krongauz, V.; Weiss, V. *Chem Rev* **2000**, *100*, 1741.

(73) Yang, H. K.; Ozcam, A. E.; Efimenko, K.; Genzer, J. *Soft Matter* **2011**, *7*, 3766.

(74) Shiraishi, Y.; Adachi, K.; Itoh, M.; Hirai, T. *Org Lett* **2009**, *11*, 3482.

(75) Calero, P.; Aznar, E.; Lloris, J. M.; Marcos, M. D.; Martinez-Manez, R.; Ros-Lis, J. V.; Soto, J.; Sancenon, F. *Chem Commun* **2008**, 1668.

(76) Tian, H.; Ren, J. Q. *Sensors-Basel* **2007**, *7*, 3166.

(77) Shao, N.; Wang, H.; Gao, X. D.; Yang, R. H.; Chan, W. H. *Analytical Chemistry* **2010**, *82*, 4628.

(78) Giordani, S.; Raymo, F. M. *Org Lett* **2003**, *5*, 3559.

(79) Piech, M.; George, M. C.; Bell, N. S.; Braun, P. V. *Langmuir* **2006**, *22*, 1379.

(80) Osterby, B.; Mckelvey, R. D.; Hill, L. *J Chem Educ* **1991**, *68*, 424.

(81) Vlassiouk, I.; Park, C. D.; Vail, S. A.; Gust, D.; Smirnov, S. *Nano Lett* **2006**, *6*, 1013.

(82) Rosario, R.; Gust, D.; Hayes, M.; Jahnke, F.; Springer, J.; Garcia, A. A. *Langmuir* **2002**, *18*, 8062.

(83) Chen, J.; Zeng, F.; Wu, S.; Chen, Q.; Tong, Z. *Chemistry* **2008**, *14*, 4851.

(84) Chen, J.; Zeng, F.; Wu, S. Z.; Zhao, J. Q.; Chen, Q. M.; Tong, Z. *Chem Commun* **2008**, 5580.

(85) Andersson, J.; Li, S. M.; Lincoln, P.; Andreasson, J. *J Am Chem Soc* **2008**, *130*, 11836.

(86) Edahiro, J.; Sumaru, K.; Tada, Y.; Ohi, K.; Takagi, T.; Kameda, M.; Shinbo, T.; Kanamori, T.; Yoshimi, Y. *Biomacromolecules* **2005**, *6*, 970.

(87) Higuchi, A.; Hamamura, A.; Shindo, Y.; Kitamura, H.; Yoon, B. O.; Mori, T.; Uyama, T.; Umezawa, A. *Biomacromolecules* **2004**, *5*, 1770.

(88) Andreasson, J.; Straight, S. D.; Kodis, G.; Park, C. D.; Hambourger, M.; Gervaldo, M.; Albinsson, B.; Moore, T. A.; Moore, A. L.; Gust, D. *J Am Chem Soc* **2006**, *128*, 16259.

(89) Gorelik, S.; Hongyan, S.; Lear, M. J.; Hobley, J. *Photoch Photobio Sci* **2010**, *9*, 141.

(90) Beyer, C.; Wagenknecht, H. A. *J Org Chem* **2010**, *75*, 2752.

(91) Doron, A.; Katz, E.; Tao, G. L.; Willner, I. *Langmuir* **1997**, *13*, 1783.

(92) Gomez, I.; Reguero, M.; Robb, M. A. *J Phys Chem A* **2006**, *110*, 3986.

(93) Rosario, R.; Gust, D.; Garcia, A. A.; Hayes, M.; Taraci, J. L.; Clement, T.; Dailey, J. W.; Picraux, S. T. *J Phys Chem B* **2004**, *108*, 12640.

(94) Aznar, E.; Casasus, R.; Garcia-Acosta, B.; Marcos, M. D.; Martinez-Manez, R. *Adv Mater* **2007**, *19*, 2228.

(95) Tamai, N.; Miyasaka, H. *Chem Rev* **2000**, *100*, 1875.

(96) Demadrille, R.; Rabourdin, A.; Campredon, M.; Giusti, G. *Journal of Photochemistry and Photobiology a-Chemistry* **2004**, *168*, 143.

(97) Li, X. L.; Wang, Y. M.; Matsuura, T.; Meng, J. B. *Mol Cryst Liq Cryst* **2000**, *344*, 301.

(98) de Leon, L.; Biewer, M. C. *Tetrahedron Lett* **2000**, *41*, 3527.

(99) Patel, K.; Castillo-Muzquiz, A.; Biewer, M. C. *Tetrahedron Lett* **2002**, *43*, 5933.

(100) Eknoian, M. W.; Worley, S. D. *J Bioact Compat Pol* **1998**, *13*, 303.

(101) Elrod, D. B.; Worley, S. D. *J Bioact Compat Pol* **1999**, *14*, 258.

(102) Kong, H.; Song, J.; Jang, J. *Environ Sci Technol* **2010**, *44*, 5672.

(103) Kreutzwiesner, E.; Noormofidi, N.; Wiesbrock, F.; Kern, W.; Rametsteiner, K.; Stelzer, F.; Slugovc, C. *J Polym Sci Pol Chem* **2010**, *48*, 4504.

(104) Kienberger, J.; Noormofidi, N.; Muhlbacher, I.; Klarholz, I.; Harms, C.; Slugovc, C. *J Polym Sci Pol Chem* **2012**, *50*, 2236.

(105) Hazzizalaskar, J.; Helary, G.; Sauvet, G. *J Appl Polym Sci* **1995**, *58*, 77.

(106) Sun, G.; Wheatley, W. B.; Worley, S. D. *Ind Eng Chem Res* **1994**, *33*, 168.

(107) Ahmed, A. E. S. I.; Hay, J. N.; Bushell, M. E.; Wardell, J. N.; Cavalli, G. *React Funct Polym* **2008**, *68*, 1448.

(108) Ahmed, A. E. S. I.; Hay, J. N.; Bushell, M. E.; Wardell, J. N.; Cavalli, G. *J Appl Polym Sci* **2009**, *113*, 2404.

(109) Strominger, J. L.; Park, J. T.; Thompson, R. E. *J Biol Chem* **1959**, *234*, 3263.

(110) Aumsuwan, N.; Heinhorst, S.; Urban, M. W. *Biomacromolecules* **2007**, *8*, 713.

(111) Hardes, J.; Ahrens, H.; Gebert, C.; Streitbuerger, A.; Buerger, H.; Erren, M.; Gunsel, A.; Wedemeyer, C.; Saxler, G.; Winkelmann, W.; Gosheger, G. *Biomaterials* **2007**, *28*, 2869.

(112) Schierholz, J. M.; Lucas, L. J.; Rump, A.; Pulverer, G. *J Hosp Infect* **1998**, *40*, 257.

(113) Eby, D. M.; Luckarift, H. R.; Johnson, G. R. *Acs Appl Mater Inter* **2009**, *1*, 1553.

(114) Strohal, R.; Schelling, M.; Takacs, M.; Jurecka, W.; Gruber, U.; Offner, F. *J Hosp Infect* **2005**, *60*, 226.

(115) Ong, S. Y.; Wu, J.; Moochhala, S. M.; Tan, M. H.; Lu, J. *Biomaterials* **2008**, *29*, 4323.

(116) Babu, R.; Zhang, J. Y.; Beckman, E. J.; Virji, M.; Pasculle, W. A.; Wells, A. *Biomaterials* **2006**, *27*, 4304.

(117) Chng, S. PRS report 2013, University of Oxford, 2013.

(118) Duan, K.; Wang, R. Z. *J Mater Chem* **2006**, *16*, 2309.

(119) Hartstock, F. W.; Kanabus-kaminska, J. M.; Griller, D. *Int J Chem Kinet* **1989**, *21*, 157.

(120) Harris, L. D. DPhil thesis, University of Oxford, 2009.

(121) Li, Y. Z.; Schuster, G. B. *J Org Chem* **1986**, *51*, 3804.

(122) Iikubo, T.; Itoh, T.; Hirai, K.; Takahashi, Y.; Kawano, M.; Ohashi, Y.; Tomioka, H. *Eur J Org Chem* **2004**, 3004.

(123) Gornostaev, L. M.; Arnold, E. V.; Lykova, E. V.; Sadoschenko, M. V. *Chem Heterocycl Com+* **2010**, *46*, 665.

(124) KotzybaHibert, F.; Kessler, P.; Zerbib, V.; Grutter, T.; Bogen, C.; Takeda, K.; Hammadi, A.; Knerr, L.; Goeldner, M. *Bioconjugate Chem* **1997**, *8*, 472.

(125) Dugave, C.; Kessler, P. *Tetrahedron Lett* **1994**, *35*, 9557.

(126) Arnold, B. R.; Scaiano, J. C.; Bucher, G. F.; Sander, W. W. *J Org Chem* **1992**, *57*, 6469.

(127) Morrison, H.; Yates, P.; Danishefsky, S. *J Org Chem* **1961**, *26*, 2617.

(128) Davies, J. R.; Kane, P. D.; Moody, C. J. *Tetrahedron* **2004**, *60*, 3967.

(129) Yates, P.; Shapiro, B. L. *J Org Chem* **1958**, *23*, 759.

(130) Droescher, H.; Jenny, E. F. *Helv Chim Acta* **1968**, *51*, 643.

(131) Reiter, G. *Langmuir* **1993**, *9*, 1344.

(132) Parker, E. PRS Report 2009, University of Oxford, 2009.

(133) Leonard, D. M. L. Part II thesis, Honour School of Chemistry, University of Oxford, 2008.

(134) Zvolinsky, O. V.; Pleshakov, V. G.; Prostakov, N. S. *Khim Geterotsikl+* **1996**, 227.

(135) Held, I.; Xu, S. J.; Zipse, H. *Synthesis-Stuttgart* **2007**, 1185.

(136) Gester, S.; Pietzsch, J.; Wuest, F. R. *J Labelled Compd Rad* **2007**, *50*, 105.

(137) Chankeshwara, S. V.; Chakraborti, A. K. *Org Lett* **2006**, *8*, 3259.

(138) Xie, H.; Ng, D.; Savinov, S. N.; Dey, B.; Kwong, P. D.; Wyatt, R.; Smith, A. B.; Hendrickson, W. A. *Journal of Medicinal Chemistry* **2007**, *50*, 4898.

(139) Andrus, M. B.; Hicken, E. J.; Stephens, J. C.; Bedke, D. K. *J Org Chem* **2005**, *70*, 9470.

(140) Tomasulo, M.; Kaanumal, S. L.; Sortino, S.; Raymo, F. M. *J Org Chem* **2007**, *72*, 595.

(141) Greenidge, P. A.; Merette, S. A. M.; Beck, R.; Dodson, G.; Goodwin, C. A.; Scully, M. F.; Spencer, J.; Weiser, J.; Deadman, J. J. *Journal of Medicinal Chemistry* **2003**, *46*, 1293.

(142) Li, X.; Gong, S. L.; Yang, W. P.; Chen, Y. Y.; Meng, X. G. *Tetrahedron* **2008**, *64*, 6230.

(143) Inoue, H.; Kikuchi, M.; Ito, J.; Nishiyama, H. *Tetrahedron* **2008**, *64*, 493.

(144) Sansom, L. K. DPhil thesis, University of Oxford, 2007.

(145) Xu, J. W.; Ling, T. C.; He, C. B. *J Polym Sci Pol Chem* **2008**, *46*, 4691.

(146) Dayal, D.; Palanimuthu, D.; Shinde, S. V.; Somasundaram, K.; Samuelson, A. G. *J Biol Inorg Chem* **2011**, *16*, 621.

(147) Jang, D. O.; Moon, K. S.; Cho, D. H.; Kim, J. G. *Tetrahedron Letters* **2006**, *47*, 6063.

(148) Tietze, L. F.; Redert, T.; Bell, H. P.; Hellkamp, S.; Levy, L. M. *Chem-Eur J* **2008**, *14*, 2527.

(149) Sato, H.; Dan, T.; Onuma, E.; Tanaka, H.; Koga, H. *Chemical & Pharmaceutical Bulletin* **1990**, *38*, 1266.

(150) Dulbecco, R.; Vogt, M. *J Exp Med* **1954**, *99*, 167.

(151) Kraus, G. A.; Kempema, A. *J Nat Prod* **2010**, *73*, 1967.

(152) Schafer, A.; Wellner, A.; Strauss, M.; Wolber, G.; Gust, R. *Chemmedchem* **2011**, *6*, 2055.

(153) Wolfe, S.; Pilgrim, W. R.; Garrard, T. F.; Chamberl.P *Can J Chemistry* **1971**, *49*, 1099.

(154) Ushijima, S.; Dohi, S.; Moriyama, K.; Togo, H. *Tetrahedron* **2012**, *68*, 1436.

Appendices

Appendix I: ATR-IR (Chapter 2)

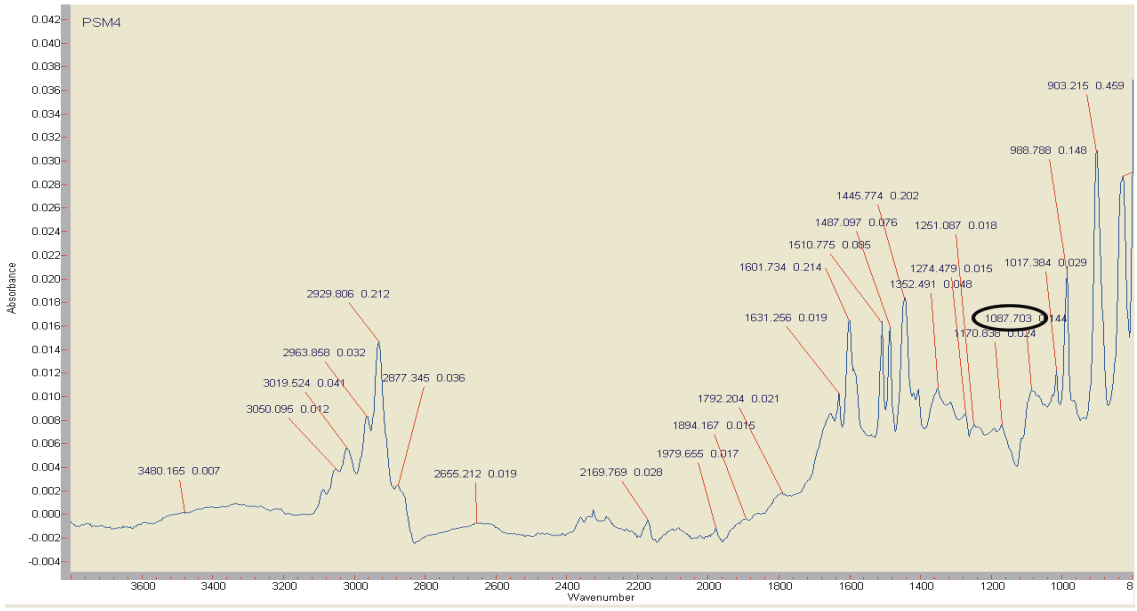

PSM4

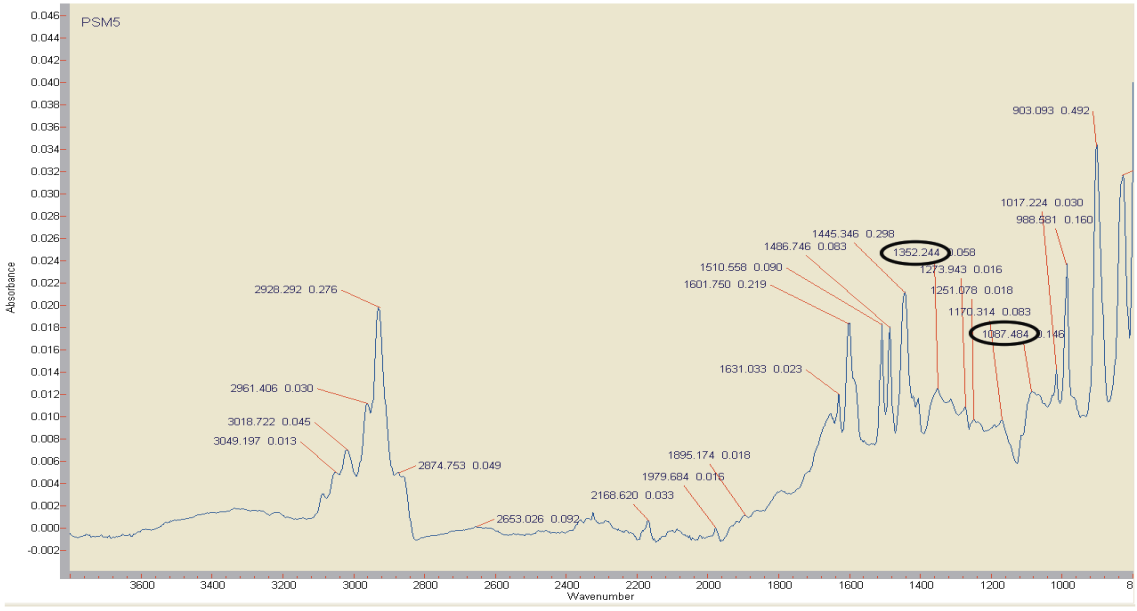

PSM5

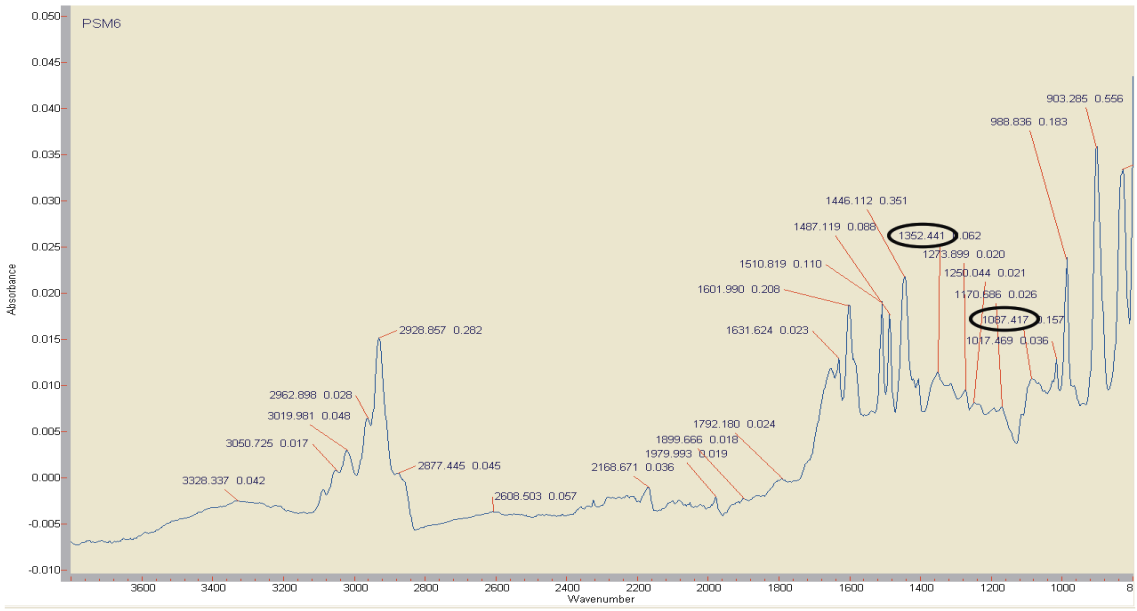
PSM6
Absorbance
Wavenumber
903.285 0.556
988.836 0.183
1446.112 0.351
1487.119 0.088
1352.441 0.062
1273.899 0.020
1510.819 0.110
1250.044 0.021
1601.990 0.208
1170.686 0.026
1087.417 0.157
1631.624 0.023
1017.469 0.036
2928.857 0.282
2962.898 0.028
3019.981 0.048
1792.180 0.024
3050.725 0.017
1899.666 0.018
1979.993 0.019
2877.445 0.045
3328.337 0.042
2168.671 0.036
2608.503 0.057

PSM6

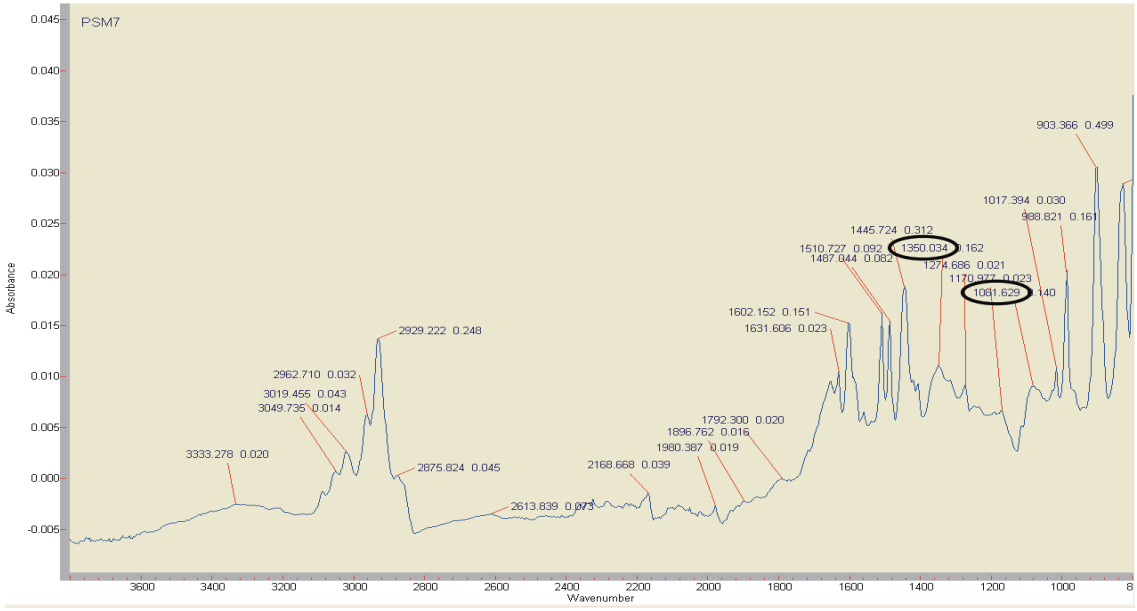
PSM7
Absorbance
Wavenumber
903.366 0.499
1017.394 0.030
988.821 0.161
1445.724 0.312
1510.727 0.092
1350.034 0.162
1487.044 0.082
1274.686 0.021
1170.977 0.023
1081.629 0.140
1602.152 0.151
1631.606 0.023
2929.222 0.248
2962.710 0.032
3019.455 0.043
3049.735 0.014
1792.300 0.020
1896.762 0.018
1980.387 0.019
3333.278 0.020
2875.824 0.045
2168.668 0.039
2613.839 0.073

PSM7

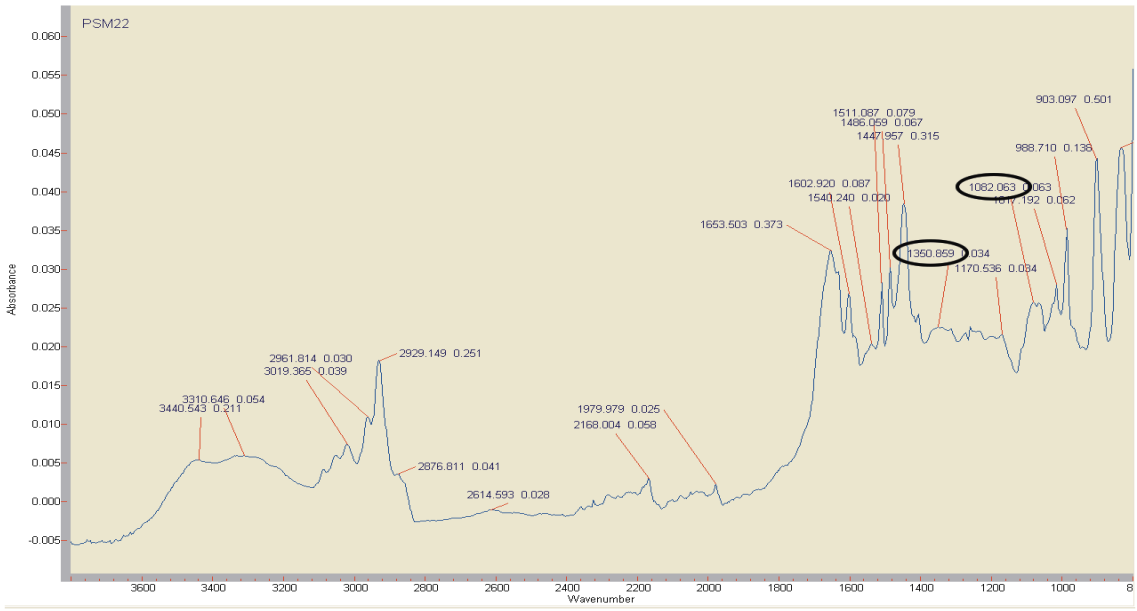
PSM22
Absorbance
Wavenumber
3440.543 0.211
3310.646 0.054
3019.365 0.039
2961.814 0.030
2929.149 0.251
2876.811 0.041
2614.593 0.028
2168.004 0.058
1979.979 0.025
1653.503 0.373
1602.920 0.087
1540.240 0.020
1511.087 0.079
1486.059 0.067
1447.957 0.315
1350.859 0.034
1170.536 0.034
1082.063 0.063
1017.192 0.062
988.710 0.138
903.097 0.501

PSM22

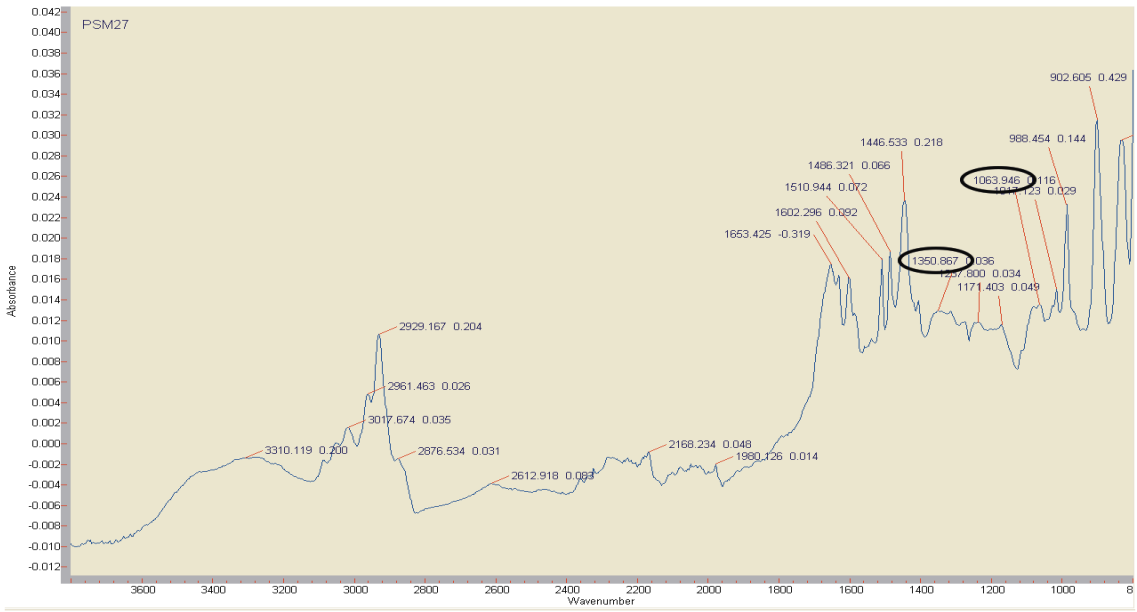
PSM27
Absorbance
Wavenumber
3310.119 0.200
3017.674 0.035
2961.463 0.026
2929.167 0.204
2876.534 0.031
2612.918 0.083
2168.234 0.048
1980.126 0.014
1653.425 -0.319
1602.296 0.092
1510.944 0.072
1486.321 0.066
1446.533 0.218
1350.867 0.036
1257.800 0.034
1171.403 0.049
1063.946 0.116
1013.123 0.029
988.454 0.144
902.605 0.429

PSM27

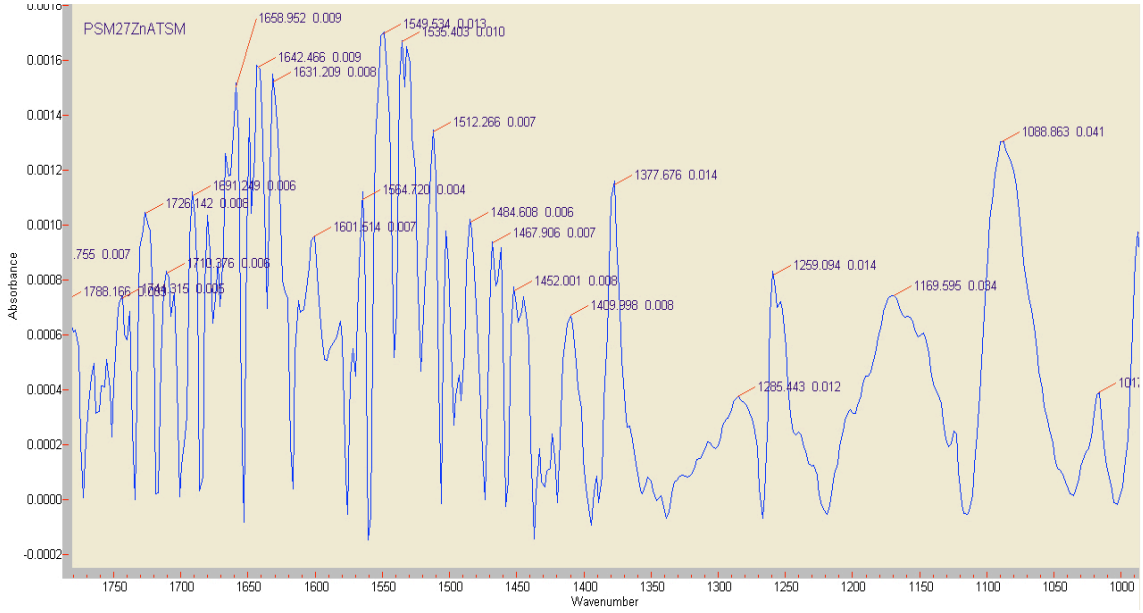

PSM27.ZnATSM

Appendix II: XPS (Chapter 2)

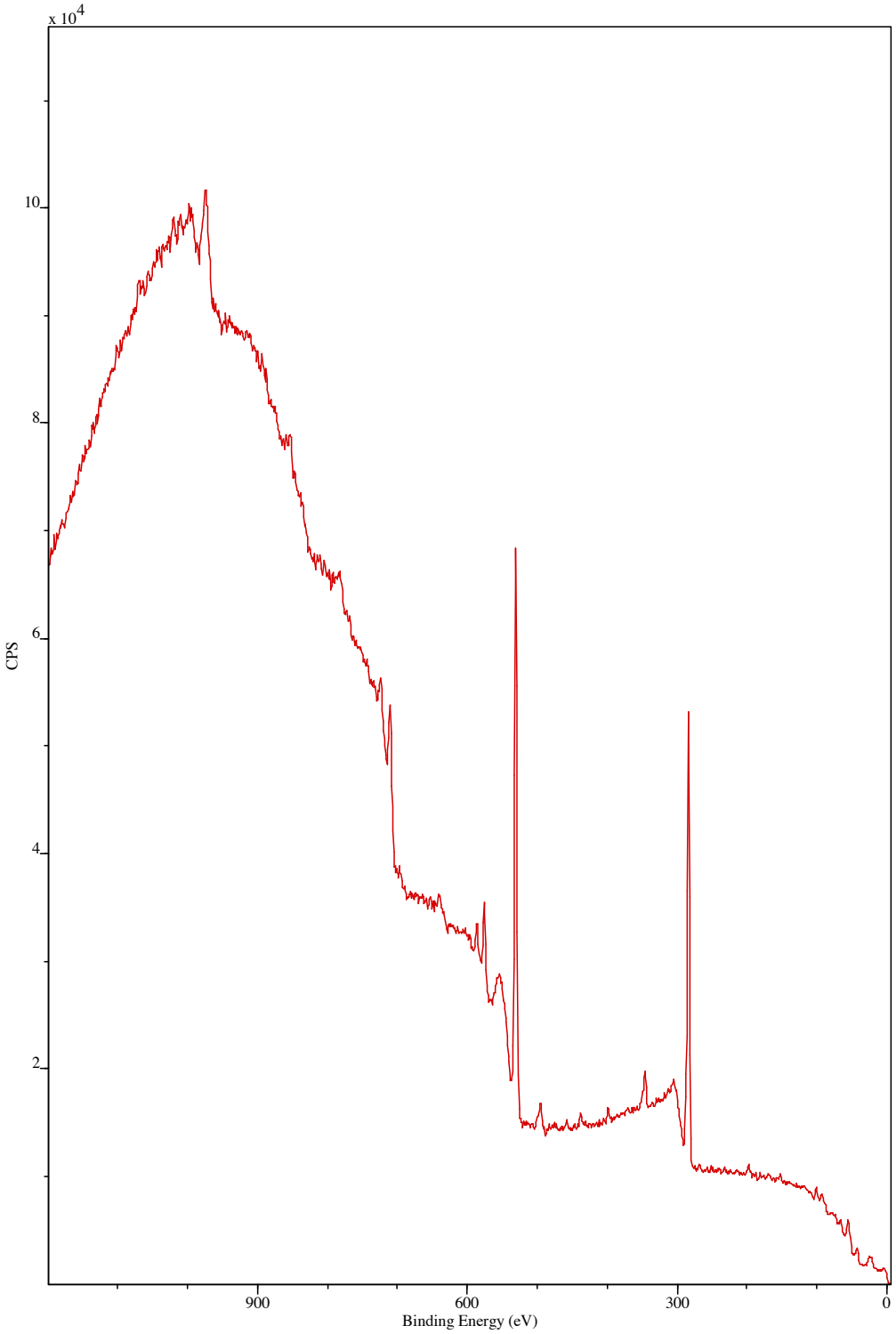

blank PS XAD

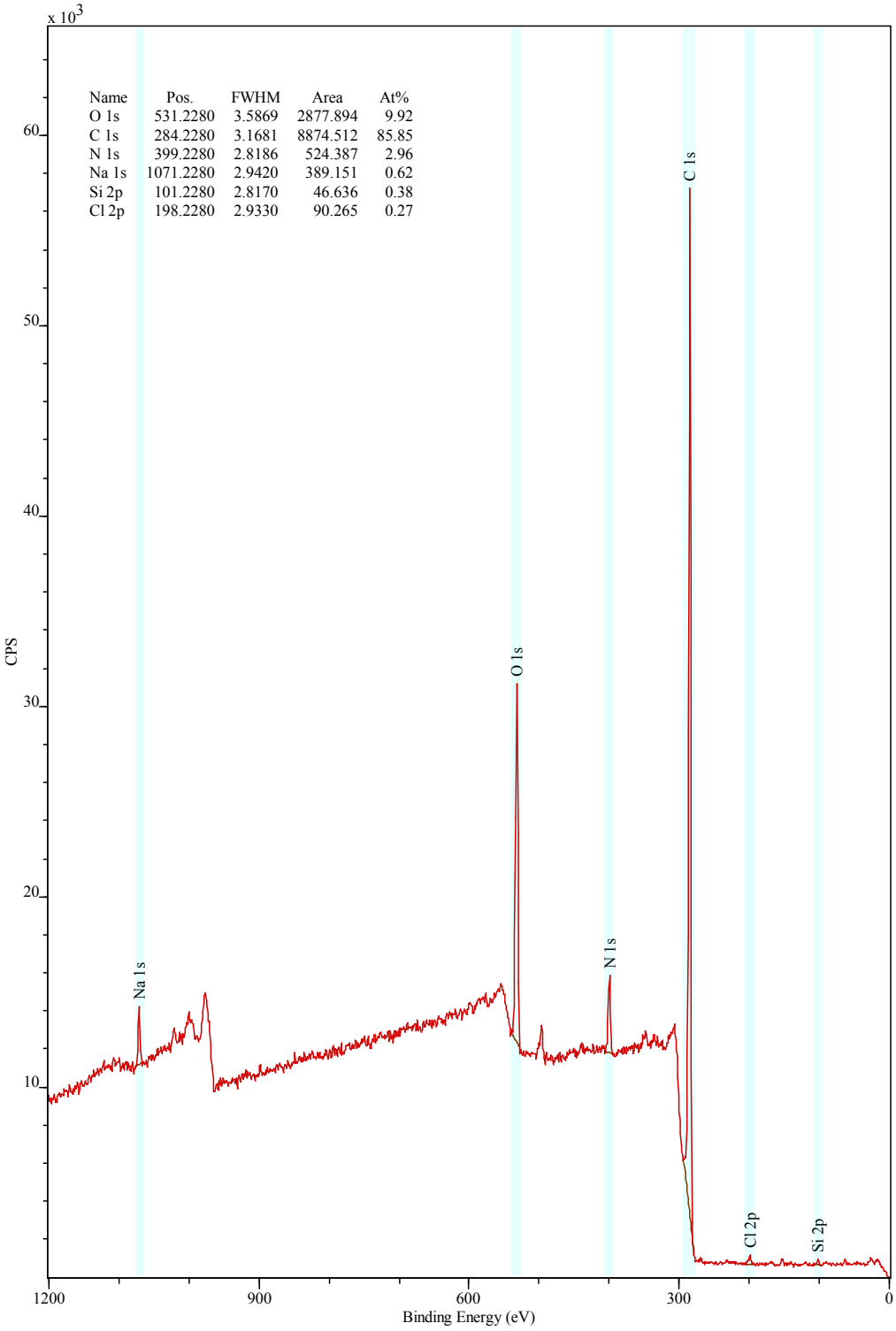
x 10^3
Name Pos. FWHM Area At%
O 1s 531.2280 3.5869 2877.894 9.92
C 1s 284.2280 3.1681 8874.512 85.85
N 1s 399.2280 2.8186 524.387 2.96
Na 1s 1071.2280 2.9420 389.151 0.62
Si 2p 101.2280 2.8170 46.636 0.38
Cl 2p 198.2280 2.9330 90.265 0.27
CPS
60
50
40
30
20
10
Na 1s
O 1s
N 1s
C 1s
Cl 2p
Si 2p
1200
900
600
300
0
Binding Energy (eV)

PSM4

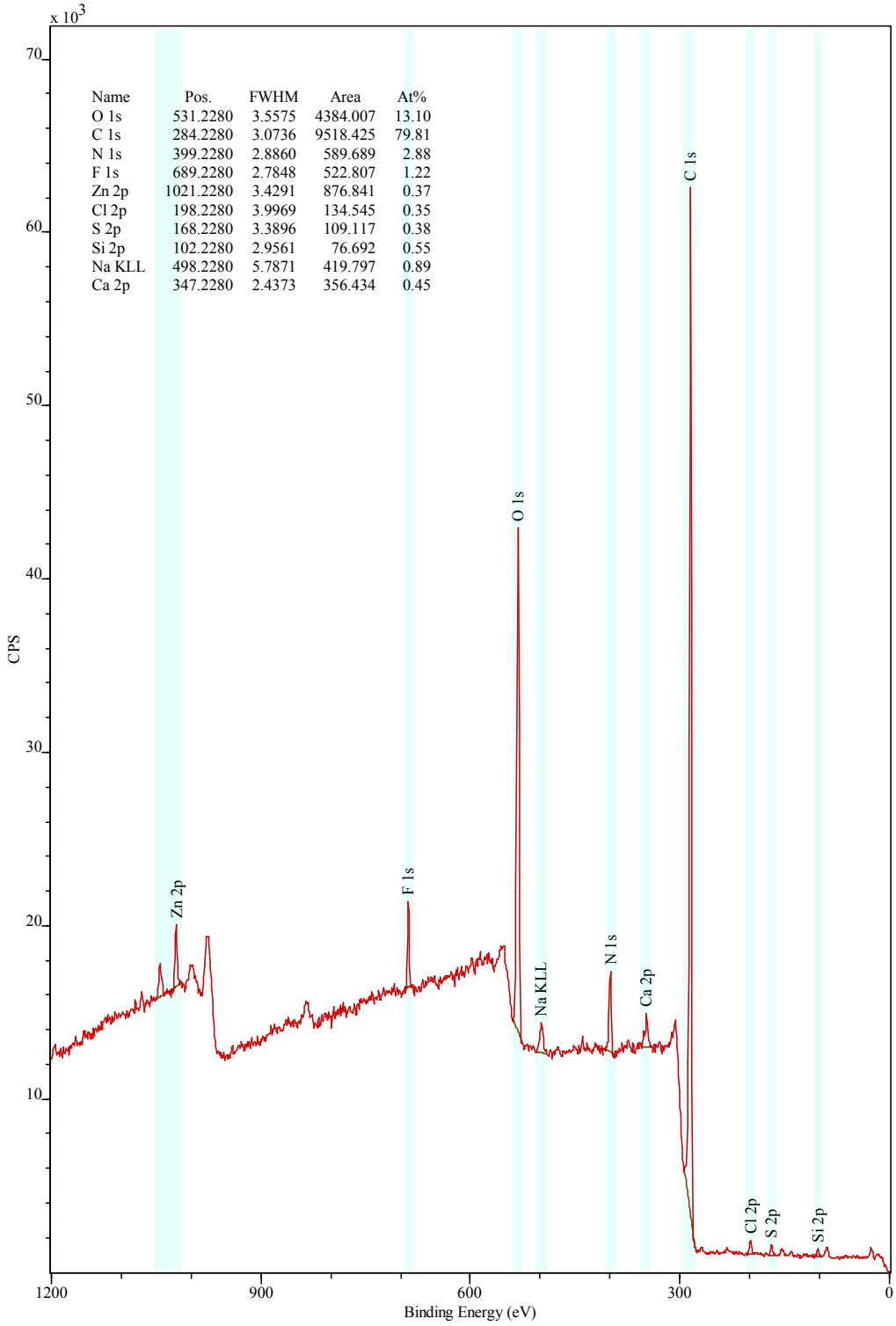
x 10^3
70
60
50
40
30
20
10
CPS
Name Pos. FWHM Area At%
O 1s 531.2280 3.5575 4384.007 13.10
C 1s 284.2280 3.0736 9518.425 79.81
N 1s 399.2280 2.8860 589.689 2.88
F 1s 689.2280 2.7848 522.807 1.22
Zn 2p 1021.2280 3.4291 876.841 0.37
Cl 2p 198.2280 3.9969 134.545 0.35
S 2p 168.2280 3.3896 109.117 0.38
Si 2p 102.2280 2.9561 76.692 0.55
Na KLL 498.2280 5.7871 419.797 0.89
Ca 2p 347.2280 2.4373 356.434 0.45
Zn 2p
F 1s
O 1s
Na KLL
N 1s
Ca 2p
C 1s
Cl 2p
S 2p
Si 2p
1200
900
600
300
0
Binding Energy (eV)

PSM4.Zn

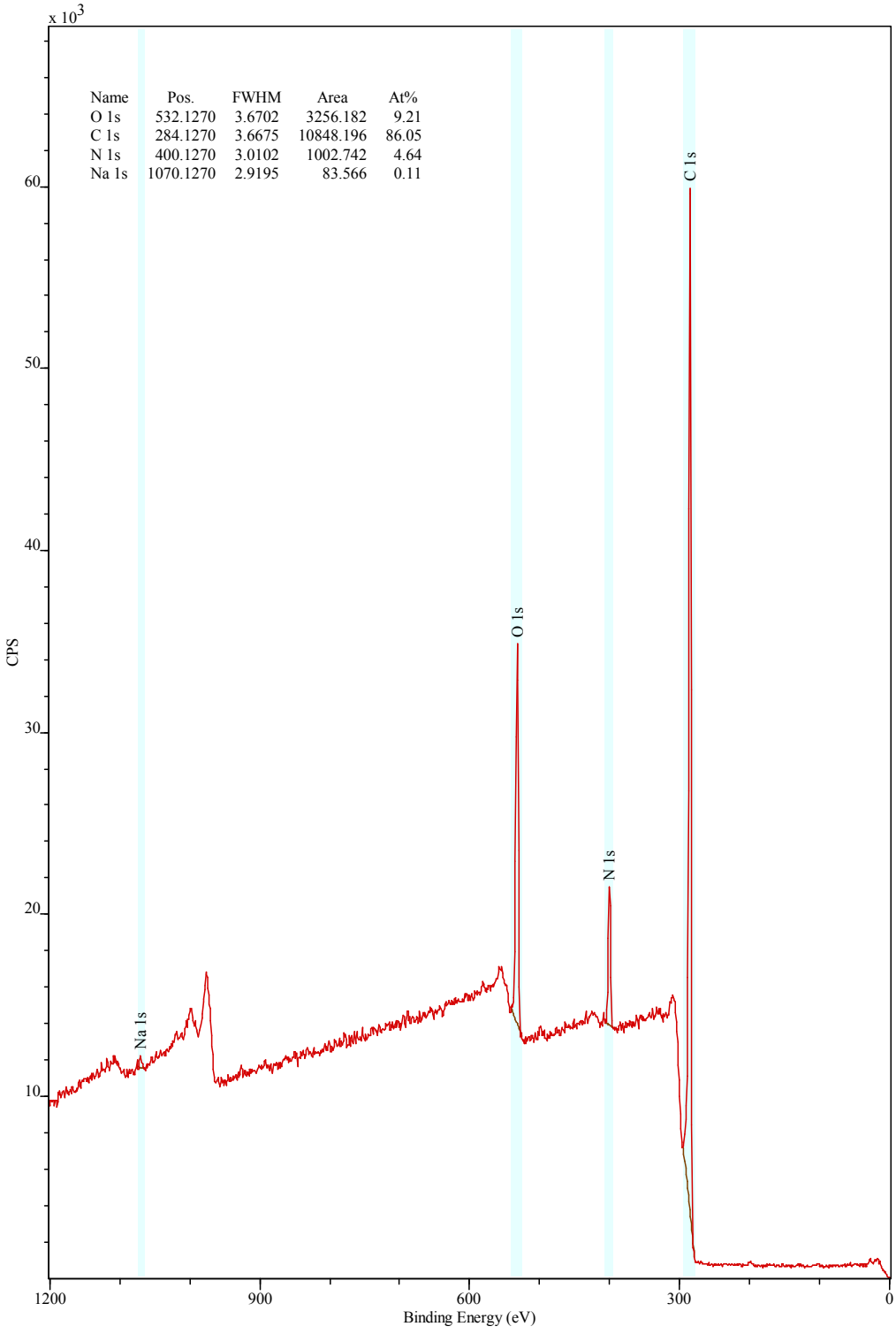
x 10^3
Name Pos. FWHM Area At%
O 1s 532.1270 3.6702 3256.182 9.21
C 1s 284.1270 3.6675 10848.196 86.05
N 1s 400.1270 3.0102 1002.742 4.64
Na 1s 1070.1270 2.9195 83.566 0.11
CPS
60
50
40
30
20
10
Na 1s
O 1s
N 1s
C 1s
1200
900
600
300
0
Binding Energy (eV)

PSM5

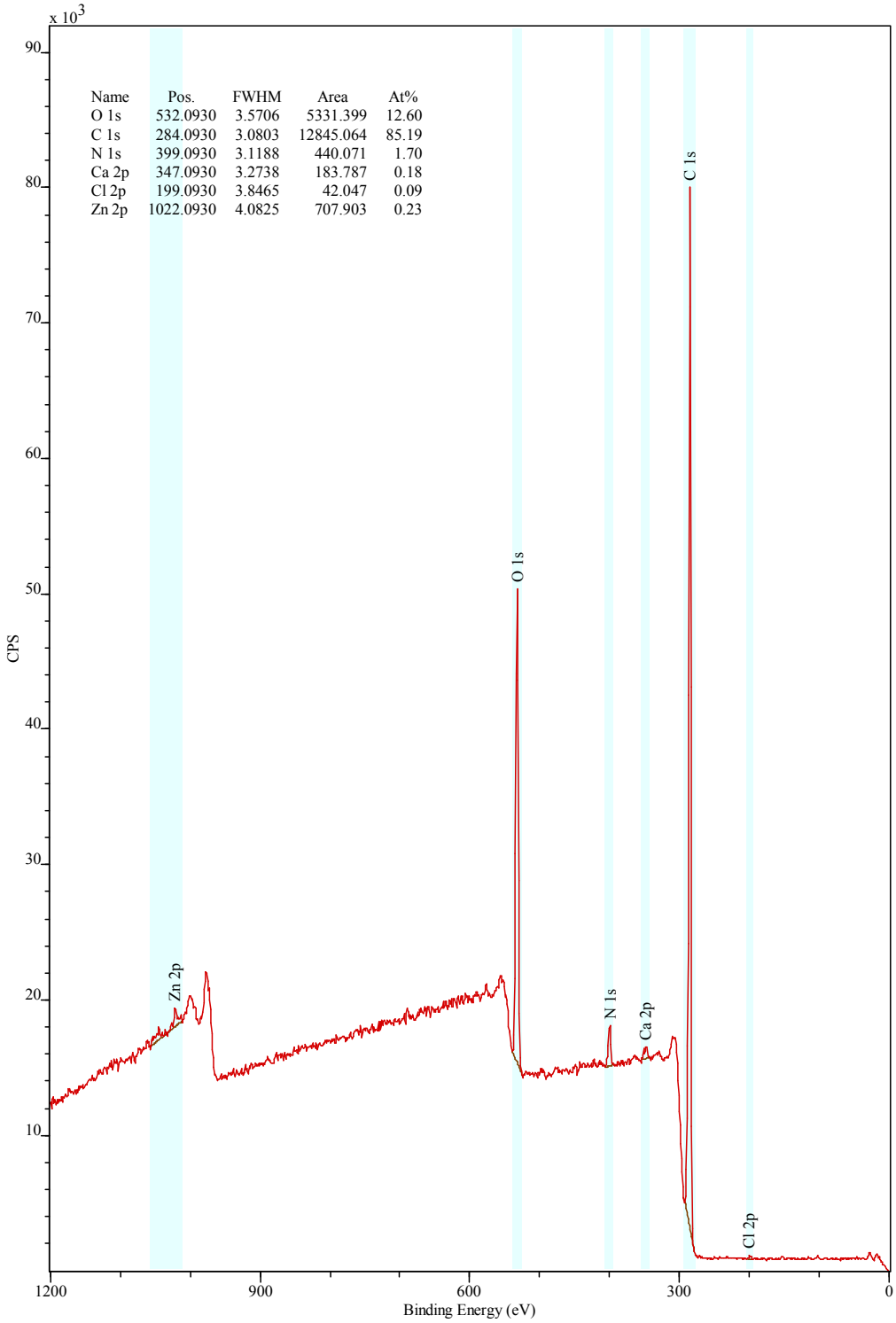
x 10^3
90
80
70
60
50
40
30
20
10
CPS
Name Pos. FWHM Area At%
O 1s 532.0930 3.5706 5331.399 12.60
C 1s 284.0930 3.0803 12845.064 85.19
N 1s 399.0930 3.1188 440.071 1.70
Ca 2p 347.0930 3.2738 183.787 0.18
Cl 2p 199.0930 3.8465 42.047 0.09
Zn 2p 1022.0930 4.0825 707.903 0.23
O 1s
C 1s
Zn 2p
N 1s
Ca 2p
Cl 2p
1200
900
600
300
0
Binding Energy (eV)

PSM5.Zn

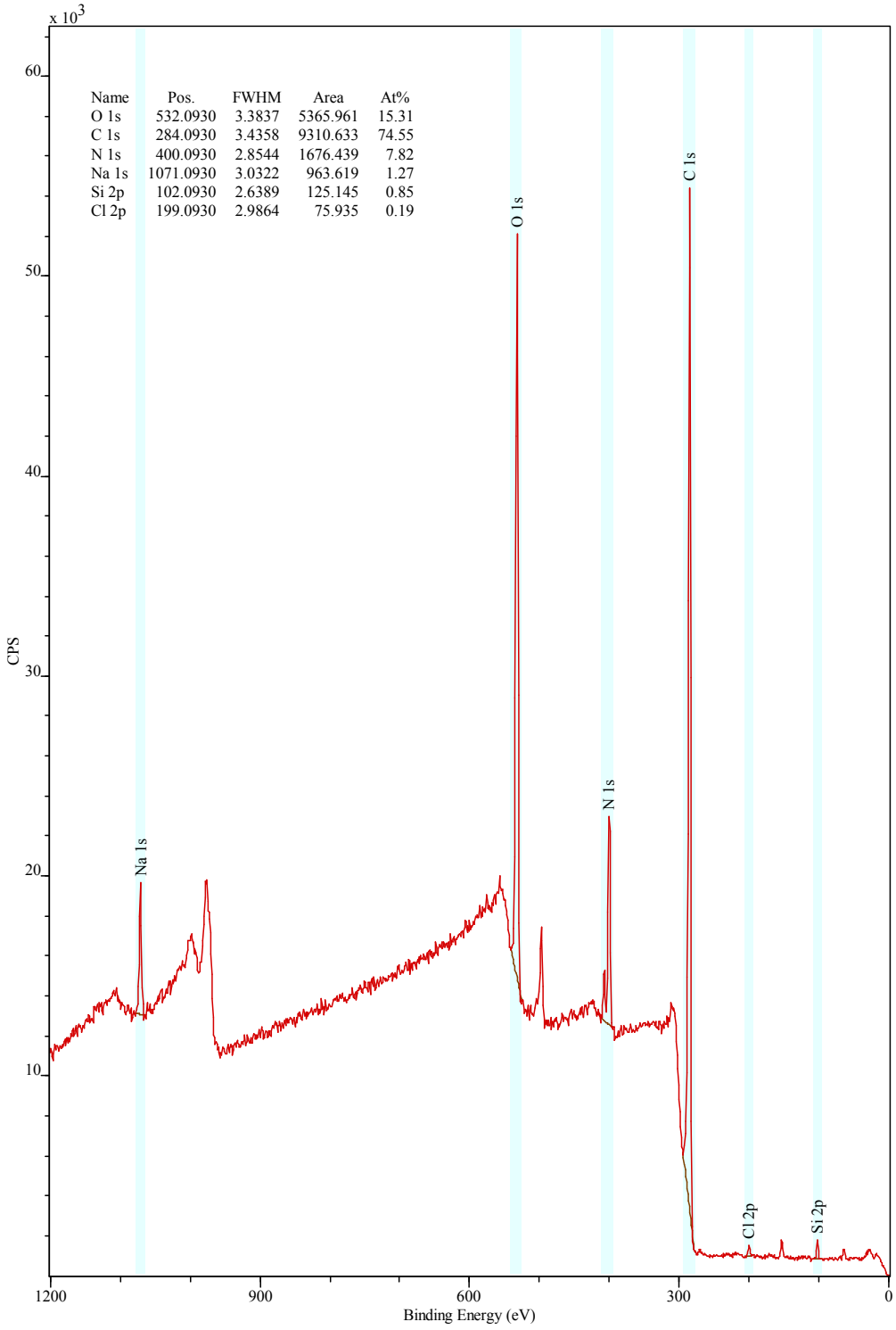
x 10^3
60
50
40
30
20
10
CPS
Name Pos. FWHM Area At%
O 1s 532.0930 3.3837 5365.961 15.31
C 1s 284.0930 3.4358 9310.633 74.55
N 1s 400.0930 2.8544 1676.439 7.82
Na 1s 1071.0930 3.0322 963.619 1.27
Si 2p 102.0930 2.6389 125.145 0.85
Cl 2p 199.0930 2.9864 75.935 0.19
O 1s
C 1s
N 1s
Na 1s
Cl 2p
Si 2p
1200
900
600
300
0
Binding Energy (eV)

PSM6

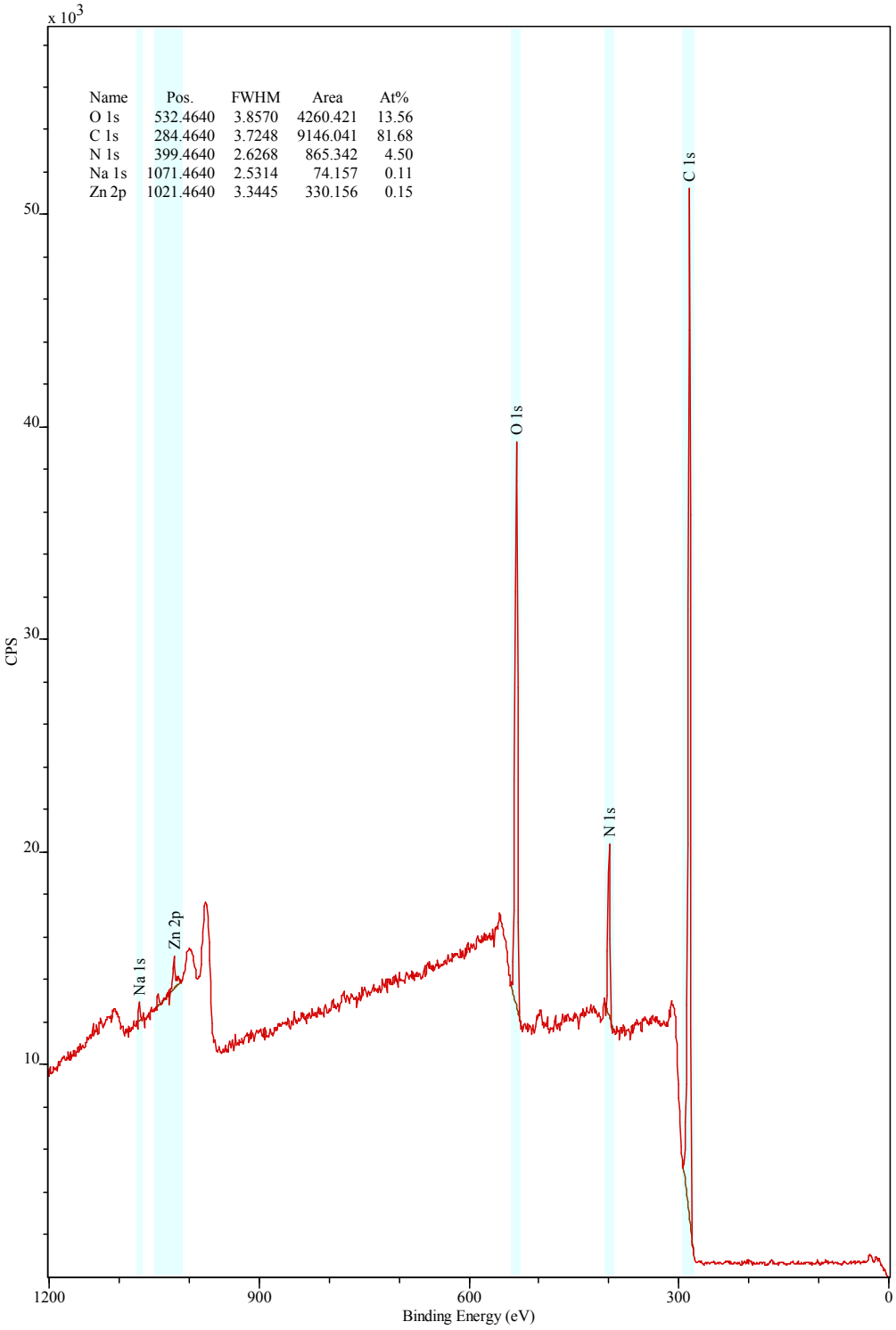
x 10^3
Name Pos. FWHM Area At%
O 1s 532.4640 3.8570 4260.421 13.56
C 1s 284.4640 3.7248 9146.041 81.68
N 1s 399.4640 2.6268 865.342 4.50
Na 1s 1071.4640 2.5314 74.157 0.11
Zn 2p 1021.4640 3.3445 330.156 0.15
CPS
50
40
30
20
10
Na 1s
Zn 2p
O 1s
N 1s
C 1s
1200
900
600
300
0
Binding Energy (eV)

PSM6.Zn

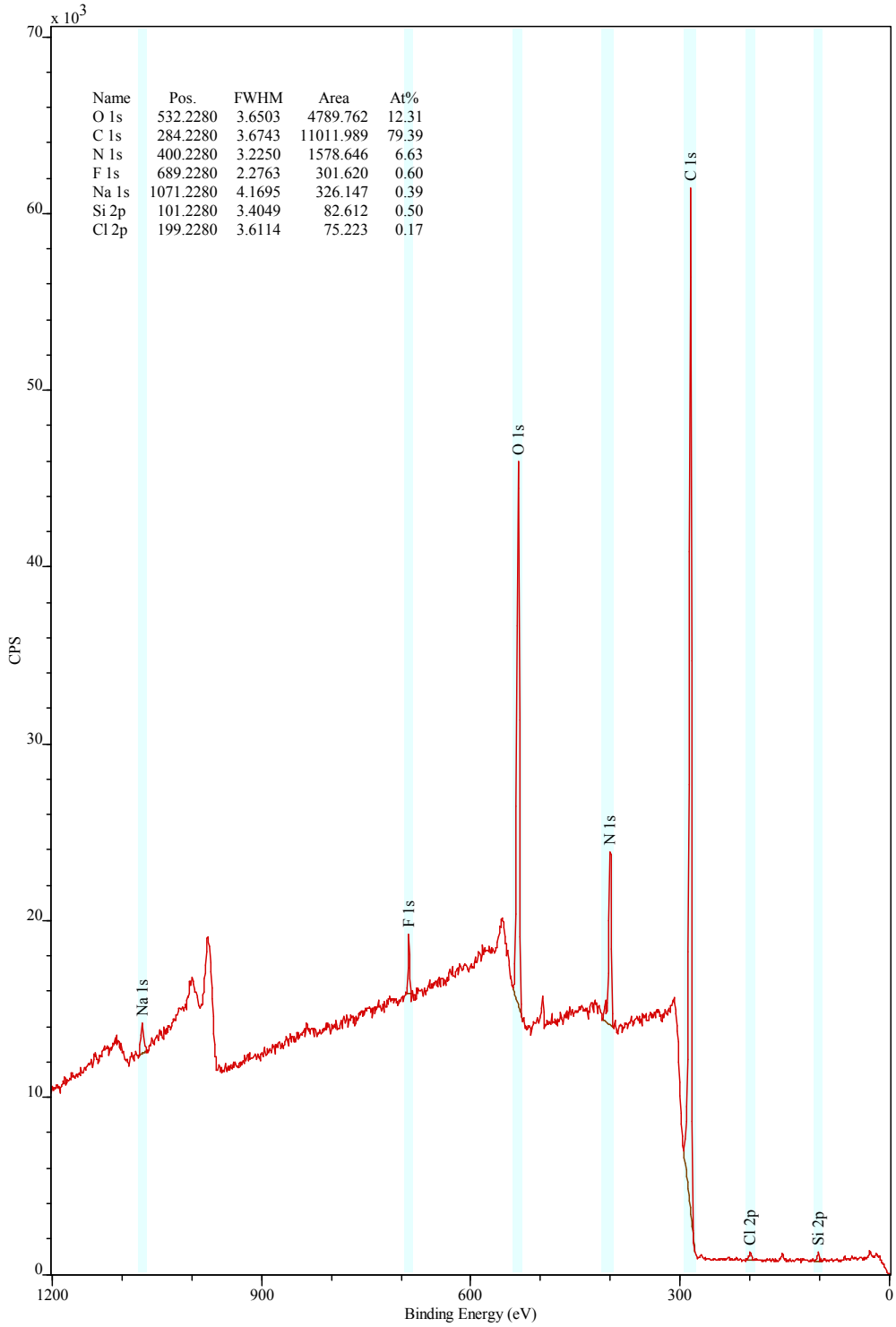
x 10^3
70
60
50
40
30
20
10
0
CPS
Name Pos. FWHM Area At%
O 1s 532.2280 3.6503 4789.762 12.31
C 1s 284.2280 3.6743 11011.989 79.39
N 1s 400.2280 3.2250 1578.646 6.63
F 1s 689.2280 2.2763 301.620 0.60
Na 1s 1071.2280 4.1695 326.147 0.39
Si 2p 101.2280 3.4049 82.612 0.50
Cl 2p 199.2280 3.6114 75.223 0.17
Na 1s
F 1s
O 1s
N 1s
C 1s
Cl 2p
Si 2p
1200
900
600
300
0
Binding Energy (eV)

PSM7

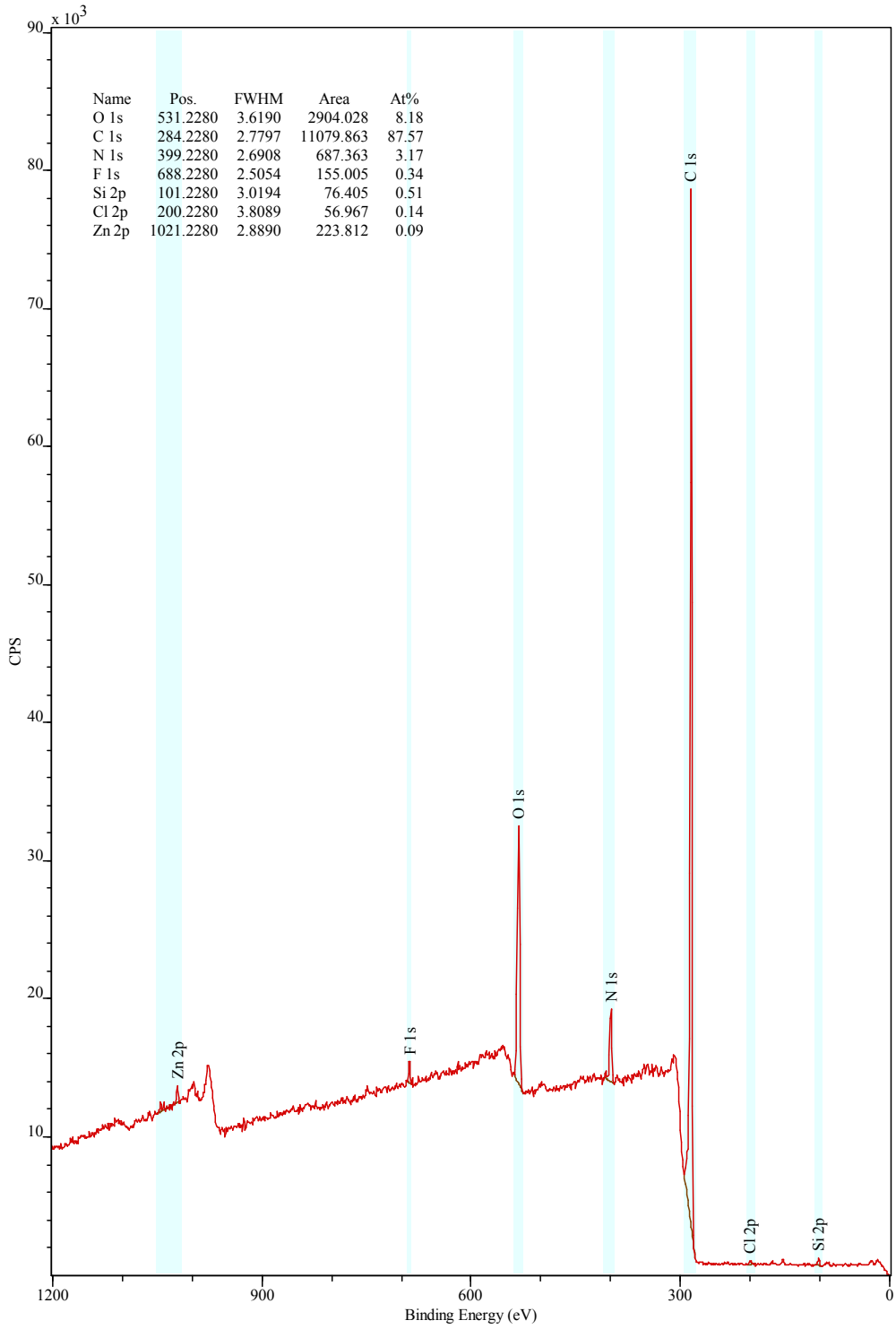
x 10^3
90
80
70
60
50
40
30
20
10
CPS
Name Pos. FWHM Area At%
O 1s 531.2280 3.6190 2904.028 8.18
C 1s 284.2280 2.7797 11079.863 87.57
N 1s 399.2280 2.6908 687.363 3.17
F 1s 688.2280 2.5054 155.005 0.34
Si 2p 101.2280 3.0194 76.405 0.51
Cl 2p 200.2280 3.8089 56.967 0.14
Zn 2p 1021.2280 2.8890 223.812 0.09
Zn 2p
F 1s
O 1s
N 1s
C 1s
Cl 2p
Si 2p
1200
900
600
300
0
Binding Energy (eV)

PSM7.Zn

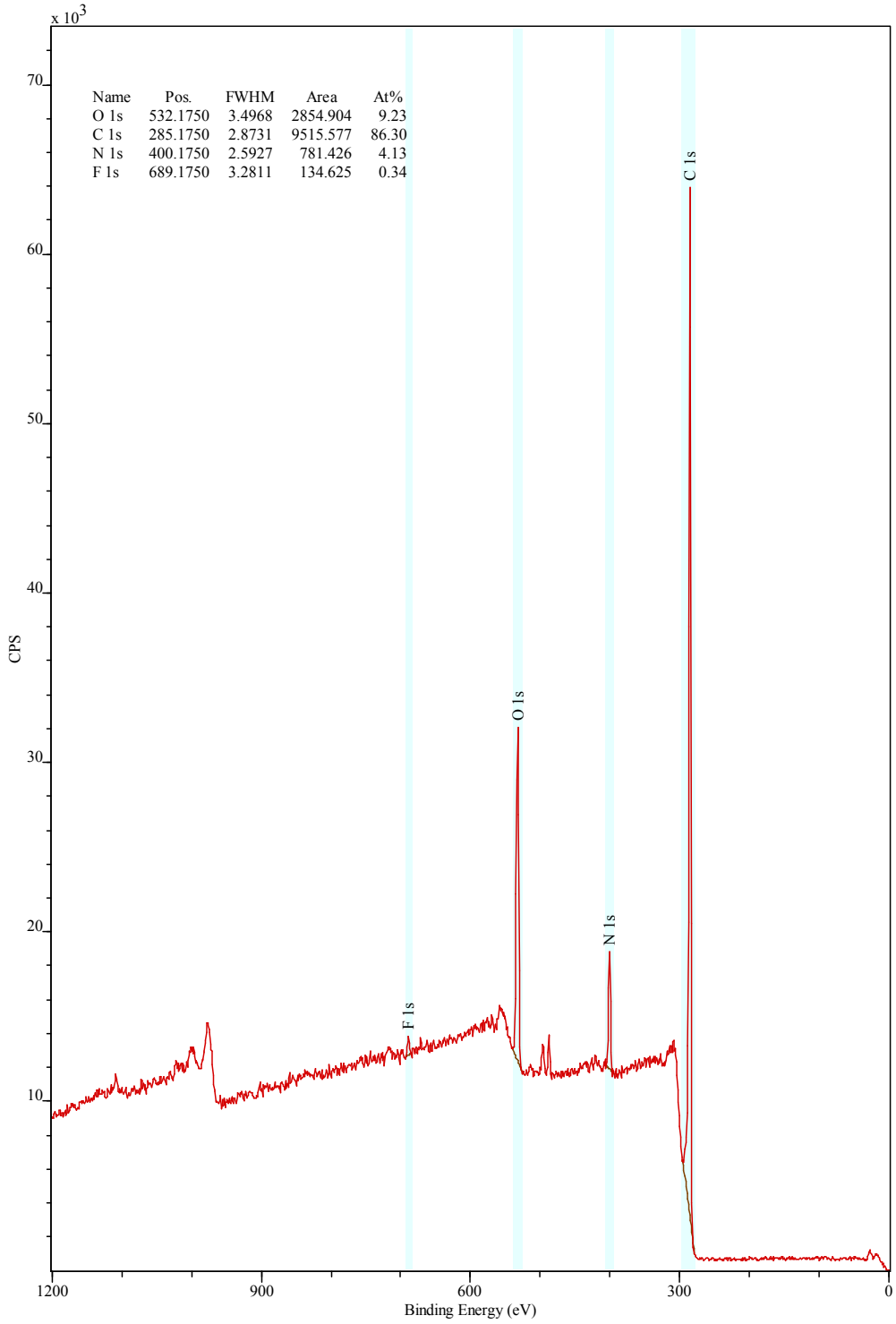
x 10^3
70
60
50
40
30
20
10
CPS
Name Pos. FWHM Area At%
O 1s 532.1750 3.4968 2854.904 9.23
C 1s 285.1750 2.8731 9515.577 86.30
N 1s 400.1750 2.5927 781.426 4.13
F 1s 689.1750 3.2811 134.625 0.34
F 1s
O 1s
N 1s
C 1s
1200
900
600
300
0
Binding Energy (eV)

PSM8

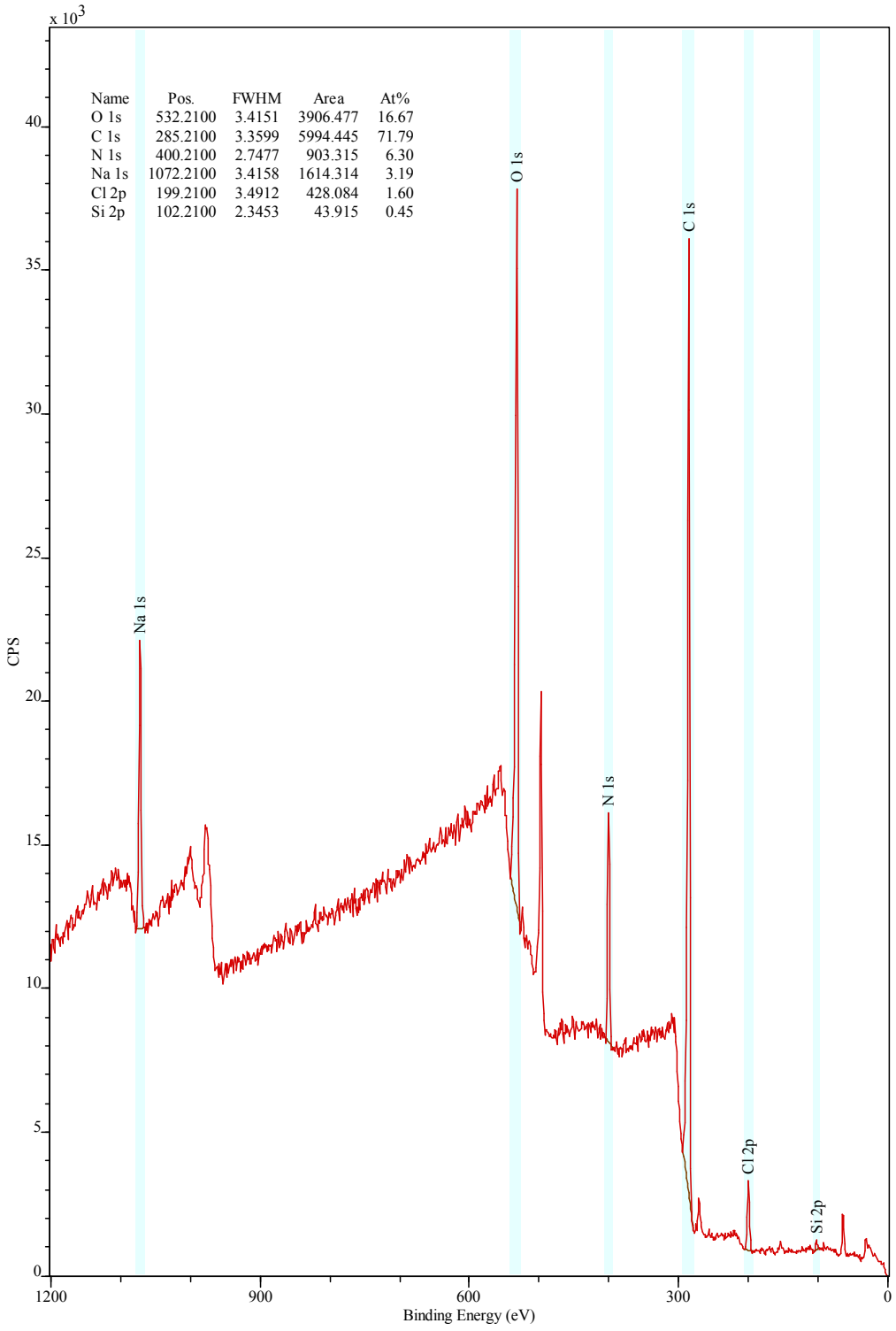
x 10^3
Name Pos. FWHM Area At%
O 1s 532.2100 3.4151 3906.477 16.67
C 1s 285.2100 3.3599 5994.445 71.79
N 1s 400.2100 2.7477 903.315 6.30
Na 1s 1072.2100 3.4158 1614.314 3.19
Cl 2p 199.2100 3.4912 428.084 1.60
Si 2p 102.2100 2.3453 43.915 0.45
O 1s
C 1s
N 1s
Na 1s
Cl 2p
Si 2p
CPS
Binding Energy (eV)
0
5
10
15
20
25
30
35
40
1200
900
600
300
0

PSM22

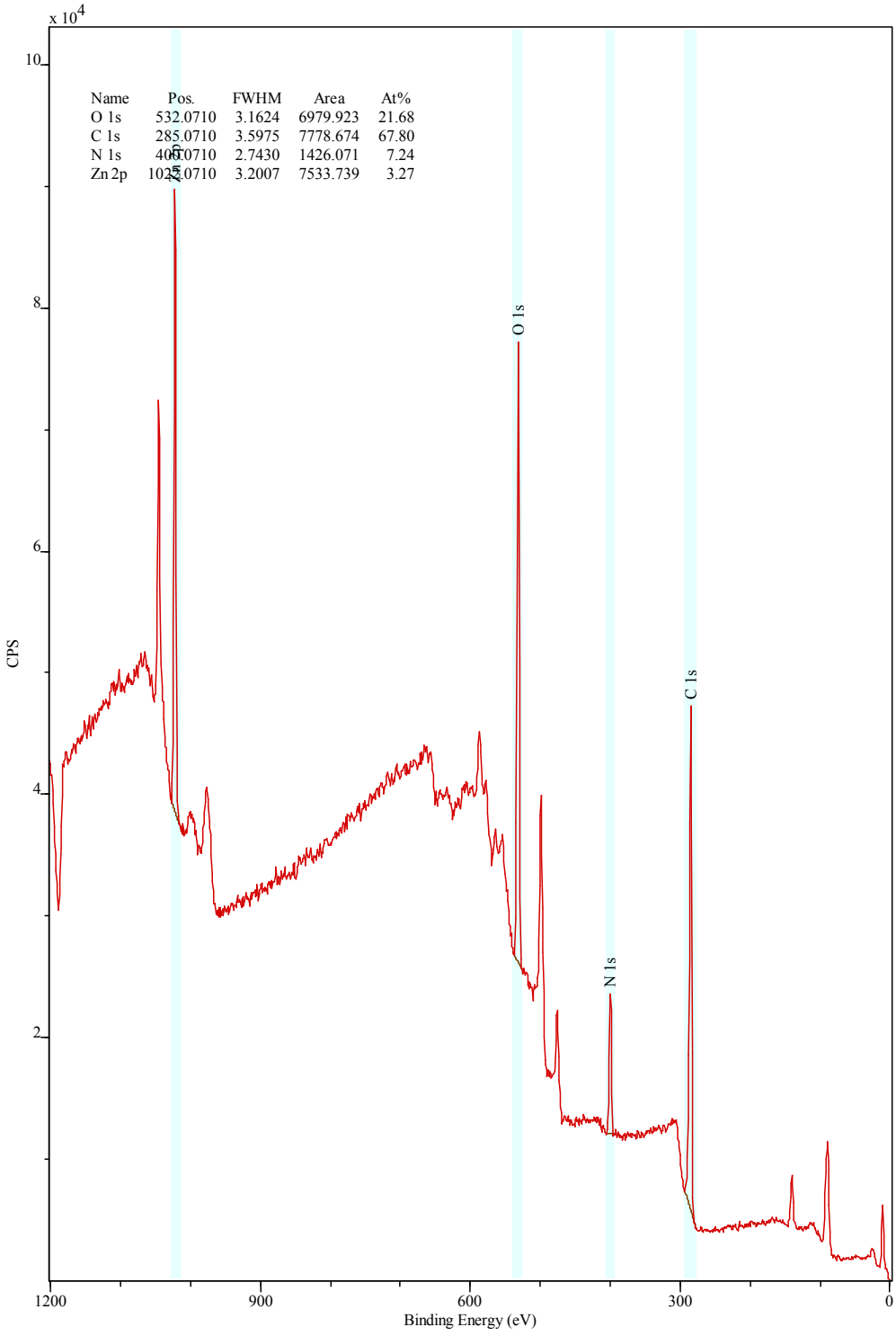
x 10^4
10
8
6
4
2
CPS
Name Pos. FWHM Area At%
O 1s 532.0710 3.1624 6979.923 21.68
C 1s 285.0710 3.5975 7778.674 67.80
N 1s 400.0710 2.7430 1426.071 7.24
Zn 2p 1025.0710 3.2007 7533.739 3.27
Zn 2p
O 1s
N 1s
C 1s
1200
900
600
300
0
Binding Energy (eV)

PSM22.Zn

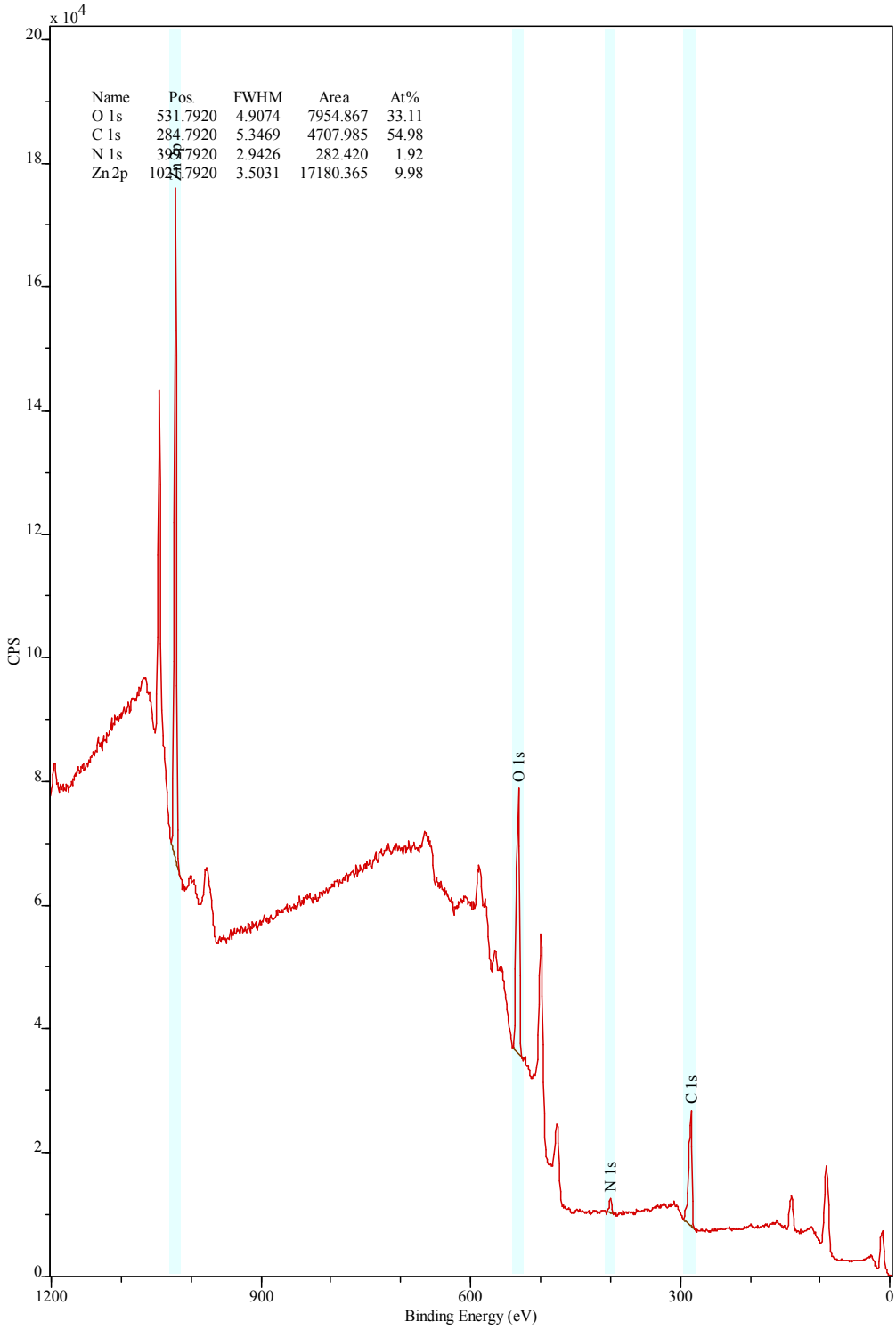
x 10^4
20
18
16
14
12
10
8
6
4
2
0
CPS
Name Pos. FWHM Area At%
O 1s 531.7920 4.9074 7954.867 33.11
C 1s 284.7920 5.3469 4707.985 54.98
N 1s 399.7920 2.9426 282.420 1.92
Zn 2p 1021.7920 3.5031 17180.365 9.98
Zn 2p
O 1s
N 1s
C 1s
1200
900
600
300
0
Binding Energy (eV)

PSM27

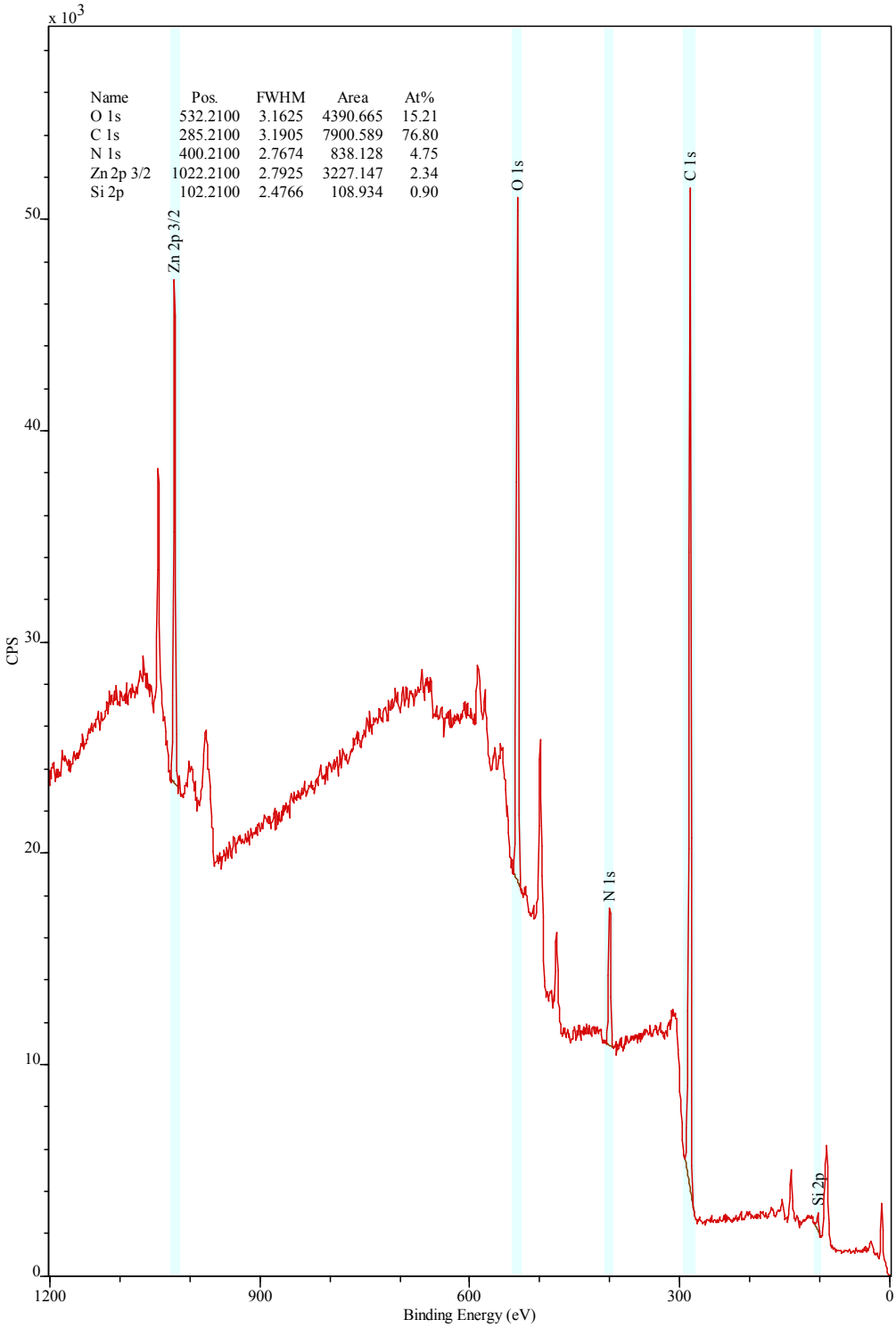
x 10^3
Name Pos. FWHM Area At%
O 1s 532.2100 3.1625 4390.665 15.21
C 1s 285.2100 3.1905 7900.589 76.80
N 1s 400.2100 2.7674 838.128 4.75
Zn 2p 3/2 1022.2100 2.7925 3227.147 2.34
Si 2p 102.2100 2.4766 108.934 0.90
Zn 2p 3/2
O 1s
N 1s
C 1s
Si 2p
CPS
0
10
20
30
40
50
1200
900
600
300
0
Binding Energy (eV)

PSM27.Zn

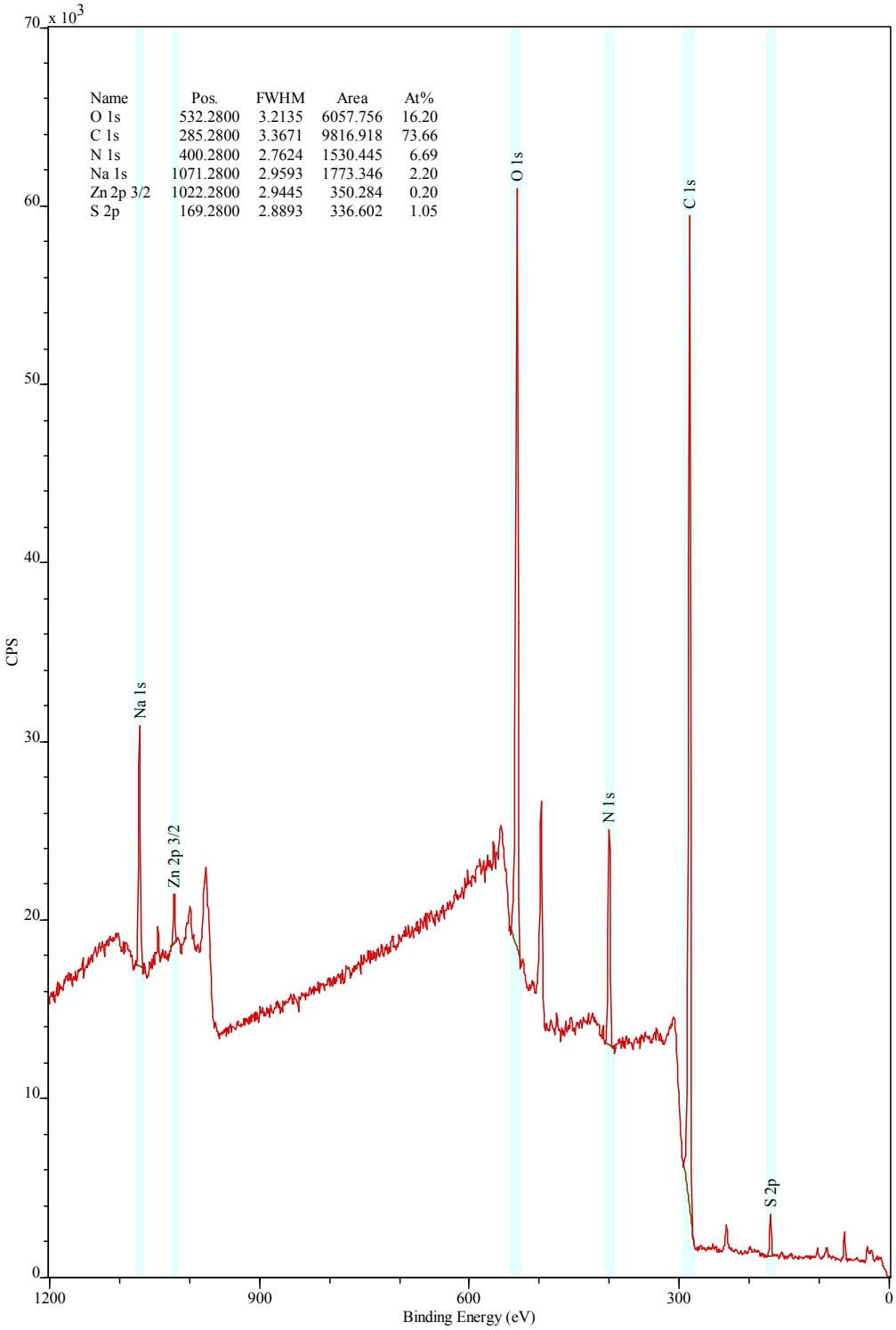

PSM27.ZnATSMA

Appendix III: ATR-IR (Chapter 3)

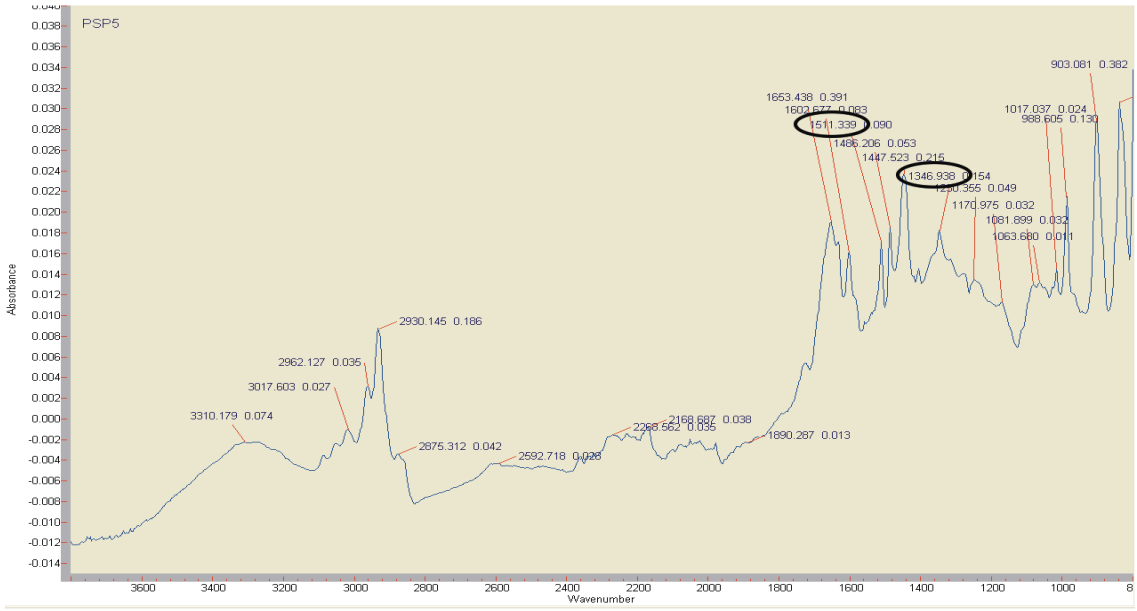

PSP5

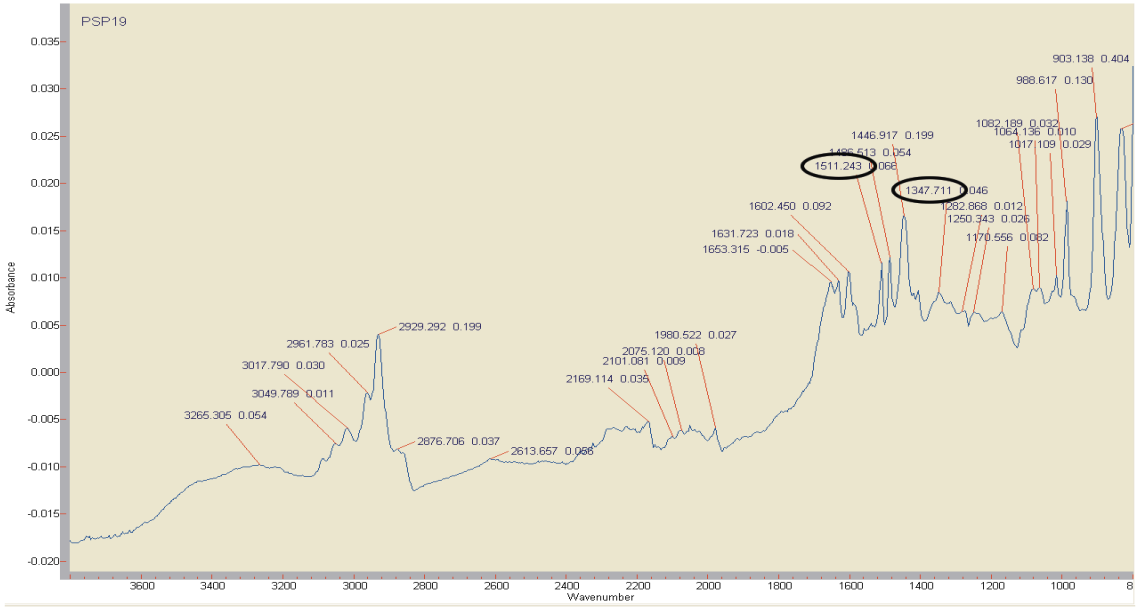

PSP19

Appendix IV: XPS (Chapter 3)

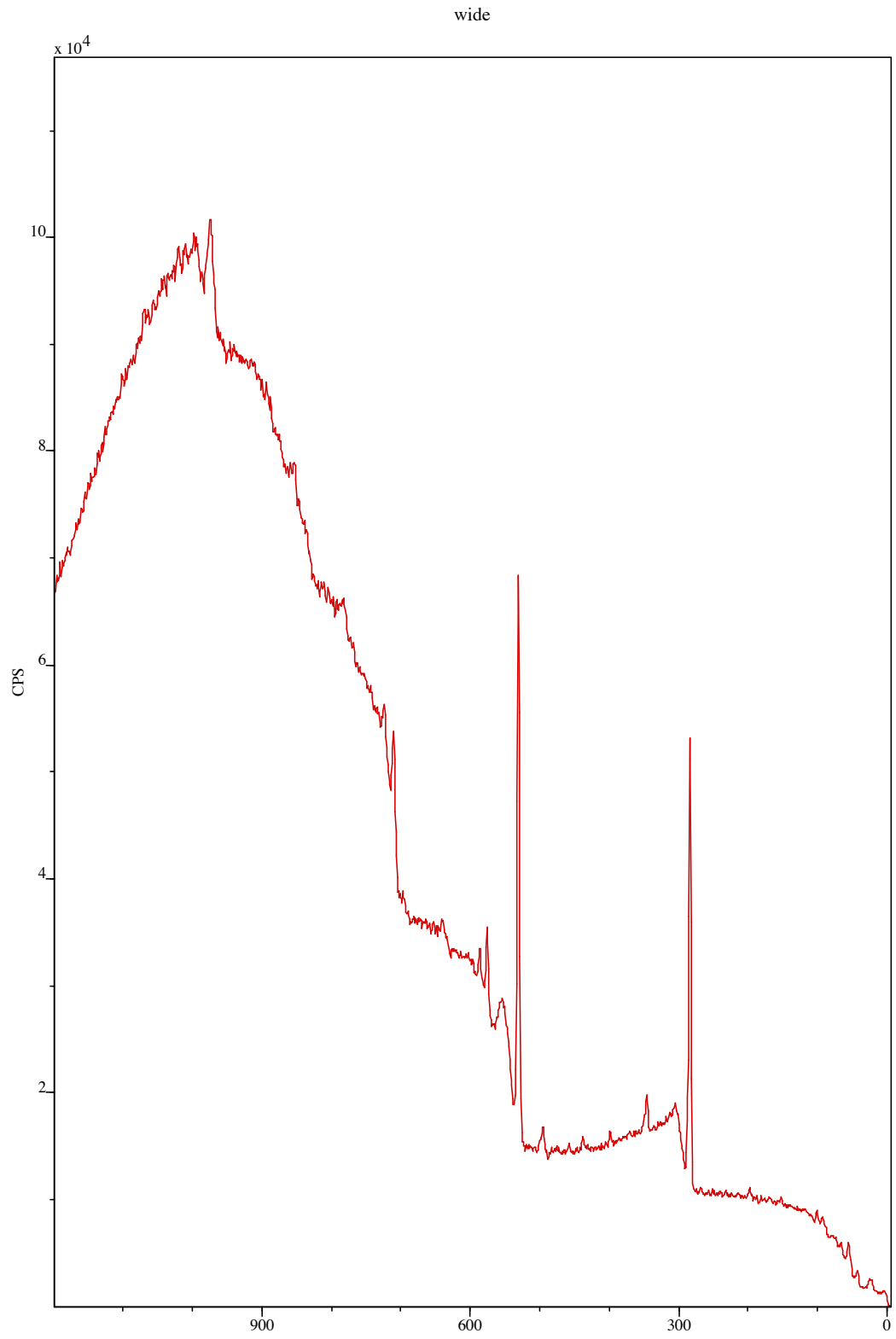

Blank PS XAD

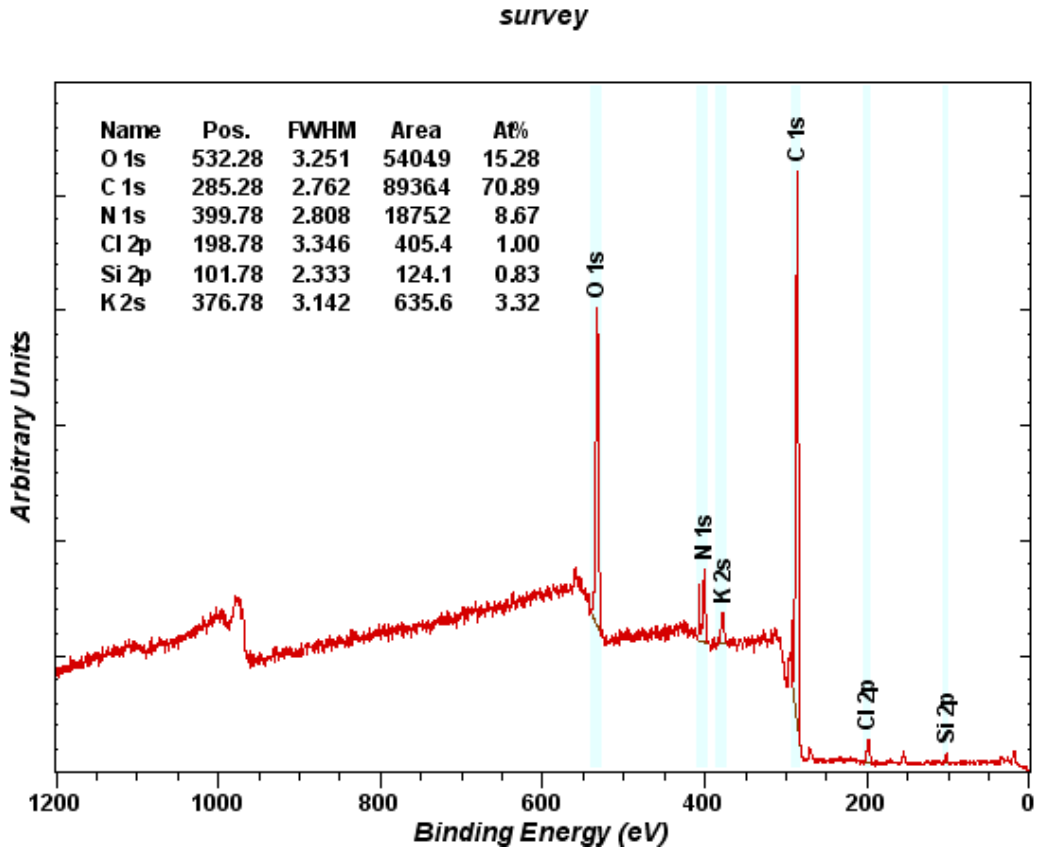
survey
Name Pos. FWHM Area At%
O 1s 532.28 3.251 54049 15.28
C 1s 285.28 2.762 89364 70.89
N 1s 399.78 2.808 18752 8.67
Cl 2p 198.78 3.346 405.4 1.00
Si 2p 101.78 2.333 124.1 0.83
K 2s 376.78 3.142 635.6 3.32
O 1s
N 1s
K 2s
C 1s
Cl 2p
Si 2p
Arbitrary Units
1200
1000
800
600
400
200
0
Binding Energy (eV)

PSP5

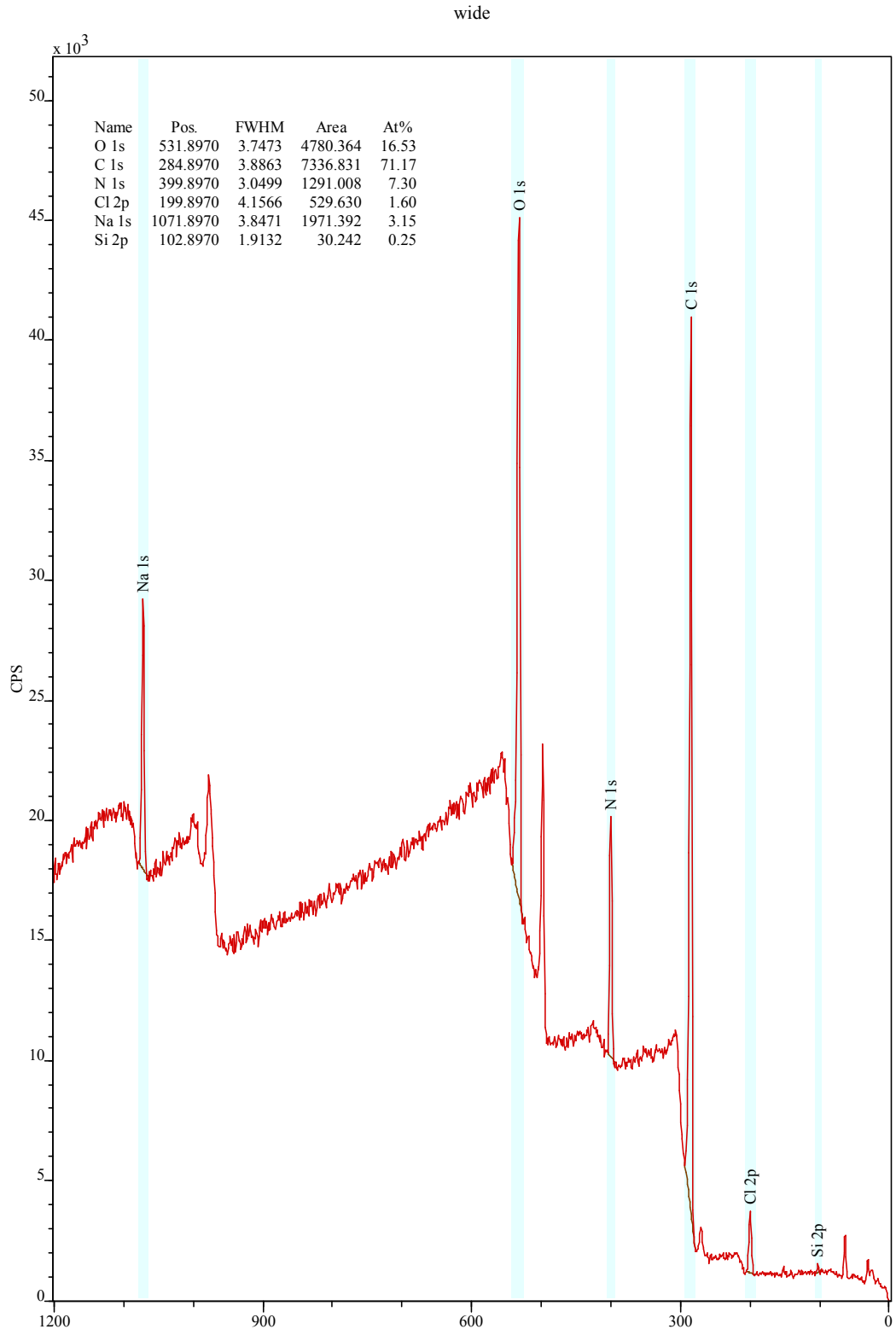
wide
x 10^3
CPS
50
45
40
35
30
25
20
15
10
5
0
1200
900
600
300
0
Name Pos. FWHM Area At%
O 1s 531.8970 3.7473 4780.364 16.53
C 1s 284.8970 3.8863 7336.831 71.17
N 1s 399.8970 3.0499 1291.008 7.30
Cl 2p 199.8970 4.1566 529.630 1.60
Na 1s 1071.8970 3.8471 1971.392 3.15
Si 2p 102.8970 1.9132 30.242 0.25
Na 1s
O 1s
N 1s
C 1s
Cl 2p
Si 2p

PSP19

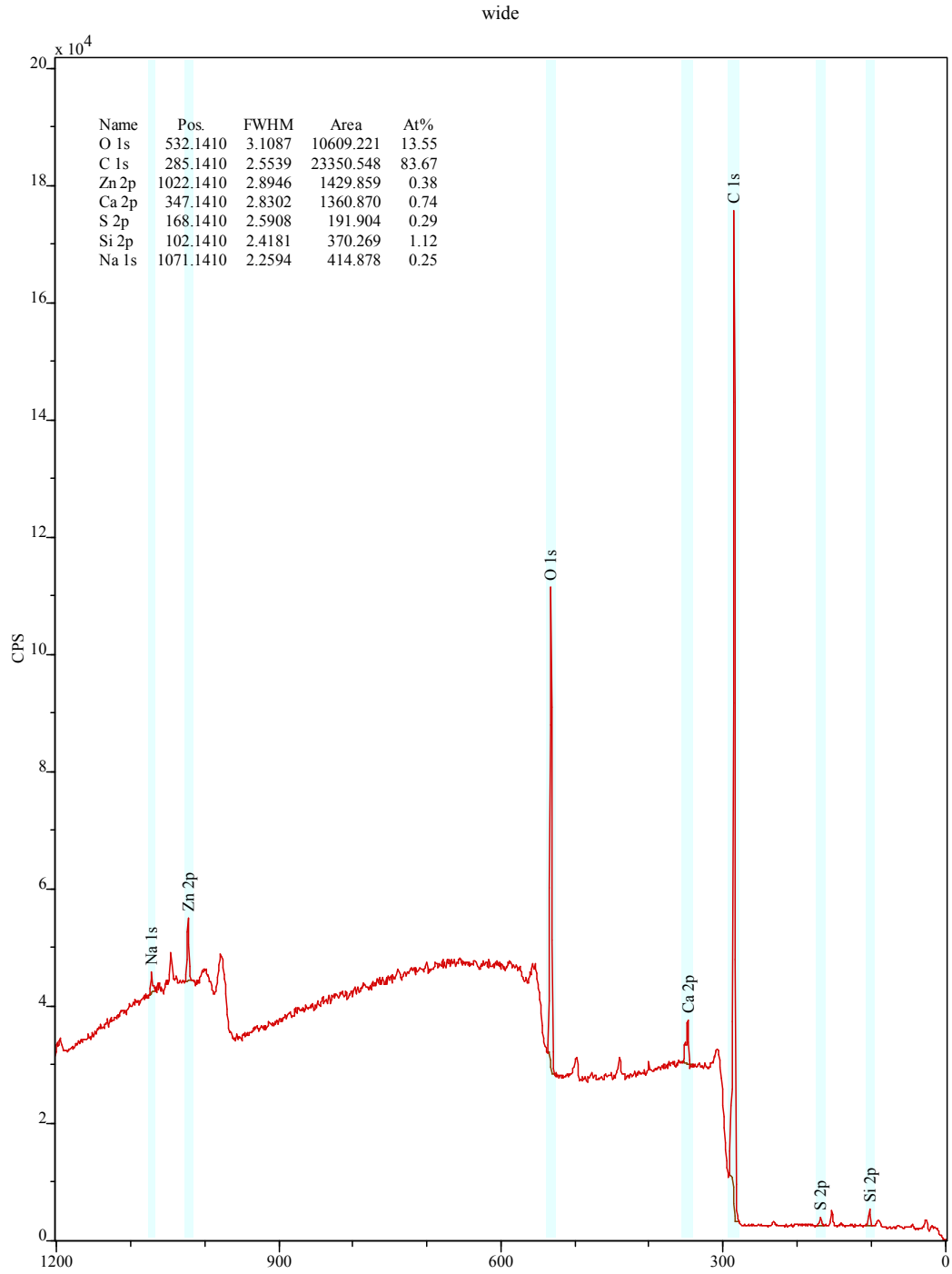
wide
x 10^4
Name Pos. FWHM Area At%
O 1s 532.1410 3.1087 10609.221 13.55
C 1s 285.1410 2.5539 23350.548 83.67
Zn 2p 1022.1410 2.8946 1429.859 0.38
Ca 2p 347.1410 2.8302 1360.870 0.74
S 2p 168.1410 2.5908 191.904 0.29
Si 2p 102.1410 2.4181 370.269 1.12
Na 1s 1071.1410 2.2594 414.878 0.25
CPS
Na 1s
Zn 2p
O 1s
Ca 2p
C 1s
S 2p
Si 2p
1200
900
600
300
0

blank PET

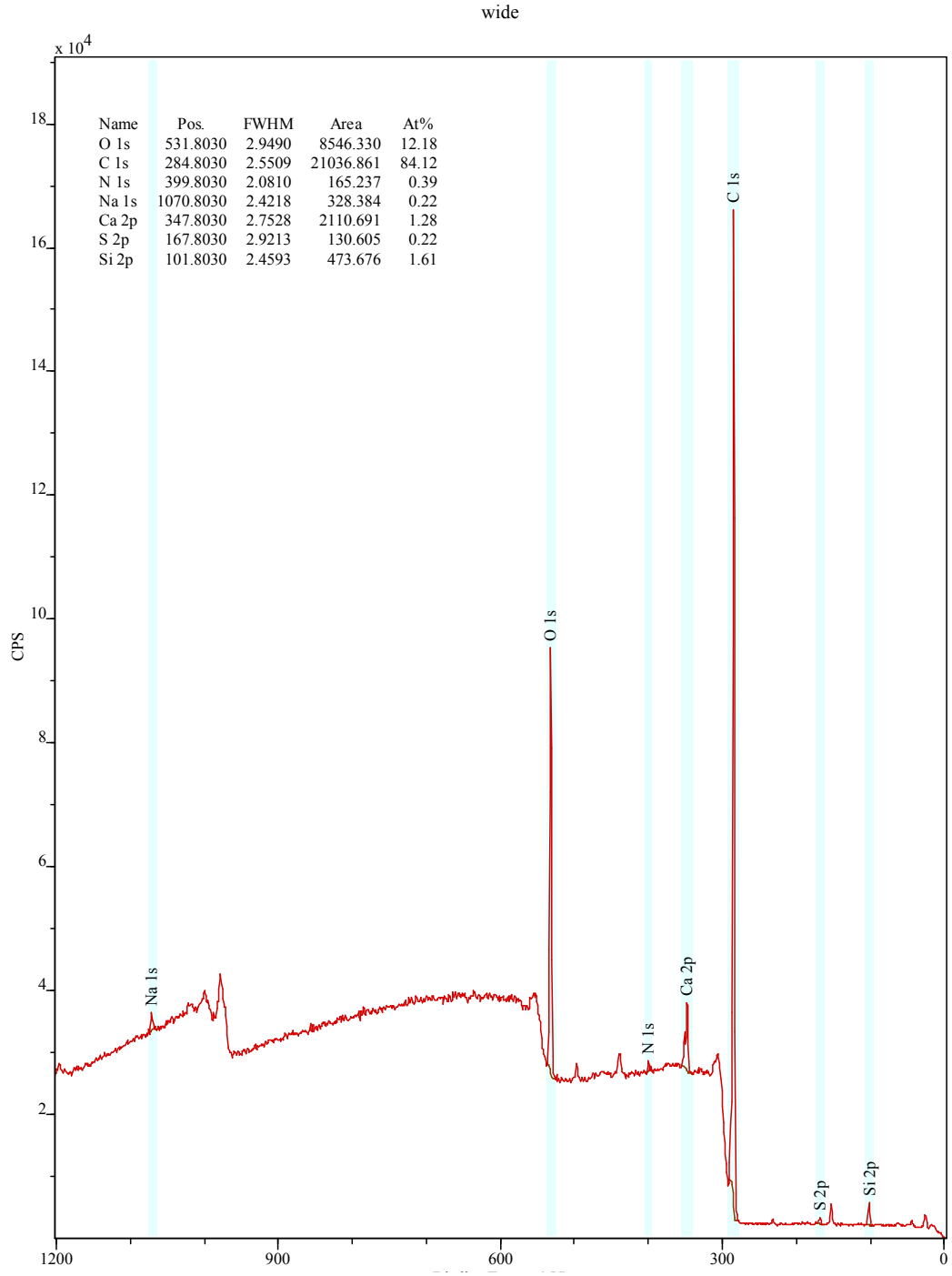
wide
x 10^4
CPS
18
16
14
12
10
8
6
4
2
Name Pos. FWHM Area At%
O 1s 531.8030 2.9490 8546.330 12.18
C 1s 284.8030 2.5509 21036.861 84.12
N 1s 399.8030 2.0810 165.237 0.39
Na 1s 1070.8030 2.4218 328.384 0.22
Ca 2p 347.8030 2.7528 2110.691 1.28
S 2p 167.8030 2.9213 130.605 0.22
Si 2p 101.8030 2.4593 473.676 1.61
Na 1s
O 1s
N 1s
Ca 2p
C 1s
S 2p
Si 2p
1200
900
600
300
0

PETP5

wide

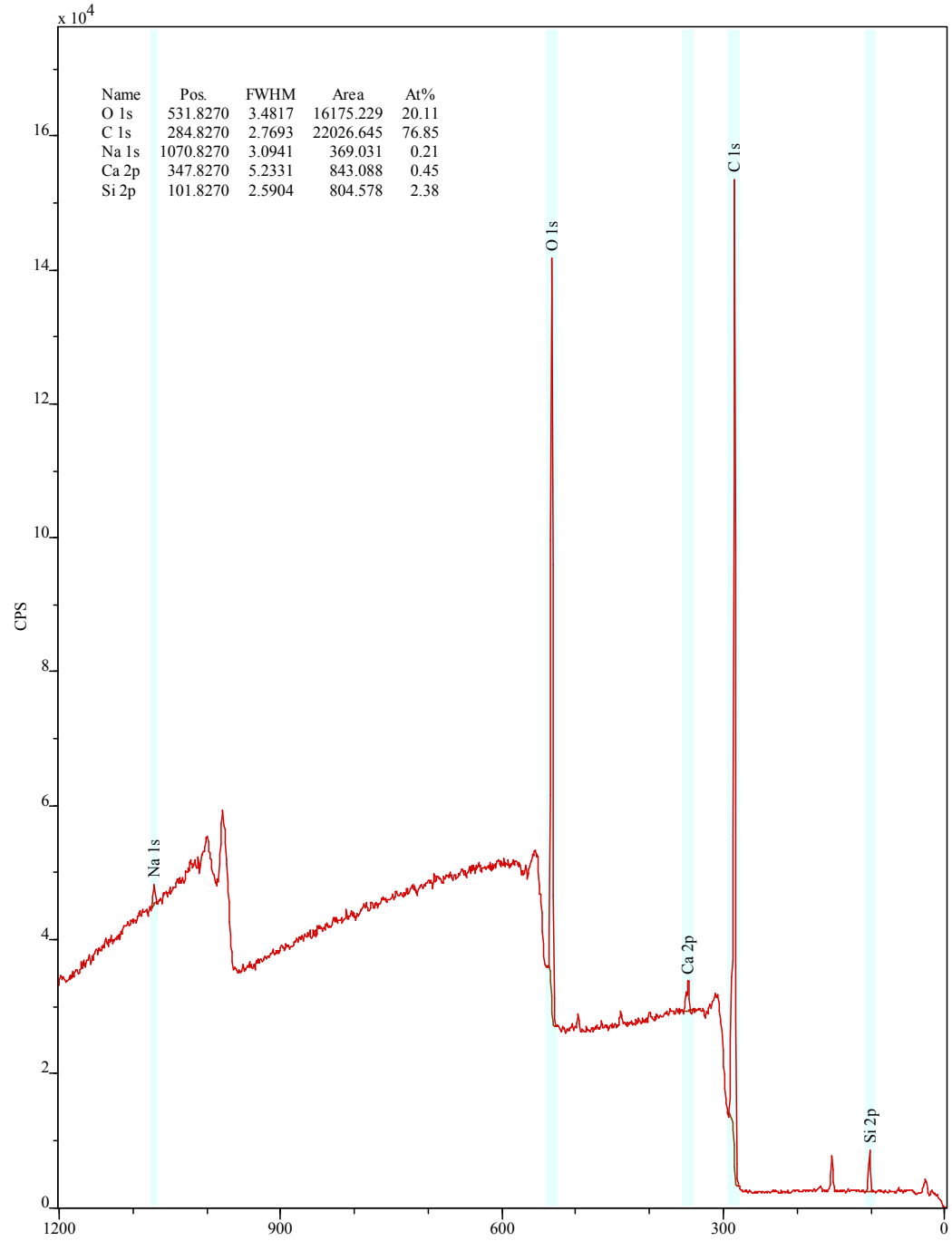
x 10^4
Name Pos. FWHM Area At%
O 1s 531.8270 3.4817 16175.229 20.11
C 1s 284.8270 2.7693 22026.645 76.85
Na 1s 1070.8270 3.0941 369.031 0.21
Ca 2p 347.8270 5.2331 843.088 0.45
Si 2p 101.8270 2.5904 804.578 2.38
CPS
O 1s
C 1s
Na 1s
Ca 2p
Si 2p
16
14
12
10
8
6
4
2
0
1200
900
600
300
0

PETP17

wide

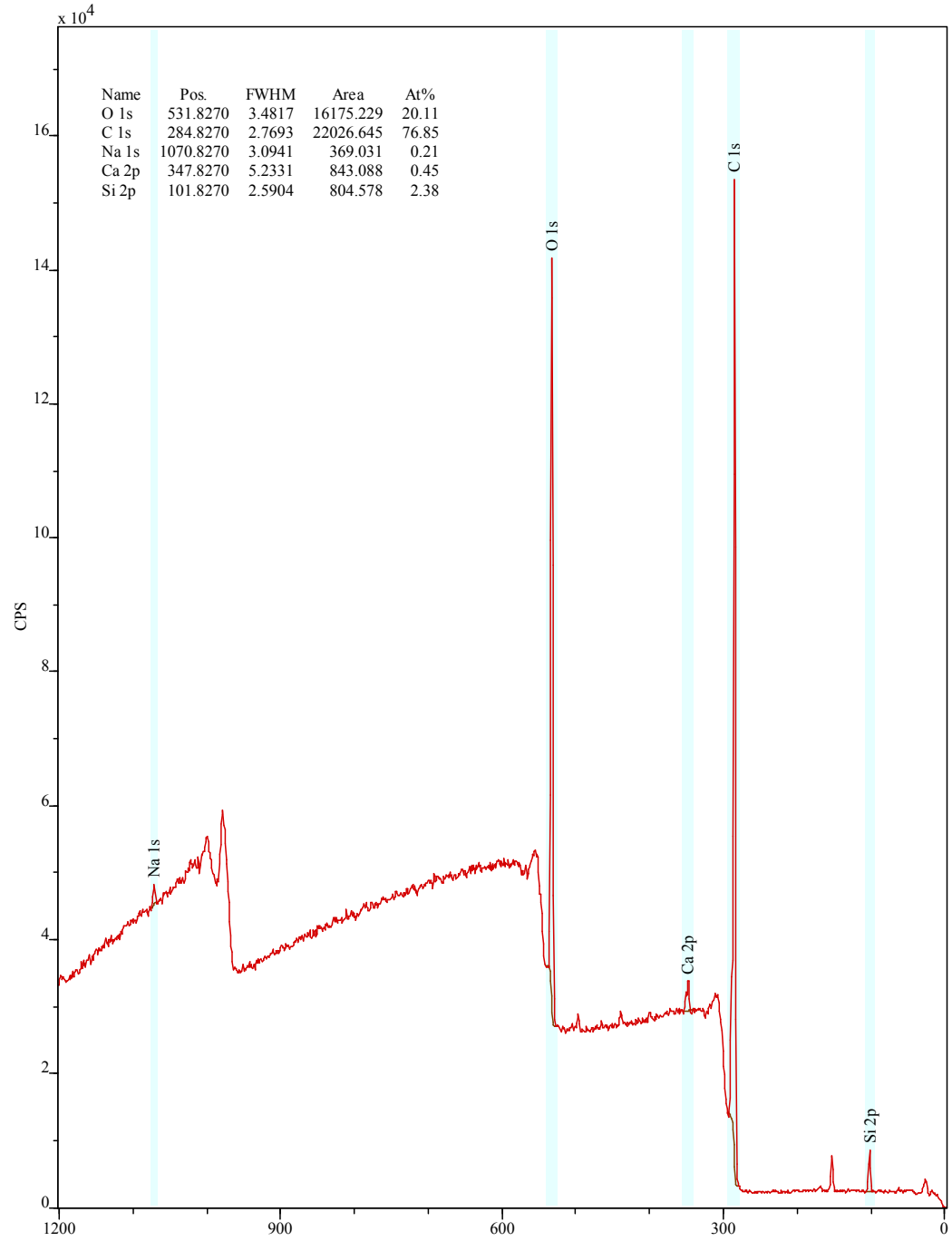
x 10^4
Name Pos. FWHM Area At%
O 1s 531.8270 3.4817 16175.229 20.11
C 1s 284.8270 2.7693 22026.645 76.85
Na 1s 1070.8270 3.0941 369.031 0.21
Ca 2p 347.8270 5.2331 843.088 0.45
Si 2p 101.8270 2.5904 804.578 2.38
O 1s
C 1s
Na 1s
Ca 2p
Si 2p
CPS
16
14
12
10
8
6
4
2
0
1200
900
600
300
0

PETP17

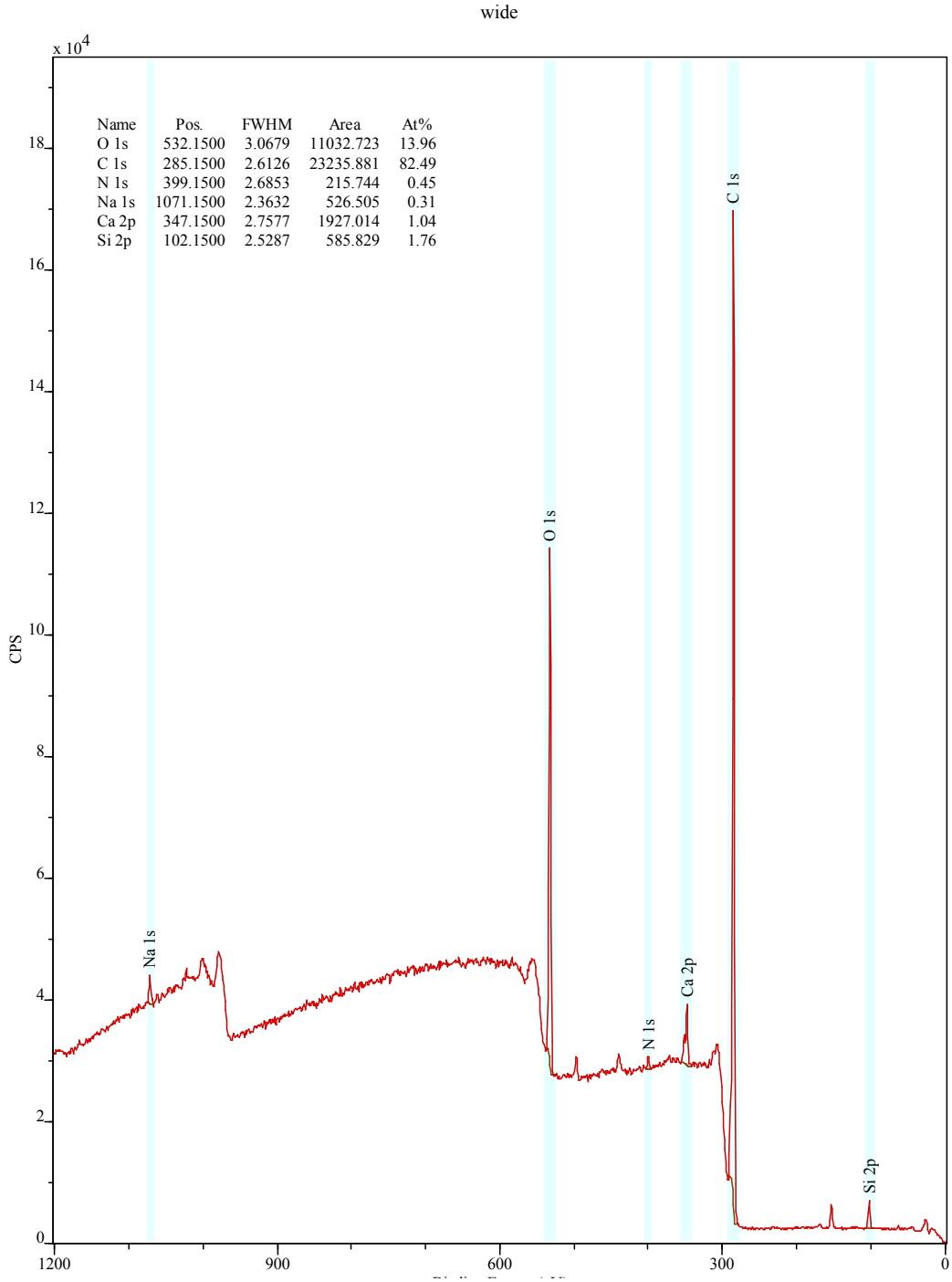
wide
x 10^4
Name Pos. FWHM Area At%
O 1s 532.1500 3.0679 11032.723 13.96
C 1s 285.1500 2.6126 23235.881 82.49
N 1s 399.1500 2.6853 215.744 0.45
Na 1s 1071.1500 2.3632 526.505 0.31
Ca 2p 347.1500 2.7577 1927.014 1.04
Si 2p 102.1500 2.5287 585.829 1.76
CPS
O 1s
C 1s
Na 1s
N 1s
Ca 2p
Si 2p
1200
900
600
300
0

PETP19

Appendix V: ATR-IR (Chapter 4)

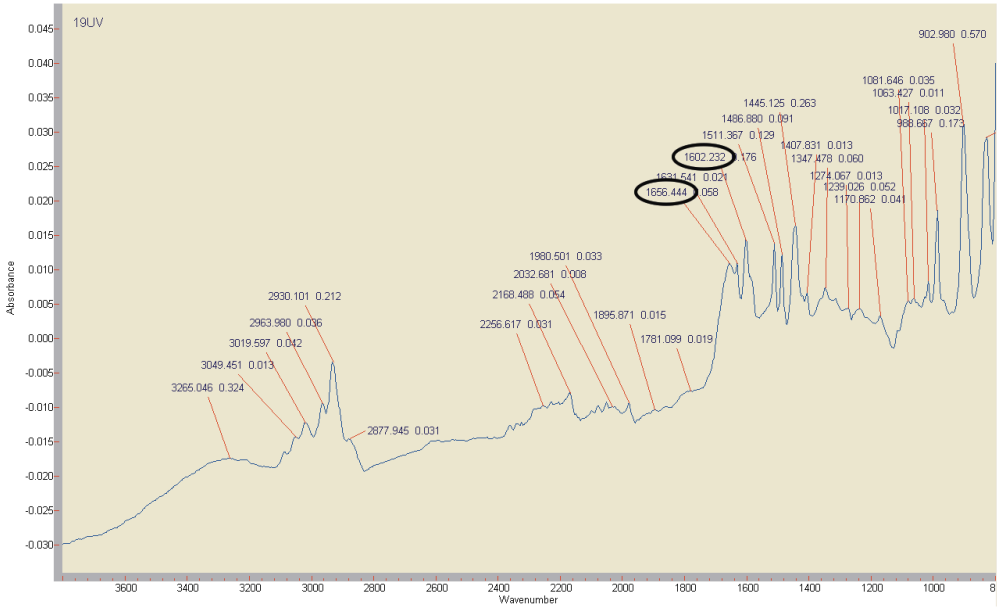

PSP19UVPenV

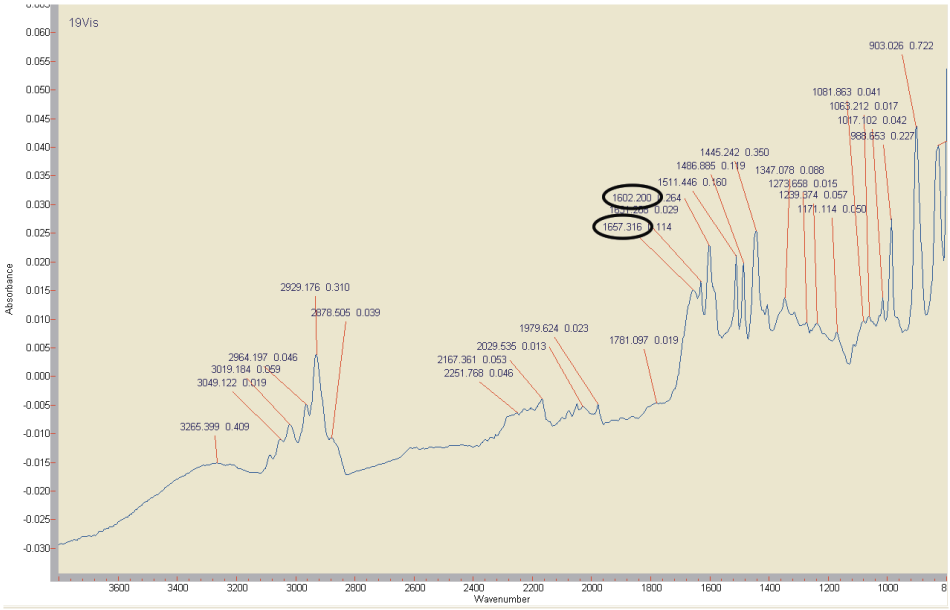

PSP19VISPenV

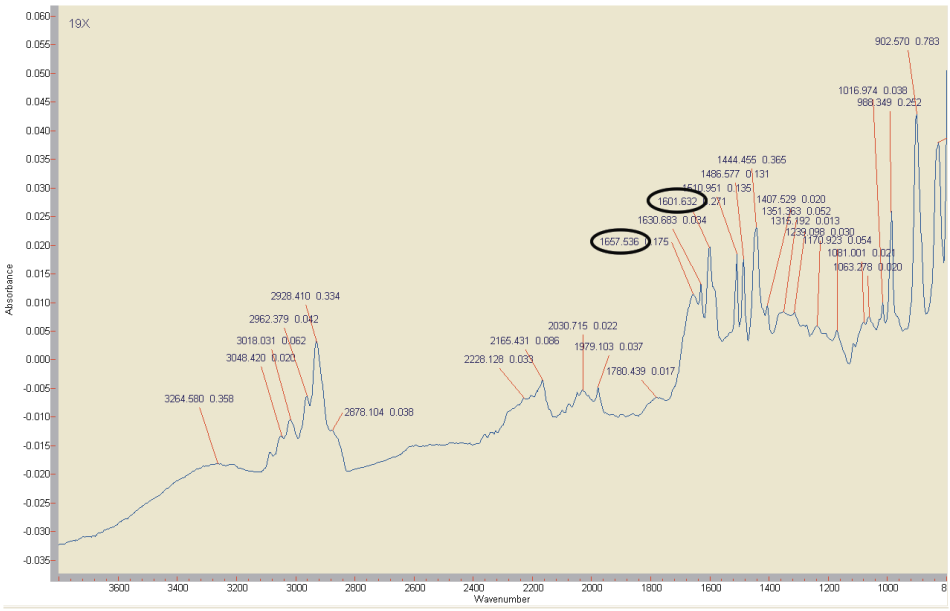

blankPSP19PenV

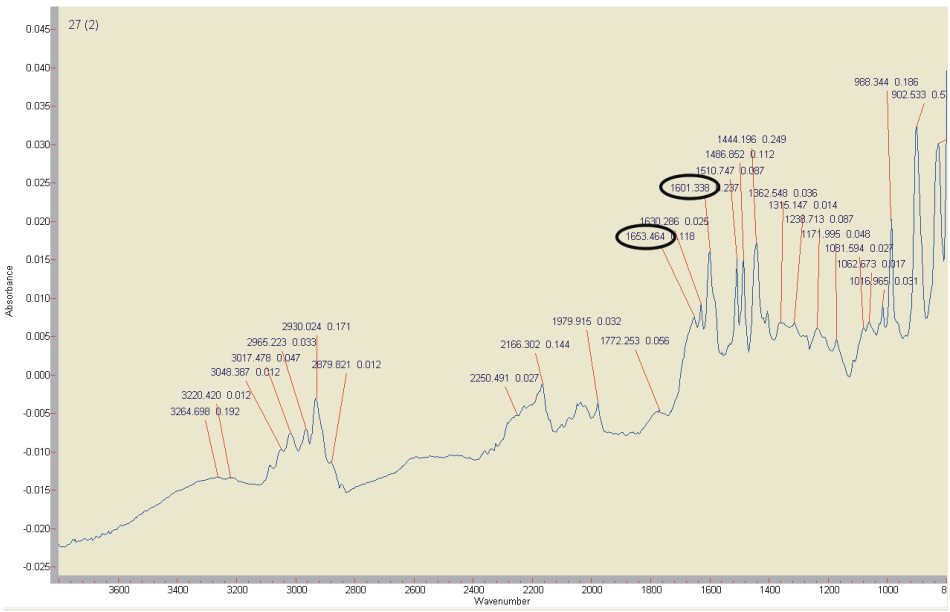

PSM27PenV

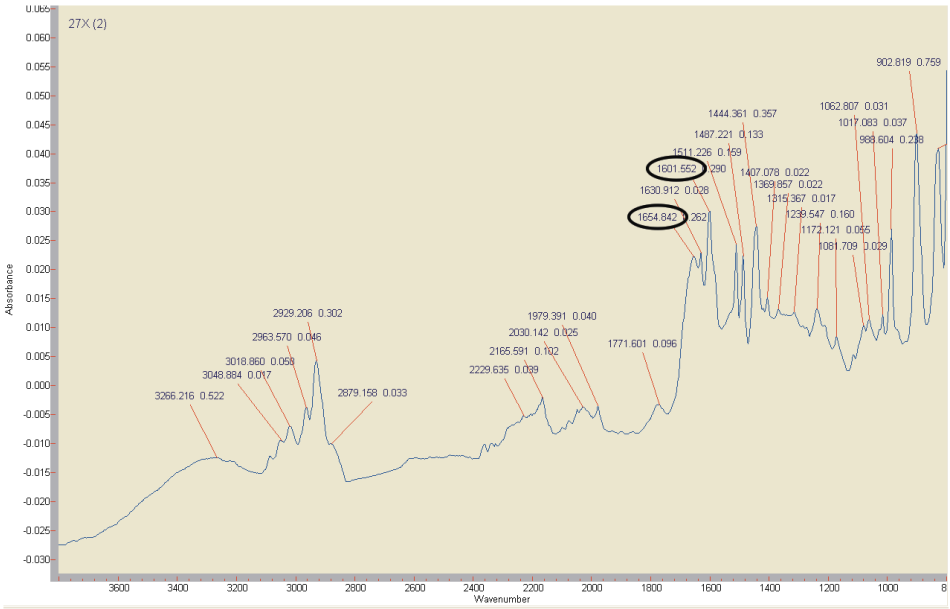

blankPSM27PenV

Appendix VI: DSC (Chapter 5)

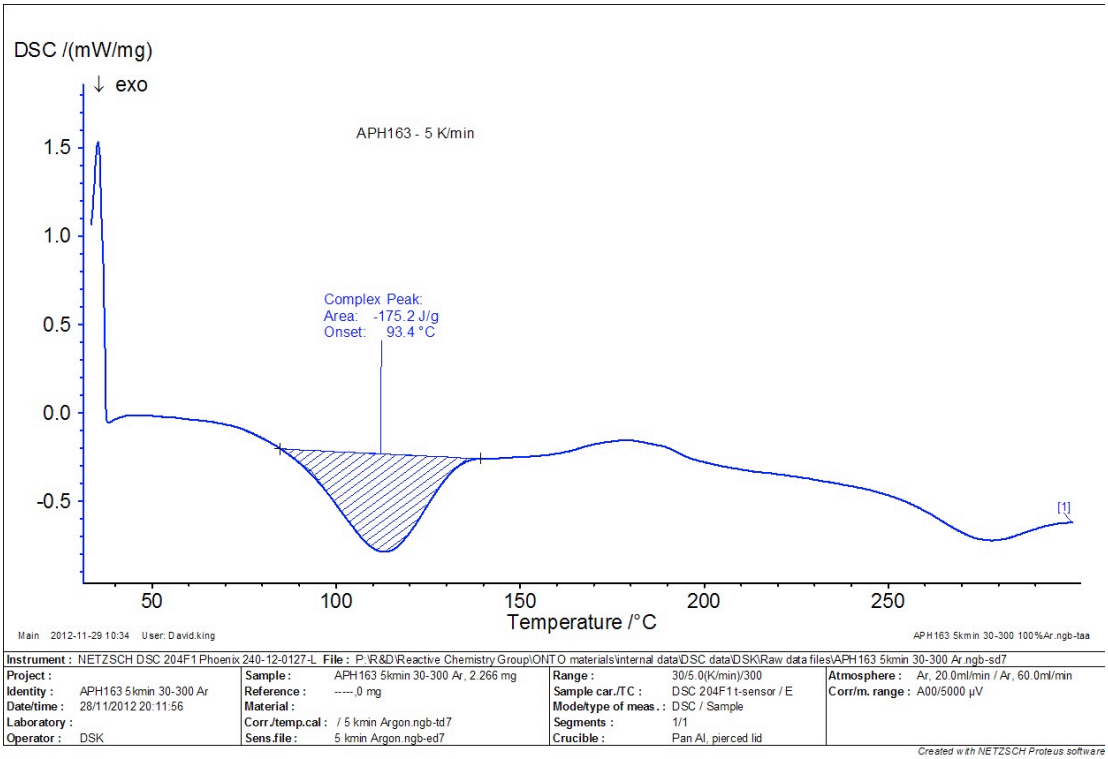

P19

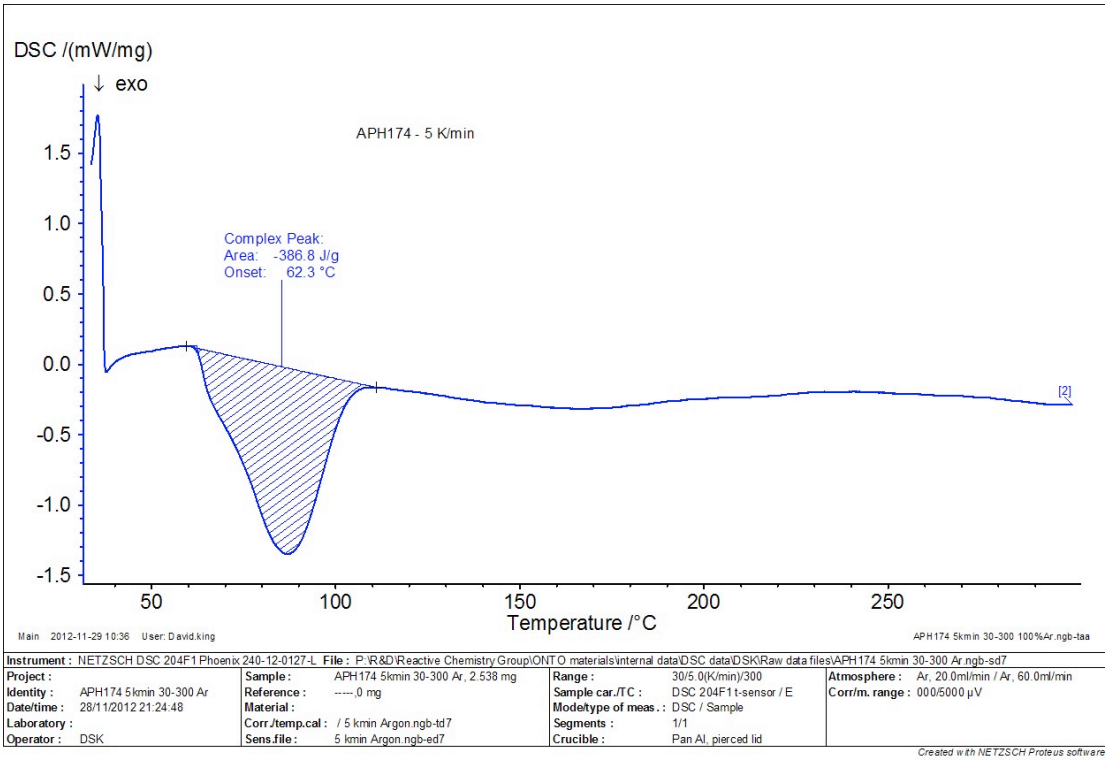

D10

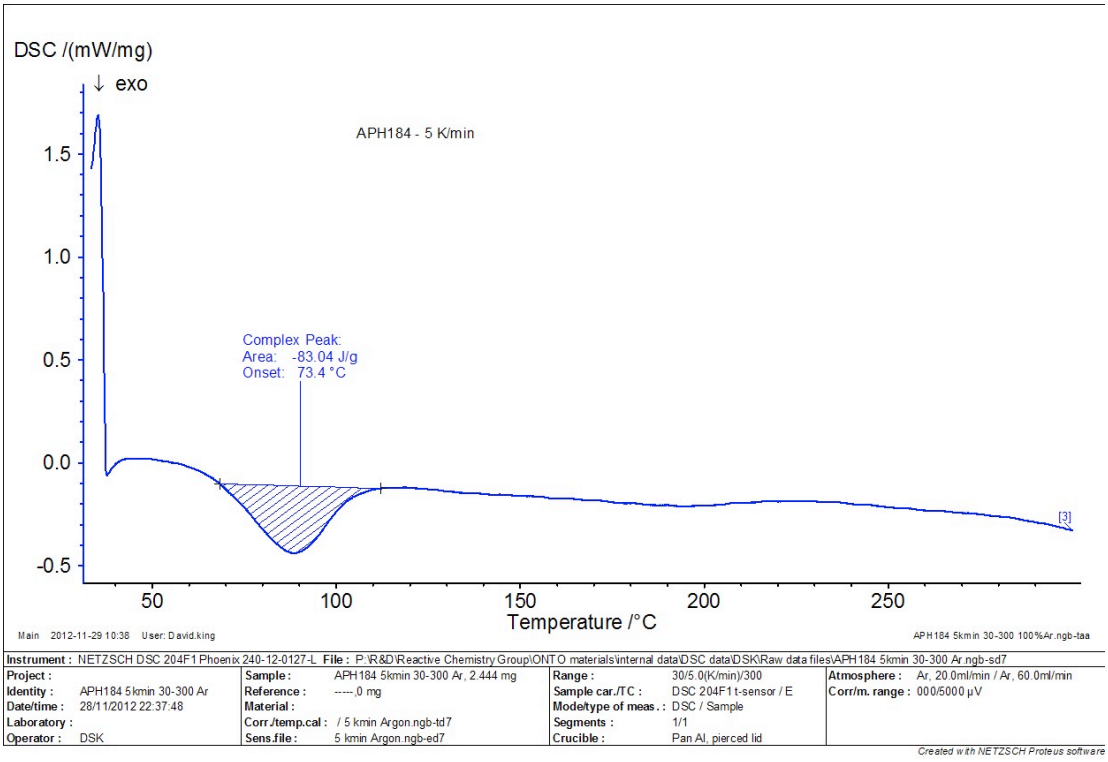
DSC /(mW/mg)
↓ exo
APH184 - 5 K/min
Complex Peak:
Area: -83.04 J/g
Onset: 73.4 °C
[3]
Temperature /°C
Main 2012-11-29 10:38 User: David.king
APH184 5kmin 30-300 100%Ar.ngb-taa
Instrument : NETZSCH DSC 204F1 Phoenix 240-12-0127-L File : P:\R&D\Reactive Chemistry Group\ONTO materials\internal data\DSC data\DSK\Raw data files\APH184 5kmin 30-300 Ar.ngb-sd7
Project :
Identity : APH184 5kmin 30-300 Ar
Date/time : 28/11/2012 22:37:48
Laboratory :
Operator : DSK
Sample : APH184 5kmin 30-300 Ar, 2.444 mg
Reference : -----,0 mg
Material :
Corr./temp.cal : / 5 kmin Argon.ngb-td7
Sens.file : 5 kmin Argon.ngb-ed7
Range : 30/5.0(K/min)/300
Sample car./TC : DSC 204F1 t-sensor / E
Mode/type of meas. : DSC / Sample
Segments : 1/1
Crucible : Pan Al, pierced lid
Atmosphere : Ar, 20.0ml/min / Ar, 60.0ml/min
Corr/m. range : 000/5000 µV
Created with NETZSCH Proteus software

D20

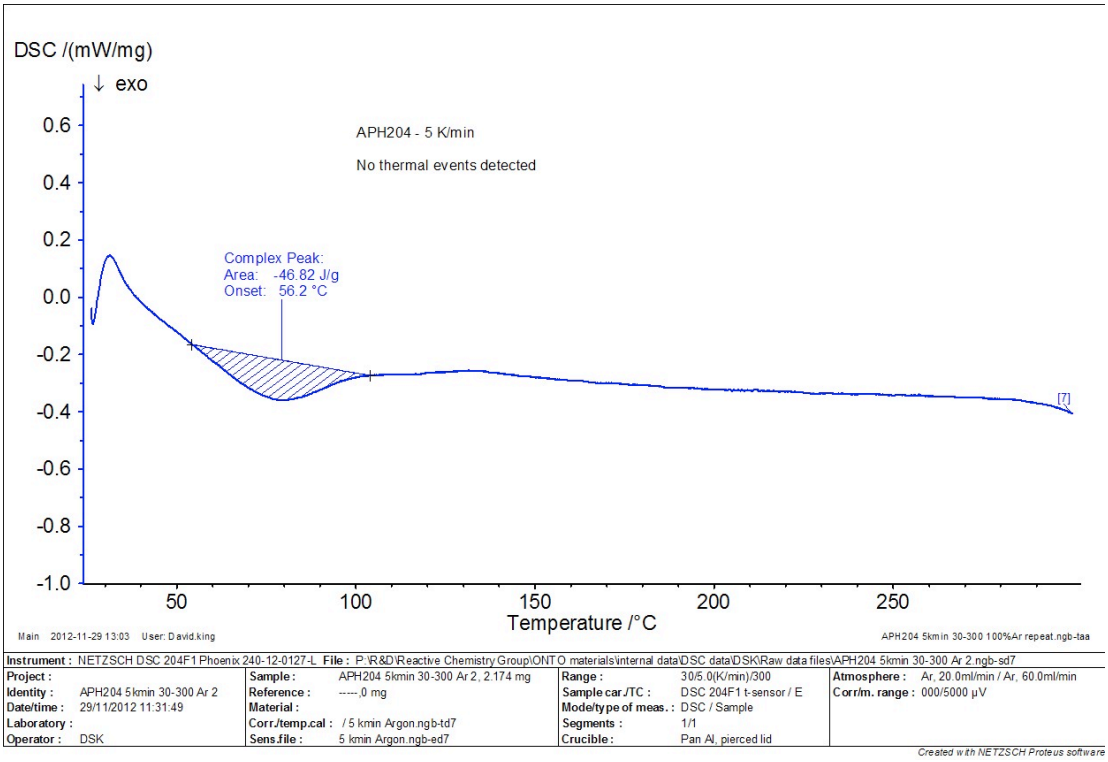
DSC /(mW/mg)
↓ exo
APH204 - 5 K/min
No thermal events detected
Complex Peak:
Area: -46.82 J/g
Onset: 56.2 °C
[7]
Temperature /°C
Main 2012-11-29 13:03 User: David.king
APH204 5kmin 30-300 100%Ar repeat.ngb-taa
Instrument : NETZSCH DSC 204F1 Phoenix 240-12-0127-L File : P:\R&D\Reactive Chemistry Group\ONTO materials\internal data\DSC data\DSK\Raw data files\APH204 5kmin 30-300 Ar 2.ngb-sd7
Project :
Identity : APH204 5kmin 30-300 Ar 2
Date/time : 29/11/2012 11:31:49
Laboratory :
Operator : DSK
Sample : APH204 5kmin 30-300 Ar 2, 2.174 mg
Reference : -----,0 mg
Material :
Corr./temp.cal : / 5 kmin Argon.ngb-td7
Sens.file : 5 kmin Argon.ngb-ed7
Range : 30/5.0(K/min)/300
Sample car./TC : DSC 204F1 t-sensor / E
Mode/type of meas. : DSC / Sample
Segments : 1/1
Crucible : Pan Al, pierced lid
Atmosphere : Ar, 20.0ml/min / Ar, 60.0ml/min
Corr/m. range : 000/5000 µV
Created with NETZSCH Proteus software

D30

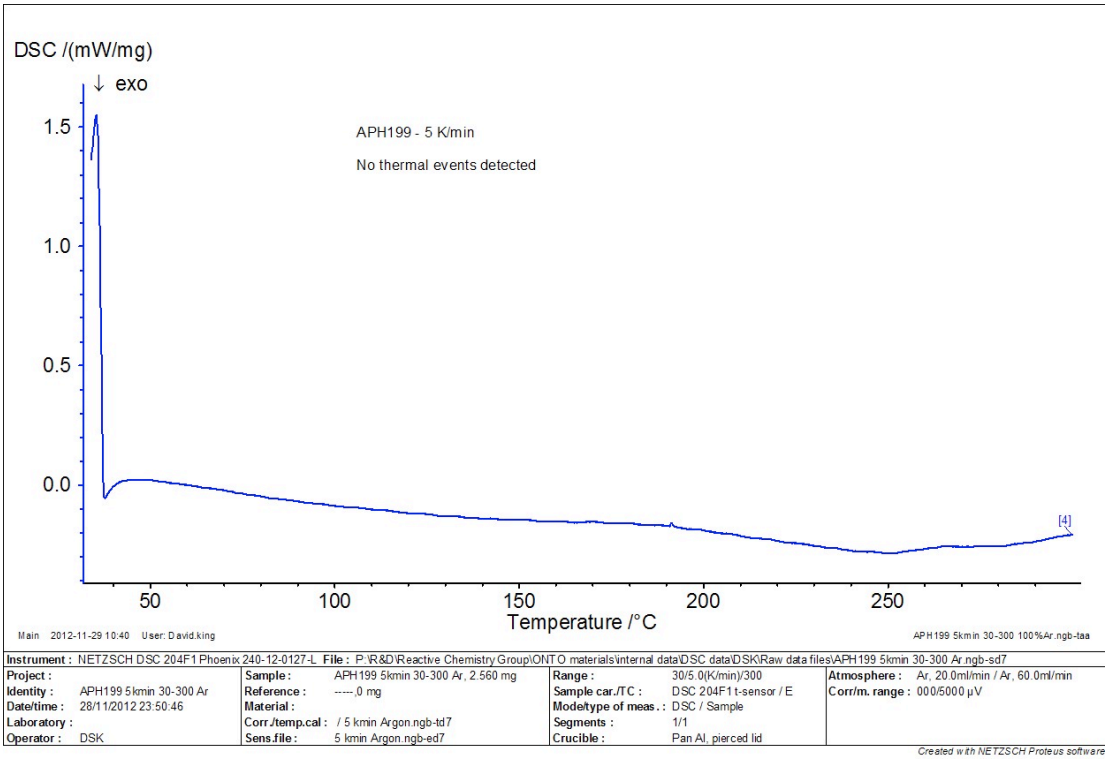
DSC /(mW/mg)
↓ exo
1.5
1.0
0.5
0.0
APH199 - 5 K/min
No thermal events detected
[4]
50
100
150
200
250
Temperature /°C
Main 2012-11-29 10:40 User: David.king
APH199 5kmin 30-300 100%Ar.ngb-taa
Instrument : NETZSCH DSC 204F1 Phoenix 240-12-0127-L File : P:\R&D\Reactive Chemistry Group\ONTO materials\internal data\DSC data\DSK\Raw data files\APH199 5kmin 30-300 Ar.ngb-sd7
Project :
Identity : APH199 5kmin 30-300 Ar
Date/time : 28/11/2012 23:50:46
Laboratory :
Operator : DSK
Sample : APH199 5kmin 30-300 Ar, 2.560 mg
Reference : -----,0 mg
Material :
Corr./temp.cal : / 5 kmin Argon.ngb-td7
Sens.file : 5 kmin Argon.ngb-ed7
Range : 30/5.0(K/min)/300
Sample car./TC : DSC 204F1 t-sensor / E
Mode/type of meas. : DSC / Sample
Segments : 1/1
Crucible : Pan Al, pierced lid
Atmosphere : Ar, 20.0ml/min / Ar, 60.0ml/min
Corr/m. range : 000/5000 µV
Created with NETZSCH Proteus software

D40

Appendix VII: Calculations

Loadings of surface-modified polymers:

$$\text{Loading } \left(\frac{\text{mmol}}{\text{g}}\right) = \left(\frac{\%\text{ of N}}{100}\right)\left(\frac{\text{g of N}}{\text{g of PS XAD}}\right) \times \left(\frac{\text{1 mol of N}}{\text{14 g of N}}\right) \times \left(\frac{\text{1 mol of precursor compound}}{\text{n mol of N atoms}}\right) \times \left(\frac{10^3\ \text{mmol}}{\text{1 mol}}\right)$$

$$\text{eg. (PSM27): } \left(\frac{0.24}{100}\right)\left(\frac{\text{g of N}}{\text{g of PS XAD}}\right) \times \left(\frac{\text{1 mol of N}}{\text{14 g of N}}\right) \times \left(\frac{\text{1 mol of precursor compound}}{\text{2 mol of N atoms}}\right) \times \left(\frac{10^3\ \text{mmol}}{\text{1 mol}}\right) = 0.086\ \left(\frac{\text{mmol}}{\text{g}}\right)$$

Assumes surface area of 725 m^2/g (manufacturer's data):

$$\text{Loading } \left(\frac{\text{molecules}}{\text{cm}^2}\right) = \text{Loading } \left(\frac{\text{mmol}}{\text{g}}\right) \times \left(\frac{10^{-3}\ \text{mol}}{\text{1 mmol}}\right) \times \left(\frac{6.02 \times 10^{23}\ \text{molecules}}{\text{1 mol}}\right) \times \left(\frac{\text{1 g}}{725\ \text{m}^2}\right) \times \left(\frac{\text{1 m}^2}{10^4\ \text{cm}^2}\right)$$

$$\text{eg. (PSM27): } 0.086\ \left(\frac{\text{mmol}}{\text{g}}\right) \times \left(\frac{10^{-3}\ \text{mol}}{\text{1 mmol}}\right) \times \left(\frac{6.02 \times 10^{23}\ \text{molecules}}{\text{1 mol}}\right) \times \left(\frac{\text{1 g}}{725\ \text{m}^2}\right) \times \left(\frac{\text{1 m}^2}{10^4\ \text{cm}^2}\right) = 7.1 \times 10^{12}\ \left(\frac{\text{molecules}}{\text{cm}^2}\right)$$

Assumes limiting area (A^o) for monolayer formation is 0.46 nm^2/molecule:

$$\text{Surface Coverage (\%)} = \text{Loading } \left(\frac{\text{molecules}}{\text{cm}^2}\right) \times \left(\frac{10^{-14}\ \text{cm}^2}{\text{1 nm}^2}\right) \times \text{Limiting area } A_0 \left(\frac{\text{nm}^2}{\text{molecules}}\right) \times 100\%$$

$$\text{eg. (PSM27): } 7.1 \times 10^{12}\ \left(\frac{\text{molecules}}{\text{cm}^2}\right) \times \left(\frac{10^{-14}\ \text{cm}^2}{\text{1 nm}^2}\right) \times 0.46\ \left(\frac{\text{nm}^2}{\text{molecules}}\right) \times 100\% = 3.3\%$$

N represents the ratio of unmodified styrene monomers to functionalised units:

FW of 1 monostyrene (C_8H_8) = 104.15 g/mol.

eg. (**PSM27**): FW of 1 modified monostyrene = 483.62 g/mol.

$$\left(\frac{\%\text{ of N}}{100}\right) = \left(\frac{14\ \frac{\text{g}}{\text{mol}}\ \text{of N}}{\text{FW of 1 modified monostyrene} + (\text{N} \times \text{FW of 1 monostyrene})}\right) \times \left(\frac{\text{n mol of N atoms}}{\text{1 mol of precursor compound}}\right)$$

$$\left(\frac{0.24}{100}\right) = \left(\frac{14\ \frac{\text{g}}{\text{mol}}\ \text{of N}}{482.61 + (\text{N} \times 104.15)}\right) \times 2,\ \text{N} = 107$$

FW of 1 monoethylene terephthalate ($C_{10}H_8O_4$) = 192.17.

eg. (**PETP19**): FW of 1 modified monoethylene terephthalate = 839.84 g/mol.

$$\left(\frac{\%\text{ of N}}{100}\right) = \left(\frac{14\ \frac{g}{mol}\text{ of N}}{\text{FW of 1 modified monomer + (N x FW of 1 monomer)}}\right) \text{x } \left(\frac{\text{n mol of N atoms}}{\text{1 mol of precursor compound}}\right)$$

$$\left(\frac{0.11}{100}\right) = \left(\frac{14\ \frac{g}{mol}\text{ of N}}{839.84 + (N \text{ x } 192.17)}\right) \text{x 3, N = 214}$$

The number of pyridine units on surface-modified polymers:

$$\text{Pyridine units } \left(\frac{mmol}{g}\right) = \frac{\text{Loading of PSMX } \left(\frac{\text{mmol of N}}{g}\right) - \text{Loading of PSM4 } \left(\frac{\text{mmol of N}}{g}\right)}{\left(\frac{\text{n mol of N atoms}}{\text{1 mol of PSMX}}\right) - \left(\frac{\text{n mol of N atoms}}{\text{1 mol of PSM4}}\right)}$$

$$\text{eg. (PSM8): } \frac{\text{Loading of PSM8 } \left(\frac{0.050 \text{ x 5 mmol of N}}{g}\right) - \text{Loading of PSM4 } \left(\frac{0.16 \text{ mmol of N}}{g}\right)}{\left(\frac{\text{5 mol of N atoms}}{\text{1 mol of PSM8}}\right) - \left(\frac{\text{1 mol of N atoms}}{\text{1 mol of PSM4}}\right)} = 0.023$$

% Diazonium coupling:

$$\%\text{ Diazonium coupling} = \frac{\text{pyridine units of PSMX } \left(\frac{mmol}{g}\right)}{\text{theoretical loading of PSM4 } \left(\frac{mmol}{g}\right)} \text{ x 100}$$

$$\text{eg. (PSM8): } \frac{\text{pyridine units of PSM8 } \left(\frac{0.023 \text{ mmol}}{g}\right)}{\text{theoretical loading of PSM4 } \left(\frac{0.136 \text{ mmol}}{g}\right)} \text{ x 100 = 17\%}$$

% Metal coordination:

$$\% \text{ Metal coordination} = \frac{\text{loading of Zn of PSMX } (\frac{\mu\text{mol}}{\text{g}}) \text{ x } (\frac{10^{-3}\ \text{mmol}}{1\ \mu\text{mol}})}{\text{pyridine units of PSMX } (\frac{\text{mmol}}{\text{g}})} \text{ x } 100$$

$$\text{eg. (PSM27): } \frac{\text{loading of Zn of PSM27 } (\frac{5.1\ \mu\text{mol}}{\text{g}}) \text{ x } (\frac{10^{-3}\ \text{mmol}}{1\ \mu\text{mol}})}{\text{pyridine units of PSM27 } (\frac{0.086\ \text{mmol}}{\text{g}})} \text{ x } 100 = 6.0\%$$

% Metal exchange:

$$\% \text{ Metal exchange} = \frac{\text{copper content of PSM28X } (\frac{\mu\text{mol}}{\text{g}})}{\text{loading of Zn of PSM27.ZnATSMX } (\frac{\mu\text{mol}}{\text{g}})} \text{ x } 100$$

$$\text{(PSM28b): } \frac{\text{copper content of PSM28b } (\frac{1.62\ \mu\text{mol}}{\text{g}})}{\text{loading of Zn of PSM27.ZnATSMA } (\frac{8.2\ \mu\text{mol}}{\text{g}})} \text{ x } 100 = 20\%$$

$$\text{(PSM28d): } \frac{\text{copper content of PSM28d } (\frac{0.38\ \mu\text{mol}}{\text{g}})}{\text{loading of Zn of PSM27.ZnATSM } (\frac{3.1\ \mu\text{mol}}{\text{g}})} \text{ x } 100 = 12\%$$